

DISCOVERY, OPTIMIZATION, AND CHARACTERIZATION
OF NOVEL SUBTYPE-SELECTIVE
M₅ MUSCARINIC ACETYLCHOLINE RECEPTOR LIGANDS

By

Patrick R. Gentry

Dissertation

Submitted to the Faculty of the
Graduate School of Vanderbilt University
in partial fulfillment of the requirements

for the degree of

DOCTOR OF PHILOSOPHY

in

Chemical and Physical Biology

August, 2014

Nashville, Tennessee

Approved:

Professor Craig Lindsley

Professor Gary Sulikowski

Professor Scott Daniels

Professor Charles Hong

Professor Lawrence Marnett

In memory of my mother,

Cynthia Gentry

ACKNOWLEDGEMENTS

I owe a great debt of gratitude to many colleagues, friends, and family for their guidance and support throughout the process of researching and writing this dissertation. Their effort and generosity have made my graduate career a productive and enjoyable time, and I would like thank a number of them here. Dr. Tom Bridges deserves much of the credit for introducing me to the research laboratory environment and the idea of pursuing a degree in biomedical research. Tom has been a mentor to me throughout my time as a research assistant and as a graduate student, and he has been an inexhaustible source of assistance and advice, for which I am tremendously grateful. Similarly, I owe thanks to Prof. Michael Treadway, who has influenced me greatly as a scientific mentor, role model, and close friend. His pep-talks, advice, and enthusiasm for academic research have played a major role in shaping my decision to pursue a career in research.

I would like to acknowledge the members of my dissertation committee: Profs. Gary Sulikowski, Scott Daniels, Charles Hong, and Larry Marnett. In the classroom they have been incredible educators and in our meetings I have greatly benefitted from their insight, experience, and guidance.

I owe my greatest thanks to my graduate advisor, Prof. Craig Lindsley. Over the course of the seven and a half years I have worked in Craig's laboratory, he has provided me with the highest quality scientific and professional education as well as countless opportunities to publish research, collaborate, develop my career, and challenge myself. Additionally, he has given me an enjoyable and thorough schooling in the nuances of

single-malt scotches, the artistry of slasher horror films, the history of 1980s hard rock, the tactics of paintball ambushes, and the importance of packing your parachute correctly.

Craig also deserves praise for surrounding himself with a laboratory full of hard-working, brilliant, and collegial scientists. Prof. Mike Wood, the project leader for research on M_5 , has been integral in shaping the course of my research and I am in debt to him for the crucial advice and guidance he has provided. Dr. Masaya Kokubo also deserves a great deal of credit as my partner in the discovery of much of the work described herein. Together Masaya and I expanded the scope of the M_5 project in ways I could have never accomplished alone. Furthermore, his knowledge and humor made him an indispensable labmate and friend; I consider myself extremely fortunate to have been able to work with him. I have been lucky enough to work closely with nearly every member of the Lindsley Laboratory, past and present, and every single one of them has encouraged, advised, and helped me throughout my time in the lab. I would especially like to thank Dr. Mike Schulte, Dr. J.T. Brogan, Dr. Hyekyung Plumley, Dr. Bruce Melançon, Prof. Mark Turlington, Prof. Corey Hopkins, Dr. Phil Kennedy, Matt Mulder, and Rocco Gogliotti for their friendship and guidance throughout my time in the laboratory.

I would like to thank the larger VCNDD group as a whole for their collaboration and collegiality throughout the course of my research at Vanderbilt. Profs. Jeff Conn and Colleen Niswender have provided me with incredible resources and support by allowing me the use of the Conn laboratory and its equipment and supplies. I thank them and all of the Conn laboratory members as well, especially Dr. Dan Foster, Becca Klar, Katrina Brewer, and Dr. Karen Gregory for their help, instruction, and friendship. Likewise,

working with the laboratory of Prof. Scott Daniels has been a magnificent collaboration and I cannot thank Scott and his lab enough for their hard work and enthusiasm for the M₅ project.

None of the research contained herein would have been possible without the generous financial support of the NIH and the Molecular Libraries Probe Center Network (MLPCN U54 MH084659). Of course, many thanks to Vanderbilt University and the Vanderbilt University Medical Center for providing the infrastructure for an outstanding research environment. I would like to thank the administration and staff of the Chemical & Physical Biology Program for providing me the means to sculpt a Ph.D. research track that allowed me to plant one foot in pharmacology and the other in organic chemistry. Within the CPBP, I especially wish to thank Lindsay Meyers, whose management of and dedication to the CPBP students is the backbone of the program.

In addition to help from within the laboratory, much of the support for my research has come from outside the scientific realm. My parents, Rick and Cindy Gentry, have given me unflinching support, encouragement, and love in my scientific endeavors and in every aspect of my life. Sadly, my mother lost her life to chronic lymphocytic leukemia shortly before I began my graduate work. It is to her that this dissertation is dedicated. My stepmother, Diane Gentry, has been a welcome addition to our family and likewise has my heartfelt thanks for her support, love, and encouragement. Lastly, I would like to give very special thanks to my best friends Jennifer Bennett, Jon Wiley, Mike Schulte, J.T. Brogan, and Pooja Brogan. Their heroic work of regularly removing me from the laboratory to go on adventures, have great conversations, and eat and drink our way across Nashville has been much enjoyed and appreciated.

TABLE OF CONTENTS

	Page
DEDICATION	ii
ACKNOWLEDGEMENTS	iii
LIST OF TABLES	x
LIST OF FIGURES	xiii
LIST OF SCHEMES.....	xix
LIST OF ABBREVIATIONS.....	xxii
Chapter	
I. INTRODUCTION	1
The M ₅ muscarinic acetylcholine receptor	1
The cholinergic system and the neurotransmitter acetylcholine	1
History and discovery of the mAChRs.....	3
Structure and function of M ₅	6
Localization of M ₅	8
Effects of the genetic deletion of M ₅	9
Therapeutic potential of M ₅	11
Allosteric modulation of the M ₅ muscarinic acetylcholine receptor	13
Allosteric modulation of mAChRs	13
Characterization of allosteric modulators.....	17
Allosteric modulators of M ₅	20
Notes on the numbering of figures, tables, schemes, and compounds	24
II. MATERIALS AND METHODS	26
General optimization strategy	26
Medicinal Chemistry	28
General synthetic methods and instrumentation	28
Isatin-based M ₅ PAM chemical experimentals and characterization	30
Non-isatin M ₅ PAM chemical experimentals and characterization	31
M ₅ NAM chemical experimentals and characterization.....	41
M ₅ orthosteric antagonist chemical experimentals and characterization	50
<i>In vitro</i> pharmacology	58

Calcium mobilization assays	58
[³ H]-NMS competition binding.....	60
[³ H]-NMS dissociation kinetics.....	61
Ancillary/off-target screening assays	62
<i>In vitro</i> DMPK.....	62
Plasma protein and brain homogenate binding	62
Hepatic microsome intrinsic clearance.....	64
LC/MS/MS bioanalysis of samples from plasma protein/brain homogenate binding and hepatic microsome intrinsic clearance assays	65
Inhibition of cytochrome P450 enzymes.....	65
Caco-2/MDCK-MDR1 transwell assays	67
<i>In vivo</i> DMPK	67
Statement on animal care and use	67
Pharmacokinetic/plasma-brain level studies in rat.....	68
Pharmacokinetic studies in non-human primate	70

III. DEVELOPMENT OF THE FIRST HIGHLY SELECTIVE, SUB-MICROMOLAR M₅ POSITIVE ALLOSTERIC MODULATOR..... 71

Prior discovery of the first M ₅ -preferring PAM.....	71
Optimization of VU0238429 to obtain the first sub-micromolar M ₅ PAM VU0467903	74
Replacement of the isatin carbonyl with tertiary hydroxyl moieties.....	74
Replacement of the isatin carbonyl with a spiro-oxetane bioisostere	79
Isatin core/phenethyl ether matrix library and the discovery of VU0467903 ...	80
<i>In vitro</i> pharmacological characterization of M ₅ PAM VU0467903	89
Characterization of mAChR subtype selectivity of VU0467903.....	89
Confirmation of the allosteric mechanism of VU0467903	90
Ancillary pharmacology of the VU0467903	91
Continued optimization of M ₅ PAM VU0467903	93
Replacement of the isatin carbonyl in the context of the phenethyl ether	93
<i>In vitro</i> and <i>in vivo</i> DMPK characterization of M ₅ PAM VU0467903.....	98
Summary and future directions	99

IV. IDENTIFICATION, OPTIMIZATION, AND CHARACTERIZATION OF A NON- ISATIN M₅ POSITIVE ALLOSTERIC MODULATOR 102

HTS identification of a novel, M ₅ -selective ligand with PAM activity	102
Optimization of VU0472882 to obtain non-isatin M ₅ PAM VU0476212	105
Optimization of eastern sulfonamide region SAR	105
Introduction of benzylic methyl and discovery of enantiospecific activity	118
Combination of benzylic methyl and sulfonamide substituent SAR	121
<i>In vitro</i> DMPK characterization of non-isatin M ₅ PAM VU0476212	124
<i>In vitro</i> DMPK characterization of VU0476212.....	124
VU0476212 metabolite identification	125

Optimization of VU0476212 to obtain non-isatin M ₅ PAM VU0481443	129
Exploration of amide and sulfonamide SAR.....	129
Attempts to constrain the <i>N</i> -alkyl moiety.....	132
Optimization of western benzamide ring substituent SAR	133
Combination of benzyl region SAR	142
Discovery of VU0481443	144
<i>In vitro</i> pharmacological characterization of non-isatin M ₅ PAM VU0481443 ...	145
Characterization of VU0481443 mAChR selectivity and fold shift	145
Ancillary pharmacology of VU0481443	147
Confirmation of the allosteric mechanism of VU0481443	149
<i>In vitro</i> and <i>in vivo</i> DMPK characterization of non-isatin M ₅ PAM	
VU0481443	150
Continued SAR exploration of non-isatin M ₅ PAM VU0481443.....	152
Exploration of piperidine core modifications.....	152
Substitution of amide <i>N</i> -alkyl substituent	155
Summary and future directions	159

V. IDENTIFICATION, OPTIMIZATION, AND CHARACTERIZATION OF THE FIRST HIGHLY SELECTIVE M₅ NEGATIVE ALLOSTERIC MODULATOR ...163

HTS identification of a novel, M ₅ -selective ligand with antagonist activity	163
Optimization of VU0352221 to obtain the first M ₅ NAM, VU0483253	165
Optimization of benzamide region SAR	165
Exploration of tricyclic core region SAR.....	179
Optimization of 9b-phenyl region SAR	183
<i>In vitro</i> pharmacological characterization of M ₅ NAM VU0483253.....	194
Characterization of mAChR subtype selectivity of VU0483253	194
Investigation of allosteric mechanism of VU0483253	195
Ancillary pharmacology of VU0483253	197
<i>In vitro</i> and <i>in vivo</i> DMPK characterization of M ₅ NAM VU0483253	199
Continued SAR exploration and physicochemical optimization of M ₅ NAM	
VU0483253	201
Continued exploration of tricyclic core region SAR.....	202
Continued exploration of benzamide region SAR	210
Continued exploration of 9b-phenyl region SAR.....	215
Summary and future directions	220

VI. IDENTIFICATION, OPTIMIZATION, AND CHARACTERIZATION OF A HIGHLY SELECTIVE M₅ ORTHOSTERIC ANTAGONIST225

HTS identification of a novel, M ₅ -selective ligand with antagonist activity	225
Optimization of VU0480131 to obtain M ₅ orthosteric antagonist VU0488130 ...	228
Exploration of eastern amide region SAR.....	228
Exploration of western aryl ether region SAR	232
Exploration of isoxazole core region SAR.....	246

Synthesis of VU0480131 enantiomers	247
<i>In vitro</i> pharmacological characterization of M ₅ orthosteric antagonist VU0488130	249
Characterization of mAChR subtype selectivity of VU0488130	249
Confirmation of the orthosteric mechanism of VU0488130	250
Ancillary pharmacology of VU0488130	251
<i>In vitro</i> and <i>in vivo</i> DMPK characterization of M ₅ orthosteric antagonist VU0483253	253
<i>In vitro</i> DMPK characterization of VU0488130	253
M ₅ Antagonist VU0488130 metabolite identification	255
<i>In vivo</i> DMPK characterization of VU0488130	256
Summary and future directions	257
 REFERENCES	 260

LIST OF TABLES

Chapter III

Table	Page
3.1 Structures for tertiary hydroxyl analogs 3.10-3.14 and associated PAM activity data from the single point (30 μ M) screen at hM ₅	77
3.2 Structures for matrix library analogs 3.18, 3.21-3.48 and associated PAM activity data from the single point (30 μ M) screen at hM ₅	83
3.3 Potencies at hM ₅ and hM ₃ for the 8 highly active matrix library analogs selected from the initial single point (30 μ M) screen	88
3.4 Ancillary/off-target competition binding screen results for 3.39 (VU0467903, ML326)	92
3.5 Structures for tertiary hydroxyl analogs 3.50-3.56 and associated PAM activity data from the single point (30 μ M) screen at hM ₅	95

Chapter IV

Table	Page
4.1 Structures for sulfonamide analogs 4.5-4.66 and associated PAM activity data from the single point (30 μ M) screen at hM ₅	107
4.2 Potencies at hM ₅ for 29 aryl and heteroaryl sulfonamide analogs selected from the single point (30 μ M) screen	115
4.3 Potencies at hM ₅ for 7 sulfonamide analogs, 4.75-4.81 , in the context of the (<i>R</i>)-oriented benzylic methyl	122
4.4 <i>In vitro</i> DMPK data for 4.75 (VU0476212) in multiple species.....	125
4.5 <i>In vitro</i> DMPK data for 4.86 (VU0477898) in multiple species.....	128
4.6 Structures for benzyl analogs 4.127-4.151 and associated PAM activity data from the single point (10 μ M) screen at hM ₅	136
4.7 Potencies at hM ₅ for substituted benzyl ring analogs selected from the single point (10 μ M) screen.....	140

4.8	Potencies at hM ₅ for combined benzyl region analogs 4.155-4.157	143
4.9	Ancillary/off-target competition binding screen results for 4.161 (VU0481443, ML380)	148
4.10	<i>In vitro</i> and <i>in vivo</i> IV PK/PBL DMPK data for 4.161 (VU0481443, ML380) in multiple species	151
4.11	Potencies at hM ₅ for <i>N</i> -alkyl library analogs 4.190-4.201 and corresponding microsomal clearance data in rat and human for selected analogs	157

Chapter V

Table	Page	
5.1	Structures for benzamide analogs 5.3-5.41 and associated inhibitory activity data from the single point (10 μM) screen at hM ₅	167
5.2	Potencies at hM ₅ for active benzamide analogs selected from the single point (10 μM) screen	174
5.3	Structures for amide analogs 5.42-5.52 and associated inhibitory activity data from the single point (10 μM) screen at hM ₅	177
5.4	Structures for core analogs 5.53-5.64 and associated inhibitory activity data from the single point (10 μM) screen at hM ₅	181
5.5	Structures for 9b-phenyl matrix library analogs 5.70-5.96 and associated inhibitory activity data from the single point (10 μM) screen at hM ₅	185
5.6	Potencies at hM ₅ for 9b-phenyl matrix library analogs 5.70-5.96	191
5.7	Ancillary/off-target competition binding screen results for 5.97 (VU0483253, ML375)	197
5.8	<i>In vitro</i> and <i>in vivo</i> DMPK data for 5.97 (VU0483253, ML375) in multiple species	200
5.9	Structures for 6-membered aminal core analogs 5.99-5.109 and associated inhibitory activity data from the single point (10 μM) screen at hM ₅	204
5.10	Structures for pyridyl core analogs 5.112-5.122 and associated inhibitory activity data from the single point (10 μM) screen at hM ₅	208

5.11 Structures for benzamide analogs 5.123-5.132 and associated inhibitory activity data from the single point (10 μ M) screen at hM ₅	211
5.12 Potencies at hM ₅ for selected benzamide analogs 5.129-5.131	214
5.13 Structures for 9b-4-methoxyphenyl analogs 5.134-5.146 and associated inhibitory activity data from the single point (10 μ M) screen at hM ₅	216
5.14 Potencies at hM ₅ for selected 9b-4-methoxyphenyl analogs 5.141, 5.144, and 5.145	219

Chapter VI

Table	Page
6.1 Structures for amide analogs 6.4-6.16 and associated inhibitory activity data from the single point (10 μ M) screen at hM ₅	230
6.2 Structures for aryl ether analogs 6.19-6.41 and associated inhibitory activity data from the single point (10 μ M) screen at hM ₅	234
6.3 Structures for amide linker analogs 6.47-6.59 and associated inhibitory activity data from the single point (10 μ M) screen at hM ₅	240
6.4 Structures for secondary amide linker analogs 6.66-6.77 and associated inhibitory activity data from the single point (10 μ M) screen at hM ₅	244
6.5 Ancillary/off-target competition binding screen results for 6.96 (VU0488130, ML380)	251
6.6 <i>In vitro</i> DMPK data for 6.96 (VU0488130) in multiple species.....	254

LIST OF FIGURES

Chapter I

Figure	Page
1.1 Illustration of acetylcholine biosynthesis at the cholinergic synapse.....	2
1.2 A) A photograph of the fly agaric mushroom (<i>Amanita muscaria</i>) in its natural state. B) The structure of the natural alkaloid muscarine, originally isolated from the extract of the fly agaric	4
1.3 Chemical probes central to the discovery and early characterization of the muscarinic acetylcholine receptors	5
1.4 Illustrated model of a mAChR depicting the general structure and the two major signaling pathways mediated by $G_{\alpha q}$ and $G_{\alpha i/o}$	7
1.5 The allosteric ternary complex model	15
1.6 Example fluorometric data illustrating the detection of a PAM in a single point, double-add assay format.....	18
1.7 Example data demonstrating the modulatory effects of a PAM and a NAM/inhibitor in full CRC assays in double-add format	19
1.8 Example data demonstrating the a PAM inducing a leftward shift in the CRC of an orthosteric ligand in a fold shift assay and a NAM depressing the CRC of an orthosteric ligand in a manner characteristic of noncompetitive antagonism	19
1.9 Structures of selected non-selective M_5 allosteric modulators.....	21
1.10 Structure, potency, and human mAChR selectivity of VU0119498.....	22
1.11 Structure, potency, and human mAChR selectivity of VU0238429.....	23

Chapter II

Figure	Page
2.1 Generalized workflow diagram illustrating multidimensional iterative parallel synthesis and testing of analog libraries optimizing multiple regions of a lead chemical series.....	28

Chapter III

Figure	Page
3.1 Structures and activities of M ₅ -preferring PAM VU0238429 (3.2) and selected M ₅ -selective PAM analogs 3.3 and 3.4	72
3.2 Structure and activity of VU0366369 (3.5)	72
3.3 Structure, planned SAR exploration, potency, and selectivity of M ₅ PAM 3.2 (VU0238429)	73
3.4 Structures and potencies of previously studied replacements for the 3-keto moiety of the isatin chemical scaffold	74
3.5 Comparison of the single point (30 μM) screen results of the tertiary hydroxyl library, analogs 3.10-3.14	77
3.6 Structure, potency, and selectivity of benzamide analog 3.10 (VU0464634).....	78
3.7 Structure of 3.18 (CID2145491), discovered in HTS of MLPCN screening deck ...	81
3.8 Structure of 3.2 (VU0238429) and the proposed structure resulting from the juxtaposition of structural elements from HTS lead compound 3.18	81
3.9 Comparison of the single point (30 μM) screen results of the isatin matrix library, analogs 3.18, 3.21-3.48	82
3.10 Potency and selectivity of compound 3.39 (VU0467903) at all human and rat mAChR subtypes.....	89
3.11 ACh CRC fold-shifts of compound 3.39 (VU0467903) at hM ₅ and rM ₅	90
3.12 [³ H]-NMS competition binding assay with 3.39 (VU0467903, ML326) in an hM ₅ membrane preparation	91
3.13 Comparison of the single point (30 μM) screen results of the tertiary hydroxyl library, analogs 3.50-3.56	95
3.14 Summary and comparison of the structure, potency, and SAR found around the first M ₅ -preferring PAM 3.2 (VU0238429, ML129) that led to the discovery of the novel, sub-micromolar M ₅ PAM 3.39 (VU0467903, ML326).....	100

Chapter IV

Figure	Page
4.1 Structure, planned SAR exploration, potency, and selectivity of HTS hit compound 4.1 (VU0472882).....	104
4.2 ACh CRC fold shifts of compound 4.1 (VU0472882) at hM ₅ and rM ₅	105
4.3 Comparison of single point (30 μM) screen results of the sulfonamide library, analogs 4.5-4.66	107
4.4 Potency and selectivity of analogs 4.47 (VU0475661) and 4.50 (VU0475778)	116
4.5 ACh CRC fold shifts of compound 4.47 (VU0475661) at hM ₅ and rM ₅	117
4.6 ACh CRC fold shifts of compound 4.50 (VU0475778) at hM ₅ and rM ₅	118
4.7 A) CRCs comparing activities of 4.73 (VU0475757), and 4.74 (VU0475756) at hM ₅ . B) Potency and selectivity of analog 4.73	120
4.8 ACh CRC fold shifts of compound 4.73 (VU0475757) at hM ₅ and rM ₅	121
4.9 Structure, potency, and selectivity of analog 4.75 (VU0476212).....	123
4.10 ACh CRC fold shifts of compound 4.75 (VU0476212) at hM ₅ and rM ₅	124
4.11 Results of metabolite identification following incubation of 4.75 (VU0476212) with rat hepatic microsomes and NADPH.....	126
4.12 Structures of inactive analogs from the constrained <i>N</i> -alkyl library, analogs 4.119-4.125	133
4.13 Comparison of single point (10 μM) screen results of the benzyl library, analogs 4.127-4.151	136
4.14 Structure, potency, and selectivity of analog 4.136 (VU0479111).....	141
4.15 ACh CRC fold shifts of compound 4.136 (VU0479111) at hM ₅ and rM ₅	141
4.16 Potency and selectivity of compound 4.161 (VU0481443) at all human and rat mAChR subtypes.....	146
4.17 ACh CRC fold shifts of compound 4.161 (VU0481443) at hM ₅ and rM ₅	147

4.18	[³ H]-NMS competition binding assay with 4.161 (VU0481443, ML380) in an hM ₅ membrane preparation	150
4.19	Results of metabolite identification following incubation of analog 4.196 (VU0549968) with rat hepatic microsomes and NADPH.....	158
4.20	Summary and comparison of the structure, potency, and SAR found around the non-isatin M ₅ PAM HTS lead 4.1 (VU0472882) that led to the discovery of the novel, sub-micromolar, non-isatin M ₅ -preferring PAM 4.161 (VU0481443, ML380)	159

Chapter V

Figure	Page	
5.1	Structure, planned SAR exploration, potency, and selectivity of HTS hit compound 5.1 (VU0352221).....	165
5.2	Comparison of single point (10 μM) screen results of the benzamide library, analogs 5.3-5.41	166
5.3	Structure, potency, and selectivity of benzamide analog 5.14 (VU0478141).....	174
5.4	Comparison of single point (10 μM) screen results of the amide library, analogs 5.42-5.52	176
5.5	Comparison of single point (10 μM) screen results of the core library, analogs 5.53-5.64	180
5.6	Comparison of single point (10 μM) screen results of the 9b-phenyl matrix library, analogs 5.70-5.96	184
5.7	Structure, potency, and selectivity of benzamide analog compound 5.78 (VU0478333)	192
5.8	(A) CRCs comparing activities of 5.78 (VU0478333), 5.97 (VU0483253), and 5.98 (VU0483252). (B) Crystal structure of the isolated active (–)-enantiomer of 5.97 , revealing its (<i>S</i>)-stereochemistry C) Structures of 5.78 , 5.97 , and 5.98	194
5.9	Potency and selectivity of compound 5.97 (VU0483253) at all human and rat mAChR subtypes.....	195
5.10	A) [³ H]-NMS competition binding assay with 5.97 (VU0483253, ML375) in an hM ₅ membrane preparation. B) [³ H]-NMS dissociation kinetics assay with 5.97 in an hM ₅ membrane preparation	197

5.11 Comparison of single point (10 μ M) screen results of the 6-membered aminal core library, analogs 5.99-5.109	204
5.12 Comparison of single point (10 μ M) screen results of the pyridyl core library, analogs 5.112-5.122	207
5.13 Comparison of single point (10 μ M) screen results of the benzamide library, analogs 5.123-5.132	211
5.14 Comparison of single point (10 μ M) screen results of the 9b-4-methoxyphenyl library, analogs 5.134-5.146	216
5.15 Summary and comparison of the structure, potency, and SAR surrounding the M ₅ antagonist HTS lead 5.1 (VU0352221) that led to the discovery of the first sub-micromolar, M ₅ -selective NAM 5.97 (VU0483253, ML375).....	221

Chapter VI

Figure	Page
6.1 Structure, planned SAR exploration, potency, and selectivity of HTS hit compound 6.1 (VU0480131).....	227
6.2 [³ H]-NMS competition binding assay with 6.1 (VU0480131) in an hM ₅ membrane preparation.....	228
6.3 Comparison of single point (10 μ M) screen results of the amide region library, analogs 6.4-6.16	229
6.4 Comparison of single point (10 μ M) screen results of the aryl ether library, compounds 6.19-6.41	233
6.5 Comparison of single point (10 μ M) screen results of the amine and amide linker library, analogs 6.47-6.59	240
6.6 Comparison of single point (10 μ M) screen results of the secondary amide linker library, analogs 6.66-6.77	244
6.7 A) CRCs comparing activities of HTS lead 6.1 (VU0480131), 6.95 (VU0487996), and 6.96 (VU0488130). B) Structures of 6.1 , 6.95 , and 6.96	249
6.8 Potency and selectivity of compound 6.96 (VU0488130, ML381) at all human and rat mAChR subtypes.....	250

6.9	[³ H]-NMS competition binding assay with 6.96 (VU0488130, ML381) in an hM ₅ membrane preparation	251
6.10	Metabolite identification results for 6.96 (VU0488130, ML381) in rat and human	256
6.11	Summary and comparison of the structure, potency, and SAR surrounding the M ₅ antagonist HTS lead 6.1 (VU0480131) that led to the discovery of the first sub-micromolar, M ₅ -selective orthosteric antagonist 6.96 (VU0488130, ML381)	258

LIST OF SCHEMES

Chapter III

Scheme	Page
3.1 Synthesis and activity of compound 3.9 (VU0462442)	75
3.2 Copper-mediated synthesis of tertiary hydroxyl library compounds 3.10 and 3.11	76
3.3 Brønsted acid catalyzed synthesis of picolines to form homologated tertiary hydroxyl library compounds 3.12-3.14	76
3.4 Synthetic pathway to spiro-oxetane isatin carbonyl analog 3.17 (VU0467863)	80
3.5 Matrix library synthesis of analogs 3.18, 3.21-3.48	82
3.6 Library synthesis of tertiary hydroxyl isatin analogs 3.50-3.56	94
3.7 Structure and synthesis of spiro-dioxolane analog 3.57 (VU0472603)	97
3.8 Structure and synthesis of spiro-pyrrolidine analog 3.62 (VU0472720)	97

Chapter IV

Scheme	Page
4.1 Synthesis of HTS lead compound 4.1 (VU0472882)	103
4.2 Synthetic scheme for sulfonamide library analogs 4.6-4.66 from intermediate 4.5	106
4.3 Synthesis of benzylic methyl analogs (<i>R</i>)- 4.73 and (<i>S</i>)- 4.74	119
4.4 Synthetic scheme for sulfonamide library analogs 4.75-4.81 from intermediate 4.71	122
4.5 Synthesis of 4.82 (VU0485582), the primary metabolite of 4.75 (VU0476212), from intermediate 4.67	126
4.6 Synthesis and activity of deuterated analog 4.86 (VU0477898) from intermediate 4.67	128

4.7	Synthesis of bisamide analog 4.87 (VU0475726) from intermediate 4.5	129
4.8	Synthesis of bissulfonamide analogs 4.92-4.94	130
4.9	Synthesis of reverse amide analog 4.99 (VU0473996).....	130
4.10	Synthesis of benzamide analogs 4.104-4.109	131
4.11	Synthesis of acetamide analogs 4.113-4.118	132
4.12	General synthesis of libraries constraining <i>N</i> -alkyl to benzyl moiety, analogs 4.119-4.125	133
4.13	General synthesis of benzyl bromide library compounds 4.127-4.151	135
4.14	Synthesis of combined benzyl region SAR compounds 4.155-4.157	142
4.15	Synthesis of compound 4.161 (VU0481443)	145
4.16	Synthesis of shifted piperidine core analogs 4.170 (VU0475663) and 4.171 (VU0475676)	153
4.17	Synthesis of spirocyclic core compounds 4.178 (VU0473644) and 4.179 (VU0482981)	154
4.18	Synthesis of central core substitutions, analogs 4.188 (VU0481897) and 4.199 (VU0482092)	155
4.19	General synthesis of <i>N</i> -alkyl library analogs 4.190-4.201	156

Chapter V

Scheme	Page	
5.1	Structure and synthetic pathway for the synthesis of HTS lead 5.1 (VU0352221)	163
5.2	Synthesis of benzamide analogs 5.4-5.41 from intermediate 5.3	166
5.3	Synthesis of des-carbonyl analog 5.42 (VU0478004).....	175
5.4	Synthesis of matrix library exploring substituents in the 9b-phenyl regions, analogs 5.70-5.96	184

5.5	Synthesis of 6-membered aminated core library analogs 5.100-5.109	203
5.6	Synthesis of pyridyl core library analogs 5.112-5.122	207
5.7	Synthesis of benzamide library analogs 5.123-5.132	210
5.8	Synthesis of 9b-phenyl library analogs 5.135-5.146	215

Chapter VI

Scheme	Page	
6.1	Structure and synthetic pathway for the synthesis of compound 6.1 (VU0480131)	226
6.2	Synthesis of amide region library analogs 6.4-6.16	229
6.3	Synthesis of aryl ether library analogs 6.19-6.41	233
6.4	Synthesis of amine and amide linker library analogs 6.47-6.59	239
6.5	Synthesis of secondary amide linker library analogs 6.66-6.77	243
6.6	Synthesis of core substitution analogs 6.85 (VU0483210) and 6.86 (VU0483109)	247
6.7	Synthesis of single enantiomers of HTS lead 6.1 , analogs (<i>R</i>) - 6.95 (VU0487996) and (<i>S</i>) - 6.96 (VU0488130).....	248

LIST OF ABBREVIATIONS

°C	Degrees Celsius
[³ H]-NMS	[³ H]- <i>N</i> -methylscopolamine
7TM	Seven-transmembrane domain
μw	Microwave radiation
AC	Adenylyl cyclase
Acetyl-CoA	Acetyl-coenzyme A
ACh	Acetylcholine
AChE	Acetylcholinesterase
ACN	Acetonitrile
AD	Alzheimer's disease
APCI	Atmospheric-pressure chemical ionization
APPI	Atmospheric-pressure photoionization
ATCM	Allosteric ternary complex model
BBB	Blood-brain barrier
Boc	<i>tert</i> -Butyloxycarbonyl
CA3	Cornu ammonis region 3
cAMP	Cyclic adenosine monophosphate
cDNA	Complementary deoxyribonucleic acid
ChAT	Choline acetyltransferase
CHO	Chinese hamster ovary
ChT	High-affinity choline transporter

CNS	Central nervous system
CRC	Concentration response curve
cyno	Cynomolgus monkey
D ₂	Dopamine D ₂ receptor
DA	Dopamine
DABCO	1,4-diazabicyclo[2.2.2]octane
DAG	Diacyl glycerol
DCE	Dichloroethane
DCM	Dichloromethane
DIAD	Diisopropyl azodicarboxylate
DIPEA	Diisopropylethylamine
DMPK	Drug metabolism and pharmacokinetics
DMSO	Dimethylsulfoxide
DPBS	Dulbecco's phosphate buffered saline
EC _{20/50/80}	Effective concentration required for 20/50/80% excitation
EDC	1-Ethyl-3-(3-dimethylaminopropyl)carbodiimide
ee	Enantiomeric excess
ESI	Electrospray ionization
EtOAc	Ethyl acetate
GDP	Guanosine diphosphate
GPCR	G protein-coupled receptor
GTP	Guanosine triphosphate
HATU	1-[Bis(dimethylamino)methylene]-1 <i>H</i> -1,2,3-triazolo[4,5-

b]pyridinium 3-oxid hexafluorophosphate

hM ₁₋₅	Human muscarinic acetylcholine receptor subtype 1 through 5
HOBt	Hydroxybenzotriazole
HPLC	High-performance liquid chromatography
HRMS	High resolution mass spectrometry
HTS	High-throughput screen(ing)
IC ₅₀	Effective concentration required for 50% inhibition
IP	Intraperitoneal
IP ₃	Inositol 1,4,5-triphosphate
IV	Intravenous(ly)
K_A/K_B	Equilibrium dissociation constant
K_i	Equilibrium dissociation constant from competition binding
K_p	Brain:plasma partition coefficient
$K_{p,uu}$	Unbound brain:plasma partition coefficient
LC/MS	Liquid chromatography/mass spectrometry
LDA	Lithium diisopropylamide
LDT	Laterodorsal tegmental nucleus
M ₁₋₅	Muscarinic acetylcholine receptor subtype 1 through 5
M ₅ ^{-/-}	M ₅ knockout
M	Molar
mAChR	Muscarinic acetylcholine receptor
MLSCN	Molecular libraries screening center network
MLPCN	Molecular libraries probe center network

MP	Macroporous polystyrene
MRM	Multiple reaction monitoring
mRNA	messenger ribonucleic acid
Ms	methanesulfonate (mesylate)
NAcc	Nucleus accumbens
nAChR	Nicotinic acetylcholine receptor
NAM	Negative allosteric modulator
NMR	Nuclear magnetic resonance
PAM	Positive allosteric modulator
PBL	Plasma-brain level
PBS	Phosphate buffered saline
PCR	Polymerase chain reaction
P-gp	P-glycoprotein
PIP ₂	Phosphatidylinositol 4,5-bisphosphate
PK	Pharmacokinetic
PLC	Phospholipase C
PNS	Peripheral nervous system
PPT	Pedunculo pontine nucleus
<i>p</i> TSA	<i>para</i> -toluenesulfonic acid
RED	Rapid equilibrium dialysis
R _f	Retardation factor
rM ₁₋₅	Rat muscarinic acetylcholine receptor subtype 1 through 5
SAR	Structure-activity relationship(s)

SEM	Standard error of the mean
SNC	Substantia nigra pars compacta
TEA	Triethylamine
Tf	Trifluoromethanesulfonate (triflate)
THF	Tetrahydrofuran
TLC	Thin-layer chromatography
TOF	Time of flight
UV	Ultraviolet
VACHT	Vesicular acetylcholine transporter
VHTSC	Vanderbilt high-throughput screening center
VTA	Ventral tegmental area
VU	Vanderbilt University

Chapter I

INTRODUCTION

The M₅ muscarinic acetylcholine receptor

The cholinergic system and the neurotransmitter acetylcholine

The M₅ muscarinic acetylcholine receptor (M₅) is a component of the cholinergic nervous system. The cholinergic system is a collection of neurons that employ the neurotransmitter acetylcholine (ACh) to convey signals within both the central nervous system (CNS) and the peripheral nervous system (PNS). Within the PNS, the cholinergic system encompasses the preganglionic neurons of the sympathetic nervous system, the pre- and post-ganglionic neurons of the parasympathetic nervous system, and the somatic nervous system¹⁻³. Within the CNS, cholinergic neurons are concentrated in cell groups located in the basal forebrain, midbrain, and hindbrain where they control and regulate a number of essential functions including cognition, sleep/wake cycles, reward-seeking behavior, motor control, and thermoregulation¹⁻³.

The neurotransmitter ACh is a polyatomic organic cation derived from dietary choline. ACh is biosynthesized when choline is taken into a neuron by the high-affinity choline transporter (ChT) whereupon the enzyme choline acetyltransferase (ChAT) catalyzes the transfer of an acetyl group from acetyl-CoA to choline (**Figure 1.1**)^{1,2}. The neurotransmitter is then concentrated in synaptic vesicles by the vesicular acetylcholine transporter (VAChT) where it awaits a release into the cholinergic synapse^{1,2}. Once in

the synapse ACh is free to bind to ACh receptors, and this activity is attenuated by the hydrolase acetylcholinesterase (AChE) which rapidly degrades ACh by hydrolyzing it to choline and acetic acid. Following hydrolysis, choline may be reabsorbed by the ChT to begin the synthetic cycle anew^{1,2}.

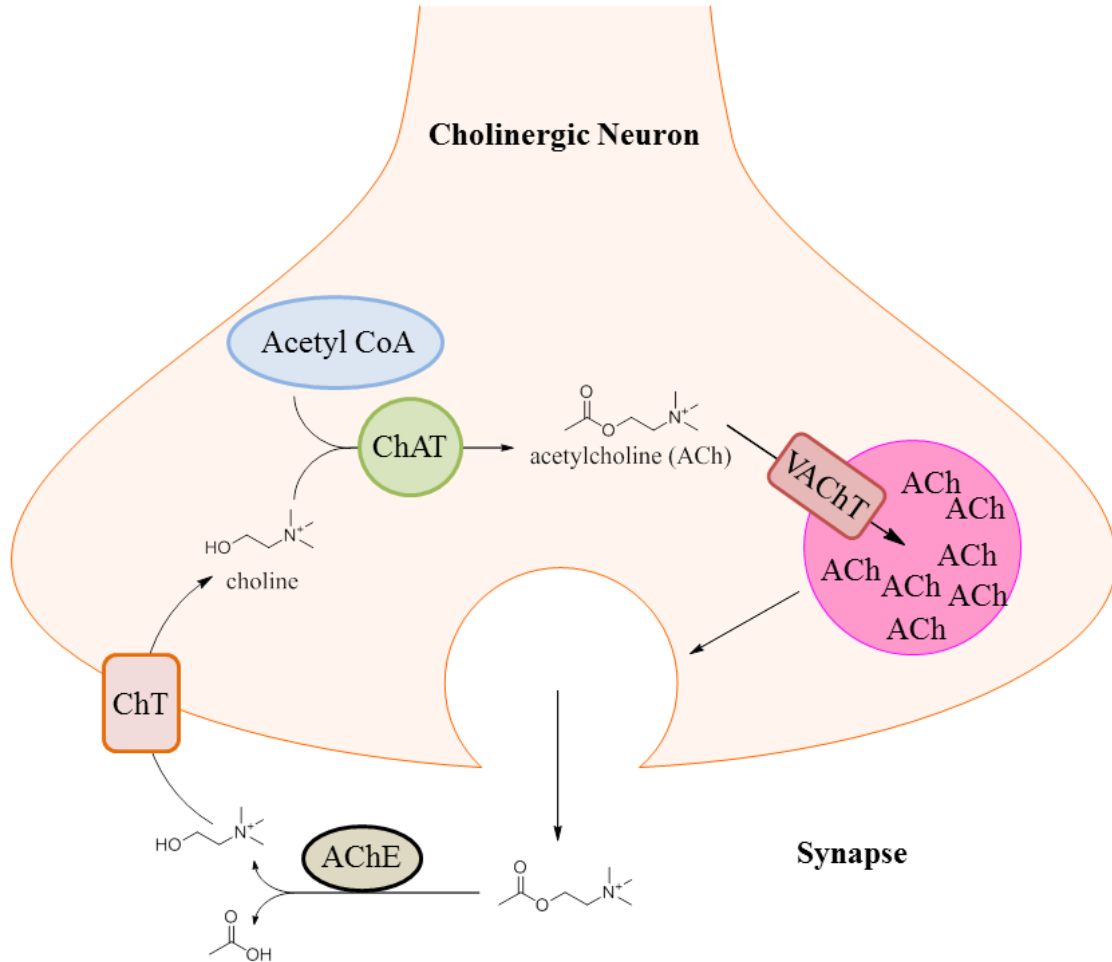


Figure 1.1. Illustration of acetylcholine biosynthesis at the cholinergic synapse. Choline is taken up by the neuron via the high-affinity choline transporter (ChT) where it is acetylated by choline acetyltransferase (ChAT) utilizing acetate from acetyl coenzyme A (Acetyl CoA) to form acetylcholine (ACh). ACh is concentrated in synaptic vesicles by the vesicular acetylcholine transporter (VACHT) until it is released into the synapse where it may be degraded by acetylcholinesterase (AChE).

ACh acts as the endogenous agonist to two classes of ACh receptors. One class, the nicotinic acetylcholine receptors (nAChRs), are pentameric, ligand-gated ion channels found in neuromuscular junctions, the CNS, and the autonomic ganglia where they mediate the ionotropic signaling of ACh^{1,3}. The other class, and the subject of this dissertation, is the muscarinic acetylcholine receptors (mAChRs). In contrast to the nAChRs, the mAChRs are G protein-coupled receptors (GPCRs) consisting of five subtypes termed M₁ through M₅. The mAChR subtypes are found throughout the CNS and periphery where they mediate the metabotropic functions of ACh^{1,3}.

History and discovery of the muscarinic acetylcholine receptors

It has only been in recent decades that the scientific community has gained an understanding of the detailed structure and pharmacology of the cholinergic system; however, the cholinergic system has been studied with chemical probes since the early days of pharmacology. One of the first examples of this was in 1869, when the pharmacologist Oswald Schmiedeberg first described muscarine, a small molecule alkaloid isolated from the fly agaric mushroom (*Amanita muscaria*; **Figure 1.2**)^{4,5}. In experiments exposing muscarine to frog hearts he noted the compound displayed a potent depressor effect similar to those effects observed upon electrical stimulation of the vagus nerve; furthermore, just as with the effects of the vagus nerve, Schmiedeberg found that the effects of muscarine could be blocked with atropine^{4,5}. In addition to the depressor effect, Schmiedeberg and others observed that muscarine generally produced effects mimicking those seen as a result of stimulating cranial and sacral involuntary nerves (e.g. – pupil constriction, lacrimation, increased salivation, and urinary and fecal

incontinence)^{4,5}. In an effort to elucidate the structure of muscarine, Schmiedeberg synthesized the nitrite ester of choline and, based on his observations that it exhibited many of the same effects as natural muscarine, reported it to be true synthetic muscarine^{5,6}.



Figure 1.2. A) A photograph of the fly agaric mushroom (*Amanita muscaria*) in its natural state⁷. B) The structure of the natural alkaloid muscarine, originally isolated from the extract of the fly agaric.

Sir Henry Dale contradicted this assertion during his study of choline esters in 1914⁸. He observed that Schmiedeberg's synthetic muscarine not only displayed effects associated with muscarine, but also exhibited effects previously attributed to the plant alkaloid nicotine⁸. Furthermore, the muscarinic or nicotinic effects could be selectively blocked using atropine or tubocurarine, respectively (**Figure 1.3**)⁸. Dale noted these dual muscarinic/nicotinic effects were displayed with much greater potency by acetylcholine, a choline ester discovered in and extracted from the ergot fungus, and further study led him to postulate that ACh was likely a naturally-occurring element of the nervous system^{8,9}. Soon thereafter, Otto Loewi's seminal experiments analyzing emissions of the

vagus nerve of frog hearts confirmed that ACh was indeed a chemical transmitter released by the vagus nerve^{5,10}. In this way, ACh was discovered as the first neurotransmitter concomitantly with the revelation that its physiological actions were divided between the two functionally distinct categories of muscarinic and nicotinic. As receptor theory came to the forefront of pharmacology in the following decades, these functional differences were attributed to two receptor classes that became known as the nicotinic and muscarinic acetylcholine receptors.

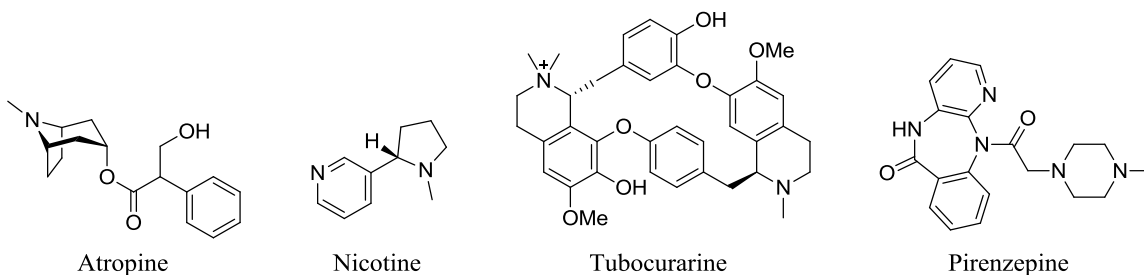


Figure 1.3. Chemical probes central to the discovery and early characterization of the muscarinic acetylcholine receptors.

As more chemical tools became available, further pharmacological scrutiny of the muscarinic effects of ACh revealed functional heterogeneity amongst the mAChRs. The muscarinic antagonist pirenzepine played a major role in this revelation and by measurement of this compound's differing binding affinities and functional selectivity the existence of at least three mAChR subtypes was established (**Figure 1.3**)¹¹⁻¹⁴. By the late 1980s, the number of confirmed mAChR subtypes was expanded as the genes for five distinct human muscarinic receptors was identified and sequenced (*CHRM1* through *CHRM5*)¹⁵⁻²⁰. Since the identification of these five subtypes, the study of mAChRs has

largely focused on the further elucidation of the structure, function, and therapeutic relevance of each mAChR subtype.

Structure and function of M₅

The examination of the human and rat mAChR gene sequences provided valuable insight into mAChR structure and subsequent transfection into stable cell lines provided the means to study the structure and function of the mAChRs in an *in vitro* context. The mAChRs are class A, rhodopsin-like GPCRs²¹. Structurally, the receptors are single subunit proteins consisting of a seven α -helical transmembrane-spanning domain (7TM) with a large cytoplasmic loop connecting the fifth and sixth transmembrane domains (**Figure 1.4**)²¹. The proteins range in size from M₁, with 460 amino acids, to M₃, with 590 amino acids. The human M₅ muscarinic acetylcholine receptor (hM₅) is a protein of 532 amino acids²¹. Across all mAChR subtypes the amino terminal, carboxy terminal, and the cytoplasmic loops were shown to share less sequence identity; however, the 7TM domain is much more conserved. This conserved sequence homology is especially evident in the ACh-binding orthosteric site situated within the 7TM domain²¹. Overall, hM₅ shares 89% sequence identity with the rat M₅ muscarinic receptor (rM₅), making M₅ the least conserved of the mAChR subtypes between the species¹⁹. Among other human mAChR subtypes, hM₅ holds the most in common with hM₃, sharing 73%, 85%, 68%, and 79% sequence identity with human M₄, M₃, M₂, and M₁, respectively^{19,21}.

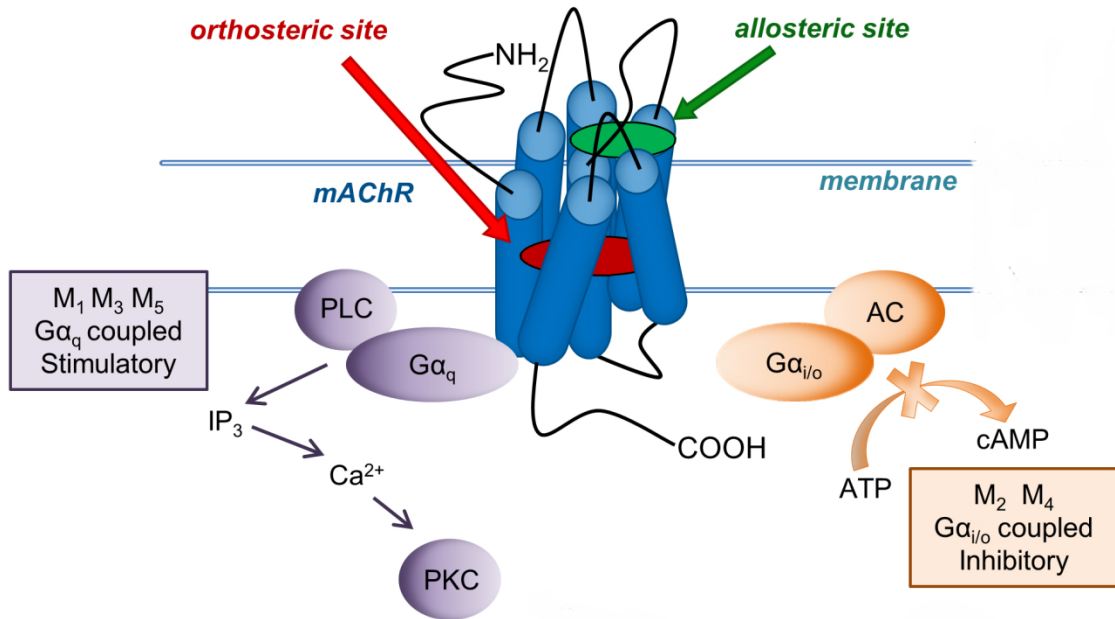


Figure 1.4. Illustrated model of a mAChR depicting the general structure and the two major signaling pathways mediated by $G_{\alpha q}$ and $G_{\alpha i/o}$. Also shown is the putative location of an allosteric site in the extracellular portion of the 7TM domain in relation to the orthosteric site situated within the 7TM.

M_5 is comparable to M_3 and M_1 in its subcellular signaling pathways as well as in its sequence identity. In an active conformation, the M_5 , M_3 , and M_1 receptors selectively bind to G protein heterotrimers possessing the $G_{\alpha q}$ subunit^{22,23}. As the G protein exchanges GTP for GDP, the heterotrimer dissociates and $G_{\alpha q}$ upregulates the activity of phospholipase C (PLC) which in turn cleaves phosphatidylinositol 4,5-bisphosphate (PIP_2) to the second messengers diacyl glycerol (DAG) and inositol 1,4,5-triphosphate (IP_3)^{22,23}. These second messengers subsequently activate multiple, predominantly stimulatory, downstream signaling pathways including calcium (Ca^{2+}) release from intracellular stores and the stimulation of protein kinase C (PKC; **Figure 1.4**)^{22,23}. In contrast, the M_2 and M_4 receptors play a predominantly inhibitory role by selectively binding to the $G_{\alpha i/o}$ subunit, which subsequently downregulates the activity of adenylyl

cyclase (AC), thus lowering cellular concentrations of the secondary messenger cyclic adenosine monophosphate (cAMP)^{22,23}.

Localization of M₅

The localization of the mAChRs has been investigated through a variety of techniques, including *in situ* mRNA hybridization, reverse transcription PCR, autoradiography, immunohistochemistry, immunocytochemistry, and immunoprecipitation. These studies have revealed mAChRs are distributed throughout the cholinergic system, in both the CNS and the periphery and in both neuronal and non-neuronal contexts²¹. Moreover, each mAChR subtype displays a unique expression pattern, with M₁, M₄, and M₅ primarily concentrated in the CNS and M₂ and M₃ located in both the CNS and the periphery²¹.

Compared to other mAChR subtypes, M₅ has a notably restricted expression pattern. Furthermore, the overall expression levels of M₅ are relatively low compared to other subtypes, and it is estimated that M₅ represents less than 2% of the total mAChR receptor load in the CNS²⁴. Of this small percentage, the highest concentration of neuronal M₅ is found within the midbrain. In the midbrain dopamine neurons of the ventral tegmental area (VTA) and the substantia-nigra pars compacta (SNc), M₅ is the only mAChR detected, where it is coexpressed with D₂ dopamine receptors²⁵⁻²⁷. Non-neuronally, M₅ is concentrated on the endothelium of the cerebral vasculature and to a lesser extent throughout other cell types of the neurovascular unit^{28,29}.

Effects of the genetic deletion of M₅

The lack of M₅-selective chemical probes combined with the relatively low abundance of the receptor presents a challenge to the study of M₅. Hence, much of what is known about the physiological relevance of M₅ has been deduced from mouse lines genetically engineered to lack functional M₅ receptors. By examining the phenotypic characteristics of these M₅ “knockout” (M₅^{-/-}) mice in comparison with wild type mice, much has been learned about the function and possible therapeutic relevance of M₅.

Outwardly, M₅^{-/-} mice appear healthy and display no major differences from their wild-type counterparts³⁰. Yet a closer physiological examination reveals that the genetic knockout of M₅ has striking effects on the cerebral vasculature. ACh is known to be a potent dilator of vascular beds, and the presence of M₅ throughout the endothelium of the cerebral vasculature led researchers to hypothesize that M₅ may play a central role in the cerebral vasodilatory process^{28,29,31}. In M₅^{-/-} mice, the ability of ACh to dilate peripheral arteries remains intact; however, ACh has no effect on the dilation of cerebral arteries and arterioles in the M₅^{-/-} mice³⁰. Moreover, the cerebral vasculature is constitutively constricted in M₅^{-/-} mice³². This constitutive constriction of the cerebral vasculature resulted in reduced cerebral blood flow and was observed alongside significant atrophy of the cortical and hippocampal pyramidal neurons³². The impact of this atrophy was reflected in behavioral studies where M₅^{-/-} mice displayed deficits in hippocampal-dependent cognitive tasks³². Additionally, electrophysiological studies of hippocampal brain slices from M₅^{-/-} mice revealed impaired long-term potentiation at the mossy fiber CA3 synapse³². While these studies seem to indicate that the lack of M₅ receptors in the CNS leads to severe impairment of hippocampal circuitry, it is unclear if this evidence

indicates direct involvement of M₅ in the development and maintenance of these brain regions or if deficits in cerebral blood flow throughout development, due to the lack of endothelial M₅, that result in the observed atrophy.

Another brain region notably affected by the genetic deletion of M₅ is the midbrain. In order to investigate of the role of M₅ in the VTA, where it is the sole mAChR subtype present on dopaminergic neurons, researchers examined the pedunculopontine (PPT) and laterodorsal tegmental (LDT) nuclei, both of which provide cholinergic inputs to the VTA. In wild type mice, the electrical stimulation of these nuclei resulted in acute and prolonged dopamine (DA) release in the nucleus accumbens (NAcc); however, this effect was absent in M₅^{-/-} mice³³⁻³⁶. DA release from the dopaminergic projections of the VTA to the NAcc is postulated to play a central role in the rewarding and reinforcing effects of drugs of addiction such as morphine and cocaine^{37,38}. Consistent with these data, M₅^{-/-} mice show impairments in reward seeking behavior. Compared to wild type mice, the rewarding effects of both cocaine and morphine were significantly attenuated in M₅^{-/-} mice, as tested in conditioned place preference and self-administration experiments³⁹⁻⁴¹.

The importance of M₅ in the midbrain extends beyond the VTA. The presence of M₅ as the only mAChR on dopaminergic projections from the SNc suggests that M₅ is also involved in mediating DA release in the dorsal striatum^{25,26}. Investigations using wild-type mouse striatal slice preparations revealed that mAChR agonists are capable of inducing DA release in the striatum; however, this effect was significantly attenuated, though not abolished, in M₅^{-/-} mice^{30,42}. Although these data suggest a pre-synaptic role for M₅ in nigrostriatal dopaminergic signaling, recent electrophysiological studies with

the first M₅-preferring ligand, VU0238429 (*vide infra*), revealed a more complicated picture wherein activation of somatodendritic M₅ receptors in the SNc increases DA release, while activation of terminally-expressed M₅ in the striatum decreases DA release²⁷.

Therapeutic potential of M₅

Taken as a whole, the results from studies of M₅^{-/-} mice strongly suggest that M₅ plays a central role in regulating the dopaminergic signaling of the midbrain as well as the vasodilation of the cerebral vasculature. Based on this information, the discovery of ligands designed to selectively activate or inhibit M₅ would not only lead to continued study and understanding of the role of M₅ in the CNS, but might also shed light on novel therapeutic strategies for a number of CNS diseases and disorders.

The selective activation of M₅ may prove most useful in the cerebral vasculature. The lack of a dilatory response to ACh in the cerebral vasculature of M₅^{-/-} mice as well as the constitutively constricted nature of their cerebral arteries and arterioles presumably indicates that the selective activation of M₅ would result in vasodilation. This hypothesis is further supported by evidence that activation of M₅ is linked to the nitric oxide-mediated vasodilatory pathway^{43,44}. A compound that could induce cerebrovascular vasodilation via the selective activation of M₅ could find therapeutic use in a range of diseases displaying deficiencies in cerebral blood flow, including acute ischemic stroke, cerebrovascular disease, cerebrovascular dementia, and Alzheimer's disease (AD). Fortuitously, such a compound would not be required to penetrate the blood-brain barrier (BBB), thereby avoiding activity at M₅ within the CNS.

On the other hand, a centrally penetrant, selective inhibitor of M₅ could prove useful in modulating the dopaminergic neurons of the midbrain. As outlined above, DA release in the NAcc appears to be regulated by M₅ in the VTA and this pathway facilitates the rewarding and reinforcing effects of substance addiction. Thus, inhibition of M₅ in the midbrain would presumably block the reward pathway activated by drugs of abuse and may represent a novel therapy for the treatment of drug addiction. Interestingly, this hypothesis is further supported by a study of a M₅ single-nucleotide polymorphism (SNP) in Australians of European ancestry. Of the 815 subjects analyzed, 19% carried an M₅ SNP that conferred an addictive phenotype characterized by increased tobacco use and a heightened propensity for cannabis dependence⁴⁵. Thus, in addition to evidence of involvement in addiction mechanisms in M₅^{-/-} mouse studies, M₅ has been directly associated with addictive behavior in humans and represents a worthwhile target for possible novel therapies for treating substance abuse.

As of yet there have been no notable drug discovery efforts to elucidate the therapeutic value of selectively activating or inhibiting M₅; however, targeting of mAChRs with small molecules for therapeutic benefit is not without precedent. For instance, deadly nightshade (*Atropa belladonna*) has been used since antiquity to treat various maladies, including opiate addiction^{46,47}. It is now known that the active compounds in nightshade include the non-selective mAChR antagonists scopolamine, hyoscyamine, and atropine⁴⁶. Unfortunately, the severe side effects of these compounds limit their usage to a few specialized circumstances⁴⁷. More recently, the mAChR agonist xanomeline was studied for use in the treatment of schizophrenia and the psychosis-like symptoms of Alzheimer's disease. Although pre-clinical and clinical studies

demonstrated efficacy, the compound was plagued by complications resulting from its severe side-effects, believed to be mediated via peripheral M₂/M₃ activation⁴⁸.

While these examples demonstrate the clear possibility for therapeutic benefits from targeting mAChRs, they also highlight that classical mAChR ligands often cause side effects that diminish their therapeutic value. The source of this limitation is the fact that the effects of classical mAChR ligands are mediated via interaction with the orthosteric binding site. As described above, the orthosteric site of mAChRs is highly conserved across the subtypes. Consequently, orthosteric mAChR ligands often have undesirable activity at multiple mAChR subtypes. Most often, the aforementioned negative side effects are the result of activation of peripheral M₂ and/or M₃ and may include bradycardia, salivation, lachrymation, sweating, and urinary and fecal incontinence^{49,50}. As a result of this challenge, recent years have seen an increase in the research of small molecules targeting mAChR allosteric sites in order to achieve unprecedented mAChR subtype selectivity while also gaining new understanding of allosteric modes of pharmacology in mAChRs.

Allosteric modulation of the M₅ muscarinic acetylcholine receptor

Allosteric modulation of mAChRs

An allosteric site is a ligand binding site on a receptor that is topographically distinct from the orthosteric site⁵¹⁻⁵³. The allosteric site is conformationally linked with the orthosteric site; thus the binding of an allosteric ligand can induce conformational changes to the receptor that modify receptor activity by modulating binding affinity

and/or efficacy of an orthosteric ligand for the receptor⁵¹⁻⁵⁴. In essence, the allosteric ligand serves to stabilize a unique conformation of the receptor protein that possesses its own equally unique pharmacology⁵⁴.

In an effort to describe the diverse and complex interactions of GPCRs, orthosteric ligands, and allosteric modulators, multiple mathematical models of varying complexity and detail have been put forth. The most basic of these is the allosteric ternary complex model (ATCM; **Figure 1.5**)⁵⁵. Within the ATCM, the binding of the orthosteric ligand (A) and the allosteric modulator (B) to the receptor (R) is described by several factors. The equilibrium dissociation constants, K_A and K_B , describe the binding of A and B, respectively, to their respective binding sites. In a traditional protein-ligand interaction, these constants may be enough to describe the interaction of the ligands with the receptor, but because the allosteric site is conformationally linked with the orthosteric site, binding of one ligand may affect the binding of the second ligand with positive or negative cooperativity. The magnitude and direction of the bound ligand's effect on the other ligand's binding affinity is described by the cooperativity factor α where $\alpha > 1$ in cases of positive cooperativity, $\alpha < 1$ in cases of negative cooperativity, and $\alpha = 1$ in cases of neutral cooperativity where allosteric binding results in unchanged binding affinity⁵⁵. In this way the ATCM has the capacity to quantitate the effects of one ligand on the second ligand's binding affinity. Similarly, the magnitude and direction of the bound ligand's effect on the second ligand's efficacy is quantitated by the efficacy modulation factor β ⁵⁵.

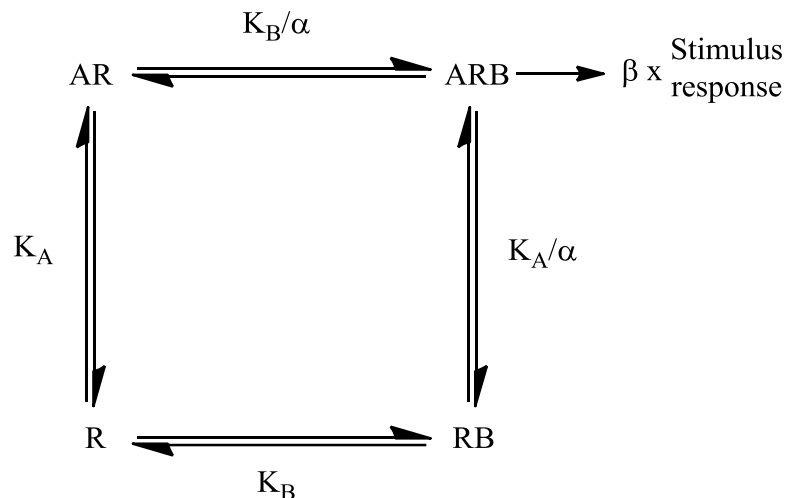


Figure 1.5. The allosteric ternary complex model (ATCM). K_A and K_B are dissociation constants describing the interaction between the orthosteric ligand (A) and the allosteric ligand (B) with the receptor (R). Cooperativity factor α describes the magnitude and direction of one ligand's effect on the binding affinity of the second ligand. Efficacy modulation factor β describes the magnitude and direction of the one ligand's effect on the second ligand's efficacy.

From the standpoint of identifying a mAChR subtype-selective chemical probe, the primary advantage offered by targeting the allosteric site is selectivity. The allosteric sites of the mAChR family are far less conserved compared to the high sequence homology of the orthosteric site. Consequently, targeting the allosteric site can provide a higher degree of subtype selectivity in binding^{53,56,57}. Even if an allosteric ligand lacks binding selectivity, the variation among mAChR allosteric sites might provide functional selectivity based on differences in cooperativity with the allosteric ligand^{53,56,57}. From a therapeutic standpoint, allosteric modulators are preferable to direct orthosteric activation since the temporal and spatial activity of the endogenous ligand is preserved^{53,56,57}. Furthermore, by avoiding the continual stimulation of the orthosteric site, an allosteric modulator may avoid development of tolerance effects often induced by exogenous orthosteric ligands (e.g. – less receptor desensitization or internalization)^{53,56,57}.

Allosteric ligands may manifest a variety of activity profiles. An allosteric ligand that potentiates the receptor response to an orthosteric agonist is termed a positive allosteric modulator (PAM) while one that decreases the receptor response is termed a negative allosteric modulator (NAM)^{53,56,57}. An allosteric ligand that in no way changes the response of the receptor to an orthosteric ligand, but simply occupies the allosteric site to no discernable effect is known as a neutral allosteric ligand (NAL)^{53,56,57}.

In addition to these ‘pure’ allosteric modulators, which possess no intrinsic activity of their own, some allosteric ligands, known as allosteric agonists, have been shown to directly activate the receptor in the absence of an orthosteric ligand^{53,56–58}. Moreover, another category of ligand, ago-allosteric modulators, displays qualities of both orthosteric ligands and allosteric ligands. That is, an ago-allosteric modulator can function as an agonist on its own or as a modulator of the activity of another orthosteric ligand^{53,56–58}. Ago-allosteric modulators are also known as bivalent ligands. In recent years the recognition and study of bivalent ligands has been further enriched by bitopic ligands. Bitopic ligands are compounds typically composed of two distinct pharmacophores covalently linked by a flexible tether region. One of these pharmacophores targets a receptor’s allosteric site while the other targets the orthosteric site^{53,59}. As a result of this unique composition, bitopic ligands display highly versatile binding properties. Current proposed modes of binding reflect how a bitopic ligand could (a) occupy both the allosteric and orthosteric site simultaneously, (b) alternate between occupation of only the orthosteric or the allosteric site, or (c) cooperatively occupy both the allosteric and orthosteric site in conjunction with a second bitopic ligand^{60,61}.

Characterization of allosteric modulators

Due to the complex nature of the pharmacology at the allosteric site, a wide range of functional and binding assays have been designed to characterize allosteric ligands. Cell-based fluorometric functional assays are among the most common assays used in screens to discover novel allosteric modulators⁶². These assays employ stably transfected cell lines expressing the receptor of interest and detect receptor activation via fluorometric measurement of various downstream indicators of receptor activation⁶². For instance, in the study of M₅, which is coupled to the G_{αq} pathway, intracellular Ca²⁺ mobilization is commonly used as a measure of receptor activation.

In order to discover allosteric ligands in a high throughput screening (HTS) scenario, a ‘single point’ assay is generally employed⁶². In this experiment, the test compound is added to the cells at a fixed concentration and allowed to incubate for several minutes. Next, a submaximal concentration of orthosteric ligand (~EC₂₀) is added. In this so-called ‘double-add’ format, PAMs will be observed to potentiate the EC₂₀ (**Figure 1.6**)^{62,63}. Contrastingly, a higher submaximal concentration (~EC₈₀) may be used to detect NAMs or other inhibitors, as these compounds will be observed to attenuate the EC₈₀ response^{62,63}. Some HTS campaigns choose to combine these two formats into a single ‘triple-add’ format in which the test compound is added to the cells, followed by an ~EC₂₀ to test for PAM activity, and finally an ~EC₈₀ to test for inhibitory activity^{62,63}.

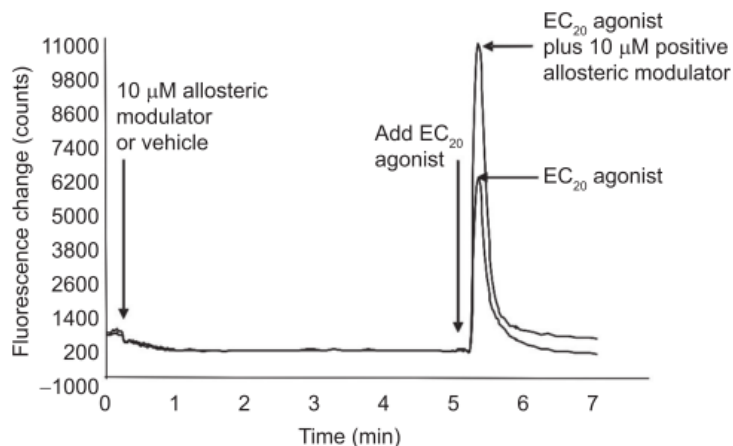


Figure 1.6. Example fluorometric data illustrating the detection of a PAM in a single point, double-add assay format (from Bridges *et al.*, 2008⁶³).

Once an allosteric modulator has been identified, multiple secondary assays will be carried out to further characterize a compound's activity and selectivity. To determine the EC_{50} of a PAM (or the IC_{50} in the case of a NAM/inhibitor) the double-add assay format will again be utilized, but in this instance the effects of multiple concentrations of test compound on the EC_{20} (or EC_{80}) will be measured in order to obtain a full concentration response curve (CRC) for the test compound (**Figure 1.7**)^{62,63}. A related functional assay measures the CRC of an orthosteric ligand in the presence and absence of fixed concentrations of an allosteric modulator. In this way an allosteric modulator's maximum efficacy may be measured in terms of the 'fold shift' induced by the modulator on the orthosteric ligand's EC_{50} (**Figure 1.8**)^{62,63}. The fold shift assay is most commonly used for PAMs. NAMs and other noncompetitive antagonists will depress the CRC of an orthosteric antagonist without shifting the EC_{50} (given a system with no receptor reserve). In general, it is the information provided by these three assays (single point, full CRC,

and fold shift), that supports and guides probe discovery campaigns in identifying, characterizing, and optimizing allosteric modulators.

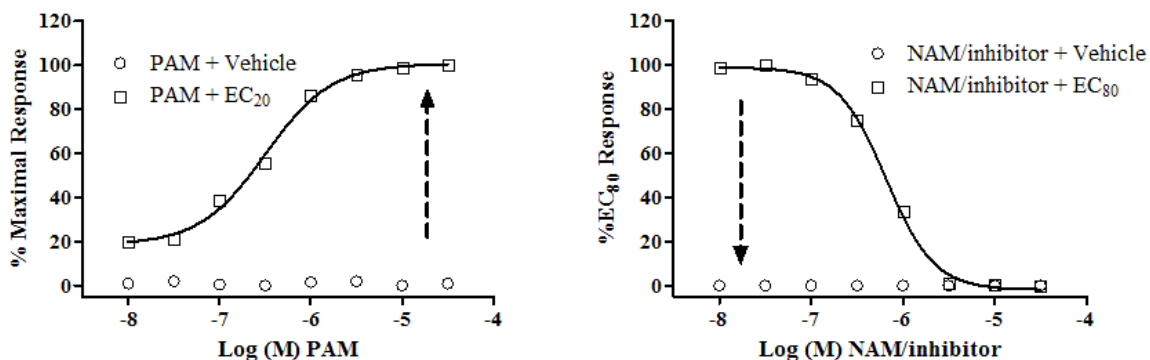


Figure 1.7. Example data demonstrating the modulatory effects of a PAM (left panel) and a NAM/inhibitor (right panel) in full CRC assays in double-add format.

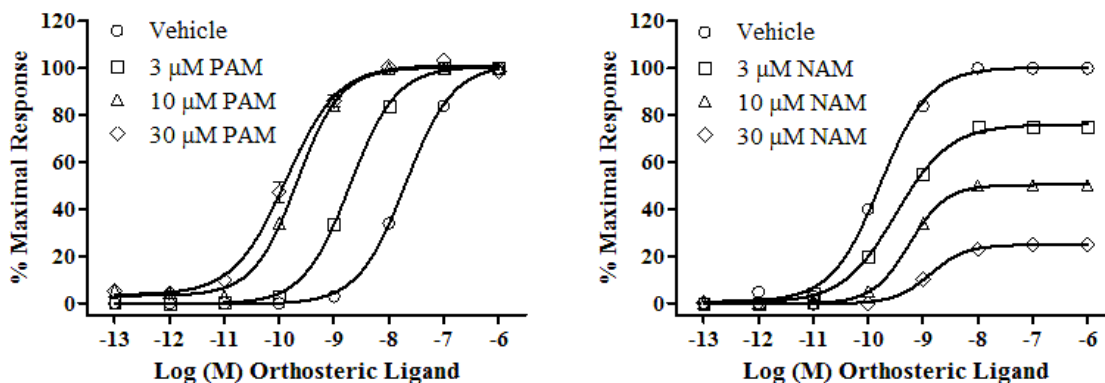


Figure 1.8. Example data demonstrating a PAM inducing a leftward shift in the CRC of an orthosteric ligand in a fold shift assay (left panel) and a NAM depressing the CRC of an orthosteric ligand in a manner characteristic of noncompetitive antagonism (right panel).

In addition to the standard repertoire of functional assays, allosteric modulators can be characterized based on binding assays as well. Binding assays generally employ membrane preparations containing the receptor of interest and use radioligands (ligands labeled with radioactive isotopes) to probe the binding of the allosteric ligand with the

receptor as measured by the radioactive decay of the radioligand. In terms of allosteric modulators, competition binding is a commonly used assay that investigates if a test compound interacts with the orthosteric site. In this assay a known orthosteric radioligand is allowed to label the orthosteric site of a portion of receptors prior to the addition of increasing concentrations of test compound. If the test compound displaces the radioligand in a concentration-dependent manner, this suggests that the test compound binds orthosterically (although pronounced negative cooperativity could conceivably elicit a similar result)⁶².

Binding assays may also be used to examine the kinetics of ligand association and dissociation. This is especially useful in the identification of NAMs. Because NAMs and orthosteric antagonists would presumably produce identical readouts in an initial functional assay (as opposed to a PAM versus an agonist), further confirmation of the mode of action is needed. Although a competition binding assay may reveal a putative NAM to be unable to displace an orthosteric radioligand, this represents negative data (inconclusive with respect to mode of action). In these cases, assays examining the dissociation kinetics of the orthosteric ligand in the presence and absence of the putative NAM may prove useful in revealing the binding cooperativity between the allosteric and the orthosteric ligands⁶².

Allosteric modulators of M₅

To date, the majority of allosteric modulators that are active at M₅ have been non-selective and exhibit allosteric activity at one or more mAChR subtypes besides M₅. Additionally, many of these compounds possess off-target activity outside of the

mAChRs that precludes their use in the detailed study of M_5 . Among this diverse collection of non-selective M_5 allosteric modulators are the neuromuscular blocking agents gallamine and alcuronium, the neurotoxins strychnine and brucine, the antiarrhythmic drug amiodarone, and the symmetrical bis-onium probe compound C₇/3-phth (Figure 1.9)^{64–68}. Clearly, non-selective mAChR allosteric modulators can possess an eclectic spectrum of chemical structures and activity profiles, yet only a single example of an allosteric modulator targeting M_5 specifically had been reported prior to the research contained in this dissertation.

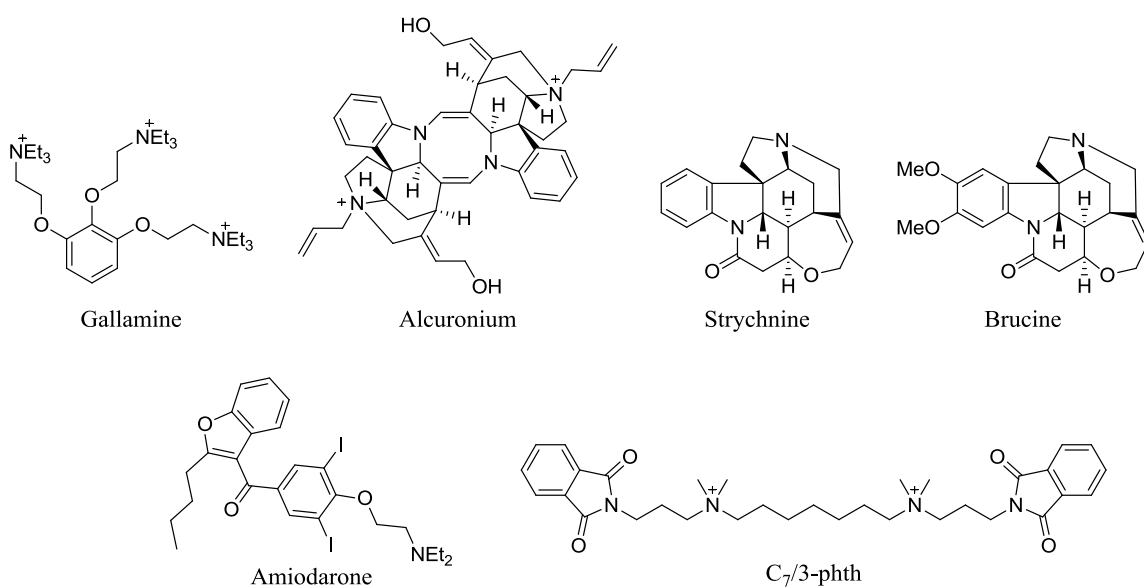


Figure 1.9. Structures of selected non-selective M_5 allosteric modulators.

The discovery of the first M_5 -preferring PAM was the serendipitous result of a drug discovery campaign at Vanderbilt University searching for an M_1 -selective PAM. A functional, cell-based HTS of the VHTSC (~160,000 compounds at the time of screening) searching for M_1 PAMs discovered a number of PAMs with varied mAChR

subtype-selectivity profiles⁶⁹. Most interesting among these was *N-p*-bromobenzyl isatin, VU0119498, which displayed activity as a *pan*-G_{αq}-coupled mAChR PAM (**Figure 1.10**). That is, in functional Ca²⁺ mobilization assays, VU0119498 exhibited PAM activity towards the natively G_{αq}-coupled M₁, M₃, and M₅ receptors with similar potency and efficacy (EC₅₀ = ~4-6 μM, %ACh_{Max} = 66-82), while having no activity at natively G_{αi/o}-coupled M₂ and M₄ receptors, which were expressed in recombinant cells co-transfected with chimeric G_{αq5} to facilitate coupling to the Ca²⁺ mobilization pathway (**Figure 1.10**)⁶⁹. This unique selectivity profile led to the hypothesis that optimization of the SAR around the chemical scaffold of VU0119498 could dial-out M₁ and M₃ activity, producing a highly selective M₅ PAM^{70,71}.

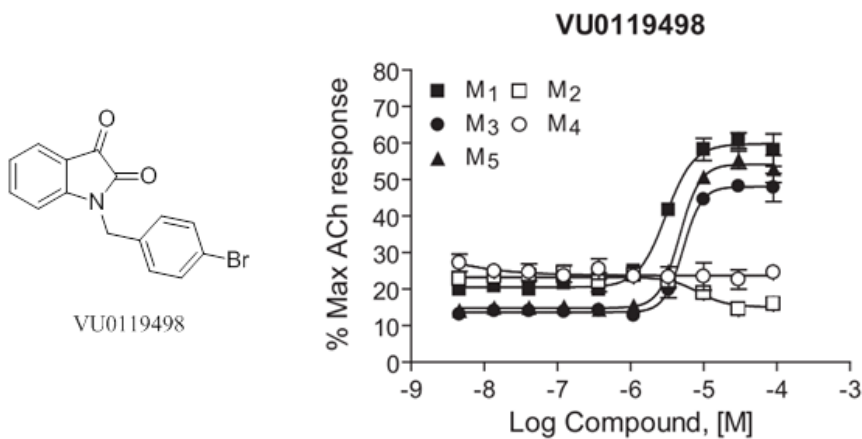


Figure 1.10. Structure, potency, and human mAChR selectivity of VU0119498. Ca²⁺ mobilization assays with hM₁-hM₅ cells were used to obtain CRCs of VU0119498 in the presence of a fixed submaximal (~EC₂₀) concentration of ACh (EC₅₀ values: hM₅ EC₅₀ = 4.1 μM, %ACh_{Max} = 74; hM₃ EC₅₀ = 6.4 μM, %ACh_{Max} = 66; hM₁ EC₅₀ = 6.0 μM, %ACh_{Max} = 82; hM₂, hM₄ EC₅₀ >30 μM. (modified from Marlo *et al.*, 2009⁶⁹).

An optimization campaign employing a strategy of multidimensional iterative parallel synthesis was subsequently initiated. Early in this campaign, a matrix-analog library exploring combinations of substitutions around the isatin benzo ring with

substitutions around the *N*-benzyl region of VU0119498 discovered that the combination of a 5-trifluoromethoxyisatin with an *N*-*p*-methoxybenzyl substitution conferred an unprecedented degree of potency and M₅-selectivity. This compound, VU0238429, displayed PAM activity at hM₅ with an EC₅₀ equal to 1.1 μM and >30-fold subtype selectivity against the remaining mAChR subtypes as measured by *in vitro* Ca²⁺ mobilization assays, earning it the distinction of being the first M₅-preferring PAM (Figure 1.11)^{70,71}.

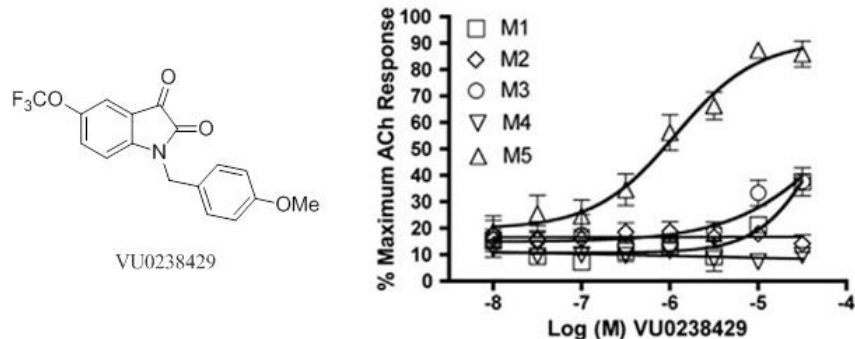


Figure 1.11. Structure, potency, and human mAChR selectivity of VU0238429. Ca²⁺ mobilization assays with hM₁-hM₅ cells were used to obtain CRCs of VU0238429 in the presence of a fixed submaximal (~EC₂₀) concentration of ACh (EC₅₀ values: hM₅ EC₅₀ = 1.1 μM, %ACh_{Max} = 91; hM₁-hM₄ EC₅₀ >30 μM. (modified from Bridges *et al.*, 2010⁷¹).

Unfortunately, upon assessment of *in vivo* pharmacokinetics and brain penetration in rat models it became clear that the compound exhibited poor systemic absorption and brain penetration, limiting the utility of VU0238429 as an *in vivo* tool; however, this impediment has not limited the compound's utility as an *in vitro* probe^{70,71}. Indeed, a recent electrophysiological study of M₅ function in mouse brain slices using VU0238429 found that the M₅ receptor mediates differential effects on nigrostriatal dopaminergic neurons based upon where on the receptor is located on the neuron; moreover, this study

marks the first time M₅ has been demonstrated pharmacologically to be functionally expressed in the dopaminergic neurons of the midbrain²⁷.

This recent electrophysiological data on M₅ represents a landmark discovery that was made possible due to the availability of an M₅-preferring ligand. The interwoven relationship between the availability of practical chemical probes and progress in understanding the pharmacology of the CNS underscores the need for more highly optimized M₅-selective ligands that are suitable not just for *in vitro* use, but for *in vivo* use as well. A novel, highly-selective M₅ PAM or NAM that could serve as an *in vivo* probe would revolutionize the study of M₅ and possibly shed light on the therapeutic relevance of modulating M₅ activity. Ideally, such a compound should have drug-like properties, meaning it should possess high potency, high M₅-selectivity, a satisfactory metabolic and pharmacokinetic (DMPK) profile, and amenable physicochemical properties. The following chapters of this dissertation describe our efforts in the optimization and characterization of four novel, M₅-selective chemical series with the goal of providing new and improved chemical tools for the study of M₅ in the CNS.

Notes on the numbering of figures, schemes, tables, and compounds

In order to present the information contained in the following chapters in a more comprehensible and orderly fashion, the numbering for all figures, tables, schemes, and compounds is uniform and specific to each Chapter. Each category of data follows the arbitrary format of “**Figure/Table/Scheme [Chapter number].[figure/table/scheme number]**” (e.g. **Figure 3.1, Figure 3.2, Figure 3.3...** etc.). Compounds and

intermediates described in each Chapter are numbered in a similar pattern (e.g. compound **3.1**, analog **3.2**, reactants **3.3a**, **3.3b**, and **3.3c**... etc.). This compound numbering system is used in place of full VU number registration codes (e.g. VU0467903) to increase readability, although relevant VU numbers are referenced with compound numbers where appropriate.

Chapter II

MATERIALS AND METHODS

General optimization strategy

The general synthetic approach to all chemical scaffold optimization projects contained herein was based on the strategy of potency optimization via multidimensional iterative parallel synthesis. That is, at the genesis of an optimization effort, a chemical scaffold would be retrosynthetically divided into regions deemed logical and amenable to library synthesis. Next, libraries ranging in size from 5-50+ members, containing analogs considered to be of interest to the exploration of the chemical scaffold's SAR, would be designed around the individual regions. These libraries were then synthesized in parallel and subsequently purified. Following purification, all final compounds would be diluted to a concentration of 10 mM in DMSO and transferred to 4 mL 2D barcoded vials. The compounds were then assigned 7-digit VU numbers (e.g. – VU0481443) and the compound's notebook number(s), structure, and accompanying data were then registered with the Vanderbilt Center for Neuroscience Drug Discovery Chemcart database to aid in storing and tracking compounds.

Once registered, all newly synthesized library analogs would be characterized in one or more *in vitro* pharmacological assays described in the pharmacology section of this Chapter. These primary assays functioned to provide feedback on how the chosen structural changes affected the activity and/or the receptor subtype selectivity of the chemical scaffold. Based on this SAR data, the field of viable structural modifications to

the region under study would be narrowed and another round of library design, synthesis, purification, and cell-based assays could proceed with greater insight into the studied region of the chemical scaffold. In this way, the SAR of individual regions of the chemical scaffolds was characterized over multiple iterative rounds to arrive at one or more optimized structures (**Figure 2.1**).

Frequently the compatibility of regional SAR discoveries would be studied in matrix libraries. These matrix libraries brought together several optimized structures that resulted from regional optimization efforts (e.g. - three optimized structures from Region I combined with three optimized structures from Region II results in 9 matrix library analogs). The SAR data gained from assaying these multidimensional libraries *in vitro* in turn informs on how to proceed with further matrix libraries; thus, the multidimensional iterative parallel synthesis process continues until a lead analog is obtained that fulfills the optimization effort's goals (**Figure 2.1**).

In this way, a multidimensional iterative parallel synthesis effort can rapidly produce a multitude of analogs based around a chemical scaffold, enabling detailed study of all aspects of a chemical scaffold's SAR. The remainder of this Chapter focuses in detail on the procedures employed in the study of the four chemical scaffolds that are the subjects of Chapters III-VI. As the synthesis of each project's chemical scaffold was based on straightforward and reliable synthetic methods, we were confident in limiting full characterization to a select handful of significant and representative compounds. In the case of compounds whose synthesis is not described in detail below, synthetic conditions and yields are summarized in the text, figures, and schemes of their respective Chapters.

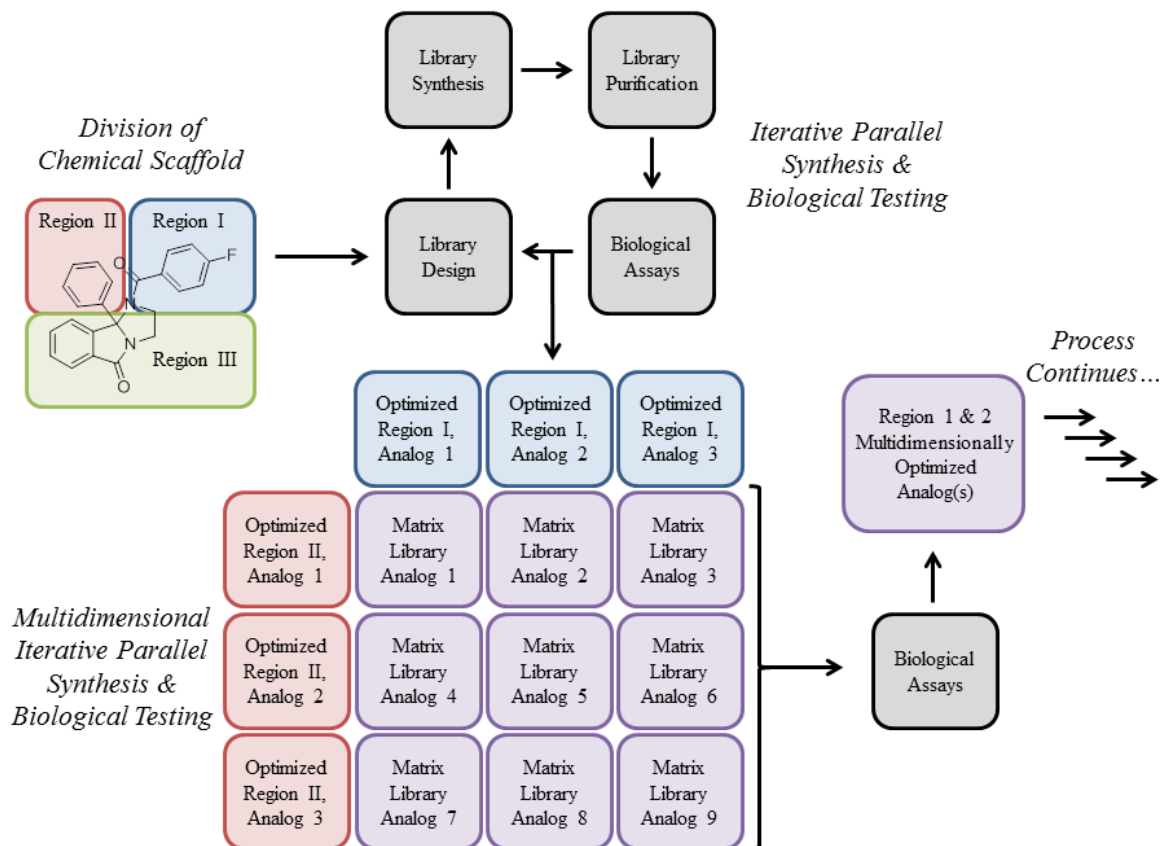


Figure 2.1. Generalized workflow diagram illustrating multidimensional iterative parallel synthesis and testing of analog libraries optimizing multiple regions of a lead chemical series.

Medicinal Chemistry

General synthetic methods and instrumentation

All chemical reactions were carried out in library format on small scale (15-100 mg). A minority of analogs were synthesized as standalone compounds (i.e. - an individual synthesis of a target not connected to a larger library). All reactions were carried out employing standard chemical techniques under inert atmosphere. Solvents used for extraction, washing, and chromatography were HPLC grade. Unless otherwise

noted, all reagents and starting materials were purchased from Aldrich Chemical Company and were used without further purification. Thermally heated reactions were warmed in temperature controlled silicone oil baths. Chilled reactions were cooled to 0 °C with a water and ice bath, and to -78 °C with an acetone and dry ice bath. Reactions cooled to < -78 °C were chilled a Thermo Scientific Neslab cc100 immersion cooler. Microwave-assisted syntheses were conducted using a Biotage Initiator 60 microwave reactor.

Analytical thin layer chromatography was performed on 250 µm silica gel plates from Sorbent Technologies. Analytical HPLC was performed on an Agilent 1200 LCMS with UV detection at 214 nm and 254 nm along with ELSD detection. All NMR spectra were recorded on a 400 MHz Brüker AV-400 instrument or a 500 Mhz Brüker DRX-500 instrument. ¹H chemical shifts are reported as δ values in ppm relative to the residual solvent peak (MeOD = 3.31, CDCl₃ = 7.26). Data are reported as follows: chemical shift, multiplicity (br = broad, s = singlet, d = doublet, t = triplet, q = quartet, quint = quintet, m = multiplet), coupling constant (Hz), and integration. ¹³C chemical shifts are reported as δ values in ppm relative to the residual solvent peak (MeOD = 49.0, CDCl₃ = 77.16). Low resolution mass spectra were obtained on an Agilent 1200 LCMS with electrospray ionization. High resolution mass spectra were recorded on a Waters QToF-API-US plus Acquity system with electrospray ionization. Automated flash column chromatography was performed on a Teledyne ISCO Combiflash Rf system. Preparative purification of library compounds was performed on a Gilson 215 preparative LC system. Chiral separations were performed on a Waters Investigator II SFC utilizing a Lux cellulose-3 column. Optical rotations were acquired on a Jasco P-2000 polarimeter at 23 °C and 589

nm. The specific rotations were calculated according to the equation $[\alpha]_D^{23} = \frac{100\alpha}{l \times c}$ where l is path length in decimeters and c is the concentration in g/100 mL.

Isatin-based M₅ PAM chemical experimentals and characterization

3.39 (VU0467903, ML326). 1-(2-phenoxyethyl)-5-(trifluoromethoxy)indoline-2,3-dione. To a solution of 5-(trifluoromethoxy)isatin (460 mg, 2.0 mmol, 1.0 eq.), K₂CO₃ (550 mg, 4.0 mmol, 2.0 eq.), KI (33 mg, 0.20 mmol, 0.1 eq.) in acetonitrile (20 mL, 0.1 M) in a 20 mL microwave reaction vial was added 2-bromoethylphenyl ether (480 mg, 2.4 mmol, 1.2 eq.). The microwave vial was sealed with a crimp cap and the vessel was heated in a microwave reactor at 160 °C for 10 minutes, with magnetic stirring. After cooling to ambient temperature, the reaction was diluted with DCM (~20 mL) and washed with brine. The organic layer was separated and dried over Na₂SO₄. Solvent was removed under reduced pressure and the crude product was purified via automated silica gel flash chromatography. Product containing fractions were combined and the solvents removed under reduced pressure to obtain 583 mg of pure product as a red-orange powder (83% yield). TLC R_f = 0.79 (hexane/ethyl acetate 1:1, UV-Vis). ¹H NMR (400.1 MHz, CDCl₃) δ (ppm): 7.52-7.46 (m, 2H); 7.31-7.25 (m, 3H); 6.98 (t, J = 7.4 Hz, 1H); 6.82 (d, J = 7.9 Hz, 2H); 4.28 (t, J = 5.0 Hz, 2H); 4.17 (t, J = 5.0 Hz, 2H); ¹³C NMR (125 MHz, CDCl₃) δ (ppm): 182.25, 158.27, 157.93, 150.01, 145.44, 131.02, 129.78, 121.75, 118.32, 114.39, 112.89, 65.94, 40.62. HRMS (TOF, ES⁺) C₁₇H₁₃NO₄F₃ [M+H]⁺ calc. mass 352.0797, found 352.0795.

4.1 (VU0472882). *N*-benzyl-1-((2,3-dihydrobenzo[*b*][1,4]dioxin-6-yl)sulfonyl)-*N*-ethylpiperidine-4-carboxamide. To a solution of *N*-benzyl-*N*-ethylpiperidine-4-carboxamide HCl (20 mg, 0.071 mmol, 1.0 eq.) and DIPEA (74 μ L, 0.213 mmol, 3.0 eq.) in DCM (1 mL, 0.071 M) was added 1,4-benzodioxan-6-sulfonyl chloride (25 mg, 0.107 mmol, 1.5 eq.). The reaction was magnetically stirred at ambient temperature for 2 hours. The reaction was quenched with saturated aqueous NaHCO₃ and the phases were separated. The aqueous layer was extracted with DCM. The combined organic layers were then washed with brine and dried over MgSO₄. Following filtration, the solvent was removed under reduced pressure. Crude product was purified via Gilson preparative LC to obtain 26 mg pure product (84% yield). TLC R_f = 0.64 (hexane/ethyl acetate 1:1). ¹H NMR (1.3:1 rotamer ratio, asterisk denotes minor rotamer peaks, 400.1 MHz, CDCl₃) δ (ppm): 7.38-6.89 (m, 8H); 4.55, 4.48* (s, 2H); 4.35-4.24 (m, 4H); 3.84-3.67 (m, 2H); 3.37*, 3.21 (q, J = 7.1 Hz, 2H); 2.51-2.22 (m, 3H), 2.08-1.88 (m, 2H), 1.84-1.65 (m, 2H), 1.15- 1.02 (m, 3H). ¹³C NMR (1.2:1 rotamer ratio, asterisk denotes minor rotamer peaks, 100.6 MHz, CDCl₃) δ (ppm): 174.17*, 174.05, 147.56, 143.66*, 137.86, 137.07*, 129.08*, 128.82*, 128.71, 128.67*, 127.93, 127.79, 127.43, 126.13*, 121.52, 121.47*, 117.80, 117.38, 117.33*, 64.64, 64.29, 50.34*, 47.83, 45.68, 45.61*, 41.38, 41.15*, 37.98*, 37.78, 28.46, 28.33*, 14.52, 12.76*. LCMS (215 nm) R_T = 1.09 min (>98%); m/z 445 [M+H]⁺. HRMS (TOF, ES+) C₂₃H₂₉N₂O₅S [M+H]⁺ calc. mass 445.1797, found 445.1796.

4.3. *tert*-butyl 4-(benzylcarbamoyl)piperidine-1-carboxylate. To a solution of 1-*tert*-butoxycarbonylpiperidine-4-carboxylic acid (600 mg, 2.62 mmol, 1.0 eq.;

Oakwood company, No. 019200, Lot No. F23F), benzylamine (273 μ L, 3.93 mmol, 1.5 eq.), and DIPEA (898 μ L, 5.24 mmol, 2.0 eq.) in DCM (10 mL, 0.26 M) was added HATU (1.99 g, 5.24 mmol, 2.0 eq.; Oakwood company, No. 023926, Lot No. G02L). The reaction was magnetically stirred at ambient temperature for 4 hours. The reaction was quenched with saturated aqueous NaHCO_3 and the phases were separated. The aqueous layer was extracted with DCM. The combined organic layers were then washed with brine and dried over MgSO_4 . Following filtration, the solvent was removed under reduced pressure. Crude product was purified via automated silica gel flash chromatography. Product containing fractions were combined and the solvents removed under reduced pressure to obtain 834 mg of product (99% yield). TLC R_f = 0.52 (hexane/ethyl acetate 1:1, *p*-anisaldehyde stain). ^1H NMR (~1:1 rotamer ratio, asterisk denotes rotamer peak, 400.1 MHz, CDCl_3) δ (ppm): 7.35-7.22 (m, 5H); 5.83 (br, 1H); 4.44*, 4.42* (s, 2H); 4.20-4.08 (m, 2H); 2.79-2.66 (m, 2H); 2.30-2.20 (m, 1H); 1.87-1.78 (m, 2H); 1.71-1.59 (m, 2H); 1.45 (s, 9H). ^{13}C NMR (100.6 MHz, CDCl_3) δ (ppm): 174.29, 154.78, 138.34, 128.89, 127.87, 127.72, 79.75, 43.65, 43.49, 28.79, 28.56. LCMS (215 nm) R_T = 1.01 min (>98%); m/z 263 $[\text{M}+\text{H}]^+$, minus *t*-butyl. HRMS (TOF, ES+) $\text{C}_{18}\text{H}_{27}\text{N}_2\text{O}_3$ $[\text{M}+\text{H}]^+$ calc. mass 319.2022, found 319.2021.

4.4. *tert*-butyl 4-(benzyl(ethyl)carbamoyl)piperidine-1-carboxylate. To a solution of *tert*-butyl 4-(benzylcarbamoyl)piperidine-1-carboxylate (700 mg, 2.20 mmol, 1.0 eq.) in THF (10 mL, 0.22 M) was added NaO^tBu (254 mg, 2.64 mmol, 1.2 eq.) and 15-crown-5 (524 μ L, 2.64 mmol, 1.2 eq.). The reaction was magnetically stirred at ambient temperature for 30 minutes at which time ethyl iodide (355 μ L, 4.40 mmol, 2.0 eq.) was added to the reaction mixture. The reaction was then magnetically stirred at

ambient temperature for 3 hours. The reaction was quenched with water and the phases were separated. The aqueous layer was extracted with ethyl acetate. The combined organic layers were then washed with brine and dried over MgSO₄. Following filtration, the solvent was removed under reduced pressure. Crude product was purified via automated silica gel flash chromatography. Product containing fractions were combined and the solvents removed under reduced pressure to obtain 596 mg of product (78% yield). TLC $R_f = 0.64$ (hexane/ethyl acetate 1:1, *p*-anisaldehyde stain). ¹H NMR (1.4:1 rotamer ratio, asterisk denotes minor rotamer peaks, 400.1 MHz, CDCl₃) δ (ppm): 7.39-7.11 (m, 5H); 4.58, 4.55* (s, 2H); 4.26-4.02 (m, 2H); 3.40*, 3.28 (q, $J = 7.1$ Hz, 2H); 2.85-2.49 (m, 3H); 1.90-1.55 (m, 4H); 1.45, 1.43* (s, 9H); 1.15, 1.08* (t, $J = 7.1$ Hz, 3H). ¹³C NMR (1.5:1 rotamer ratio, asterisk denotes minor rotamer peaks, 100.6 MHz, CDCl₃) δ (ppm): 174.78*, 174.64, 154.78, 138.02, 137.35*, 129.04*, 128.66, 127.90, 127.74*, 127.34, 126.26*, 79.64, 79.59*, 50.46*, 47.79, 43.38, 41.40, 41.16*, 39.09*, 38.87, 28.88, 28.71*, 28.54, 14.54, 12.77*. LCMS (215 nm) $R_T = 1.14$ min (>98%); m/z 291 [M+H]⁺, minus *t*-butyl. HRMS (TOF, ES+) C₂₀H₃₁N₂O₃ [M+H]⁺ calc. mass 347.2335, found 347.2333.

4.5. *N*-benzyl-*N*-ethylpiperidine-4-carboxamide HCl. *tert*-butyl 4-(benzyl(ethyl)carbamoyl)piperidine-1-carboxylate (500 mg, 1.44 mmol, 1.0 eq.) was dissolved neat in 4N HCl/dioxane. The reaction was magnetically stirred at ambient temperature for 1 hour. Solvent was then removed under reduced pressure to obtain 407 mg of product (quantitative yield). TLC $R_f = 0.01$ (hexane/ethyl acetate 1:1, *p*-anisaldehyde stain). ¹H NMR (1.3:1 rotamer ratio, asterisk denotes minor rotamer peaks, 400.1 MHz, MeOD) δ (ppm): 7.33-7.09 (m, 5H); 4.63*, 4.50 (s, 2H); 3.41-3.25 (m, 4H);

3.21 (quint, $J = 1.6$ Hz, 1H); 3.11-2.84 (m, 3H); 1.97-1.70 (m, 4H), 1.10, 1.00* (t, $J = 7.1$, 3H). ^{13}C NMR (1.5:1 rotamer ratio, asterisk denotes minor rotamer peaks, 100.6 MHz, MeOD) δ (ppm): 175.67*, 175.60, 138.90, 138.65*, 129.99*, 129.64, 128.71*, 128.62, 128.37, 127.68*, 51.79, 44.28, 44.19*, 43.25, 42.84*, 37.30*, 36.93, 26.94, 26.75*, 14.73, 12.83*. LCMS (215 nm) $R_T = 0.62$ min (>98%); m/z 247 $[\text{M}+\text{H}]^+$. HRMS (TOF, ES+) $\text{C}_{15}\text{H}_{23}\text{N}_2\text{O}$ $[\text{M}+\text{H}]^+$ calc. mass 247.1810, found 247.1810.

4.67. (R)-tert-butyl 4-((1-phenylethyl)carbamoyl)piperidine-1-carboxylate. To a solution of 1-*tert*-butoxycarbonylpiperidine-4-carboxylic acid (500 mg, 2.18 mmol, 1.0 eq.; Oakwood company, No. 019200, Lot No. F23F), (*R*)-(+)- α -methylbenzylamine (334 μL , 2.62 mmol, 1.2 eq.), and DIPEA (747 μL , 4.36 mmol, 2.0 eq.) in DCM (10 mL, 0.22 M) was added HATU (1.04 g, 2.73 mmol, 1.25 eq.; Oakwood company, No. 023926, Lot No. G02L). The reaction was magnetically stirred at ambient temperature for 4 hours. The reaction was quenched with saturated aqueous NaHCO_3 and the phases were separated. The aqueous layer was extracted with DCM. The combined organic layers were then washed with brine and dried over MgSO_4 . Following filtration, the solvent was removed under reduced pressure. Crude product was purified via automated silica gel flash chromatography. Product containing fractions were combined and the solvents removed under reduced pressure to obtain 584 mg of product (81% yield). TLC $R_f = 0.52$ (hexane/ethyl acetate 1:1, *p*-anisaldehyde stain). ^1H NMR (~1:1 rotamer ratio, asterisk denotes rotamer peak, 400.1 MHz, CDCl_3) δ (ppm): 7.38-7.22 (m, 5H); 5.70 (br, 1H); 5.12 (quint, $J = 7.2$ Hz, 1H); 4.12 (br, 2H); 2.79-2.64 (m, 2H); 2.27-2.15 (m, 1H); 1.85-1.73 (m, 2H); 1.70-1.54 (m, 2H); 1.49*, 1.47* (s, 3H); 1.45 (s, 9H). ^{13}C NMR (100.6 MHz, CDCl_3) δ (ppm): 173.47, 154.80, 143.24, 128.86, 127.56, 126.22, 79.74, 48.67,

43.51, 28.78, 28.73, 28.56, 21.82. LCMS (215 nm) $R_T = 1.05$ min (>98%); m/z 277 [M+H]⁺, minus *t*-butyl. HRMS (TOF, ES+) C₁₉H₂₈N₂O₃FNa [M+H]⁺ calc. mass 355.1998, found 355.1996. Specific rotation $[\alpha]_D^{23} = 62.9^\circ$ ($c = 0.57$, CHCl₃).

4.69. (R)-tert-butyl 4-(ethyl(1-phenylethyl)carbamoyl)piperidine-1-carboxylate. To a solution of (*R*)-*tert*-butyl 4-((1-phenylethyl)carbamoyl)piperidine-1-carboxylate (100 mg, 0.301 mmol, 1.0 eq.) in THF (2 mL, 0.15 M) was added NaO^tBu (43 mg, 0.451 mmol, 1.5 eq.) and 15-crown-5 (90 μ L, 0.451 mmol, 1.5 eq.). The reaction was magnetically stirred at ambient temperature for 30 minutes at which time ethyl iodide (49 μ L, 0.602 mmol, 2.0 eq.) was added to the reaction mixture. The reaction was then magnetically stirred at ambient temperature for 24 hours. The reaction was quenched with water and the phases were separated. The aqueous layer was extracted with DCM. The combined organic layers were then washed with brine and dried over MgSO₄. Following filtration, the solvent was removed under reduced pressure. Crude product was purified via automated silica gel flash chromatography. Product containing fractions were combined and the solvents removed under reduced pressure to obtain 27 mg of product (25% yield). TLC $R_f = 0.65$ (hexane/ethyl acetate 1:1, *p*-anisaldehyde stain). ¹H NMR (~2:1 rotamer ratio, asterisk denotes minor rotamer peaks, 400.1 MHz, CDCl₃) δ (ppm): 7.40-7.18 (m, 5H); 6.04, 5.13* (q, $J = 6.9$ Hz, 1H); 4.18 (br, 2H); 3.52-2.86 (m, 2H); 2.86-2.48 (m, 3H); 1.95-1.73 (m, 2H); 1.72-1.57 (m, 3H); 1.56-1.49 (m, 2H); 1.48- 1.38* (m, 9H); 1.03*, 0.98 (t, $J = 6.9$, 3H). ¹³C NMR (~2:1 rotamer ratio, asterisk denotes minor rotamer peaks, 100.6 MHz, CDCl₃) δ (ppm): 174.96, 174.46*, 154.82, 141.38, 141.05*, 128.85*, 128.51, 127.65*, 127.51, 127.39, 126.60*, 79.70, 79.64*, 54.98*, 50.73, 39.73, 39.50*, 38.58*, 37.91, 29.12, 29.08*, 28.83*, 28.76, 28.57, 19.20*, 17.27,

16.94, 14.56*. LCMS (215 nm) $R_T = 1.18$ min (>98%); m/z 305 $[M+H]^+$, minus *t*-butyl. HRMS (TOF, ES+) $C_{21}H_{32}N_2O_3Na$ $[M+H]^+$ calc. mass 383.2311, found 383.2309. Specific rotation $[\alpha]_D^{23} = 124.7^\circ$ ($c = 0.61$, $CHCl_3$).

4.71. (*R*)-*N*-ethyl-*N*-(1-phenylethyl)piperidine-4-carboxamide HCl. (*R*)-*tert*-butyl 4-(ethyl(1-phenylethyl)carbamoyl)piperidine-1-carboxylate (347 mg, 0.963 mmol, 1.0 eq.) was dissolved neat in 4N HCl/dioxane. The reaction was magnetically stirred at ambient temperature for 1 hour. Solvent was then removed under reduced pressure to obtain 255 mg of product (89% yield). TLC $R_f = 0.01$ (hexane/ethyl acetate 1:1, *p*-anisaldehyde stain). 1H NMR (1.5:1 rotamer ratio, asterisk denotes minor rotamer peaks, 400.1 MHz, MeOD) δ (ppm): 7.43-7.24 (m, 5H); 5.86, 5.38* (q, $J = 7.1$ Hz, 1H); 3.51-2.93 (m, 7H); 2.08-1.87 (m, 4H); 1.70*, 1.55 (d, $J = 7.0$ Hz, 3H); 0.99, 0.97* (t, $J = 7.1$ Hz, 3H). ^{13}C NMR (1.5:1 rotamer ratio, asterisk denotes minor rotamer peaks, 100.6 MHz, MeOD) δ (ppm): 175.78, 175.29*, 142.02, 129.82*, 129.59, 128.75*, 128.60, 128.45, 127.97*, 56.66*, 53.02, 44.31*, 44.28, 39.58*, 39.41, 37.80, 37.47*, 27.12*, 27.06, 26.99*, 26.88, 19.20*, 17.17, 17.12, 14.52*. LCMS (215 nm) $R_T = 0.74$ min (>98%); m/z 261 $[M+H]^+$. HRMS (TOF, ES+) $C_{16}H_{25}N_2O$ $[M+H]^+$ calc. mass 261.1967, found 261.1968. Specific rotation $[\alpha]_D^{23} = 121.4^\circ$ ($c = 0.65$, $CHCl_3$).

4.75 (VU0476212). (*R*)-1-((1*H*-indazol-5-yl)sulfonyl)-*N*-ethyl-*N*-(1-phenylethyl)piperidine-4-carboxamide. To a solution of (*R*)-*N*-ethyl-*N*-(1-phenylethyl)piperidine-4-carboxamide HCl (20 mg, 0.067 mmol, 1.0 eq.) and DIPEA (23 μ L, 0.134 mmol, 2.0 eq.) in DCM (0.7 mL, 0.1 M) was added 1*H*-indazole-5-sulfonyl chloride (22 mg, 0.101 mmol, 1.5 eq.). The reaction was magnetically stirred at ambient temperature for 2 hours. The reaction was quenched with saturated aqueous $NaHCO_3$ and

the phases were separated. The aqueous layer was extracted with DCM. The combined organic layers were then washed with brine and dried over MgSO₄. Following filtration, the solvent was removed under reduced pressure. Crude product was purified via Gilson preparative LC to obtain 26 mg pure product (88% yield). TLC R_f = 0.23 (hexane/ethyl acetate 1:1). ¹H NMR (1.7:1 rotamer ratio, asterisk denotes minor rotamer peaks, 400.1 MHz, CDCl₃) δ (ppm): 8.32-8.17 (m, 2H); 7.79-7.56 (m, 2H); 7.35-7.10 (m, 5H); 5.99, 5.00* (q, J = 7.1 Hz, 1H); 3.96-3.76 (m, 2H), 3.50-2.80 (m, 2H), 2.57-2.30 (m, 3H); 2.12-1.88 (m, 2H); 1.85-1.69 (m, 2H); 1.60*, 1.47 (d, J = 7.1 Hz, 3H); 0.99*, 0.87 (t, J = 7.1, 3H). ¹³C NMR (1.7:1 rotamer ratio, asterisk denotes minor rotamer peaks, 100.6 MHz, CDCl₃) δ (ppm): 174.47, 173.94*, 141.40, 140.64*, 136.20, 129.41, 129.26*, 128.88*, 128.57, 127.75*, 127.52, 127.49, 126.49, 125.46, 122.80, 110.76, 55.06*, 50.98, 45.71, 38.65*, 38.55, 38.34*, 37.97, 28.66*, 28.41, 19.15*, 17.18, 16.92, 14.51*. LCMS (215 nm) R_T = 1.01 min (>98%); m/z 441 [M+H]⁺. HRMS (TOF, ES+) C₂₃H₂₉N₄O₃S [M+H]⁺ calc. mass 441.1960, found 441.1961. Specific rotation $[\alpha]_D^{23}$ = 65.1° (c = 0.11, CHCl₃).

4.158. *tert*-butyl 4-((2-(trifluoromethyl)benzyl)carbamoyl)piperidine-1-carboxylate. To a solution of 1-*tert*-butoxycarbonylpiperidine-4-carboxylic acid (573 mg, 2.5 mmol, 1.0 eq.; Oakwood company, No. 019200, Lot No. F23F), 2-(trifluoromethyl)benzylamine (421 μL, 3 mmol, 1.2 eq.), and DIPEA (857 μL, 5 mmol, 2.0 eq.) in DCM (12 mL, 0.21 M) was added HATU (1.43 g, 3.75 mmol, 1.5 eq.; Oakwood company, No. 023926, Lot No. G02L). The reaction was magnetically stirred at ambient temperature for 24 hours. The reaction was quenched with saturated aqueous NaHCO₃ and the phases were separated. The aqueous layer was extracted with DCM. The combined organic layers were then washed with brine and dried over MgSO₄.

Following filtration, the solvent was removed under reduced pressure. Crude product was purified via automated silica gel flash chromatography. Product containing fractions were combined and the solvents removed under reduced pressure to obtain 607 mg of product (63% yield). TLC $R_f = 0.55$ (hexane/ethyl acetate 1:1). ^1H NMR (400.1 MHz, CDCl_3) δ (ppm): 7.68-7.62 (m, 1H); 7.55-7.49 (m, 2H); 7.43- 7.34 (m, 1H); 5.85 (br, 1H); 4.67-4.56 (m, 2H); 4.20-4.04 (m, 2H); 2.80-2.64 (m, 2H); 2.31-2.18 (m, 1H); 1.85-1.74 (m, 2H); 1.70-1.55 (m, 2H); 1.44 (s, 9H). ^{13}C NMR (100.6 MHz, CDCl_3) δ (ppm): 174.27, 154.78, 136.76, 132.55, 131.07 (q, $J_{CF} = 1.4$ Hz), 128.04 (q, $J_{CF} = 32.3$ Hz), 127.88, 126.19 (q, $J_{CF} = 5.5$ Hz), 124.59 (q, $J_{CF} = 272.5$ Hz), 79.78, 43.42, 40.29, 40.27, 28.69, 28.56. LCMS (215 nm) $R_T = 1.18$ min (>98%); m/z 330 $[\text{M}+\text{H}]^+$, minus *t*-butyl. HRMS (TOF, ES+) $\text{C}_{19}\text{H}_{25}\text{N}_2\text{O}_3\text{F}_3\text{Na}$ $[\text{M}+\text{H}]^+$ calc. mass 409.1715, found 409.1713.

4.159. *tert*-butyl 4-(ethyl(2-(trifluoromethyl)benzyl)carbamoyl)piperidine-1-carboxylate. To a solution of *tert*-butyl 4-((2-(trifluoromethyl)benzyl)carbamoyl)piperidine-1-carboxylate (394 mg, 1.020 mmol, 1.0 eq.) in THF (6.8 mL, 0.15 M) was added NaO^tBu (147 mg, 1.529 mmol, 1.5 eq.) and 15-crown-5 (405 μL , 2.039 mmol, 2 eq.). The reaction was magnetically stirred at ambient temperature for 30 minutes at which time ethyl iodide (164 μL , 2.0392 mmol, 2.0 eq.) was added to the reaction mixture. The reaction was then magnetically stirred at ambient temperature overnight. The reaction was quenched with brine and the phases were separated. The aqueous layer was extracted with EtOAc. The combined organic layers were then dried over MgSO_4 . Following filtration, the solvent was removed under reduced pressure. Crude product was purified via automated silica gel flash chromatography. Product containing fractions were combined and the solvents removed

under reduced pressure to obtain 350 mg of product (83% yield). TLC $R_f = 0.69$ (hexane/ethyl acetate 1:1, UV-Vis). ^1H NMR (~1:1 rotamer ratio, asterisk denotes rotamer peak, 400.1 MHz, CDCl_3) δ (ppm): 7.75-7.18 (m, 4H); 4.80*, 4.72* (s, 2H); 4.28-4.03 (m, 2H); 3.45*, 3.31* (q, $J = 7.3$ Hz, 2H); 2.87-2.30 (m, 3H); 1.94-1.51 (m, 4H); 1.46*, 1.43* (s, 9H); 1.18*, 1.13* (t, $J = 7.1$ Hz, 3H). ^{13}C NMR (~1:1 rotamer ratio, asterisk denotes rotamer peak, 100.6 MHz, CDCl_3) δ (ppm): 175.15, 154.83*, 154.76*, 136.76*, 136.39*, 132.67*, 132.30*, 128.30 (q, $J_{CF} = 30.7$ Hz), 128.11*, 127.77*, 127.15*, 126.65*, 126.62*, 125.97* (q, $J_{CF} = 5.4$ Hz), 124.44*, 124.50* (q, $J_{CF} = 273.5$ Hz), 79.77*, 79.65*, 46.98*, 44.02*, 43.39; 42.05*, 41.88*, 39.20*, 38.87*, 28.93*, 28.65*, 28.58*, 28.55*, 14.53*, 12.79*. LCMS (215 nM) $R_T = 0.69$ min (>98%); m/z 359 $[\text{M}+\text{H}]^+$, minus *t*-butyl. HRMS (TOF, ES+) $\text{C}_{21}\text{H}_{30}\text{N}_2\text{O}_3\text{F}_3$ $[\text{M}+\text{H}]^+$ calc. mass 415.2209, found 415.2207.

4.160. *N*-ethyl-*N*-(2-(trifluoromethyl)benzyl)piperidine-4-carboxamide HCl.
tert-butyl 4-(ethyl(2-(trifluoromethyl)benzyl)carbamoyl)piperidine-1-carboxylate (297 mg, 0.717 mmol, 1.0 eq.) was dissolved neat in 4N HCl/dioxane. The reaction was magnetically stirred at ambient temperature for 1 hour. Solvent was then removed under reduced pressure to obtain 247 mg of product (98% yield). TLC $R_f = 0.01$ (hexane/ethyl acetate 1:1, *p*-anisaldehyde stain). ^1H NMR (~2.5:1 rotamer ratio, asterisk denotes minor rotamer peaks, 400.1 MHz, MeOD) δ (ppm): 7.82-7.22 (m, 4H); 4.88*, 4.79 (s, 2H); 3.54-3.36 (m, 4H); 3.25-3.11 (m, 2H); 3.01-2.82 (m, 1H); 2.14-1.86 (m, 4H); 1.22, 1.12* (t, $J = 7.2$ Hz, 3H). ^{13}C NMR (2.5:1 rotamer ratio, asterisk denotes minor rotamer peaks, 100.6 MHz, MeOD) δ (ppm): 176.09, 175.85*, 137.17, 137.07*, 134.08*, 133.61, 129.21*, 128.96 (q, $J_{CF} = 30.7$ Hz), 128.77, 128.58, 128.40*, 127.6*, 127.13 (q, $J_{CF} = 5.6$

Hz), 126.10 (q, $J_{CF} = 272.6$ Hz), 126.02*, 45.93*, 45.89, 44.28, 44.12*, 43.83, 42.98*, 37.20*, 36.88, 26.94, 26.70*, 14.62, 12.63*. LCMS (215 nm) $R_T = 0.86$ min (>98%); m/z 315 $[M+H]^+$. HRMS (TOF, ES+) $C_{16}H_{22}N_2OF_3$ $[M+H]^+$ calc. mass 315.1684, found 315.1682.

4.161 (VU0481443, ML380). 1-((1H-indazol-5-yl)sulfonyl)-N-ethyl-N-(2-(trifluoromethyl)benzyl)piperidine-4-carboxamide. To a solution of *N*-ethyl-*N*-(2-(trifluoromethyl)benzyl)piperidine-4-carboxamide HCl (20 mg, 0.063 mmol, 1.0 eq.) and DIPEA (33 μ L, 0.196 mmol, 2.0 eq.) in DCM (0.7 mL, 0.1 M) was added 1*H*-indazole-5-sulfonyl chloride (20.5 mg, 0.095 mmol, 1.5 eq.). The reaction was magnetically stirred at ambient temperature for 2 hours. The reaction was quenched with MeOH and solvent was removed under reduced pressure. Crude product was purified via Gilson preparative LC to obtain 4.2 mg pure product (15.3% yield). TLC $R_f = 0.35$ (hexane/ethyl acetate 1:1). 1H NMR (1.25:1 rotamer ratio, asterisk denotes minor rotamer peak, 400.1 MHz, $CDCl_3$) δ (ppm): 8.31 (s, 1H); 8.25 (m, 1H); 7.78, 7.72* (d, $J = 8.8$ Hz, 1H); 7.68-7.57 (m, 2H); 7.52*, 7.46 (t, $J = 7.6$ Hz, 1H); 7.38*, 7.32 (t, $J = 7.6$ Hz, 1H); 7.21-7.13 (m, 1H); 4.76, 4.64* (s, 2H); 3.95-3.86, 3.85-3.76* (m, 2H); 3.41*, 3.22 (q, $J = 7.2$ Hz, 2H); 2.60-2.46 (m, 2H); 2.37-2.26 (m, 1H); 2.11-1.92 (m, 2H); 1.91-1.81, 1.74-1.65* (m, 2H); 1.16-1.05 (m, 3H). ^{13}C NMR (1.35:1 rotamer ratio, asterisk denotes minor rotamer peak, 100.6 MHz, $CDCl_3$) δ (ppm): 174.70; 141.40, 141.34*; 136.29, 135.77*; 135.95; 132.67*, 132.31; 129.31*, 129.19; 127.94, 127.86*; 127.90 (q, $J = 30.3$ Hz); 126.65 (q, $J_{CF} = 5.3$ Hz); 126.47; 126.26 (q, $J_{CF} = 245$ Hz); 126.04 (q, $J = 5.6$ Hz); 122.81, 122.73*; 122.66; 110.92, 110.89*; 46.94*, 44.23; 45.64, 45.46*; 42.12, 41.87*; 37.96*, 37.68;

28.48, 28.27*; 14.44, 12.67*. LCMS (215 nm) $R_T = 1.11$ min (>98%); m/z 495 [M+H]⁺. HRMS (TOF, ES+) C₂₃H₂₆N₄O₃F₃S [M+H]⁺ calc. mass 495.1678, found 495.1679.

M₅ NAM chemical experimentals and characterization

5.1 (VU0352221), 1-(4-fluorobenzoyl)-9b-phenyl-2,3-dihydro-1H-imidazo[2,1-a]isoindol-5(9bH)-one. To a solution of 9b-phenyl-1, 2, 3, 9b-tetrahydro-5H-imidazo[2,1-a]isoindol-5-one (20 mg, 0.080 mmol, 1.0 eq.; Bionet, 2M-569S, Batch No. 26684) and DIPEA (27 μ L, 0.160 mmol, 2.0 eq.) in DCM (0.8 mL, 0.1 M) was added 4-fluorobenzoyl chloride (14 μ L, 0.120 mmol, 1.5 eq.). The reaction was magnetically stirred at ambient temperature for 2 hours. The reaction was quenched with methanol and the organics were concentrated on a heated air-drying block. Crude product was purified via Gilson preparative LC. Product containing fractions were combined and the solvents removed under reduced pressure to obtain 24.8 mg of product (83% yield). TLC $R_f = 0.60$ (hexane/ethyl acetate 1:1). ¹H NMR (400.1 MHz, CDCl₃) δ (ppm): 8.04 (d, $J = 7.4$ Hz, 1H); 7.89-7.86 (m, 1H); 7.64-7.55 (m, 2H); 7.52-7.46 (m, 2H); 7.40-7.34 (m, 3H); 7.25-7.20 (m, 2H); 7.13-7.06 (m, 2H); 4.35-4.28 (m, 1H); 4.04-3.95 (m, 1H); 3.82-3.76 (m, 1H); 3.36-3.26 (m, 1H). ¹³C NMR (100.6 MHz, CDCl₃) δ (ppm): 172.22, 168.21, 165.12, 162.62, 146.33, 138.11, 133.32, 132.58 (d, $J_{C-F} = 3.2$ Hz), 132.09, 130.29, 129.25, 129.20 (d, $J = 3.4$ Hz), 128.87, 128.81, 126.07, 123.81, 115.86 (d, $J = 22$ Hz), 87.74, 52.37, 39.56. LCMS (214 nM) $R_T = 1.08$ min (>98%); m/z 373 [M+H]⁺. HRMS (TOF, ES+) C₂₃H₁₈N₂O₂F [M+H]⁺ calc. mass 373.1352, found 373.1349.

5.14 (VU0478141). 1-(3,4-difluorobenzoyl)-9b-phenyl-2,3-dihydro-1H-imidazo[2,1-a]isoindol-5(9bH)-one. To a solution of 9b-phenyl-1, 2, 3, 9b-tetrahydro-

5H-imidazo[2,1-a]isoindol-5-one (15 mg, 0.060 mmol, 1.0 eq.; Bionet, 2M-569S, Batch No. 26684) and DIPEA (267 μ L, 0.120 mmol, 2.0 eq.) in DCM (0.6 mL, 0.1 M) was added 3,4-difluorobenzoyl chloride (11 μ L, 0.090 mmol, 1.5 eq.). The reaction was magnetically stirred at ambient temperature for 2 hours. The reaction was quenched with methanol and the organics were concentrated on a heated air-drying block. Crude product was purified via Gilson preparative LC. Product containing fractions were combined and the solvents removed under reduced pressure to obtain 13.4 mg of product (57% yield). TLC R_f = 0.74 (hexane/ethyl acetate 1:1). ^1H NMR (400.1 MHz, CDCl_3) δ (ppm): 8.06-8.00 (m, 1H); 7.91-7.86 (m, 1H); 7.64-7.56 (m, 2H); 7.40-7.31 (m, 4H); 7.25-7.17 (m, 4H); 4.37-4.29 (m, 1H); 4.03-3.94 (m, 1H); 3.83-3.76 (m, 1H); 3.38-3.28 (m, 1H). ^{13}C NMR (100.6 MHz, CDCl_3) δ (ppm): 172.16, 166.82, 151.72 (dd, $J_{\text{C-F}}$ = 253.3 Hz, 12.0 Hz), 150.35 (dd, $J_{\text{C-F}}$ = 251.2 Hz, 13.1 Hz), 146.12, 137.9, 133.37, 133.22 (t, J = 4.6 Hz), 132.05, 130.40, 129.15, 128.98, 128.87, 126.02, 123.89, 123.58 (dd, J = 7.1 Hz, 4.0 Hz), 117.90 (d, 17.8 Hz), 116.80 (d, 18.9 Hz), 87.84, 52.32, 39.55. LCMS (214 nM) R_T = 1.12 min (>98%); m/z 391 $[\text{M}+\text{H}]^+$. HRMS (TOF, ES+) $\text{C}_{23}\text{H}_{17}\text{N}_2\text{O}_2\text{F}_2$ $[\text{M}+\text{H}]^+$ calc. mass 391.1258, found 391.1257.

5.66 (VU006006). 9b-(4-chlorophenyl)-2,3-dihydro-1H-imidazo[2,1-a]isoindol-5(9bH)-one. To a mixture of 2-(4-chlorobenzoyl)benzoic acid (5.21 g, 20.0 mmol, 1 eq.) and ethylenediamine (2.67 mL, 40.0 mmol, 2 eq.) in toluene (30 mL, 0.67 M) was added *p*-toluenesulfonic acid monohydrate (~0.1 g, 3 mol%). A Dean-Stark trap was used to remove water while the mixture was magnetically stirred and heated to reflux for 4 hours. After cooling to ambient temperature, the reaction mixture was dissolved in dichloromethane. The organic layer was washed with a saturated aqueous solution of

sodium bicarbonate and then with brine. Solvent was removed under reduced pressure and the crude product was recrystallized from ethanol to give 2.86 g of pure product (50.2% yield). TLC $R_f = 0.38$ (hexane/ethyl acetate 1:1). ^1H NMR (400.1 MHz, CDCl_3) δ (ppm): 7.81-7.76 (m, 1H); 7.66-7.60 (m, 2H); 7.49-7.44 (m, 2H); 7.34-7.30 (m, 2H); 7.28-7.23 (m, 1H); 3.85-3.77 (m, 1H); 3.70-3.62 (m, 1H); 3.28-3.13 (m, 2H); 2.10-2.02 (m, 1H). ^{13}C NMR (100.6 MHz, CDCl_3) δ (ppm): 172.65, 147.54, 137.74, 134.44, 132.94, 131.79, 130.01, 129.03, 127.91, 124.60, 123.40, 89.25, 50.83, 41.85. LCMS (214 nM) $R_T = 0.837$ min (>98%); m/z 285 $[\text{M}+\text{H}]^+$. HRMS (TOF, ES+) $\text{C}_{16}\text{H}_{14}\text{N}_2\text{OCl}$ $[\text{M}+\text{H}]^+$ calc. mass 285.0795, found 285.0794.

5.67 (VU0331642). 9b-(4-fluorophenyl)-2,3-dihydro-1H-imidazo[2,1-a]isoindol-5(9bH)-one. To a mixture of 2-(4-fluorobenzoyl)benzoic acid (2.44 g, 10.0 mmol, 1 eq.) and ethylenediamine (1.34 mL, 20.0 mmol, 2 eq.) in toluene (15 mL, 0.67 M) was added *p*-toluenesulfonic acid monohydrate (~0.5 g, 3 mol%). A Dean-Stark trap was used to remove water while the mixture was magnetically stirred and heated to reflux for 4 hours. After cooling to ambient temperature, the reaction mixture was dissolved in dichloromethane. The organic layer was washed with a saturated aqueous solution of sodium bicarbonate and then with brine. Solvent was removed under reduced pressure and the crude product was recrystallized from ethanol to give 1.49 g of pure product (55.5% yield). TLC $R_f = 0.40$ (hexane/ethyl acetate 1:1). ^1H NMR (400.1 MHz, CDCl_3) δ (ppm): 7.81-7.75 (m, 1H); 7.70-7.63 (m, 2H); 7.50-7.43 (m, 2H); 7.29-7.24 (m, 1H); 7.06-6.70 (m, 2H); 3.85-3.78 (m, 1H); 3.69-3.62 (m, 1H); 3.28-3.13 (m, 2H); 2.14-1.97 (br, 1H). ^{13}C NMR (100.6 MHz, CDCl_3) δ (ppm): 172.65, 164.18, 161.73, 147.81, 134.80 (d, $J_{\text{C-F}} = 28$ Hz), 132.90, 131.76, 129.92, 128.24 (d, $J = 8.29$ Hz), 124.56, 123.40,

115.69 (d, $J = 21.63$ Hz), 89.29, 50.82, 41.82. LCMS (214 nM) $R_T = 0.766$ min (>98%); m/z 269 $[M+H]^+$. HRMS (TOF, ES+) $C_{16}H_{14}N_2OF$ $[M+H]^+$ calc. mass 269.1090, found 269.1089.

5.68 (VU0478193). 9b-(*p*-tolyl)-2,3-dihydro-1*H*-imidazo[2,1-*a*]isoindol-5(9b*H*)-one. To a mixture of 2-(4-methylbenzoyl)benzoic acid (4.81 g, 20.0 mmol, 1 eq.) and ethylenediamine (2.67 mL, 40.0 mmol, 2 eq.) in toluene (30 mL, 0.67 M) was added *p*-toluenesulfonic acid monohydrate (~0.1 g, 3 mol%). A Dean-Stark trap was used to remove water while the mixture was magnetically stirred and heated to reflux for 4 hours. After cooling to ambient temperature, the reaction mixture was dissolved in dichloromethane. The organic layer was washed with a saturated aqueous solution of sodium bicarbonate and then with brine. Solvent was removed under reduced pressure and the crude product was recrystallized from ethanol to give 2.88 g of pure product (54.5% yield). TLC $R_f = 0.38$ (hexane/ethyl acetate 1:1). 1H NMR (400.1 MHz, $CDCl_3$) δ (ppm): 7.81-7.74 (m, 1H); 7.57 (d, $J = 7.93$ Hz, 2H); 7.48-7.41 (m, 2H); 7.33-7.27 (m, 1H); 7.16 (d, $J = 7.93$ Hz, 2H); 3.86-3.77 (m, 1H); 3.68-3.59 (m, 1H); 3.33-3.13 (m, 2H); 2.34 (s, 3H); 2.04 (br, 1H). ^{13}C NMR (100.6 MHz, $CDCl_3$) δ (ppm): 172.66, 148.14, 138.25, 136.00, 132.77, 131.86, 129.70, 129.54, 126.22, 124.42, 123.43, 89.58, 50.84, 41.76, 21.23. LCMS (214 nM) $R_T = 0.741$ min (>98%); m/z 265 $[M+H]^+$. HRMS (TOF, ES+) $C_{17}H_{17}N_2O$ $[M+H]^+$ calc. mass 265.1341, found 265.1340.

5.76 (VU0326724). 9b-(4-chlorophenyl)-1-(4-fluorobenzoyl)-2,3-dihydro-1*H*-imidazo[2,1-*a*]isoindol-5(9b*H*)-one. To a solution of 9b-(4-chlorophenyl)-2,3-dihydro-1*H*-imidazo[2,1-*a*]isoindol-5(9b*H*)-one (15 mg, 0.053 mmol, 1.0 eq.) and DIPEA (18 μ L, 0.105 mmol, 2.0 eq.) in DCM (0.53 mL, 0.1 M) was added 4-fluorobenzoyl chloride (9.5

μL , 0.079 mmol, 1.5 eq.). The reaction was magnetically stirred at ambient temperature for 2 hours. The reaction was quenched with methanol and the organics were concentrated on a heated air-drying block. Crude product was purified via Gilson preparative LC. Product containing fractions were combined and the solvents removed under reduced pressure to obtain 12.5 mg of product (58.0 % yield). TLC R_f = 0.69 (hexane/ethyl acetate 1:1). ^1H NMR (400.1 MHz, MeOD) δ (ppm): 7.87-7.81 (m, 3H); 7.65-7.54 (m, 2H); 7.45-7.41 (m, 2H); 7.39-7.35 (m, 2H); 7.34-7.31 (m, 1H); 7.24-7.12 (m, 2H); 3.92-3.83 (m, 1H); 3.74-3.66 (m, 1H); 3.54-3.46 (m, 1H); 3.32-3.25 (m, 1H). ^{13}C NMR (100.6 MHz, MeOD) δ (ppm): 170.48, 169.18, 167.45, 164.96, 150.86, 139.49, 135.51, 134.31, 131.79 (d, J_{C-F} = 2.4 Hz), 131.37, 130.90, 130.81, 130.74, 129.80, 129.05, 123.99 (d, J = 5.7 Hz), 116.46, 116.24, 92.45, 40.69, 39.87. LCMS (214 nM) R_T = 1.205 min (>98%); m/z 407 $[\text{M}+\text{H}]^+$. HRMS (TOF, ES+) $\text{C}_{23}\text{H}_{17}\text{N}_2\text{O}_2\text{FCl}$ $[\text{M}+\text{H}]^+$ calc. mass 407.0963, found 407.0964.

5.78 (VU0478333). 9b-(4-chlorophenyl)-1-(3,4-difluorobenzoyl)-2,3-dihydro-1H-imidazo[2,1-a]isoindol-5(9bH)-one. To a solution of 9b-(4-chlorophenyl)-2,3-dihydro-1H-imidazo[2,1-a]isoindol-5(9bH)-one (15 mg, 0.053 mmol, 1.0 eq.) and DIPEA (18 μL , 0.105 mmol, 2.0 eq.) in DCM (0.53 mL, 0.1 M) was added 3,4-difluorobenzoyl chloride (9.9 μL , 0.079 mmol, 1.5 eq.). The reaction was magnetically stirred at ambient temperature for 2 hours. The reaction was quenched with methanol and the organics were concentrated on a heated air-drying block. Crude product was purified via Gilson preparative LC. Product containing fractions were combined and the solvents removed under reduced pressure to obtain 12.0 mg of product (53.3 % yield). TLC R_f = 0.71 (hexane/ethyl acetate 1:1). ^1H NMR (400.1 MHz, CDCl_3) δ (ppm): 8.03-8.00 (m, 1H);

7.90-7.86 (m, 1H); 7.65-7.57 (m, 2H); 7.37-7.31 (m, 3H); 7.25-7.19 (m, 2H); 7.19-7.14 (m, 2H); 4.37-4.31 (m, 1H); 4.02-3.93 (m, 1H); 3.82-3.75 (m, 1H); 3.42-3.25 (m, 1H). ^{13}C NMR (100.6 MHz, CDCl_3) δ (ppm): 172.08, 166.85, 151.87 (dd, $J_{\text{C-F}} = 254$ Hz, 12.4 Hz), 150.34 (dd, $J_{\text{C-F}} = 252$ Hz, 12.9 Hz) 145.77, 136.65, 134.94, 133.56, 132.95 (t, $J = 4.5$ Hz), 131.89, 130.61, 129.06, 128.97, 127.53, 124.04, 123.62 (dd, $J_1 = 6.8$ Hz, 3.9 Hz), 117.94 (d, $J = 17.9$ Hz), 116.3 (d, $J = 18.5$ Hz), 87.37, 52.25, 39.70. LCMS (214 nM) $R_T = 1.189$ min (>98%); m/z 425 $[\text{M}+\text{H}]^+$. HRMS (TOF, ES+) $\text{C}_{23}\text{H}_{17}\text{N}_2\text{O}_2\text{F}_2\text{Cl}$ $[\text{M}+\text{H}]^+$ calc. mass 425.0868, found 425.0869.

5.97 (VU0483253, ML375). (S)-9b-(4-chlorophenyl)-1-(3,4-difluorobenzoyl)-2,3-dihydro-1H-imidazo[2,1-a]isoindol-5(9bH)-one. From **5.78**, the second eluting pure enantiomer was separated via CO_2 supercritical fluid chromatography (Lux cellulose-3 10 x 250 mm column at 40 °C, backpressure regulated at 100 bar, MeOH co-solvent, 10% isocratic prep over 7 minutes at 15 mL/min) and was determined to have an ee of >98% by chiral HPLC analysis (Lux cellulose-3 4.6 x 250 mm column at 40 °C, backpressure regulated at 100 bar, MeOH co-solvent, 5-50% over 7 minutes at 3.5 mL/min). Crystals of pure compound were obtained by allowing a solution of MeOH saturated with pure compound to rest in a scored flask, for 5 hours. An x-ray crystal structure was determined using an Agilent Xcalibur PX II diffractometer employing an Enhance (Cu) X-ray source. ^1H NMR (400.1 MHz, CDCl_3) δ (ppm): 8.04-7.99 (m, 1H); 7.90-7.85 (m, 1H); 7.65-7.56 (m, 2H); 7.38-7.30 (m, 3H); 7.25-7.19 (m, 2H); 7.18-7.14 (m, 2H); 4.38-4.30 (m, 1H); 4.01-3.93 (m, 1H); 3.82-3.75 (m, 1H); 3.34-3.25 (m, 1H). ^{13}C NMR (100.6 MHz, CDCl_3) δ (ppm): 172.07, 166.84, 151.81 (dd, $J_{\text{C-F}} = 254$ Hz, 12.7 Hz), 150.33 (dd, $J_{\text{C-F}} = 252$ Hz, 13 Hz) 145.77, 136.65, 134.94, 133.55, 132.91 (t, $J = 4.8$

Hz), 131.88, 130.61, 129.06, 128.97, 127.53, 124.03, 123.62 (dd, $J = 6.8$ Hz, 4 Hz), 117.94 (d, $J = 17$ Hz), 116.83 (d, $J = 18$ Hz), 87.37, 52.24, 39.70. SFC (214 nM) $R_T = 3.591$ min (>98%). HRMS (TOF, ES+) $C_{23}H_{16}N_2O_2F_2Cl$ $[M+H]^+$ calc. mass 425.0868, found 425.0872. Specific rotation $[\alpha]_D^{23} = -168.6^\circ$ ($c = 0.75$, $CHCl_3$).

5.98 (VU0483252). (R)-9b-(4-chlorophenyl)-1-(3,4-difluorobenzoyl)-2,3-dihydro-1H-imidazo[2,1-*a*]isoindol-5(9bH)-one. From **5.78**, the first eluting pure enantiomer was separated via CO_2 supercritical fluid chromatography (Lux cellulose-3 10 x 250 mm column at 40 °C, backpressure regulated at 100 bar, MeOH co-solvent, 10% isocratic prep over 7 minutes at 15 mL/min) and was determined to have an ee of >98% by chiral HPLC analysis (Lux cellulose-3 4.6 x 250 mm column at 40 °C, backpressure regulated at 100 bar, MeOH co-solvent, 5-50% over 7 minutes at 3.5 mL/min). 1H NMR (400.1 MHz, $CDCl_3$) δ (ppm): 8.03-7.99 (m, 1H); 7.89-7.86 (m, 1H); 7.65-7.57 (m, 2H); 7.37-7.31 (m, 3H); 7.25-7.19 (m, 2H); 7.18-7.14 (m, 2H); 4.38-4.31 (m, 1H); 4.01-3.94 (m, 1H); 3.82-3.75 (m, 1H); 3.34-3.25 (m, 1H). ^{13}C NMR (100.6 MHz, $CDCl_3$) δ (ppm): 172.07, 166.84, 151.80 (dd, $J_{C-F} = 254$ Hz, 12.3 Hz), 150.33 (dd, $J_{C-F} = 252$ Hz, 12.8 Hz) 145.76, 136.65, 134.93, 133.55, 132.91 (t, $J = 4.5$ Hz), 131.88, 130.60, 129.05, 128.97, 127.53, 124.03, 123.63 (dd, $J = 6.7$ Hz, 4 Hz), 117.94 (d, $J = 17.7$ Hz), 116.82 (d, $J = 18.8$ Hz), 87.37, 52.24, 39.70. SFC (214 nM) $R_T = 3.187$ min (>98%). HRMS (TOF, ES+) $C_{23}H_{16}N_2O_2F_2Cl$ $[M+H]^+$ calc. mass 425.0868, found 425.0870. Specific rotation $[\alpha]_D^{23} = +167.2^\circ$ ($c = 0.87$, $CHCl_3$).

5.99 (VU0485459). 10b-(4-chlorophenyl)-1,3,4,10b-tetrahydropyrimido[2,1-*a*]isoindol-6(2H)-one. To a solution of 2-(4-chlorobenzoyl)benzoic acid (4.81 g, 20.0 mmol, 1 eq.) and 1,3-diaminopropane (3.33 mL, 40.0 mmol, 2 eq.) in toluene (30 mL,

0.67 M) was added *p*-toluenesulfonic acid monohydrate (~0.1 g, 3 mol%). A Dean-Stark trap was used to remove water while the mixture was magnetically stirred and heated to reflux for 3 hours. After cooling to ambient temperature, a precipitate was isolated via vacuum filtration. The precipitate was then recrystallized from ethanol to give 3.75 g of pure product (62.8% yield). TLC R_f = 0.48 (hexane/ethyl acetate 1:1). ^1H NMR (400.1 MHz, CDCl_3) δ (ppm): 7.88-7.82 (m, 1H); 7.52 (d, J = 8.6 Hz, 2H); 7.46-7.40 (m, 2H); 7.34 (d, J = 8.8 Hz, 2H); 7.30-7.25 (m, 1H); 4.57-4.50 (m, 1H); 3.11-3.01 (m, 2H); 2.98-2.85 (m, 1H); 1.84-1.67 (m, 1H); 1.59-1.51 (m, 1H). ^{13}C NMR (100.6 MHz, CDCl_3) δ (ppm): 166.64, 148.96, 137.24, 134.26, 132.23, 130.52, 129.54, 129.34, 128.33, 124.07, 122.56, 78.74, 40.81, 36.83, 26.67. LCMS (214 nM) R_T = 0.83 min (>98%); m/z 299 $[\text{M}+\text{H}]^+$. HRMS (TOF, ES+) $\text{C}_{17}\text{H}_{16}\text{N}_2\text{OCl}$ $[\text{M}+\text{H}]^+$ calc. mass 299.0951, found 299.0950.

5.106 (VU0478894). 10b-(4-chlorophenyl)-1-(3,4-difluorobenzoyl)-1,3,4,10b-tetrahydropyrimido[2,1-a]isoindol-6(2H)-one. To a solution of 10b-(4-chlorophenyl)-1,3,4,10b-tetrahydropyrimido[2,1-a]isoindol-6(2H)-one (20 mg, 0.067 mmol, 1.0 eq.) and DIPEA (23 μL , 0.134 mmol, 2.0 eq.) in DCM (0.7 mL, 0.1 M) was added 3,4-difluorobenzoyl chloride (13 μL , 0.101 mmol, 1.5 eq.). The reaction was magnetically stirred at ambient temperature for 2 hours. The reaction was quenched with methanol and the organics were concentrated on a heated air-drying block. Crude product was purified via Gilson preparative LC. Product containing fractions were combined and the solvents removed under reduced pressure to obtain 17.8 mg of product (60.5 % yield). TLC R_f = 0.59 (hexane/ethyl acetate 1:1). ^1H NMR (400.1 MHz, CDCl_3) δ (ppm): 7.95-7.87 (m, 2H); 7.77-7.73 (m, 1H); 7.51-7.43 (m, 2H); 7.40-7.31 (m, 3H); 7.30-7.17 (m, 3H); 4.58-

4.49 (m, 1H); 3.64-3.48 (m, 2H); 3.06-2.96 (m, 1H); 2.01-1.89 (m, 1H); 1.87-1.76 (m, 1H). ^{13}C NMR (100.6 MHz, CDCl_3) δ (ppm): 170.44, 167.66, 152.14 (dd, $J_{\text{C-F}} = 254.7$ Hz, 12.6 Hz), 150.41 (dd, $J_{\text{C-F}} = 251.5$ Hz, 12.6 Hz), 146.37, 136.06, 134.81, 132.81 (t, $J = 4.5$ Hz), 132.14, 130.60, 129.59, 127.84, 127.70, 124.40 (dd, $J = 6.9$ Hz, 3.9 Hz), 123.65, 117.91 (d, $J = 17.9$ Hz), 117.70 (d, $J = 18.1$ Hz), 117.57 (d, $J = 18.3$ Hz), 81.89, 45.87, 34.60, 24.18. LCMS (214 nM) $R_T = 1.18$ min (>98%); m/z 372 $[\text{M}+\text{H}]^+$. HRMS (TOF, ES+) $\text{C}_{24}\text{H}_{18}\text{N}_2\text{O}_2\text{F}_2\text{Cl}$ $[\text{M}+\text{H}]^+$ calc. mass 439.1025, found 439.1022.

5.111 (VU0481528). 9b-phenyl-2,3-dihydro-1H-imidazo[1',2':1,5]pyrrolo[3,4-b]pyridin-5(9bH)-one. To a mixture of 3-benzoylpicolinic acid (500 mg, 2.20 mmol, 1 eq.) and ethylenediamine (294 μL , 4.40 mmol, 2 eq.) in toluene (10 mL, 0.2 M) was added *p*-toluenesulfonic acid monohydrate (~12 mg, 3 mol%). A Dean-Stark trap was used to remove water while the mixture was magnetically stirred and heated to reflux for 2 hours. After cooling to ambient temperature, the reaction mixture was made basic with aqueous 1N NaOH. The organic layer was then separated and the aqueous layer was extracted with dichloromethane. The organic layers were then combined, washed with brine, and dried over magnesium sulfate. After filtration, the solvent was removed under reduced pressure and 378 mg of crude product was carried forward without purification (68% crude yield). TLC $R_f = 0.65$ (hexane/ethyl acetate 1:1). ^1H NMR (400.1 MHz, CDCl_3) δ (ppm): 8.76-8.71 (m, 1H); 7.69-7.64 (m, 3H); 7.39-7.29 (m, 4H); 3.95-3.86 (m, 1H); 3.74-3.65 (m, 1H); 3.32-3.20 (m, 1H), 2.18 (br, 1H). ^{13}C NMR (100.6 MHz, CDCl_3) δ (ppm): 170.12, 152.40, 150.16, 142.35, 138.00, 131.71, 129.06, 128.86, 126.19, 126.12, 87.48, 50.67, 41.95. LCMS (214 nM) $R_T = 0.61$ min (>98%); m/z 252 $[\text{M}+\text{H}]^+$. HRMS (TOF, ES+) $\text{C}_{15}\text{H}_{14}\text{N}_3\text{O}$ $[\text{M}+\text{H}]^+$ calc. mass 252.1137, found 252.1137.

5.117 (VU0481760). 1-(3,4-difluorobenzoyl)-9b-phenyl-2,3-dihydro-1H-imidazo[1',2':1,5]pyrrolo[3,4-b]pyridin-5(9bH)-one. To a solution of 9b-phenyl-2,3-dihydro-1H-imidazo[1',2':1,5]pyrrolo[3,4-b]pyridin-5(9bH)-one (20 mg, 0.080 mmol, 1.0 eq.) and DIPEA (27 μ L, 0.160 mmol, 2.0 eq.) in DCM (0.8 mL, 0.1 M) was added 3,4-difluorobenzoyl chloride (15 μ L, 0.120 mmol, 1.5 eq.). The reaction was magnetically stirred at ambient temperature for 2 hours. The reaction was quenched with methanol and the organics were concentrated on a heated air-drying block. Crude product was purified via Gilson preparative LC. Product containing fractions were combined and the solvents removed under reduced pressure to obtain 9.7 mg of product (31.0 % yield). TLC R_f = 0.25 (hexane/ethyl acetate 1:1). ^1H NMR (400.1 MHz, CDCl_3) δ (ppm): 8.88-8.85 (m, 1H); 8.39-8.36 (m, 1H); 7.48 (dd, $J_1 = 7.8$ Hz, $J_2 = 4.8$ Hz, 1H); 7.42-7.33 (m, 5H); 7.29-7.21 (m, 3H); 4.47-4.40 (m, 1H); 4.07-3.99 (m, 1H); 3.86-3.80 (m, 1H); 3.43-3.34 (m, 1H). ^{13}C NMR (100.6 MHz, CDCl_3) δ (ppm): 169.69, 167.10, 153.06, 151.72 (dd, $J_{\text{C-F}} = 231.5$ Hz, 12.0 Hz), 150.39 (dd, $J_{\text{C-F}} = 252.0$ Hz, 12.7 Hz), 149.89, 141.05, 137.55, 136.76, 132.64 (t, $J = 4.5$ Hz), 129.40, 129.17, 126.59, 125.91, 123.51 (dd, $J = 6.7$ Hz, 4 Hz), 118.05 (d, $J = 17.8$ Hz), 116.77 (d, $J = 18.7$ Hz), 85.87, 52.11, 39.64. LCMS (214 nM) $R_T = 0.98$ min (>98%); m/z 392 $[\text{M}+\text{H}]^+$. HRMS (TOF, ES+) $\text{C}_{22}\text{H}_{16}\text{N}_3\text{O}_2\text{F}_2$ $[\text{M}+\text{H}]^+$ calc. mass 392.1211, found 392.1210.

M₅ orthosteric antagonist chemical experimentals and characterization

6.1 (VU0480131). 5-((3-acetylphenoxy)methyl)-N-methyl-N-(1-(pyridin-2-yl)ethyl)isoxazole-3-carboxamide. To a solution of 5-((3-acetylphenoxy)methyl)isoxazole-3-carboxylic acid (20 mg, 0.077 mmol, 1 eq.; Enamine,

BBV-32990746, Lot No. R36151), *N*-methyl-1-(pyridin-2-yl)ethanamine (12.5 mg, 0.092 mmol, 1.2 eq.; ChemBridge, 4102794, Batch # 02), and DIPEA (26.4 μ L, 0.154 mmol, 2 eq.) in DCM (0.8 mL, 0.1 M) was added HATU (43.9 mg, 0.116 mmol, 1.5 eq.). The reaction was magnetically stirred at ambient temperature for 2 hours. The reaction mixture was quenched with aqueous NaHCO₃ and the organic layer was separated. The aqueous layer was extracted with DCM and the combined organic layers were dried over MgSO₄. After filtration, the solvent was removed under reduced pressure. The crude product was purified via Gilson preparative LC to obtain 24.9 mg pure product (85% yield). TLC R_f = 0.21 (hexane/ethyl acetate 1:1). ¹H NMR (~1:1 rotamer ratio, asterisk denotes rotamer peak, 500.1 MHz, MeOD) δ (ppm): 8.58-8.49 (m, 1H); 7.88-7.77 (m, 1H); 7.66-7.53 (m, 2H); 7.50-7.23 (m, 4H); 6.79*, 6.77* (s, 1H); 5.94*, 5.50* (q, J = 6.7 Hz, 1H); 5.34 (s, 2H); 3.00*, 2.82* (s, 3H); 2.57*, 2.56* (s, 3H), 1.70-1.65 (m, 3H). ¹³C NMR (~1:1 rotamer ratio, asterisk denotes rotamer peak, 125.8 MHz, MeOD) δ (ppm): 199.76, 170.14*, 169.98*, 163.40*, 163.13*, 160.27*, 160.20*, 159.96*, 159.63*, 159.43*, 159.39*, 150.08*, 149.76*, 139.82, 139.13*, 138.78*, 131.07, 124.20, 123.76, 123.28, 123.17, 121.23*, 121.16*, 114.90*, 114.89*, 105.46*, 105.34*, 61.89*, 61.86*, 59.40*, 55.34*, 32.73*, 28.99*, 26.83, 16.89*, 15.75*. LCMS (215 nM) R_T = 0.84 min (>98%); m/z 380 [M+H]⁺. HRMS (TOF, ES+) C₂₁H₂₂N₃O₄ [M+H]⁺ calc. mass 380.1610, found 380.1613.

6.89. (*R*)-2-nitro-*N*-(1-(pyridin-2-yl)ethyl)benzenesulfonamide. To a solution of (*R*)-1-(pyridin-2-yl)ethanamine (200 mg, 1.64 mmol, 1 eq.; Ark Pharm, Inc., AK-37082, Lot No. WZG111226-023A) and DIPEA (422 μ L, 2.46 mmol, 1.5 eq.) in DCM (5 mL, 0.33 M) was added nitrobenzenesulfonyl chloride (435 mg, 1.96 mmol, 1.2 eq.). The

reaction was magnetically stirred at ambient temperature for 1 hour. The reaction was quenched with aqueous NaHCO₃ and the organic phase was separated. The aqueous layer was extracted with DCM and the combined organic layers were dried over MgSO₄. After filtration, the solvent was removed under reduced pressure. The crude product was purified via silica gel column chromatography to obtain 459.2 mg of product (91% yield). TLC $R_f = 0.33$ (hexane/ethyl acetate 1:1). ¹H NMR (~1:1 rotamer ratio, asterisk denotes rotamer peak, 400.1 MHz, CDCl₃) δ (ppm): 8.31 (d, $J = 4.6$ Hz, 1H); 7.92*, 7.90* (d, $J = 1.4$ Hz, 1H); 7.79*, 7.77* (d, $J = 1.1$ Hz, 1H); 7.61-7.50 (m, 3H); 7.16*, 7.14* (s, 1H); 7.06*, 7.04* (d, $J = 4.9$ Hz, 1H); 6.75 (d, $J = 7.7$ Hz, 1H); 4.75 (quin, $J = 7.2$ Hz, 1H), 1.52 (d, $J = 6.8$ Hz, 3H). ¹³C NMR (100.6 MHz, CDCl₃) δ (ppm): 159.67, 149.16, 147.84, 137.24, 134.96, 133.40, 132.92, 130.89, 125.52, 122.91, 121.38, 55.28, 23.75. LCMS (215 nM) $R_T = 0.67$ min (>98%); m/z 308 [M+H]⁺. HRMS (TOF, ES+) C₁₃H₁₄N₃O₄S [M+H]⁺ calc. mass 308.0705, found 308.0708. Specific rotation $[\alpha]_D^{23} = 169.0^\circ$ ($c = 0.83$, CHCl₃).

6.90. (S)-2-nitro-N-(1-(pyridin-2-yl)ethyl)benzenesulfonamide. To a solution of (S)-1-(pyridin-2-yl)ethanamine (500 mg, 4.09 mmol, 1 eq.; Ark Pharm, Inc., AK-37110, Lot No. WZG120207-006) and DIPEA (1.05 mL, 6.14 mmol, 1.5 eq.) in DCM (10 mL, 0.41 M) was added nitrobenzenesulfonyl chloride (1.09 g, 4.91 mmol, 1.2 eq.). The reaction was magnetically stirred at ambient temperature for 1 hour. The reaction was quenched with aqueous NaHCO₃ and the organic phase was separated. The aqueous layer was extracted with DCM and the combined organic layers were dried over MgSO₄. After filtration, the solvent was removed under reduced pressure. The crude product was purified via silica gel column chromatography to obtain 974 mg of product (78% yield).

TLC $R_f = 0.33$ (hexane/ethyl acetate 1:1). ^1H NMR (~1:1 rotamer ratio, asterisk denotes rotamer peak, 400.1 MHz, CDCl_3) δ (ppm): 8.31 (d, $J = 4.6$ Hz, 1H); 7.92*, 7.90* (d, $J = 1.4$ Hz, 1H); 7.79*, 7.77* (d, $J = 1.1$ Hz, 1H); 7.61-7.50 (m, 3H); 7.15*, 7.13* (s, 1H); 7.06*, 7.04* (d, $J = 4.9$ Hz, 1H); 6.75 (d, $J = 7.7$ Hz, 1H); 4.75 (quin, $J = 7.2$ Hz, 1H), 1.52 (d, $J = 6.8$ Hz, 3H). ^{13}C NMR (100.6 MHz, CDCl_3) δ (ppm): 159.67, 149.12, 147.84, 137.29, 134.95, 133.40, 132.93, 130.90, 125.52, 122.93, 121.40, 55.26, 23.74. LCMS (215 nM) $R_T = 0.62$ min (>98%); m/z 308 $[\text{M}+\text{H}]^+$. HRMS (TOF, ES+) $\text{C}_{13}\text{H}_{14}\text{N}_3\text{O}_4\text{S}$ $[\text{M}+\text{H}]^+$ calc. mass 308.0705, found 308.0707. Specific rotation $[\alpha]_{\text{D}}^{23} = -160.0^\circ$ ($c = 0.79$, CHCl_3).

6.91. (*R*)-*N*-methyl-2-nitro-*N*-(1-(pyridin-2-yl)ethyl)benzenesulfonamide. To a solution of (*R*)-2-nitro-*N*-(1-(pyridin-2-yl)ethyl)benzenesulfonamide (1.13 g, 3.68 mmol, 1 eq.), MeOH (223 μL , 5.52 mmol, 1.5 eq.), and PPh_3 (1.93 g, 7.36 mmol, 2 eq.) in DCM (10 mL, 0.37 M) was added DIAD (1.45 mL, 7.36 mmol, 2 eq). The reaction was magnetically stirred at ambient temperature for 1 hour. The reaction was diluted with DCM and washed with aqueous 1N HCl and brine. The organic layer was separated and dried over MgSO_4 . After filtration, the solvent was removed under reduced pressure. The crude product was purified via silica gel column chromatography to obtain 772 mg of product (65% yield). TLC $R_f = 0.55$ (hexane/ethyl acetate 1:1). ^1H NMR (1:1 rotamer ratio, asterisk denotes rotamer peak, 500.1 MHz, CDCl_3) δ (ppm): 8.54 (d, $J = 4.3$ Hz, 1H); 8.06*, 8.04* (br, 1H), 7.73-7.60 (m, 4H); 7.46*, 7.45* (s, 1H); 7.25-7.20 (m, 1H); 5.35 (q, $J = 6.8$ Hz, 1H); 2.85 (s, 3H); 1.57 (d, $J = 7.0$ Hz, 3H). ^{13}C NMR (125.8 MHz, CDCl_3) δ (ppm): 158.85, 156.71, 148.67, 148.37, 137.83, 133.79, 133.46, 131.96, 131.26, 124.49, 123.21, 57.12, 29.86, 16.08. LCMS (215 nM) $R_T = 0.744$ min (>98%); m/z 322

[M+H]⁺. HRMS (TOF, ES+) C₁₄H₁₆N₃O₄S [M+H]⁺ calc. mass 322.0862, found 322.0860. Specific rotation $[\alpha]_{D}^{23} = 48.2^{\circ}$ (*c* = 0.72, CHCl₃).

6.92. (S)-N-methyl-2-nitro-N-(1-(pyridin-2-yl)ethyl)benzenesulfonamide. To a solution of (S)-2-nitro-N-(1-(pyridin-2-yl)ethyl)benzenesulfonamide (970 mg, 3.16 mmol, 1 eq.), MeOH (192 μL, 4.73 mmol, 1.5 eq.), and PPh₃ (1.66 g, 6.32 mmol, 2 eq.) in DCM (10 mL, 0.30 M) was added DIAD (1.24 mL, 6.32 mmol, 2 eq.). The reaction was magnetically stirred at ambient temperature for 1 hour. The reaction was diluted with DCM and washed with aqueous 1N HCl and brine. The organic layer was separated and dried over MgSO₄. After filtration, the solvent was removed under reduced pressure. The crude product was purified via silica gel column chromatography to obtain 750 mg of product (74% yield). TLC *R_f* = 0.55 (hexane/ethyl acetate 1:1). ¹H NMR (~1:1 rotamer ratio, asterisk denotes rotamer peak, 400.1 MHz, CDCl₃) δ (ppm): 8.48 (d, *J* = 4.3 Hz, 1H); 8.02*, 8.00* (d, *J* = 1.8 Hz, 1H), 7.70-7.58 (m, 4H); 7.38*, 7.36* (s, 1H); 7.16*, 7.14* (d, *J* = 4.8 Hz, 1H); 5.30 (q, *J* = 7.0 Hz, 1H); 2.81 (s, 3H); 1.52 (d, *J* = 7.0 Hz, 3H). ¹³C NMR (100.6 MHz, CDCl₃) δ (ppm): 158.64, 148.77, 147.93, 136.79, 133.45, 133.03, 131.59, 130.71, 124.03, 122.61, 122.46, 56.87, 29.35, 15.63. LCMS (215 nM) *R_T* = 0.72 min (>98%); *m/z* 322 [M+H]⁺. HRMS (TOF, ES+) C₁₄H₁₆N₃O₄S [M+H]⁺ calc. mass 322.0862, found 322.0862. Specific rotation $[\alpha]_{D}^{23} = -76.3^{\circ}$ (*c* = 0.48, CHCl₃).

6.93. (R)-N-methyl-1-(pyridin-2-yl)ethanamine. To a solution of (R)-N-methyl-2-nitro-N-(1-(pyridin-2-yl)ethyl)benzenesulfonamide (770 mg, 2.40 mmol, 1 eq.) and K₂CO₃ (995 mg, 7.20 mmol, 3 eq.) in acetonitrile (10 mL, 0.24 M) was added 2-chlorothiophenol (335 μL, 2.88 mmol, 1.2 eq.). The reaction was magnetically stirred at ambient temperature for 4 hours. The reaction was quenched with aqueous 1N NaOH and

the organic layer was separated. The aqueous layer was extracted with DCM and the combined organic layers were washed with brine and dried over MgSO₄. After filtration, the solvent was removed under reduced pressure. The crude product was purified via silica gel column chromatography to obtain 166.4 mg of product (51% yield). TLC R_f = 0.68 (hexane/ethyl acetate 1:1, ninhydrin stained). ¹H NMR (500.1 MHz, MeOD) δ (ppm): 8.86 (d, J = 4.4 Hz, 1H); 8.47 (t, J = 7.5 Hz, 1H); 8.01 (d, J = 8.1 Hz, 1H); 7.8 (t, J = 6.1 Hz, 1H); 4.75 (q, J = 6.6 Hz, 1H); 2.76 (s, 3H); 1.78 (d, J = 6.7 Hz, 3H). ¹³C NMR (125.8 MHz, MeOD) δ (ppm): 154.17, 147.82, 144.41, 127.45, 125.89, 58.90, 32.21, 18.64. HRMS (TOF, ES+) C₈H₁₃N₂ [M+H]⁺ calc. mass 137.1079, found 137.1077. Specific rotation $[\alpha]_D^{23} = 20.5^\circ$ ($c = 0.95$, MeOH).

6.94. (S)-N-methyl-1-(pyridin-2-yl)ethanamine. To a solution of (S)-N-methyl-2-nitro-N-(1-(pyridin-2-yl)ethyl)benzenesulfonamide (750 mg, 2.33 mmol, 1 eq.) and K₂CO₃ (966 mg, 6.99 mmol, 3 eq.) in acetonitrile (10 mL, 0.23 M) was added 2-chlorothiophenol (327 μ L, 2.8 mmol, 1.2 eq.). The reaction was magnetically stirred at ambient temperature for 4 hours. The reaction was quenched with aqueous 1N NaOH and the organic layer was separated. The aqueous layer was extracted with DCM and the combined organic layers were washed with brine and dried over MgSO₄. After filtration, the solvent was removed under reduced pressure. The crude product was purified via silica gel column chromatography to obtain 62.8 mg of product (20% yield). TLC R_f = 0.68 (hexane/ethyl acetate 1:1, ninhydrin stained). ¹H NMR (400.1 MHz, MeOD) δ (ppm): 8.91 (br, 1H); 8.49 (br, 1H); 8.13 (br, 1H); 7.95 (br, 1H); 4.80 (br, 1H); 2.78 (s, 3H); 1.83 (br, 3H). ¹³C NMR (100.6 MHz, MeOD) δ (ppm): 154.12, 147.85, 146.84,

128.70, 127.12, 59.27, 33.24, 19.29. HRMS (TOF, ES+) C₈H₁₃N₂ [M+H]⁺ calc. mass 137.1079, found 137.1078. Specific rotation $[\alpha]_D^{23} = -20.3^\circ$ ($c = 0.97$, MeOH).

6.95 (VU0487996). (R)-5-((3-acetylphenoxy)methyl)-N-methyl-N-(1-(pyridin-2-yl)ethyl)isoxazole-3-carboxamide. To a solution of 5-((3-acetylphenoxy)methyl)isoxazole-3-carboxylic acid (100 mg, 0.383 mmol, 1 eq.; Enamine, BBV-32990746, Lot No. R36151), (R)-N-methyl-1-(pyridin-2-yl)ethanamine (62.6 mg, 0.459 mmol, 1.2 eq.), and DIPEA (131.3 μ L, 0.766 mmol, 2 eq.) in DCM (1.5 mL, 0.25 M) was added HATU (218.6 mg, 0.575 mmol, 1.5 eq). The reaction was magnetically stirred at ambient temperature for 2 hours. The reaction mixture was quenched with aqueous NaHCO₃ and the organic layer was separated. The aqueous layer was extracted with DCM and the combined organic layers were dried over MgSO₄. After filtration, the solvent was removed under reduced pressure. The crude product was purified via Gilson preparative LC to obtain 136.1 mg of product (94% yield). TLC $R_f = 0.27$ (hexane/ethyl acetate 1:1). ¹H NMR (~1:1 rotamer ratio, asterisk denotes rotamer peak, 500.1 MHz, CDCl₃) δ (ppm): 8.60-8.55 (m, 1H); 7.71-7.64 (m, 1H); 7.59*, 7.58* (br, 1H); 7.54 (br, 1H); 7.42-7.31 (m, 2H); 7.24-7.13 (m, 2H); 6.71*, 6.69* (br, 1H); 6.05*, 5.74* (q, $J = 6.7$ Hz, 1H); 5.23 (s, 2H); 3.08*, 2.85* (s, 3H); 2.58 (s, 3H), 1.72-1.64 (m, 3H). ¹³C NMR (~1:1 rotamer ratio, asterisk denotes rotamer peak, 125.8 MHz, CDCl₃) δ (ppm): 197.59, 167.88*, 167.68*, 161.13*, 160.90*, 159.33*, 159.18*, 158.91*, 158.80*, 157.98, 149.24*, 148.92*, 138.76, 137.17*, 136.90*, 130.04, 122.98*, 122.78*, 122.72*, 122.45, 122.16*, 120.30, 113.37*, 113.35*, 105.08*, 105.03*, 61.19*, 61.14*, 57.87*, 53.77*, 32.06*, 28.70*, 26.81, 16.71*, 15.41*. LCMS (215 nM) $R_T =$

0.87 min (>98%); m/z 380 $[M+H]^+$. HRMS (TOF, ES+) $C_{21}H_{22}N_3O_4$ $[M+H]^+$ calc. mass 380.1610, found 380.1611. Specific rotation $[\alpha]_D^{23} = 134.8^\circ$ ($c = 0.78$, $CHCl_3$).

6.96 (VU0488130, ML381). (S)-5-((3-acetylphenoxy)methyl)-N-methyl-N-(1-(pyridin-2-yl)ethyl)isoxazole-3-carboxamide. To a solution of 5-((3-acetylphenoxy)methyl)isoxazole-3-carboxylic acid (100 mg, 0.383 mmol, 1 eq.; Enamine, BBV-32990746, Lot No. R36151), (S)-N-methyl-1-(pyridin-2-yl)ethanamine (62.6 mg, 0.459 mmol, 1.2 eq.), and DIPEA (131.3 μ L, 0.766 mmol, 2 eq.) in DCM (1.5 mL, 0.25 M) was added HATU (218.6 mg, 0.575 mmol, 1.5 eq) The reaction was magnetically stirred at ambient temperature for 2 hours. The reaction mixture was quenched with aqueous $NaHCO_3$ and the organic layer was separated. The aqueous layer was extracted with DCM and the combined organic layers were dried over $MgSO_4$. After filtration, the solvent was removed under reduced pressure. The crude product was purified via Gilson preparative LC to obtain 129.3 mg of product (89% yield). TLC $R_f = 0.27$ (hexane/ethyl acetate 1:1). 1H NMR (~1:1 rotamer ratio, asterisk denotes rotamer peak, 400.1 MHz, $CDCl_3$) δ (ppm): 8.59-8.55 (m, 1H); 7.70-7.63 (m, 1H); 7.59*, 7.57* (m, 1H); 7.55-7.52 (m, 1H); 7.42-7.31 (m, 2H); 7.23-7.14 (m, 2H); 6.71*, 6.68* (s, 1H); 6.05*, 5.74* (q, $J = 6.9$ Hz, 1H); 5.23 (s, 2H); 3.07*, 2.85* (s, 3H); 2.58 (s, 3H), 1.70-1.64 (m, 3H). ^{13}C NMR (~1:1 rotamer ratio, asterisk denotes rotamer peak, 100.6 MHz, $CDCl_3$) δ (ppm): 197.59, 167.88*, 167.67*, 161.13*, 160.88*, 159.33*, 159.17*, 158.96*, 158.79*, 157.97, 149.27*, 149.05*, 138.75, 137.03*, 136.86*, 130.03, 122.91*, 122.73*, 122.70*, 122.44, 122.13*, 120.29, 113.36*, 113.34*, 105.07*, 105.02*, 61.17*, 61.12*, 57.87*, 53.73*, 31.98*, 28.69*, 26.80, 16.69*, 15.39*. LCMS (215 nM) $R_T =$

0.85 min (>98%); m/z 380 $[M+H]^+$. HRMS (TOF, ES+) $C_{21}H_{22}N_3O_4$ $[M+H]^+$ calc. mass 380.1610, found 380.1607. Specific rotation $[\alpha]_D^{23} = -125.8^\circ$ ($c = 0.69$, $CHCl_3$).

***In vitro* pharmacology**

Calcium mobilization assays

All functional cell-based Ca^{2+} mobilization assays were performed on a FLEXStation II (Molecular Devices, Sunnyvale, CA) essentially as previously described^{69,72,73}. Initial, single point (10 or 30 μM) characterization of test compounds was performed in stable Chinese hamster ovary (CHO) cell lines constitutively expressing hM₅ receptors. These were plated at 50,000 cells per well in Costar 96-well black-walled, TC-treated, clear-bottomed plates (Fisher) in Ham's F12 medium supplemented with 10% FBS and 20 mM HEPES. Cells were incubated overnight at 37 °C under 5% CO₂. The following day, medium was removed and replaced with 50 μL of 2 μM Fluo-4 AM (Invitrogen) calcium sensitive dye in calcium assay buffer (Hank's Balanced Salt Solution supplemented with 20 mM HEPES and 2.5 mM Probenecid, pH 7.4) and the cells were then incubated 45 minutes at 37 °C under 5% CO₂. Dye was then removed and replaced with 45 μL of fresh assay buffer. Test compounds were serially diluted into assay buffer at 2X (20 μM) stock concentration in 0.6% dimethylsulfoxide (DMSO); stock compounds were added to the assay for a final stock concentration of 10 or 30 μM and a final DMSO concentration of 0.3%. Acetylcholine (Sigma-Aldrich) was serially diluted into assay buffer to 10X submaximal ($\sim EC_{20}$ or EC_{80} , determined empirically on day of assay) and 10X maximal (10 μM) stock concentrations. After

establishing baseline fluorescence, test compounds (45 μL) were added to the cells using the FLEXStation II's integrated pipettor and allowed to equilibrate for 150 seconds before addition of acetylcholine (10 μL). Data were obtained as max-min fluorescent ratios and then normalized to a percentage of maximal acetylcholine response. The single point values represent mean values obtained from at least three independent determinations performed in triplicate or greater (error bars represent +/- SEM) unless otherwise specified.

For Ca^{2+} mobilization assays measuring ACh CRC fold shift, CHO cells stably expressing hM_5 were plated in the manner described above. Test compounds were serially diluted into assay buffer to a 2X (20 or 60 μM) stock concentration in 0.6% DMSO; stock compounds were added to the assay for a final stock concentration of 10 or 30 μM and a final DMSO concentration of 0.3%. An eight-point concentration range of ACh was serially diluted in assay buffer to 10X final concentration. FLEXStation II protocols were carried out as described above; data were obtained as max-min fluorescent ratios and then normalized to a percentage of the maximum ACh response. Calculation of the ACh EC_{50} was performed using the curve-fitting software of GraphPad Prism (version 5.01). ACh fold shift was calculated as a ratio of ACh EC_{50} in the presence of vehicle to the ACh EC_{50} in the presence of test compound. Data shown represent mean values obtained from at least three independent determinations performed in triplicate or greater (error bars represent +/- SEM) unless otherwise specified.

For selectivity assays, CHO cells stably expressing hM_1 , $\text{hM}_2/\text{G}_{\text{qi}5}$, hM_3 , $\text{hM}_4/\text{G}_{\text{qi}5}$, hM_5 , rM_1 , $\text{rM}_2/\text{G}_{\text{qi}5}$, rM_3 , $\text{rM}_4/\text{G}_{\text{qi}5}$, or rM_5 were plated in the manner described above. An eight-point concentration range of test compound was serially diluted in assay

buffer to 2X final concentration and acetylcholine was diluted in assay buffer to 10X submaximal (\sim EC₂₀ or EC₈₀, determined empirically on day of assay) and 10X maximal (10 μ M for M₁₋₅; 100 μ M for M₂, M₄) stock concentrations. FLEXstation II protocols were carried out as described above; data were obtained as max-min fluorescent ratios and then normalized to percentage of maximum acetylcholine response. Calculation of EC₅₀ or IC₅₀ was performed using the curve-fitting software of GraphPad Prism (version 5.01). Data shown represent mean values obtained from at least three independent determinations performed in triplicate or greater (error bars represent \pm SEM) unless otherwise specified.

[³H]-NMS competition binding

Membranes were prepared from stable CHO cell lines constitutively expressing human M₅ receptors according to previously described protocols^{69,72,73}. Binding reactions were carried out in 2 mL, clear, 96-well, deep well plates (Axygen Scientific) and contained 0.3 nM [³H]-NMS (PerkinElmer), 10 μ g of membrane protein, and an eleven-point concentration range of test compound or atropine in a total volume of 500 μ L assay buffer (100 mM NaCl, 10 mM MgCl₂, 20 mM HEPES, pH 7.4). Nonspecific binding was determined in the presence of 10 μ M atropine. The K_D of [³H]-NMS was determined empirically to be 0.264 nM. Binding reactions were performed at ambient temperature and allowed to incubate for 3 hours on a Lab-Line Titer plate shaker at setting 7 (\sim 750 rpm). Reactions were terminated by rapid filtration through GF/B glass microfiber filter plates (1 μ m pore size) using a 96-well Brandel harvester and washed 3X with ice-cold harvesting buffer (50 mM Tris-HCl, 0.9% NaCl, pH 7.4). Filter plates were dried

overnight and counted in a PerkinElmer TopCount scintillation counter (PerkinElmer Life and Analytical Sciences). Actual [³H]-NMS concentration was back-calculated after counting aliquots of 10X [³H]-NMS used in the reaction. For all assays, radioligand depletion was kept to approximately 18% or less. Plotting of data and calculation of K_i was performed using the curve-fitting software of GraphPad Prism (version 5.01). Data shown represent mean values obtained from three independent determinations performed using three or more replicates (error bars represent +/- SEM).

[³H]-NMS dissociation kinetics

Membranes were prepared from stable CHO cell lines constitutively expressing human M₅ receptors cells according to a previously described protocol^{69,72,73}. Binding reactions were carried out in 2 mL, clear, 96-well, deep well plates (Axygen Scientific) and initially contained M₅ CHO cell membranes (10 µg) and a saturating amount (0.3 nM) of [³H]-NMS. Binding was allowed to equilibrate at ambient temperature for 3 hours on a Lab-Line Titer plate shaker at setting 7 (~750 rpm). Atropine (10 µM) and either vehicle or test compound (10 µM) were then added at various time points over 3.5 hours in a final volume of 500 µL. Plate agitation was continued between additions. Nonspecific binding was determined in the presence of 10 µM atropine. Reactions were terminated by rapid filtration through GF/B glass microfiber filter plates (1 µm pore size) using a 96-well Brandel harvester and washed 3X with ice-cold harvesting buffer (50 mM Tris-HCl, 0.9% NaCl, pH 7.4). Filter plates were dried overnight and counted in a PerkinElmer TopCount scintillation counter (PerkinElmer Life and Analytical Sciences). Actual [³H]-NMS concentration was back-calculated after counting aliquots of 10X [³H]-

NMS used in the reaction. For all assays, radioligand depletion was kept to approximately 15% or less. Plotting of data and calculation of $t_{1/2}$ was performed using the curve-fitting software of GraphPad Prism (version 5.01). Data shown represent mean values obtained from three independent determinations performed using three or more replicates (error bars represent +/- SEM).

Ancillary/off-target screening assays

Prior to conducting *in vivo* experiments, compounds were submitted to Eurofins Panlabs Leadprofiling screening panel of 68 GPCRs, ion channels, enzymes, transporters, and nuclear hormone receptors. Test compounds (10 μ M) were evaluated in competition binding assays using standard orthosteric radioligands for each target ($n = 2$). Results were calculated as % inhibition of radioligand binding, with >50% inhibition representing significant activity at a given target.

***In vitro* DMPK**

Plasma protein and brain homogenate binding

Plasma protein and brain homogenate binding measurements were performed essentially as previously described⁷³. The protein binding of each compound was determined in plasma via equilibrium dialysis employing rapid equilibrium dialysis (RED) plates (ThermoFisher Scientific, Rochester, NY). Plasma was added to a 96 well plate containing test compound and mixed thoroughly for a final compound concentration of 5 μ M. Subsequently, an aliquot of the plasma-compound mixture was transferred to

the *cis* chamber (red) of the RED plate, with phosphate buffer (25 mM, pH 7.4) in the *trans* chamber. The RED plate was sealed and incubated for 4 hours at 37 °C with shaking. At completion, aliquots from each chamber were diluted 1:1 with either plasma (*cis*) or buffer (*trans*) and transferred to a new 96 well plate, at which time ice-cold acetonitrile containing internal standard (50 ng/mL carbamazepine) (2 volumes) was added to extract the matrices. The plate was centrifuged (3000 rcf, 10 min) and supernatants transferred and diluted 1:1 (supernatant: water) into a new 96 well plate, which was then sealed in preparation for LC/MS/MS analysis. Each compound was assayed in triplicate within the same 96-well plate. Fraction unbound was determined using the following equation:

$$f_u = \frac{Conc_{buffer}}{Conc_{plasma}}$$

A similar approach was used to determine the degree of brain homogenate binding, which employed the same methodology and procedure with the following modifications: 1) a final compound concentration of 1 µM was used, 2) naïve rat brains were homogenized in DPBS (1:3 composition of brain:DPBS, w/w) using a Mini-Bead Beater™ machine in order to obtain brain homogenate, which was then utilized in the same manner as plasma in the previously described plasma protein binding assay. Fraction unbound was determined using the following equations:

$$\text{Diluted: } f_{u,d} = \frac{Conc_{buffer}}{Conc_{plasma}}$$

$$\text{Undiluted: } f_u = \frac{1/D}{\left\{ \left(\frac{1}{f_{u,d}} \right) - 1 \right\} + 1/D}, \text{ where D = dilution factor}$$

Hepatic microsome intrinsic clearance

The intrinsic clearance of each test compound was determined essentially as previously described⁷³. Human or rat hepatic microsomes (0.5 mg/mL) and 1 μ M test compound were incubated in 100 mM potassium phosphate pH 7.4 buffer with 3 mM MgCl₂ at 37 °C with constant shaking. After a 5 min preincubation, the reaction was initiated by addition of NADPH (1 mM). At selected time intervals (0, 3, 7, 15, 25, and 45 min), aliquots were taken and subsequently placed into a 96-well plate containing cold acetonitrile with internal standard (50 ng/mL carbamazepine). Plates were then centrifuged at 3000 rcf (4° C) for 10 min, and the supernatant was transferred to a separate 96-well plate and diluted 1:1 with water for LC/MS/MS analysis. The in vitro half-life ($T_{1/2}$, min, Eq. 1), intrinsic clearance (CL_{int} , mL/min/kg, Eq. 2) and subsequent predicted hepatic clearance (CL_{hep} , mL/min/kg, Eq. 3) was determined employing the following equations:

$$(1) \quad T_{1/2} = \frac{\ln(2)}{k}$$

where k represents the slope from linear regression analysis of the natural log percent remaining of test compound as a function of incubation time.

$$(2) \quad CL_{int} = \frac{0.693}{in\ vitro\ T_{1/2}} \times \frac{mL\ incubation}{mg\ microsomes} \times \frac{45\ mg\ microsomes}{gram\ liver} \times \frac{20^a\ gram\ liver}{kg\ body\ wt}$$

^ascale-up factor: 20 (human) or 45 (rat)

$$(3) \quad CL_{hep} = \frac{Q_h \cdot CL_{int}}{Q_h + CL_{int}}$$

where Q_h (hepatic blood flow in mL/min/kg) is 21 (human) or 70 (rat).

LC/MS/MS bioanalysis of samples from plasma protein/brain homogenate binding and hepatic microsome intrinsic clearance assays

Samples were analyzed essentially as previously described⁷³ on a Thermo Electron TSQ Quantum Ultra triple quad mass spectrometer (San Jose, CA) via electrospray ionization (ESI) with two Thermo Electron Accella pumps (San Jose, CA), and a Leap Technologies CTC PAL autosampler (Carrboro, NC). Analytes were separated by gradient elution on a dual column system with two Thermo Hypersil Gold (2.1 x 30 mm, 1.9 μ m) columns (San Jose, CA) thermostated at 40 °C. HPLC mobile phase A was 0.1% formic acid in water and mobile phase B was 0.1% formic acid in acetonitrile. The gradient started at 10% B after a 0.2 min hold and was linearly increased to 95% B over 0.8 min; hold at 95% B for 0.2 min; returned to 10% B in 0.1 min. The total run time was 1.3 min and the HPLC flow rate was 0.8 mL/min. While pump 1 ran the gradient method, pump 2 equilibrated the alternate column isocratically at 10% B. Compound optimization, data collection and processing was performed using Thermo Electron's QuickQuan software (v2.3) and Xcalibur (v2.0.7 SP1).

Inhibition of cytochrome P450 enzymes

Cytochrome P450 inhibition studies were performed essentially as previously described⁷³. A cocktail of substrates for cytochrome P450 enzymes (1A2: Phenacetin, 10 μ M; 2C9: Diclofenac, 5 μ M; 2D6: Dextromethorphan, 5 μ M; 3A4: Midazolam, 2 μ M) were mixed for cocktail analysis. The positive control for pan-P450 inhibition (miconazole) was included alongside each test compound in analysis.

A reaction mixture of 100 mM potassium phosphate buffer, pH 7.4, 0.1 mg/mL human liver microsomes (HLM) and Substrate Mix is prepared and aliquoted into a 96-deepwell block. Test compound and positive control (in duplicate) were then added such that the final concentration of test compound ranged from 0.1 – 30 μ M. The plate was vortexed briefly and then pre-incubated at 37° C while shaking for 15 minutes. The reaction was initiated with the addition of NADPH (1 mM final concentration). The incubation continued for 8 min and the reaction quenched by 2x volume of cold acetonitrile containing internal standard (50 nM carbamazepine). The plate was centrifuged for 10 minutes (4000 rcf, 4 °C) and the resulting supernatant diluted 1:1 with water for LC/MS/MS analysis. A 12-point standard curve of substrate metabolites (1A2: Acetaminophen; 2C9: 4-Hydroxydiclofenac; 2D6: Dextrorphan tartrate; 3A4: 1-Hydroxymidazolam) over the range of 0.98 nM to 2000 nM was utilized.

Samples were analyzed via electrospray ionization (ESI) on an AB Sciex API-4000 (Foster City, CA) triple-quadrupole instrument that was coupled with Shimadzu LC-10AD pumps (Columbia, MD) and a Leap Technologies CTC PAL auto-sampler (Carrboro, NC). Analytes were separated by gradient elution using a Fortis C18 3.0 x 50 mm, 3 μ m column (Fortis Technologies Ltd, Cheshire, UK) thermostated at 40 °C. HPLC mobile phase A was 0.1% formic acid in water (pH unadjusted), mobile phase B was 0.1% formic acid in acetonitrile (pH unadjusted). The gradient started at 10% B after a 0.2 min hold and was linearly increased to 90% B over 1.2 min; held at 90% B for 0.1 min and returned to 10% B in 0.1 min followed by a re-equilibration (0.9 min). The total run time was 2.5 min and the HPLC flow rate was 0.5 mL/min. The source temperature was set at 500 °C and mass spectral analyses were performed using multiple reaction

monitoring (MRM), with transitions specific for each compound utilizing a Turbo-Ionspray® source in positive ionization mode (5.0 kV spray voltage).

The IC₅₀ values for each compound were obtained for the individual CYP enzymes by quantitating the inhibition of metabolite formation for each probe substrate. A 0 µM compound condition (or control) was set to 100% enzymatic activity and the effect of increasing test compound concentrations on enzymatic activity could then be calculated from the % of control activity. Curves were fitted using XLfit 5.2.2 (four-parameter logistic model, equation 201) to determine the concentration that produces half-maximal inhibition (IC₅₀).

Caco-2/MDCK-MDR1 transwell assays

Measurements of bidirectional efflux in Caco-2 or MDCK-MDR1 (P-gp) cell monolayer transwell assays were performed via contract with Absorption Systems (Exton, PA; <http://www.absorption.com>).

***In vivo* DMPK**

Statement on animal care and use

All animal study procedures were approved by the Institutional Animal Care and Use Committee and were conducted in accordance with the National Institutes of Health regulations of animal care covered in Principles of Laboratory Animal Care (National Institutes of Health).

Pharmacokinetic/plasma-brain level studies in rat

Intravenous (IV) pharmacokinetics (PK) of non-isatin M₅ PAM compound **4.161** (VU0481443, ML380) and M₅ orthosteric antagonist **6.96** (VU0488130, ML381) were obtained via contract with Frontage Laboratories (Exton, PA). Serial sampling of plasma (10 time points) following a single intravenous administration (1 mg/kg: formulated at 1 mg/mL in 10% ethanol, 50% PEG400, 40% saline vehicle) to male Sprague-Dawley rats ($n = 3$). Non-compartmental analysis was performed in order to obtain PK parameters. After 24 hours re-administration of the same dose (and formulation) was performed, and single time point (0.25 hours post re-administration) samples of plasma and brain were collected in order to assess brain distribution (brain:plasma partition coefficient, K_p).

Rat IV/PO PK of M₅ NAM compound **5.97** (VU0483253, ML375) was carried out using four male, Sprague Dawley adult rats, each weighing approximately 360 – 380 grams. Two rats received a single dose (1 mg/kg) of a 1 mg/mL dosing solution (10% ethanol, 50% PEG 400, and 40% saline vehicle) of **5.97** administered as an intravenous (IV) bolus via a surgically implanted jugular vein catheter. In the other arm of the study, two rats received a single dose (10 mg/kg) of a 1 mg/mL dosing solution (0.1% Tween 80 in 0.5% methyl cellulose) of **5.97** administered orally. Plasma was collected serially at 0.0333, 0.117, 0.25, 0.5, 1, 2, 4, 7, and 24 hours in the IV arm and at 0.25, 0.5, 1, 2, 4, 7, and 24 hours in the PO arm. Plasma samples were prepared in chilled, EDTA-fortified tubes by centrifugation (10 minutes; 3000 RCF; 4 °C) of blood samples; brain samples (collected after the final time point) were rinsed (cold, phosphate-buffered saline) and frozen (dry ice), and all samples were stored (-80 °C) until analysis by LC-MS/MS.

On the day of analysis, frozen whole-rat brains were weighed and diluted with 1:3 (w/w) parts of 70:30 isopropanol:water. The mixture was then subjected to mechanical homogenation employing a Mini-Beadbeater™ and 1.0 mm Zirconia/Silica Beads (BioSpec Products) followed by centrifugation. The sample extraction of plasma (20 µL) or brain homogenate (20 µL) was analyzed by a method based on protein precipitation using three volumes of ice-cold acetonitrile containing an internal standard (50 ng/mL carbamazepine). The samples were centrifuged (3000 rcf, 5 min) and supernatants transferred and diluted 1:1 (supernatant: water) into a new 96 well plate, which was then sealed in preparation for LC/MS/MS analysis.

In vivo samples were analyzed via electrospray ionization (ESI) on an AB Sciex API-5500 QTrap (Foster City, CA) instrument that was coupled with Shimadzu LC-20AD pumps (Columbia, MD) and a Leap Technologies CTC PAL auto-sampler (Carrboro, NC). Analytes were separated by gradient elution using a Fortis C18 3.0 x 50 mm, 3 µm column (Fortis Technologies Ltd, Cheshire, UK) thermostated at 40 °C. HPLC mobile phase A was 0.1% formic acid in water (pH unadjusted), mobile phase B was 0.1% formic acid in acetonitrile (pH unadjusted). The gradient started at 30% B after a 0.2 min hold and was linearly increased to 90% B over 0.8 min; held at 90% B for 0.5 min and returned to 30% B in 0.1 min followed by a re-equilibration (0.9 min). The total run time was 2.5 min and the HPLC flow rate was 0.5 mL/min. The source temperature was set at 500 °C and mass spectral analyses were performed using MRM, with transitions specific for each compound utilizing a Turbo-Ionspray® source in positive ionization mode (5.0 kV spray voltage). The calibration curves were constructed in blank plasma. All data were analyzed using AB Sciex Analyst software v1.5.1.

Pharmacokinetic study in non-human primate

An *in vivo* PK study of M₅ NAM **5.97** (VU0483253, ML375) in non-human primates (cynomolgus monkey) was performed by contract with Frontage Laboratories (Exton, PA). **5.97** was administered IV as a single dose (1 mg/kg: formulated at 1 mg/mL in 10% ethanol 70% PEG400 20% saline vehicle) to male cynomolgus monkeys ($n = 3$), and plasma was collected serially at 0.033, 0.083, 0.25, 0.5, 1, 2, 4, 6, 8, and 24 hours. Non-compartmental analysis was performed to obtain PK parameters.

Chapter III

DEVELOPMENT OF THE FIRST HIGHLY SELECTIVE, SUB-MICROMOLAR M₅ POSITIVE ALLOSTERIC MODULATOR

Prior discovery of the first M₅-preferring PAM

To date, very few PAMs selective for M₅ have been reported^{70,71,74}. As discussed in the introduction (Chapter I), our laboratory previously reported the first highly M₅-preferring PAM, the isatin-based compound VU0238429 (**3.2**), which was discovered after a campaign exploring and optimizing the SAR surrounding the chemical scaffold of M_{1/3/5} PAM VU0119498 (**3.1**)^{70,71}. Further rounds of iterative parallel synthesis extensively characterized the SAR of biaryl ether substitutions in the southern *N*-benzyl region of the **3.2** pharmacophore, producing multiple potent and M₅-selective analogs (**Figure 3.1**)³. Unfortunately, as with **3.2**, these early M₅ PAMs failed to display the DMPK and physicochemical profile necessary to serve as an *in vivo* probe into the role of selective M₅ activation^{70,71,74}. Despite this hindrance, aspects of the **3.2** chemical scaffold remained to be explored, so a new optimization campaign was launched with the goals of improving the chemical series' physicochemical and DMPK profile whilst maintaining potency and M₅ selectivity⁷⁵.

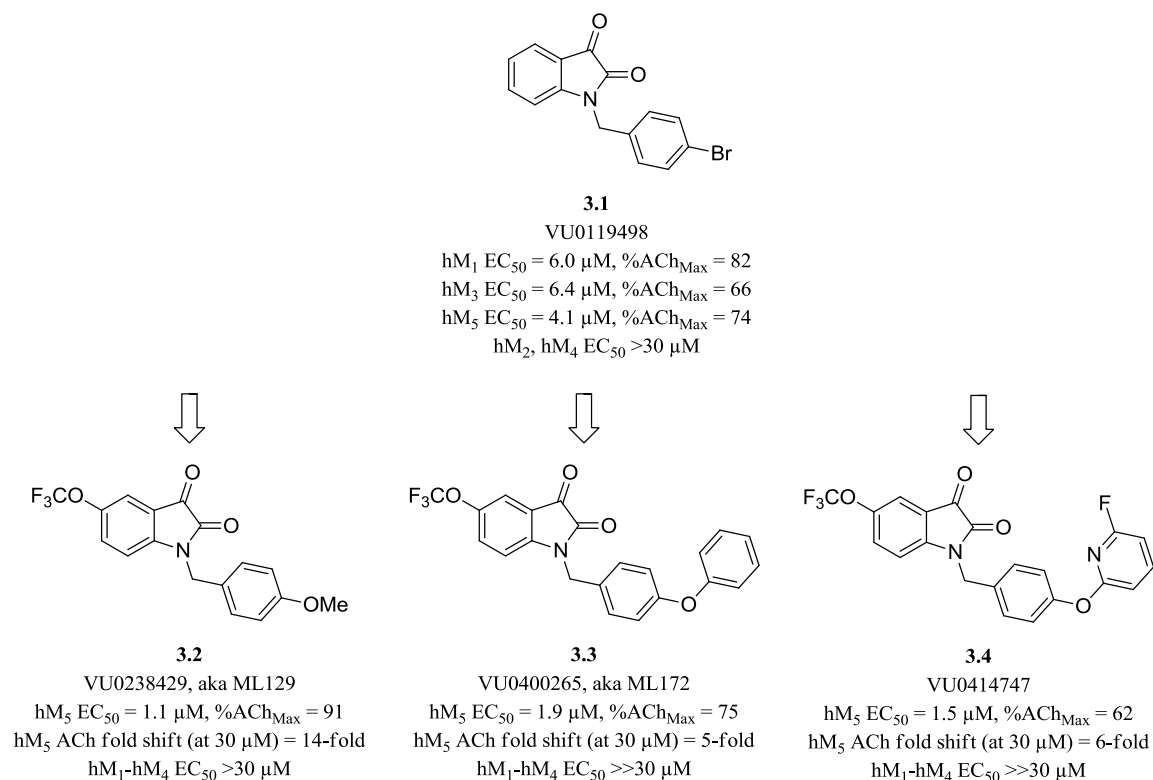


Figure 3.1. Structures and activities of M₅-preferring PAM VU0238429 (**3.2**) and selected M₅-selective PAM analogs **3.3** and **3.4**. All three were developed from a *pan*-M₁, M₃, M₅ PAM, VU0119498 (**3.1**) that afforded both M₁-selective PAMs and, by virtue of the 5-OCF₃ moiety, M₅-selective PAMs^{70,71,74}.

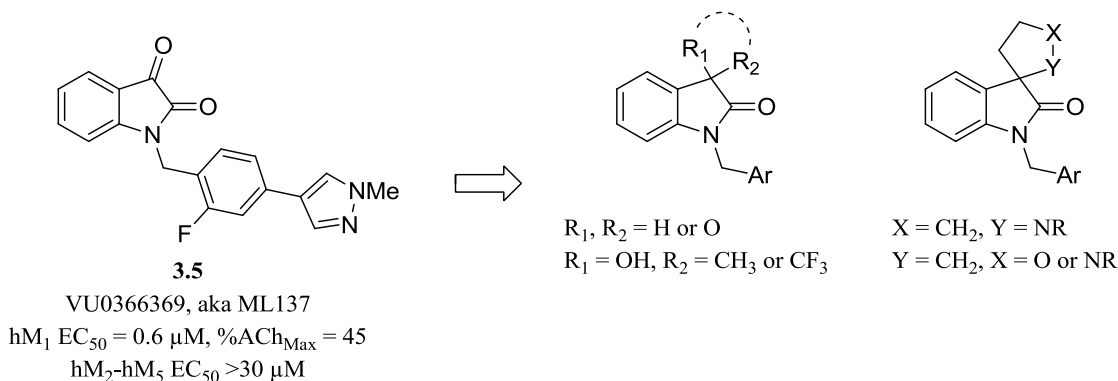
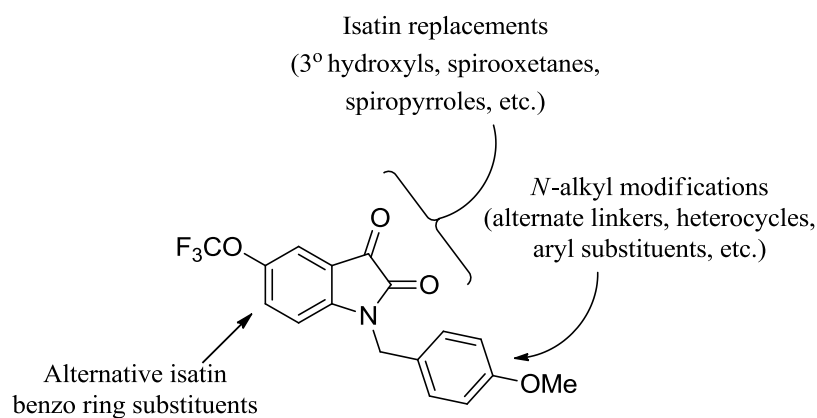


Figure 3.2. Structure and activity of VU0366369 (**3.5**). Multiple productive replacements (tertiary hydroxyls, dioxolanes, and spirocyclic tetrahydrofurans/pyrrolidines) were identified for the isatin core of **3.5** that maintained selective M₁ PAM activity⁷⁶⁻⁷⁸.

We were encouraged in this effort by a previous project in our lab based around a similar isatin pharmacophore: the highly selective, isatin-based M₁ PAM, **3.5**

(VU0366369; **Figure 3.2**)⁷⁶⁻⁷⁸. In exploring the SAR surrounding **3.5**, a number of replacements for the isatin moiety were discovered that maintained M₁ PAM activity while offering novel SAR and relieving the potential DMPK liability of the isatin ketone⁷⁶⁻⁷⁸. Therefore, our optimization plan for **3.2** emulated this campaign, evaluating spirocyclic and tertiary hydroxyl replacements for the isatin moiety, while also continuing to investigate the rich SAR of the southern *N*-benzyl region in an effort to furnish a novel M₅ PAM possessing a satisfactory DMPK profile and potency in the submicromolar range (**Figure 3.3**).



3.2

VU0238429, aka ML129

hM₅ EC₅₀ = 1.1 μM, %ACh_{Max} = 91

hM₅ ACh fold shift (at 30 μM) = 14-fold

hM₁-hM₄ EC₅₀ >30 μM

Figure 3.3. Structure, planned SAR exploration, potency, and selectivity of M₅ PAM **3.2** (VU0238429).

Optimization of VU0238429 to obtain the first sub-micromolar M₅ PAM VU0467903

Replacement of the isatin carbonyl with tertiary hydroxyl moieties

The keto-amide moiety of **3.2** (VU0238429) was of particular interest for removal or substitution due to the 3-keto moiety's reactivity as an electrophile. This reactivity could lead to multiple problems in a biological system, including transient reactions with endogenous nucleophiles or the irreversible covalent inhibition of cysteine proteases⁷⁹. Furthermore, it was hypothesized that the 3-keto may also represent a DMPK liability as a substrate for efflux pumps.

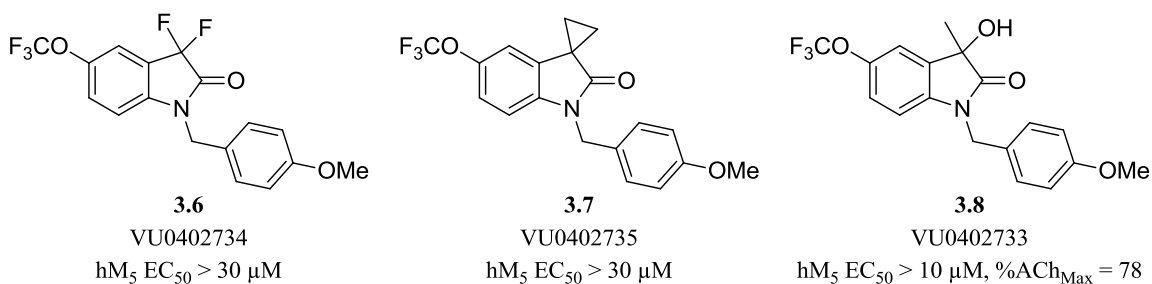
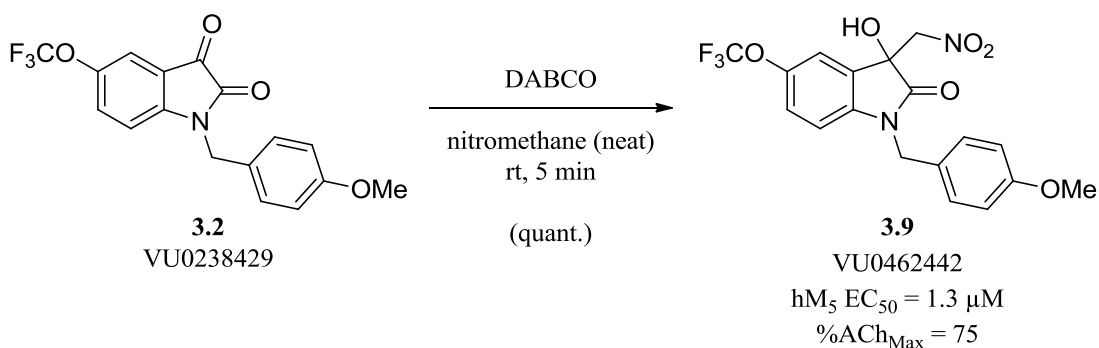


Figure 3.4. Structures and potencies of previously studied replacements for the 3-keto moiety of the isatin chemical scaffold⁸⁰.

Previous SAR in this region revealed that any attempt to remove the 3-position ketone resulted in loss of activity. The exception to this pattern was a 3-hydroxyl-3-methyl analog **3.8** which maintained activity, albeit at greatly decreased potency (**Figure 3.4**)⁸⁰. Thus we set out to more extensively explore tertiary hydroxyl moieties possessing diverse functionalities.

Treatment of **3.2** with DABCO in neat nitromethane afforded our first tertiary alcohol analog **3.9** in quantitative yield (**Scheme 3.1**)⁸¹. Upon evaluating compound **3.9**

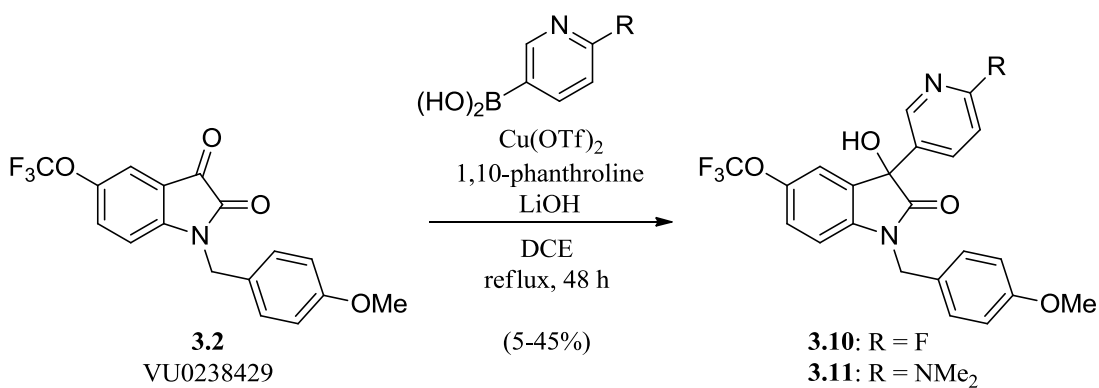
in a full CRC Ca^{2+} mobilization assay at hM_5 in the presence of an ACh EC_{20} , we observed that **3.9** maintained PAM activity and was of comparable potency and efficacy to **3.2** ($\text{hM}_5 \text{EC}_{50} = 1.3 \mu\text{M}$, 75% ACh_{Max}). Although this result encouraged us to further pursue a library of tertiary alcohol analogs, **3.9** itself was not attractive as a probe due to the metabolic instability of its nitro moiety.



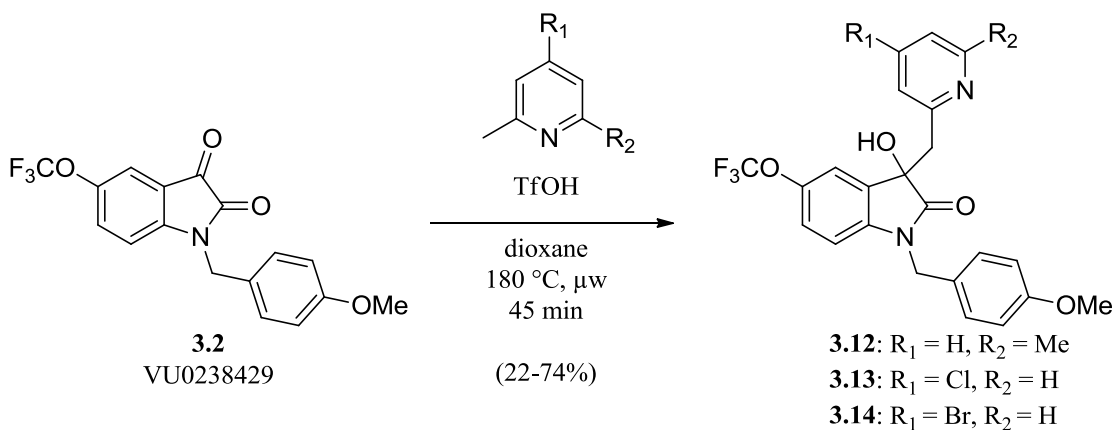
Scheme 3.1. Synthesis and activity of compound **3.9** (VU0462442). Ca^{2+} mobilization assays in hM_5 cells were used to obtain CRCs of compound **3.9** in the presence of a fixed submaximal ($\sim \text{EC}_{20}$) concentration of ACh. Data represent the mean of at least 3 independent experiments with similar results.

We next pursued a small library of tertiary alcohols possessing substituted pyridines. Here, we employed two synthetic routes to survey pyridyl analogs **3.10** and **3.11**, and pyridyl methyl homologs **3.12-3.14**. Utilizing **3.2** as a starting material, exposure to functionalized pyridyl boronic acids under $\text{Cu}(\text{OTf})_2$ catalysis afforded analogs **3.10** and **3.11** (Scheme 3.2)⁸². It should be noted that the synthesis of multiple pyridyl analogs was attempted using this procedure; however, yields were miniscule and pure compound could not be isolated for biological testing. The homologated congeners **3.12-3.14** were accessed utilizing substituted picolines under Brønsted acid catalysis (Scheme 3.3)⁸³. When tested in single point (30 μM) Ca^{2+} mobilization assays at hM_5 in

the presence of an ACh \sim EC₂₀, SAR proved to be shallow, with most analogs demonstrating little or no PAM activity (**Figure 3.5, Table 3.1**). Only compound **3.10** displayed any considerable activity, potentiating the ACh EC₂₀ to 77% of the ACh maximum in the 30 μ M single point assay. When Ca²⁺ mobilization assays were performed at hM₅ to obtain full CRCs of **3.10** in the presence of an ACh EC₂₀, we observed the compound to have low micromolar activity (hM₅ EC₅₀ = 2.0 μ M, ACh_{Max} = 73; **Figure 3.6**).



Scheme 3.2. Copper-mediated synthesis of tertiary hydroxyl library compounds **3.10** and **3.11**⁸².



Scheme 3.3. Brønsted acid catalyzed synthesis of picolines to form homologated tertiary hydroxyl library compounds **3.12-3.14**⁸³.

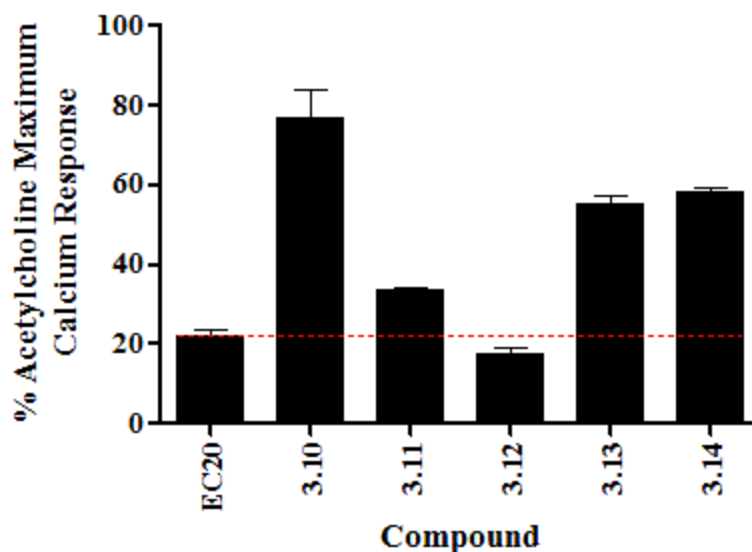
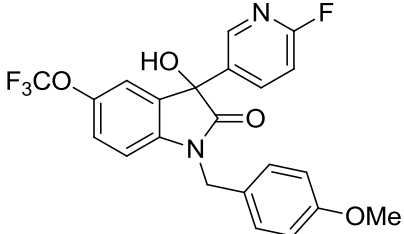
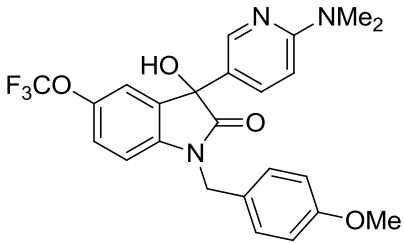
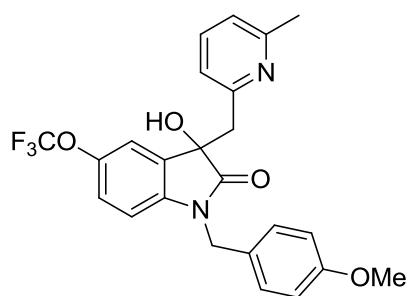


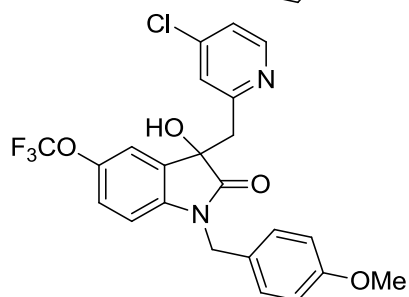
Figure 3.5. Comparison of the single point (30 μ M) screen results of the tertiary hydroxyl library, analogs **3.10-3.14**. Ca^{2+} mobilization was used to obtain $\%ACh_{\text{Max}}$ values for each compound in the presence of a fixed submaximal ($\sim EC_{20}$) concentration of ACh in cell lines expressing hM_5 . Data represent the mean \pm S.E.M. of at least 3 replicate experiments with similar results.

Table 3.1. Structures for tertiary hydroxyl analogs **3.10-3.14** and associated PAM activity data from the single point (30 μ M) screen at hM_5 . Ca^{2+} mobilization responses for each compound are reported as a percentage of the maximum ACh response. VU number denotes the compound identifier assigned by Vanderbilt University. Data represent the mean of at least 3 replicate experiments with similar results.

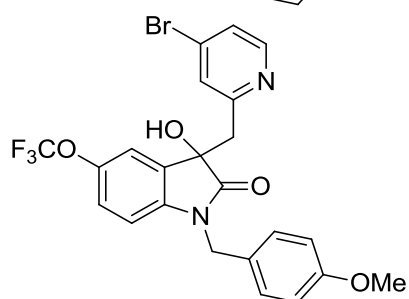
Structure	Cmpd #	VU #	hM_5 $\%ACh_{\text{Max}}$
	3.10	VU0464634	76.9
	3.11	VU0464633	33.7



3.12 VU0465833 17.5



3.13 VU0465746 55.3



3.14 VU0465801 58.3

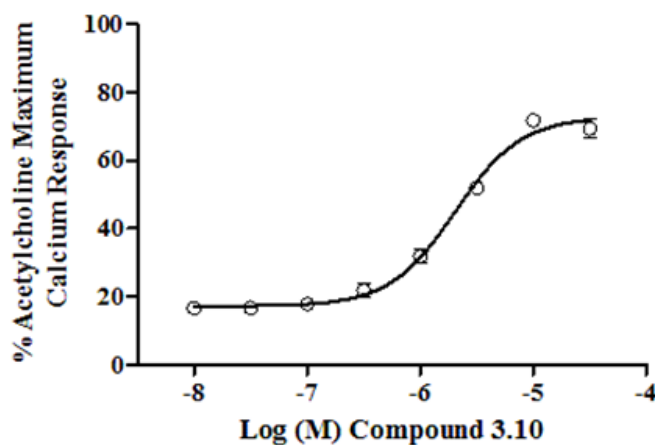
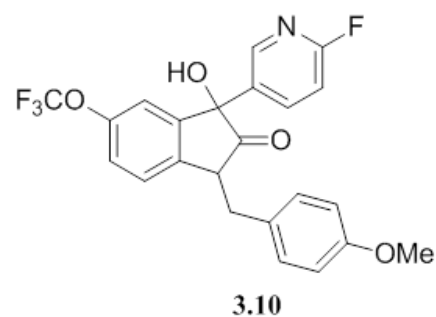
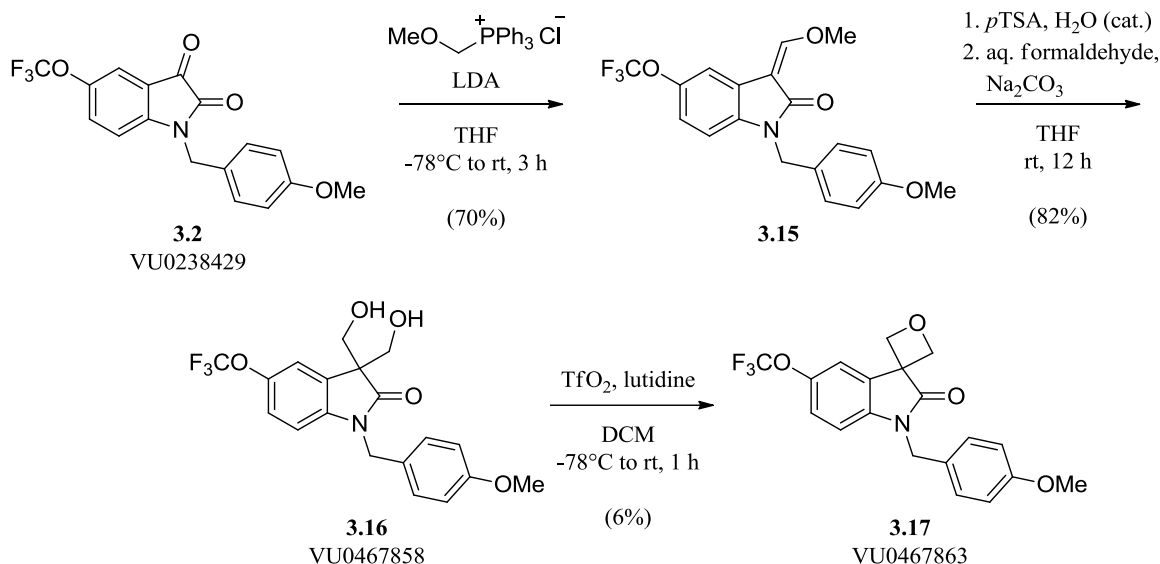


Figure 3.6. Structure, potency, and selectivity of benzamide analog **3.10** (VU0464634). Ca^{2+} mobilization assays with hM₅ cells were used to obtain CRCs of compound **3.10** in the presence of a fixed submaximal (~EC₂₀) concentration of ACh (EC₅₀ values: hM₅ EC₅₀ = 2.0 μM , %ACh_{Max} = 72.8). Data represent the mean \pm S.E.M. of at least 3 independent experiments with similar results.

Replacement of the isatin carbonyl with a spiro-oxetane bioisostere

In response to the shallow SAR surrounding the 3-carbonyl position, we elected to introduce a more subtle variant of the isatin carbonyl in the form of a spiro-oxetane, a common bioisostere of a carbonyl. In terms of improving the isatin DMPK profile, the oxetane offers several advantages over the carbonyl. Like a carbonyl, an spiro-oxetane has a similar spatial disposition and is an H-bond acceptor; however, unlike a carbonyl, the oxetane is more metabolically stable⁸⁴.

From **3.2**, a Wittig reaction with (methoxymethyl)triphenylphosphonium chloride provided **3.15**. In one pot, **3.15** was treated with pTSA to reveal the aldehyde which was subsequently converted to diol **3.16** under Aldol-Tishchenko reaction conditions. Mono-triflation of **3.16** and subsequent nucleophilic displacement proceeded in low yield (~6%) to the spiro-oxetane **3.17** (**Scheme 3.4**). Interestingly, both diol **3.16** and spiro-oxetane **3.17** were completely inactive in Ca^{2+} mobilization assays at hM_5 in the presence of an ACh $\sim\text{EC}_{20}$ ($\text{EC}_{50} \gg 30 \mu\text{M}$).



Scheme 3.4. Synthetic pathway to spiro-oxetane isatin carbonyl analog **3.17** (VU0467863).

Isatin core/phenethyl ether matrix library and the discovery of VU0467903

Concurrent with our efforts to optimize of **3.2**, an HTS campaign was initiated in 2012 in conjunction with SRIMSC under the MLPCN to directly interrogate the chemical landscape possessing selective M₅ functional activity. The HTS employed the MLPCN screening deck and was conducted using a single-point, triple-add, functional, fluorescence-based Ca²⁺ mobilization assay in CHO cell lines stably expressing hM₅ (see Chapter IV for a more detailed description of the 2012 M₅ HTS). Early in the analysis of this HTS, prior to official ‘hit’ confirmation, we noticed an isatin-based compound, CID2145491 (**3.18**), that registered as a weak single-point (31% ACh_{Max} at 30 μM) hit at hM₅ (**Figure 3.7**). This ‘hit’ possessed the familiar isatin core, but also a unique *N*-phenethyl ether substitution. Furthermore, we were intrigued to find an isatin compound lacking the 5-OCF₃ moiety, a SAR element previously observed to be vital to M₅-selectivity, which maintained activity at M₅.

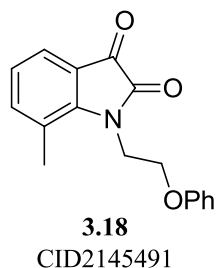


Figure 3.7. Structure of **3.18** (CID2145491), discovered in HTS of MLPCN screening deck.

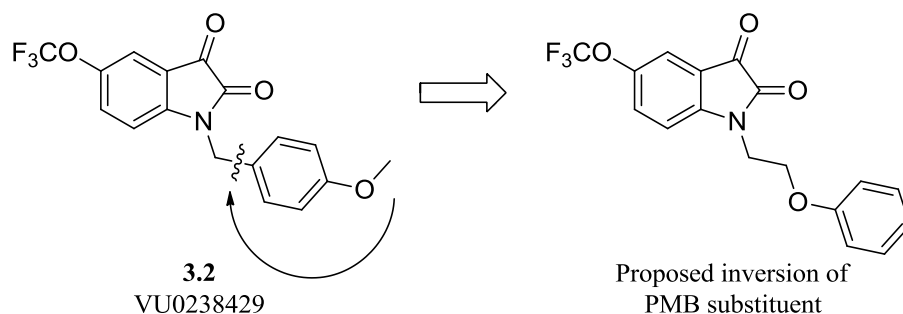
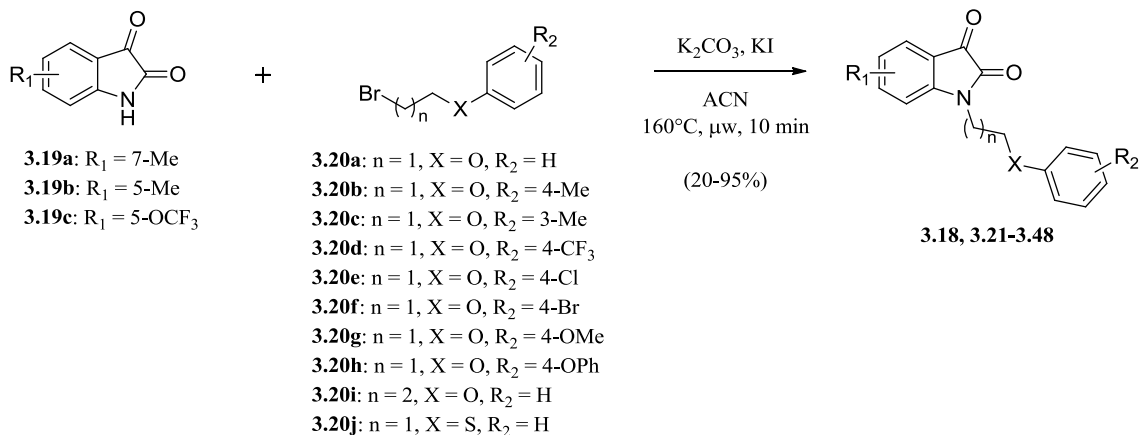


Figure 3.8. Structure of **3.2** (VU0238429) and the proposed structure resulting from the juxtaposition of structural elements from HTS lead compound **3.18**.

We immediately questioned whether the juxtaposition of the **3.2** 5-OCF₃ isatin core with the phenethyl ether moiety of compound **3.18** would lead to an improved M₅ PAM. Structurally, a juxtaposed analog would be comparable to a disconnection and inversion of the **3.2** *N*-*p*-methoxybenzyl group (**Figure 3.8**). Thus a matrix library was constructed comparing 5-OCF₃ and 7-methyl isatin cores. We also included 5-methyl isatin cores in order to determine if the activity of an isatin methyl substituent might transfer to alternative positions. Ten *N*-phenethyl ether variants were then selected to cross with the three isatin cores. These phenethyl ether analogs were selected with the goal of exploring multiple dimensions of SAR around this moiety, including substitution of the phenyl ring, variation of the ether, and homologation of the alkyl chain.



Scheme 3.5. Matrix library synthesis of analogs **3.18, 3.21-3.48**.

All matrix library analogs, including a resynthesis of the HTS lead **3.18**, were prepared by alkylating the core isatin with alkyl halide versions of the phenethyl ether analogs under microwave-assisted conditions (**Scheme 3.5**). The PAM activity of the library analogs was subsequently tested in single-point (30 μ M) Ca²⁺ mobilization assays at hM₅ in the presence of an ACh \sim EC₂₀ (**Figure 3.9, Table 3.2**).

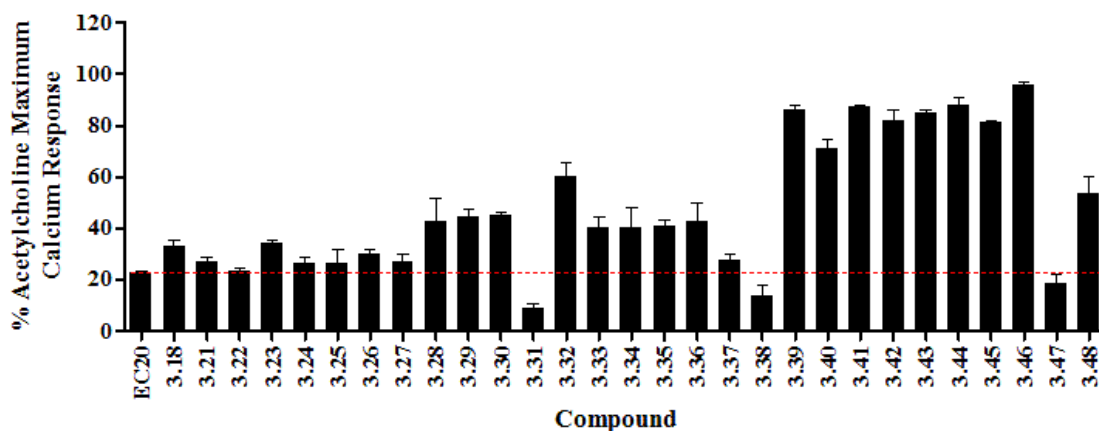
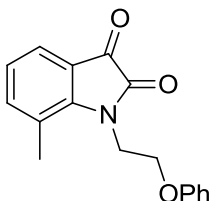
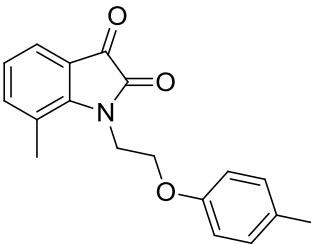
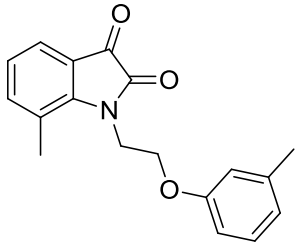
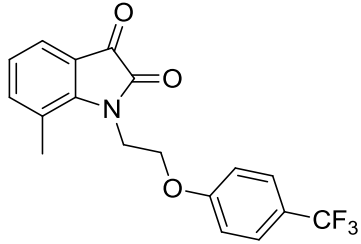
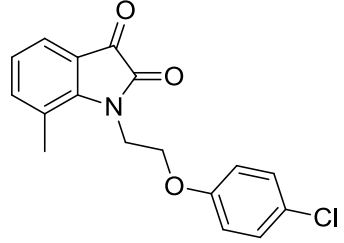
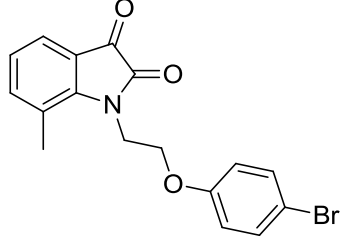
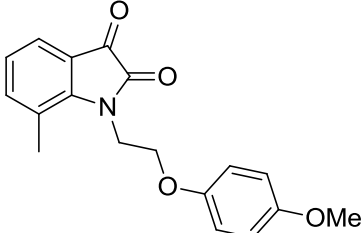
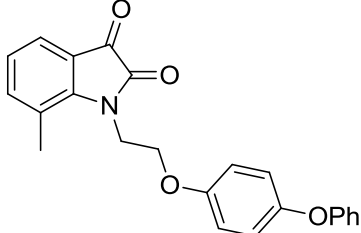
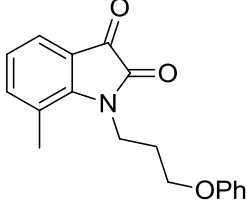
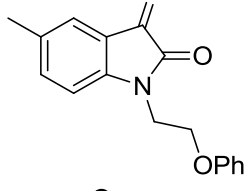
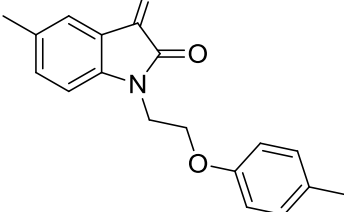
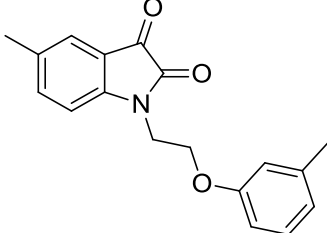
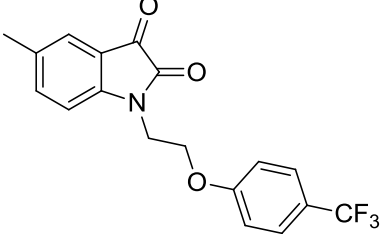
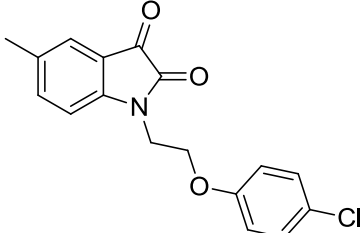
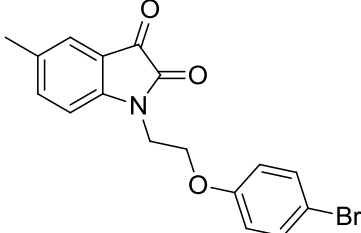
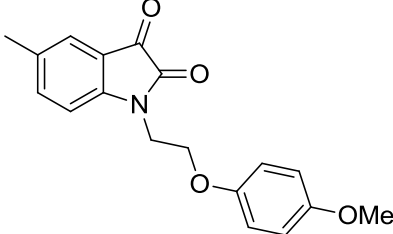
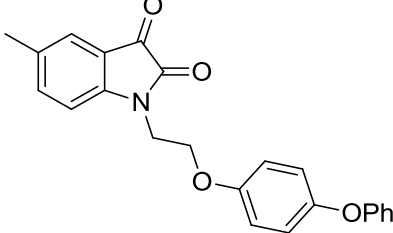
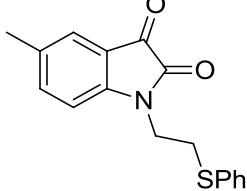
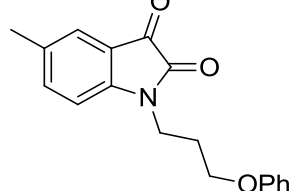
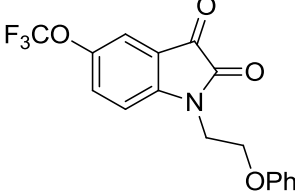


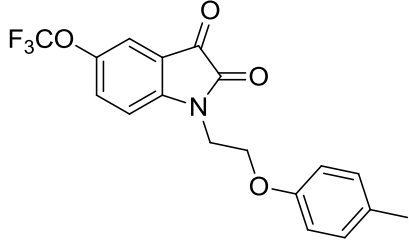
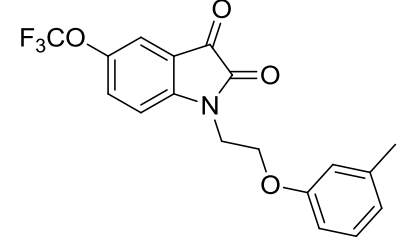
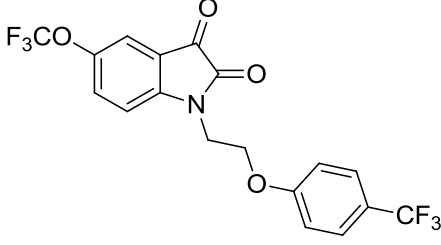
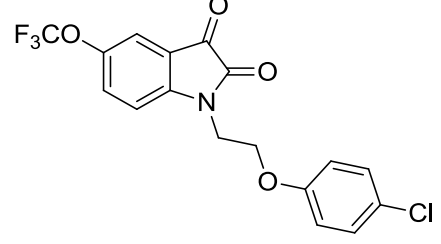
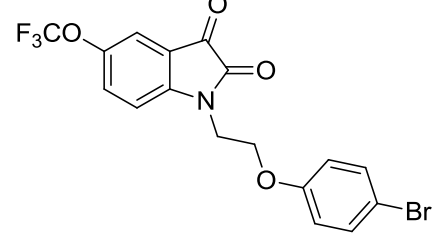
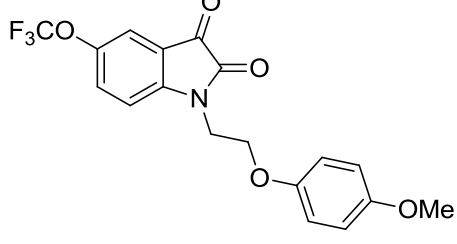
Figure 3.9. Comparison of the single point (30 μ M) screen results of the isatin matrix library, analogs **3.18, 3.21-3.48**. Ca²⁺ mobilization was used to obtain %ACh_{Max} values for each compound in the presence of a fixed submaximal (\sim EC₂₀) concentration of ACh in cell lines expressing hM₅. Data represent the mean \pm S.E.M. of at least 3 replicate experiments with similar results.

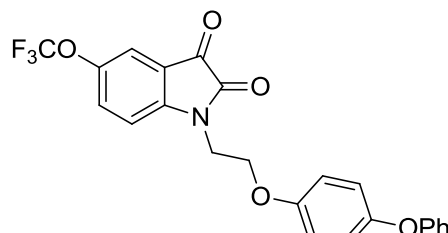
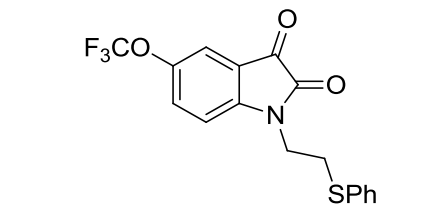
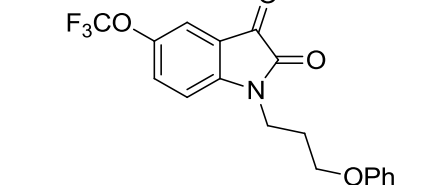
Table 3.2. Structures for matrix library analogs **3.18**, **3.21-3.48** and associated PAM activity data from the initial single point (30 μ M) screen at hM₅. Ca²⁺ mobilization responses for each compound are reported as a percentage of the maximum ACh response. VU number denotes the compound identifier assigned by Vanderbilt University. Data represent the mean of at least 3 replicate experiments with similar results.

Structure	Cmpd #	VU #	hM ₅ %ACh _{Max}
	3.18	VU0336754	33.1
	3.21	VU0297422	26.8
	3.22	VU0267572	23.1
	3.23	VU0468696	34.2
	3.24	VU0468939	26.5
	3.25	VU0468703	26.7

	3.26	VU0469051	29.9
	3.27	VU0469065	27.3
	3.28	VU0195631	42.6
	3.29	VU0294899	44.7
	3.30	VU0297289	45.0
	3.31	VU0300264	8.8
	3.32	VU0468709	60.5

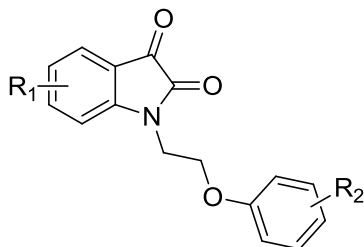
	3.33	VU0468998	40.4
	3.34	VU0468654	40.4
	3.35	VU0468952	40.9
	3.36	VU0468949	42.6
	3.37	VU0468683	27.9
	3.38	VU0288396	13.6
	3.39	VU0467903	85.8

	3.40	VU0467974	70.8
	3.41	VU0468196	87.5
	3.42	VU0468690	81.9
	3.43	VU0468957	84.7
	3.44	VU0468685	87.8
	3.45	VU0468948	81.5

	3.46	VU0469054	95.8
	3.47	VU0468702	18.6
	3.48	VU0467973	53.5

The single-point data revealed eight compounds that potentiated the ACh EC₂₀ to >70% at 30 μM. Notably, all of these compounds possessed the 5-OCF₃ substituted isatin core, while all methyl substituted isatin core analogs appeared relatively inactive. Furthermore, this group of highly active compounds included compound **3.39**, which represents the envisioned juxtaposition of structural elements from **3.2** and **3.18** shown in **Figure 3.8**. Potency data for all eight highly active compounds as well as the HTS lead compound **3.18** was subsequently obtained in CRC Ca²⁺ mobilization assays at hM₅ in the presence of an ACh ~EC₂₀ (**Table 3.3**).

Table 3.3. Potencies at hM₅ and hM₃ for the 8 highly active matrix library analogs selected from the initial single point (30 μM) screen. Also included is the hM₅ CRC data for the HTS lead **3.18**. Ca²⁺ mobilization assays with hM₅ cells were used to obtain CRCs of compounds in the presence of a fixed submaximal (~EC₂₀) concentration of ACh. Data represent the mean of at least 3 independent experiments with similar results. ---, not determined.



Cmpd #	R ₁ =	R ₂ =	hM ₅		hM ₃	
			EC ₅₀ (μM)	%ACh _{Max}	EC ₅₀ (μM)	%ACh _{Max}
3.18	7-Me	H	>>30	---	---	---
3.39	5-OCF ₃	H	0.41	90.5	>30	52.9
3.40	5-OCF ₃	4-Me	0.52	89.8	---	---
3.41	5-OCF ₃	3-Me	0.52	91.4	---	---
3.42	5-OCF ₃	4-CF ₃	0.35	94.1	6.7	78.4
3.43	5-OCF ₃	4-Cl	0.45	92.3	---	---
3.44	5-OCF ₃	4-Br	1.4	96.7	---	---
3.45	5-OCF ₃	4-OMe	0.59	88.6	---	---
3.46	5-OCF ₃	4-OPh	1.1	92.7	---	---

Curiously, HTS lead compound **3.18** proved to be devoid of PAM activity. Despite this, we were pleased to see that six of the eight compounds tested displayed potencies in the submicromolar range. The most potent of these, **3.39** (VU0467903) and **3.42** (VU0468690), were counterscreened in Ca²⁺ mobilization assays at hM₃ in the presence of an ACh ~EC₂₀ to ascertain their general selectivity for M₅ (**Table 3.3**). Both compounds showed weak activity at hM₃; however, **3.39** displayed a greater selectivity window for M₅.

In vitro pharmacological characterization of M₅ PAM VU0467903

Characterization of mAChR subtype selectivity of VU0467903

Encouraged by the selectivity of **3.39** (VU0467903) for hM₅ versus hM₃, a full mAChR subtype-selectivity profile was obtained. Counterscreening was carried out against the remaining human mAChR subtypes as well as for all rat mAChR subtypes (with M₂ and M₄ co-expressing G_{αq15}; **Figure 3.10**). The latter selectivity panel was performed to ensure that **3.39**, which had so far been only tested on human isoforms of the mAChRs, was active and selective at rat isoforms as well. This examination of species difference was an important step as we ultimately desired an *in vivo* tool compound with which to study M₅ in the CNS, and rat is the standard *in vivo* model system for such studies.

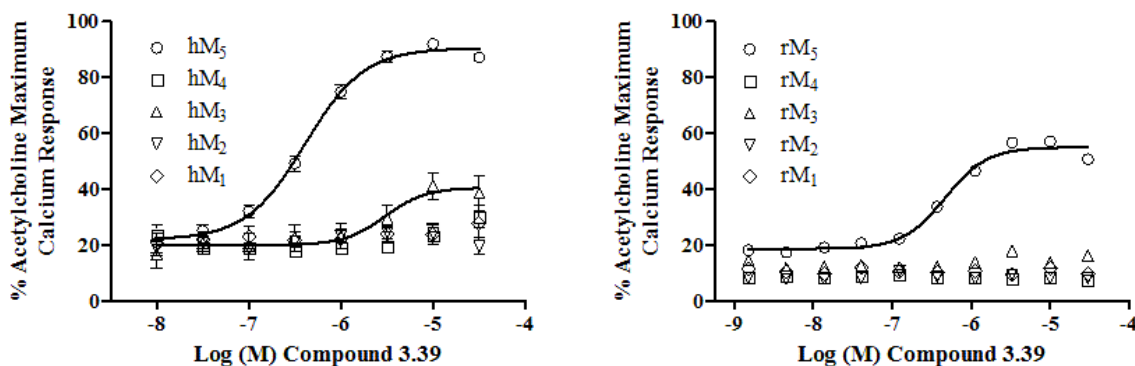


Figure 3.10. Potency and selectivity of compound **3.39** (VU0467903) at all human and rat mAChR subtypes. Ca²⁺ mobilization assays with hM₁-hM₅ cells and with rM₁-rM₅ cells (M₂ and M₄ co-expressing G_{αq15}) were used to obtain CRCs of **3.39** in the presence of a fixed submaximal (~EC₂₀) concentration of ACh (EC₅₀ values: hM₅ EC₅₀ = 0.41 μM, %ACh_{Max} = 91; hM₃ EC₅₀ = 3.0 μM, %ACh_{Max} = 41; hM₁, hM₂, hM₄ EC₅₀ >30 μM; rM₅ EC₅₀ = 0.47 μM, %ACh_{Max} = 55; rM₁-rM₄ EC₅₀ >30 μM). Data represent the mean ± S.E.M. of at least 3 independent experiments with similar results. Note: human selectivity studies were performed in standard double-add mode on a Molecular Devices FLEXStation II, while rat studies were performed in triple-add mode on a Hamamatsu FDSS 6000. Rat selectivity studies performed by A. Lamasal.

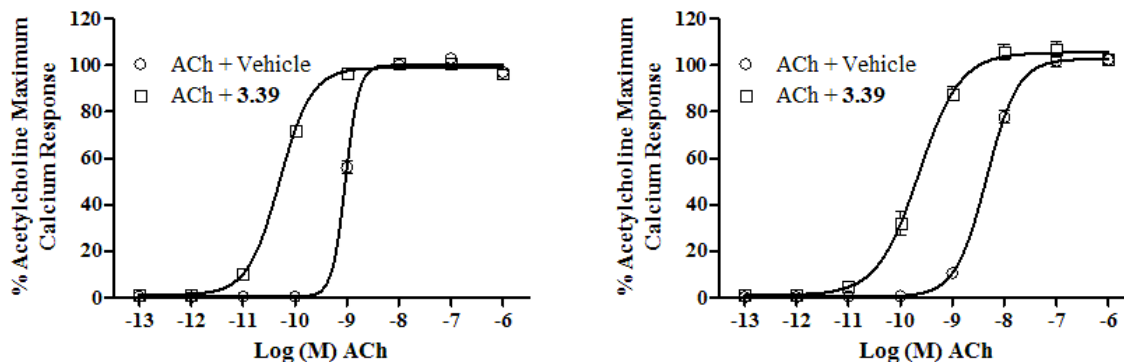


Figure 3.11. ACh CRC fold-shifts of compound **3.39** (VU0467903) at hM₅ (left panel) and rM₅ (right panel). Ca²⁺ mobilization assays with hM₅ cells and rM₅ cells were used to obtain ACh CRCs in the presence of vehicle or 30 μ M compound **3.39** (EC₅₀ values: hM₅ EC₅₀ of ACh + vehicle = 933 pM, hM₅ EC₅₀ of ACh + **3.39** = 50.4 pM, hM₅ fold-shift = 18.5; rM₅ EC₅₀ of ACh + vehicle = 4.58 nM, rM₅ EC₅₀ of ACh + **3.39** = 225 pM, rM₅ fold-shift = 20.4). Data represent the mean \pm S.E.M. of at least 3 independent experiments with similar results.

The mAChR selectivity panel revealed that **3.39** possesses good selectivity for M₅ in both rat and human isoforms (hM₅ EC₅₀ = 0.41 μ M, %ACh_{Max} = 91; hM₃ EC₅₀ = 3.0 μ M, %ACh_{Max} = 41; hM₁, hM₂, hM₄ EC₅₀ >30 μ M; rM₅ EC₅₀ = 0.47 μ M, %ACh_{Max} = 55; rM₁-rM₄ EC₅₀ >30 μ M). Further characterization of the compound's efficacy was probed in ACh fold shift assays. In these assays **3.39** (30 μ M) induced a robust 20-fold leftward shift of the ACh CRC in rM₅ and 19-fold leftward shift in hM₅ (**Figure 3.11**). Based on the unprecedented submicromolar potency, M₅-selectivity, and ACh fold shift exhibited by compound **3.39**, it was declared an MLPCN probe and given the identifier ML326.

Confirmation of the allosteric mechanism of VU0467903

Although evidence of an allosteric mode of action for **3.39** (VU0467903, ML326) was strongly supported by its behavior in double-add Ca²⁺ mobilization assays (i.e. – **3.39** displays no intrinsic activity, yet potentiates an ACh EC₂₀) and by prior [³H]-NMS competition binding data on the parent compound **3.2**, we nonetheless desired to confirm

an allosteric mechanism via [³H]-NMS competition binding with **3.39** (Figure 3.12). As predicted, the study revealed that, when competing with the orthosteric antagonist [³H]-NMS in hM₅ membrane preparations, **3.39** does not compete for the orthosteric site. This competition binding data, when taken into account with the aforementioned evidence of an allosteric mechanism, strongly suggests that **3.39** is indeed an allosteric modulator.

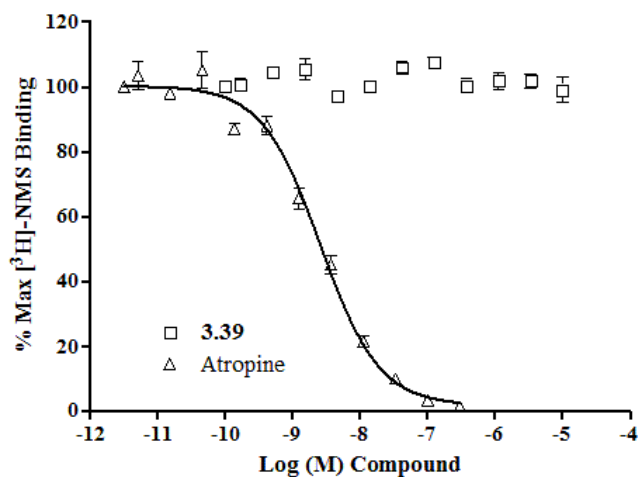


Figure 3.12. [³H]-NMS competition binding assay with **3.39** (VU0467903, ML326) in an hM₅ membrane preparation. [³H]-NMS and a CRC of either Atropine (control) or **3.39** were allowed to equilibrate for 3 hours in the hM₅ membrane preparation before filtration and scintillation counting (K_i values: Atropine $K_i = 1.57$ nM, **3.39** $K_i \gg 10$ μ M). Data represent the mean \pm S.E.M. of at least 3 independent experiments with similar results.

Ancillary pharmacology of the VU0467903

In order to obtain a general impression of the propensity for off-target binding by compound **3.39**, it was entered into a commercial radioligand competition binding screen of 67 GPCRs, ion channels, and transporters (Table 3.4). Unfortunately this screen revealed that **3.39** competed with ligand binding significantly at numerous off-target GPCRs and transporters, including NET.

Table 3.4. Ancillary/off-target competition binding screen results for **3.39** (VU0467903, ML326). **3.39** was dosed at 10 μ M for single point competition binding assays. Targets displaying significant binding ($\geq 50\%$ at 10 μ M) are outlined. Data represent the mean of 2 independent experiments with similar results. Studies performed by Eurofins Panlabs, Inc.

Target/Protein	Species	% Inhibition
Adenosine A ₁	Human	-3
Adenosine A _{2A}	Human	7
Adenosine A ₃	Human	57
Adrenergic α_{1A}	Rat	71
Adrenergic α_{1B}	Rat	66
Adrenergic α_{1D}	Human	44
Adrenergic β_1	Human	33
Adrenergic β_2	Human	8
Androgen (Testosterone) AR	Rat	24
Bradykinin B ₁	Human	12
Bradykinin B ₂	Human	5
Calcium Channel L-Type, Benzothiazepine	Rat	-16
Calcium Channel L-Type, Dihydropyridine	Rat	44
Calcium Channel N-Type	Rat	1
Cannabinoid CB ₁	Human	72
Dopamine D ₁	Human	73
Dopamine D _{2S}	Human	31
Dopamine D ₃	Human	59
Dopamine D _{4.2}	Human	46
Endothelin ET _A	Human	44
Endothelin ET _B	Human	3
Epidermal Growth Factor (EGF)	Human	4
Estrogen ER α	Human	5
GABA _A , Flunitrazepam, Central	Rat	-2
GABA _A , Muscimol, Central	Rat	6
GABA _{B1A}	Human	-3
Glucocorticoid	Human	88
Glutamate, Kainate	Rat	-5
Glutamate, NMDA, Agonism	Rat	9
Glutamate, NMDA, Glycine	Rat	19
Glutamate, NMDA, Phencyclidine	Rat	4
Histamine H ₁	Human	41
Histamine H ₂	Human	95
Histamine H ₃	Human	-3
Imidazoline I ₂ , Central	Rat	33
Interleukin IL-1	Mouse	-2
Leukotriene, Cysteinyl CysLT ₁	Human	26
Melatonin MT ₁	Human	40
Muscarinic M ₁	Human	22
Muscarinic M ₂	Human	-2
Muscarinic M ₃	Human	-2

Neuropeptide Y Y ₁	Human	29
Neuropeptide Y Y ₂	Human	12
Nicotinic Acetylcholine	Human	-26
Nicotinic Acetylcholine α 1, Bungarotoxin	Human	5
Opiate δ ₁ (OP1, DOP)	Human	12
Opiate κ (OP2, KOP)	Human	42
Opiate μ (OP3, MOP)	Human	78
Phorbol Ester	Mouse	9
Platelet Activating Factor (PAF)	Human	37
Potassium Channel [K _{ATP}]	Human	10
Potassium Channel hERG	Human	21
Prostanoid EP ₄	Human	-3
Purinergic P2X	Rabbit	4
Purinergic P2Y	Rat	4
Rolipram	Rat	-6
Serotonin (5-HT _{1A})	Human	-9
Serotonin (5-HT _{2B})	Human	1
Serotonin (5-HT ₃)	Human	-12
Sigma σ ₁	Human	-35
Sodium Channel, Site 2	Rat	38
Tachykinin NK ₁	Human	-19
Thyroid Hormone	Rat	2
Transporter, Dopamine (DAT)	Human	42
Transporter, GABA	Rat	7
Transporter, Norepinephrine (NET)	Human	77
Transporter, Serotonin (SERT)	Human	8

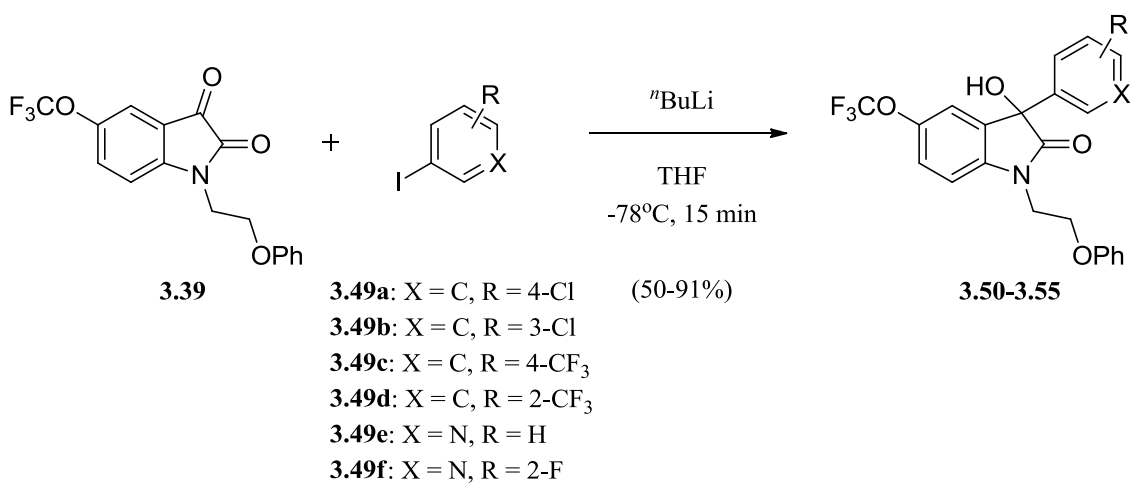
Continued optimization of M₅ PAM VU0467903

Replacement of the isatin carbonyl in the presence of the phenethyl ether moiety

In light of the great increase in potency provided by the *N*-phenethyl ether substitution, we questioned if the chemical scaffold may now tolerate a substitution of the isatin carbonyl. Thus we again turned our efforts to substituting the isatin carbonyl with spirocyclic heterocycles and tertiary hydroxyl moieties.

The low yields of the reactions previously employed to synthesize tertiary hydroxyl analogs (*vide supra*) compelled us to employ the more reliable method of direct

lithiation to construct a small library of tertiary hydroxyl analogs in the context of the southern phenethyl ether moiety. The treatment of heteroaryl iodides with ${}^n\text{BuLi}$ before the addition of **3.39** produces the desired tertiary hydroxyl analogs **3.50-3.55** swiftly and in high yields (**Scheme 3.6**). In addition to heterocyclic analogs, we utilized methyl lithium to synthesize the 3-hydroxy-3-methyl analog **3.56** to mimic the substitution previously observed to be weakly active in analog **3.8** of the **3.2** series of M_5 PAMs (**Figure 3.4**). The library analogs were subsequently tested in single-point (30 μM) Ca^{2+} mobilization assays to assess their activity (**Figure 3.13**, **Table 3.5**).



Scheme 3.6. Library synthesis of tertiary hydroxyl isatin analogs **3.50-3.55**.

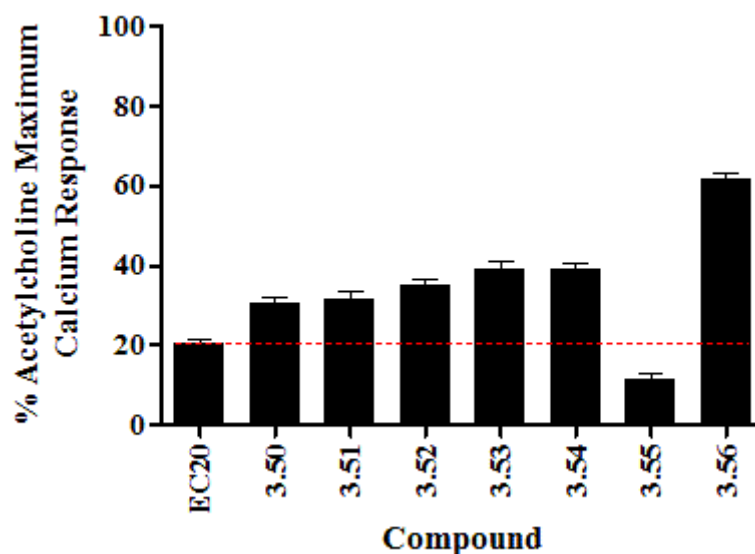
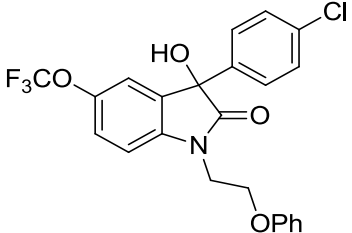
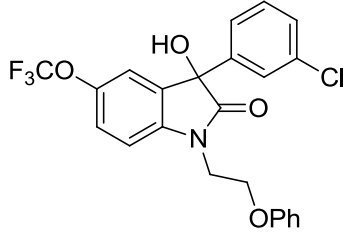
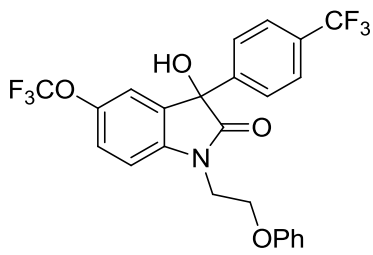
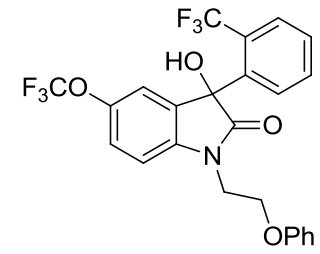
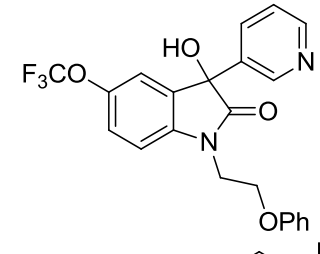
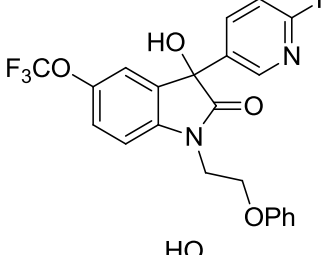
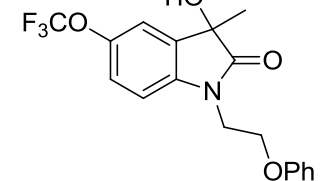


Figure 3.13. Comparison of the single point (30 μM) screen results of the tertiary hydroxyl library, analogs **3.50-3.56**. Ca^{2+} mobilization was used to obtain $\%ACh_{\text{Max}}$ values for each compound in the presence of a fixed submaximal ($\sim EC_{20}$) concentration of ACh in cell lines expressing hM_5 . Data represent the mean \pm S.E.M. of at least 3 replicate experiments with similar results.

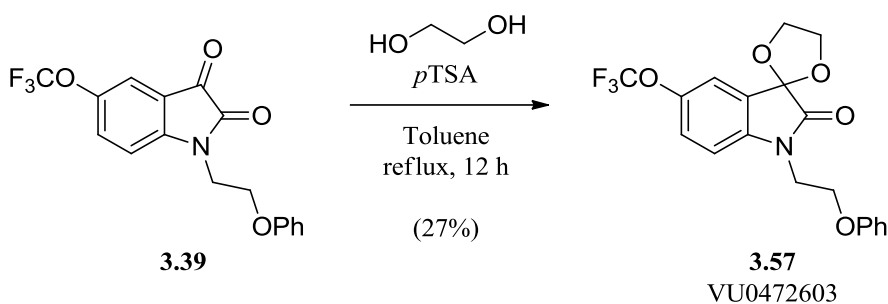
Table 3.5. Structures for tertiary hydroxyl analogs **3.50-3.56** and associated PAM activity data from the single point (30 μM) screen at hM_5 . Ca^{2+} mobilization responses for each compound are reported as a percentage of the maximum ACh response. VU number denotes the compound identifier assigned by Vanderbilt University. Data represent the mean of at least 3 replicate experiments with similar results.

Structure	Cmpd #	VU #	hM_5 $\%ACh_{\text{Max}}$
	3.50	VU0472634	30.6
	3.51	VU0472612	31.5

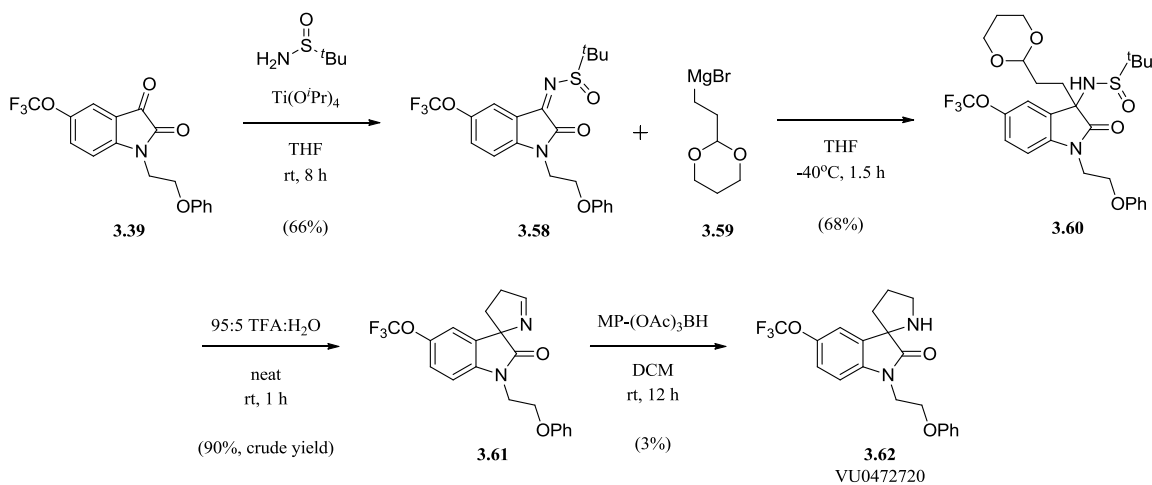
	3.52	VU0472606	35.1
	3.53	VU0472601	38.8
	3.54	VU0472617	39.1
	3.55	VU0472826	11.4
	3.56	VU0470221	61.5

Even in the context of the southern phenethyl ether moiety, no tertiary hydroxyl analogs exhibited any notable PAM activity at 30 μM . The best response was given by the 3-hydroxy-3-methyl analog **3.56**; however, upon testing in a full CRC Ca^{2+} mobilization assay at hM_5 in the presence of an ACh $\sim\text{EC}_{20}$ this analog displayed weak potency ($\text{hM}_5 \text{EC}_{50} > 10 \mu\text{M}$, $\% \text{ACh}_{\text{Max}} = 67$).

We next combined the phenethyl ether SAR with spirocyclic replacements for the isatin ketone. Spiro-pyrrolidine and spiro-dioxolane analogs were chosen as targets due to the activity these moieties displayed when applied to the M₁ PAM isatin scaffold **3.5**.



Scheme 3.7. Structure and synthesis of spiro-dioxolane analog **3.57** (VU0472603).



Scheme 3.8. Structure and synthesis of spiro-pyrrolidine analog **3.62** (VU0472720).

The spiro-dioxolane analog **3.57** was easily accessed by treating **3.39** with *p*TSA and ethylene glycol (**Scheme 3.7**). The spiro-pyrrolidine analog synthesis began from **3.39** as well. Condensation with Ellman's sulfonamide provided intermediate **3.58** which was subsequently treated with Grignard reagent **3.59** to furnish intermediate **3.60**.

Deprotection of the aldehyde and amine was simultaneously accomplished by treatment with TFA to provide the dihydropyrrole **3.61**. Finally, MP-(OAc)₃BH was used to reduce the spirocycle to the pyrrolidine **3.62** (**Scheme 3.8**). Interestingly, when subjected to full CRC Ca²⁺ mobilization assays, neither of the spirocyclic analogs displayed PAM activity at hM₅, signifying a notable disconnect in isatin SAR between M₁ and M₅ PAMs.

***In vitro* and *in vivo* DMPK characterization of M₅ PAM VU0467903**

Discouraged by the intractable SAR around the isatin moiety, we returned to the highly potent and M₅-selective **3.39** (VU0467903, ML326) to characterize its DMPK profile via multiple assays, including plasma protein binding, rat brain homogenate binding, rat and human microsomal stability, and CYP inhibition studies. In addition to these *in vitro* assays, **3.39** was intravenously administered to male Sprague-Dawley rats at a dose of 1 mg/kg to determine *in vivo* rat PK/CNS exposure.

The CYP inhibition assay revealed that **3.39** possessed a relatively clean CYP profile (IC₅₀s: 1A2 = 1.5 μM; 2C9 = 8.6 μM; 2D6 = 11.3 μM; 3A4 = 7.5 μM); however, the remainder of the DMPK studies were halted as insurmountable LCMS/MS analytical quantization issues were encountered. Ionization of **3.39** using ESI, APPI, and APCI ionization probes all resulted in untraceable daughter ions which prevented the determination of DMPK parameters and *in vivo* rat exposure. Alternative methods of analysis, including chemical derivatization and UV absorbance also failed to provide the requisite sensitivity for detection of **3.39**. As a result of these issues, we were unable to complete DMPK characterization of **3.39**.

In response to our complications in characterizing the DMPK profile of **3.49**, we attempted DMPK characterization of other promising, highly potent M₅ PAM analogs such as **3.42**, **3.43**, **3.45** and **3.46**. Unfortunately, they too suffered from poor ionization profiles which precluded DMPK profiling.

Taking into account the lack of tractable SAR found in continued optimization attempts of **3.39**, the LCMS/MS ionization issues that precluded DMPK characterization, and the promising nature of separate, concurrently studied M₅-selective ligands (Chapters IV, V, and VI), further work at the optimization of compound **3.39** was put on hold.

Summary and future directions

In summary, we endeavored to improve the potency and metabolic stability of the first-generation, isatin-based M₅ PAM **3.2** (VU0238429, ML129) via targeted SAR exploration and optimization of the chemical scaffold. In the course of this optimization campaign we synthesized over 60 novel analogs, but SAR was found to be intractable and many of these analogs exhibited no activity at M₅. Insight from a weak M₅ PAM HTS lead **3.18** led to its hybridization with **3.2** and resulted in compound **3.39** (VU0467903, ML326), the first highly M₅-preferring and sub-micromolar M₅ PAM (**Figure 3.14**).

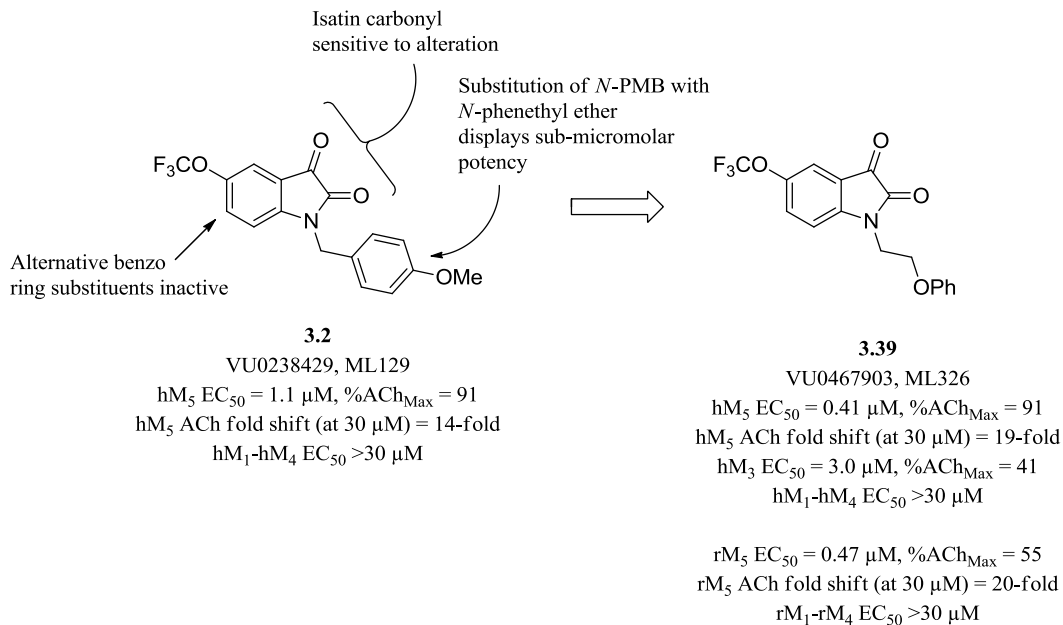


Figure 3.14. A summary and comparison of the structure, potency, and SAR found around the first M₅-preferring PAM **3.2** (VU0238429, ML129) that led to the discovery of the novel, sub-micromolar M₅ PAM **3.39** (VU0467903, ML326).

Future directions for the **3.39** chemical series are limited. Further optimization of the isatin M₅ PAM scaffold was halted due to the inability to obtain a detailed DMPK profile of **3.39** or its analogs due to the scaffold's poor ionization profile. As a result of this barrier to analysis, **3.39** and its analogs are unlikely to be utilized as *in vivo* tool compounds. This does not, however, preclude the use of the **3.39** M₅ PAM series as *in vitro* or *ex vivo* probes. Recently, M₅ was shown to be functional in a native system via an electrophysiological study of M₅ function carried out in mouse brain slices using the M₅ PAM **3.2** in conjunction with the acetylcholine analogs oxotremorine-M and carbachol. By using **3.2** to selectively potentiate M₅, this study revealed the differential effects of the M₅ receptor on dopaminergic neurons based upon where the receptor is physically located on the neuron²⁷. Thus, despite their limited utility as *in vivo* probes, the

present series of isatin-based M_5 PAMs hold the potential to be valuable *in vitro* probes for pharmacological studies of the potentiation of M_5 in the CNS.

Chapter IV

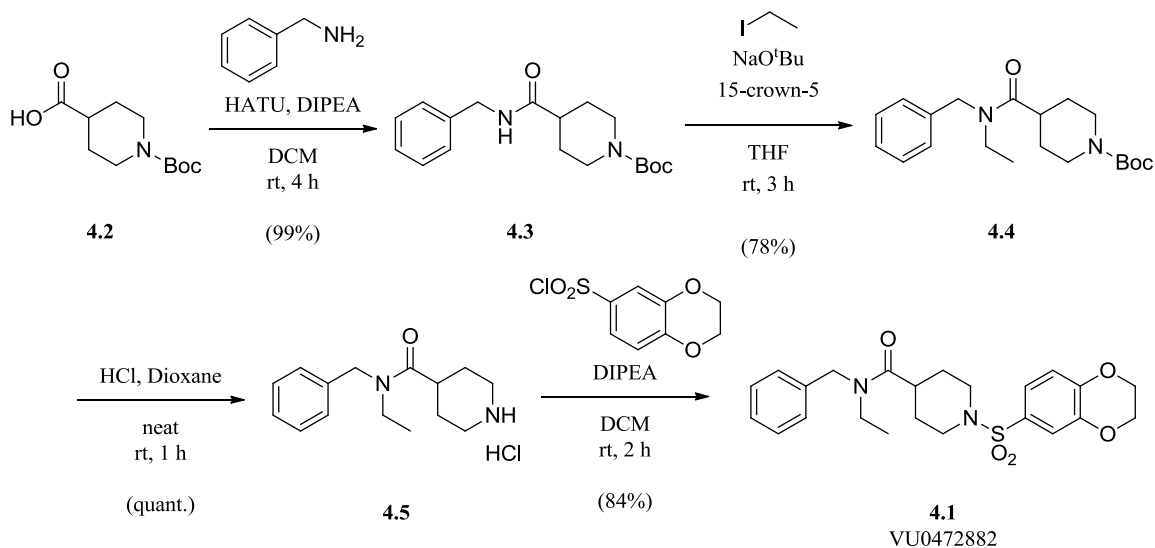
IDENTIFICATION, OPTIMIZATION, AND CHARACTERIZATION OF A NON-ISATIN M₅ POSITIVE ALLOSTERIC MODULATOR

HTS identification of a novel, M₅-selective ligand with PAM activity

The extensive study of the SAR surrounding isatin-based M₅ PAMs VU0238429 and VU0467903 (Chapter III) confirmed targeting the M₅ allosteric site as a viable strategy of gaining a high degree of M₅ selectivity^{70,71,74,75}. In response to this, an HTS campaign was initiated in 2012 in conjunction with SRIMSC under the MLPCN to directly interrogate the chemical landscape possessing selective M₅ functional activity. The HTS employed the MLPCN screening deck (~360,000 compounds at the time of screening, PubChem AID 624103), and was conducted using a single-point, triple-add, functional, fluorescence-based Ca²⁺ mobilization assay in CHO cell lines stably expressing hM₅. The triple-add mode (i.e. – test compound addition, followed by ACh EC₂₀ addition, followed by ACh EC₈₀ addition) is particularly advantageous to a HTS as it enables the screen to identify activators (agonists and PAMs), while also searching for inhibitors (antagonists and NAMs). The initial screen identified 3920 M₅ primary hits (1.07% hit rate). The primary hits were next counterscreened in the same manner against the parental CHO cell line and two CHO cell lines expressing hM₁ and hM₄, respectively (with M₄ co-expressing G_{αq15}). The compounds that appeared most promising as M₅ activators were then purchased from commercial sources as fresh powder and

reconfirmed in triple-add 10-point CRC experiments. This process resulted in the identification of nine confirmed M₅ PAMs as well as nine M₅ antagonists (two of which are discussed in chapters V and VI).

Owing to its novel chemotype and the modular composition, compound **4.1** (VU0472882) was deemed the most intriguing and structurally tractable M₅ PAM lead. The activity of the **4.1** was reconfirmed via in-house resynthesis and retesting in double-add CRC Ca²⁺ mobilization assays at all human mAChR subtypes as well as rM₅ (**Scheme 4.1, Figure 4.1**). This in-house resynthesis and reconfirmation was a vital step as lead compounds from HTS campaigns can occasionally fail to reconfirm. This failure can be caused by a variety of factors, including sample impurity, sample contamination, or incorrect structural assignment from the compound vendor or the HTS effort's compound management system.



Scheme 4.1. Synthesis of HTS lead compound **4.1** (VU0472882).

Beginning from the *N*-Boc protected carboxylic acid core **4.2**, a HATU-mediated peptide coupling with benzylamine furnished the secondary amide **4.3**. The amide was deprotonated with *tert*-butoxide followed by treatment with iodoethane to form tertiary amide **4.4**. Removal of the Boc protecting group was accomplished under standard anhydrous HCl conditions to provide HCl salt **4.5**. Finally, the secondary amine was sulfonylated with 1,4-benzodioxan-6-sulfonyl chloride to form the HTS lead compound **4.1** (Scheme 4.1). **4.1** was tested in CRC Ca²⁺ mobilization assays in CHO cell lines stably expressing individual human mAChR subtypes as well as rM₅. The HTS lead was verified to possess weak PAM activity at both human and rat isoform of M₅ (EC₅₀ >10 μM) and no activity was observed at hM₁-hM₄ (EC₅₀ >>30 μM; **Figure 4.1**); furthermore, at 10 μM **4.1** was found to shift the ACh CRC 2.3-fold at hM₅ and 2.5-fold at rM₅ (**Figure 4.2**).

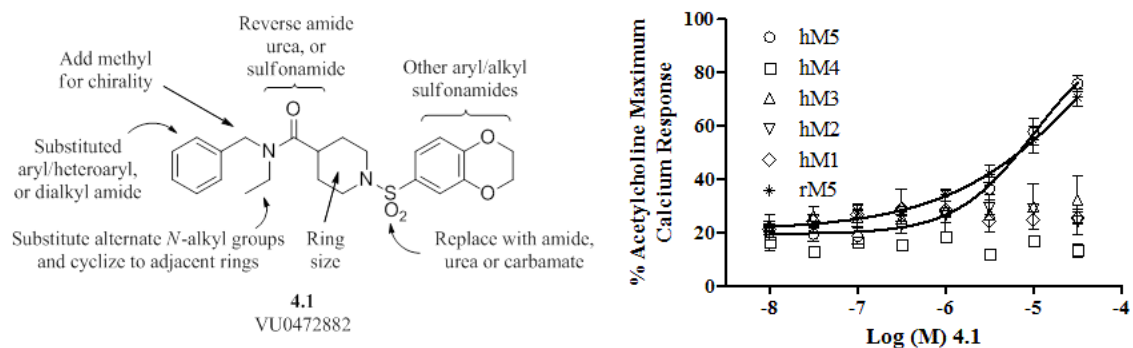


Figure 4.1. Structure, planned SAR exploration, potency, and selectivity of HTS hit compound **4.1** (VU0472882). Ca²⁺ mobilization assays with hM₁-hM₅ (M₂ and M₄ co-expressing G_{αq15}) and rM₅ cells were used to obtain CRCs of resynthesized compound **4.1** in the presence of a fixed submaximal (~EC₂₀) concentration of ACh (EC₅₀ values: hM₅ EC₅₀ > 10 μM, %ACh_{Max} = 76; hM₁-hM₄ EC₅₀ >>30 μM; rM₅ EC₅₀ > 10 μM, %ACh_{Max} = 71). Data represent the mean ± S.E.M. of at least 3 independent experiments with similar results.

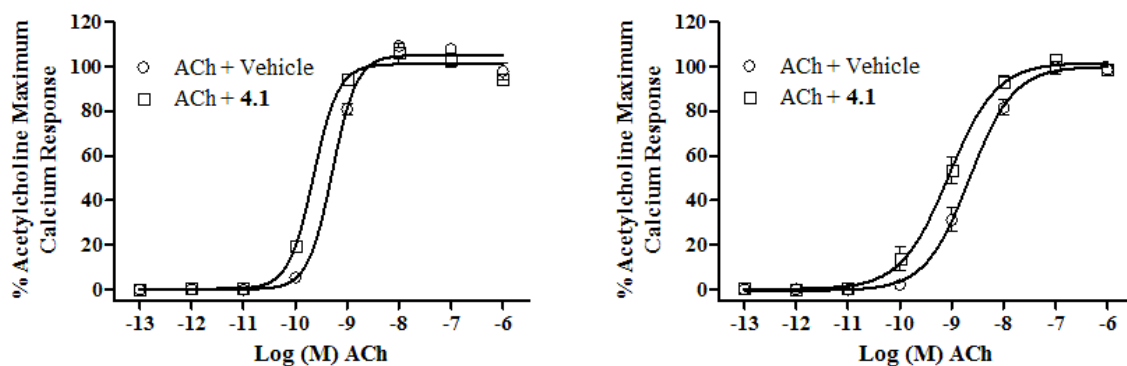


Figure 4.2. ACh CRC fold shifts of compound **4.1** (VU0472882) at hM₅ (left panel) and rM₅ (right panel). Ca²⁺ mobilization assays with hM₅ cells and rM₅ cells were used to obtain ACh CRCs in the presence of vehicle or 10 μM compound **4.1** (EC₅₀ values: hM₅ EC₅₀ of ACh + vehicle = 517 pM, hM₅ EC₅₀ of ACh + **4.1** = 224 pM, hM₅ fold shift = 2.3; rM₅ EC₅₀ of ACh + vehicle = 2.20 nM, rM₅ EC₅₀ of ACh + **4.1** = 873 pM, rM₅ fold shift = 2.5). Data represent the mean ± S.E.M. of at least 3 independent experiments with similar results.

Despite the weak potency and fold shift of **4.1** we were heartened to see the compound's selectivity for M₅. Previous to this HTS campaign the only known M₅ selective compounds were invariably centered on an isatin-based chemical scaffold with few tractable points of SAR (Chapters I and III). We now possessed a lead that, in stark contrast to the isatin M₅ PAM scaffold, exhibited a modular scaffold amenable to a broad range of modifications; thus, we hypothesized that further exploration of the wide range of SAR possibilities around the chemical scaffold would result in improved potency whilst maintaining M₅ selectivity⁸⁵.

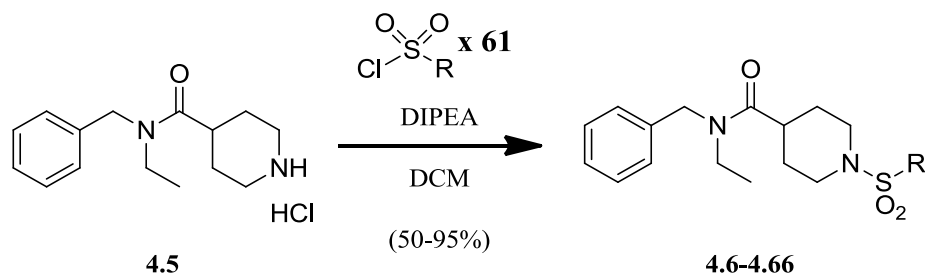
Optimization of VU0472882 to obtain non-isatin M₅ PAM VU0476212

Optimization of eastern sulfonamide region SAR

Our laboratory's experiences with previous medicinal chemistry projects optimizing GPCR allosteric modulators often found that subtle structural changes can have a drastic effect on a chemical scaffold's physicochemical and pharmacological

characteristics. Given the several structural regions of the non-isatin M₅ PAM lead scaffold we proposed to address the exploration of each region in an iterative manner, optimizing a single region whilst holding the rest of the molecule constant. Once an optimal structure for one region was found, it was held constant while the next region was addressed, and so on.

The first region that we turned our attention to was the eastern sulfonamide substituent. We coupled the piperidine amine, compound **4.5**, to a wide variety of substituted sulfonyl halides, including aryl, heteroaryl, and alkyl substituents. The starting material **4.5** was easily obtained in high yields from the synthetic pathway depicted in **Scheme 4.1** and was sulfonylated with a library of >60 sulfonyl chlorides under standard acyl chloride amide coupling conditions (**Scheme 4.2**). The resulting analogs (compounds **4.6-4.66**), as well as the unreacted amine **4.5** were then screened in single point (30 μM) Ca²⁺ mobilization assays in the presence of an ACh ~EC₂₀ in CHO cells stably expressing hM₅. The results of this single point screen are shown in **Figure 4.3** and **Table 4.1**.



Scheme 4.2. Synthetic scheme for sulfonylamine library analogs **4.6-4.66** from intermediate **4.5**.

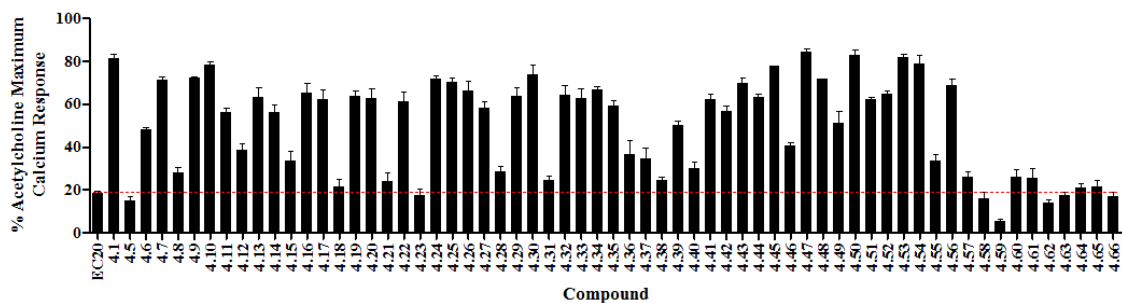
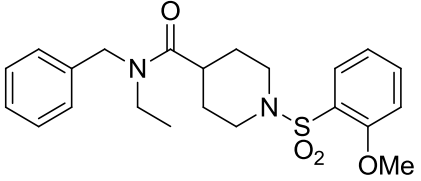
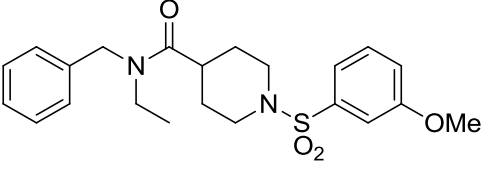
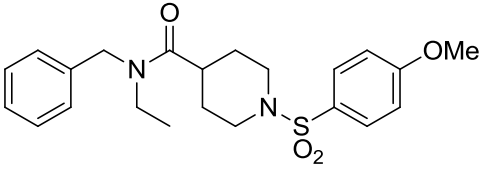
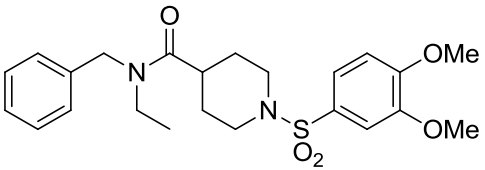
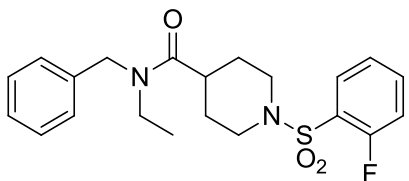
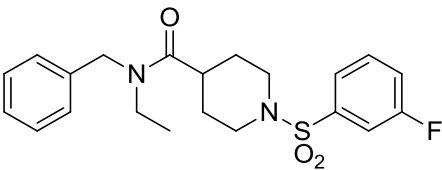
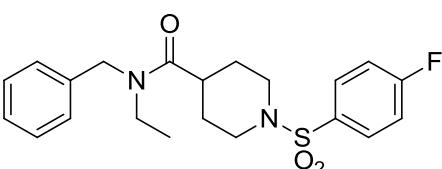
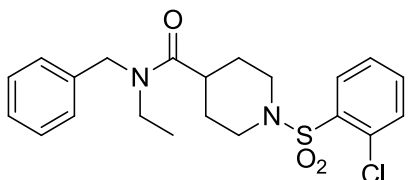
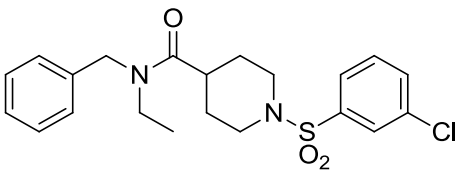
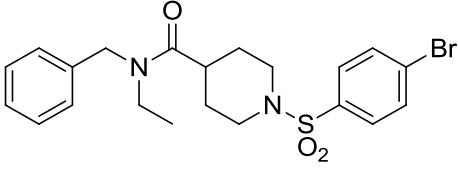
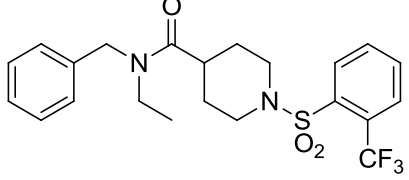
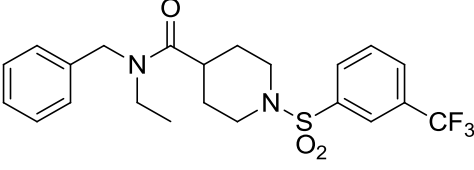
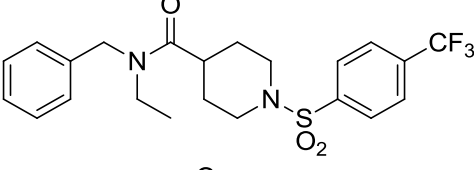
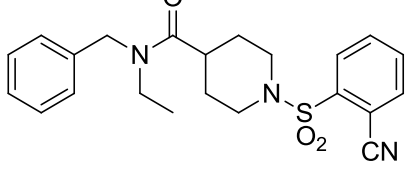
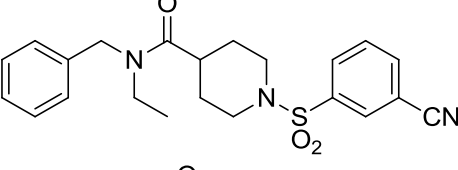
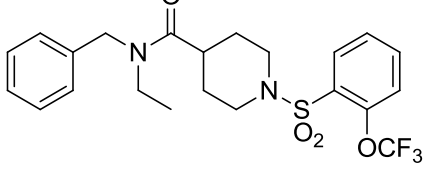
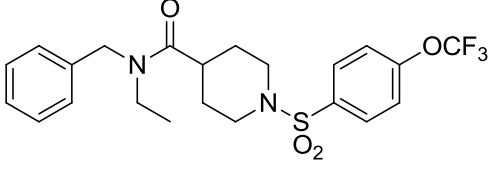
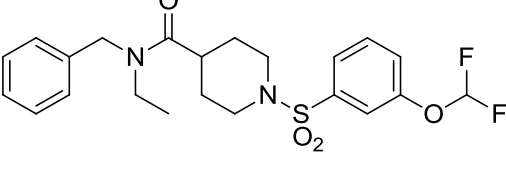


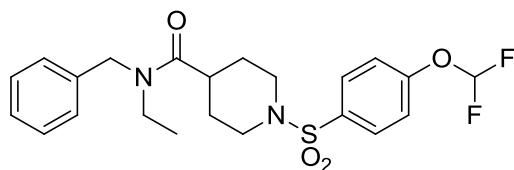
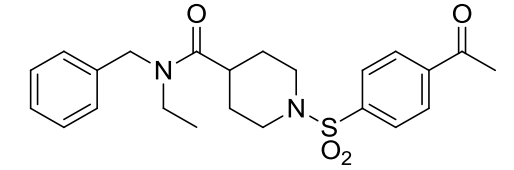
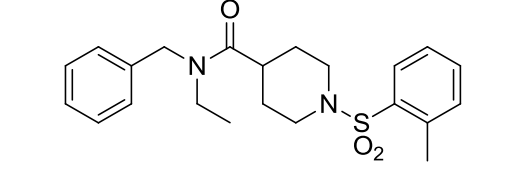
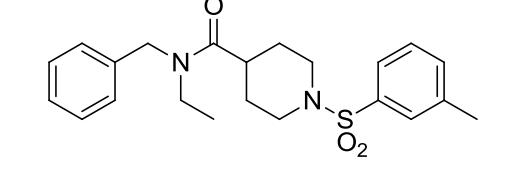
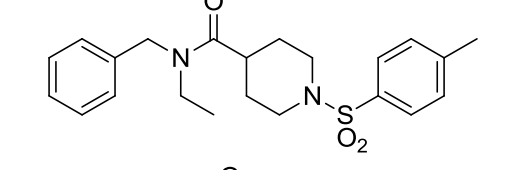
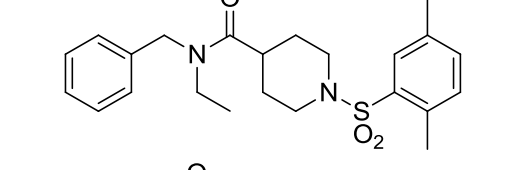
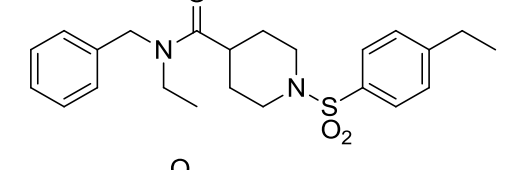
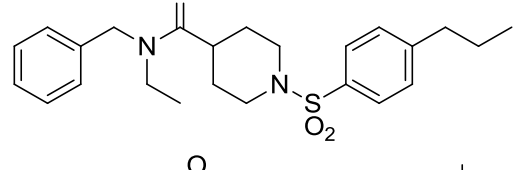
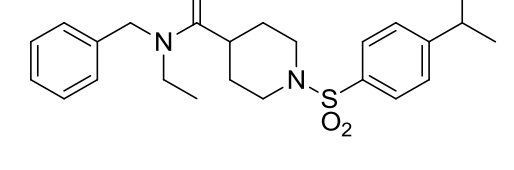
Figure 4.3. Comparison of single point (30 μ M) screen results of the sulfonamide library, analogs **4.5-4.66**. Also included is the single point Ca^{2+} mobilization response of the initial hit, compound **4.1**. Ca^{2+} mobilization was used to obtain % ACh_{Max} values for each compound in the presence of a fixed submaximal ($\sim\text{EC}_{20}$) concentration of ACh. Data represent the mean \pm S.E.M. of at least 3 replicate experiments with similar results.

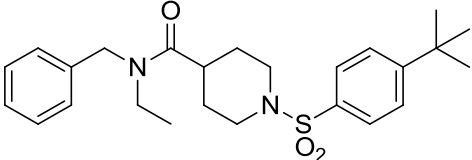
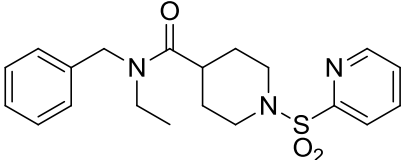
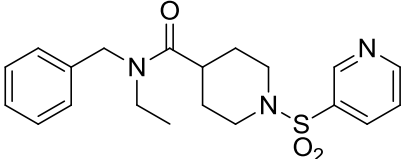
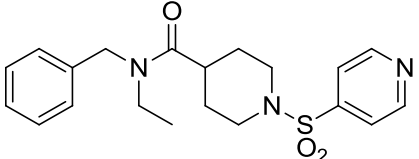
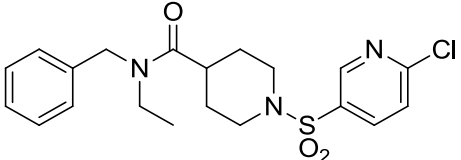
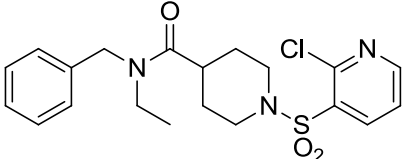
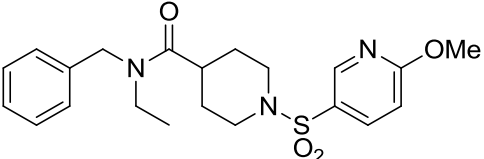
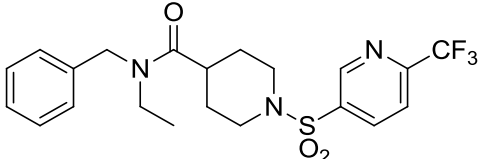
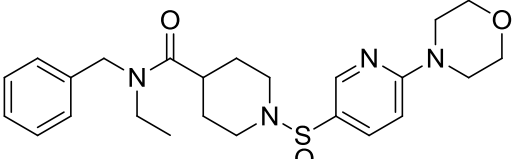
Table 4.1. Structures for sulfonamide analogs **4.5-4.66** and associated PAM activity data from the single point (30 μ M) screen at hM_5 . Also included is the structure and single point Ca^{2+} mobilization response of the HTS hit, compound **4.1**. Ca^{2+} mobilization responses for each compound are reported as a percentage of the maximum ACh response. VU number denotes the compound identifier assigned by Vanderbilt University. Data represent the mean of at least 3 replicate experiments with similar results.

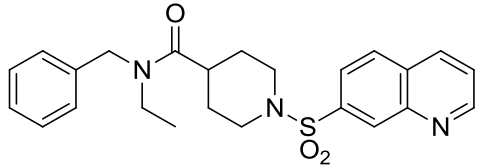
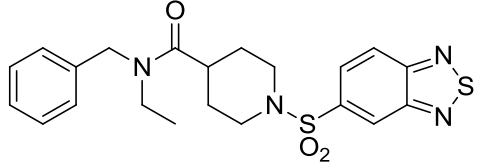
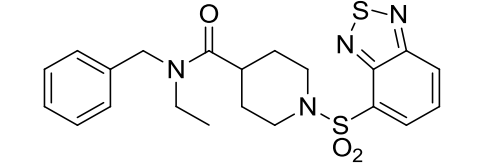
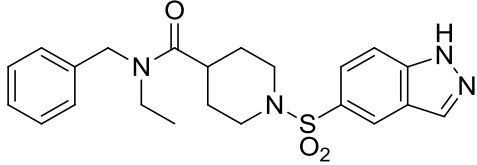
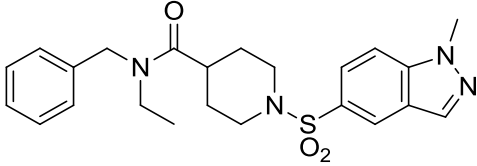
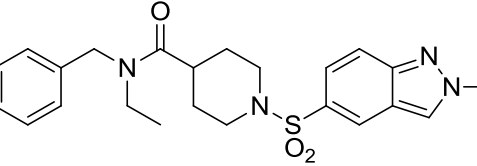
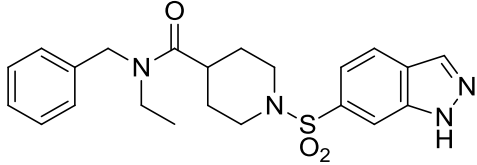
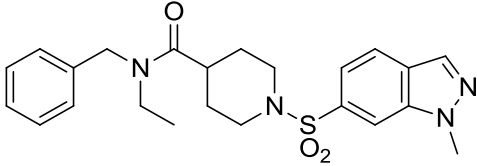
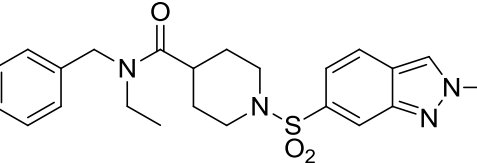
Structure	Cmpd #	VU #	hM_5 % ACh_{Max}
	4.1	VU0472882	81.4
	4.5	VU0472883	14.9
	4.6	VU0472804	48.0
	4.7	VU0472801	71.5

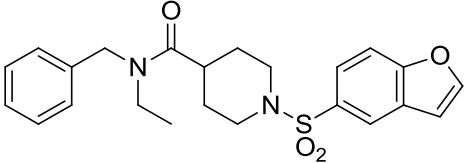
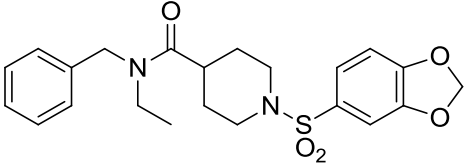
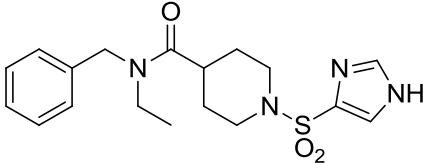
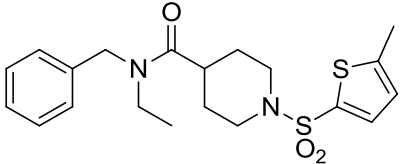
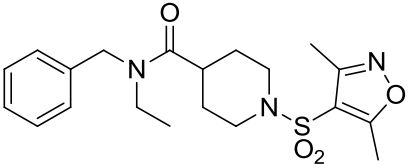
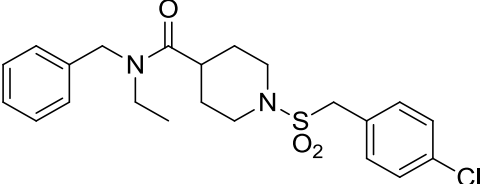
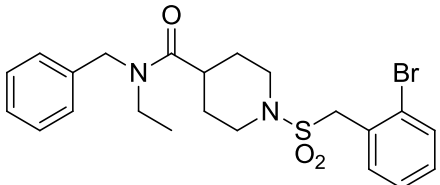
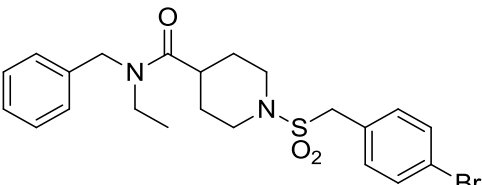
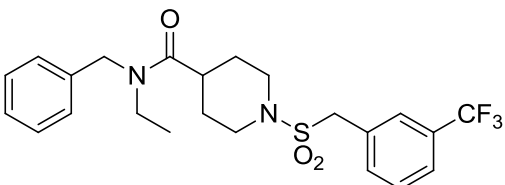
	4.8	VU0475780	28.1
	4.9	VU0472822	72.2
	4.10	VU0472783	78.4
	4.11	VU0472815	56.0
	4.12	VU0475696	38.4
	4.13	VU0475727	63.2
	4.14	VU0475750	56.2
	4.15	VU0475706	33.6
	4.16	VU0475695	65.3

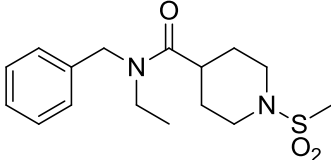
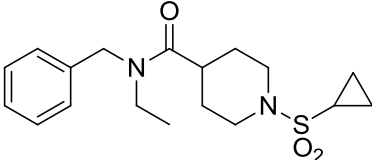
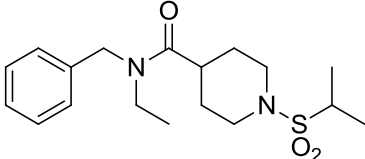
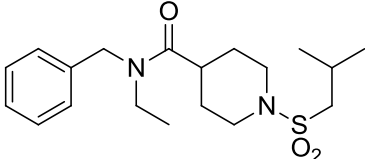
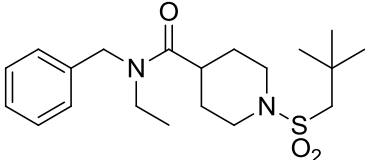
	4.17	VU0475772	62.1
	4.18	VU0475723	21.7
	4.19	VU0475782	63.9
	4.20	VU0475728	62.6
	4.21	VU0475681	24.0
	4.22	VU0475674	61.0
	4.23	VU0475771	17.5
	4.24	VU0475773	71.7
	4.25	VU0475698	70.2

	4.26	VU0475774	66.1
	4.27	VU0475751	58.4
	4.28	VU0475785	28.6
	4.29	VU0475700	63.8
	4.30	VU0475699	73.7
	4.31	VU0475763	24.5
	4.32	VU0475764	64.3
	4.33	VU0475783	62.9
	4.34	VU0475786	66.7

	4.35	VU0475682	59.3
	4.36	VU0486994	36.4
	4.37	VU0487015	34.5
	4.38	VU0487479	24.7
	4.39	VU0475701	50.1
	4.40	VU0475777	30.0
	4.41	VU0475720	62.5
	4.42	VU0475787	56.9
	4.43	VU0475749	70.0

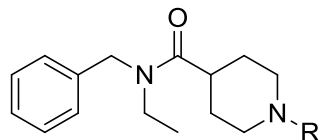
	4.44	VU0472827	63.4
	4.45	VU0472800	77.9
	4.46	VU0111215	40.8
	4.47	VU0475661	84.3
	4.48	VU0486967	71.5
	4.49	VU0487026	51.4
	4.50	VU0475778	83.1
	4.51	VU0487157	62.3
	4.52	VU0487160	64.9

	4.53	VU0475765	82.1
	4.54	VU0487151	78.6
	4.55	VU0475713	33.7
	4.56	VU0475677	68.8
	4.57	VU0475678	25.9
	4.58	VU0475784	16.0
	4.59	VU0475680	5.3
	4.60	VU0475721	26.2
	4.61	VU0475714	25.5

	4.62	VU0474010	14.1
	4.63	VU0474011	17.3
	4.64	VU0475722	20.8
	4.65	VU0475760	21.3
	4.66	VU0475679	17.0

This initial single point screen revealed that SAR around the sulfonamide substituent was rich and highly flexible. Many of the aryl and heteroaryl sulfonamide analogs potentiated of the ACh EC₂₀ to over 70% of the maximal ACh response. In exception to this, *ortho*-substituted aryl sulfonamides were notably disfavored. Likewise, alkyl and benzyl sulfonamide analogs showed little potentiator response, as did the unreacted starting material, compound **4.5**. Based on this screen, 29 compounds were tested in full CRC Ca²⁺ mobilization assays at hM₅ to determine potency (**Table 4.2**).

Table 4.2. Potencies at hM₅ for 29 aryl & heteroaryl sulfonamide analogs selected from the single point (30 μM) screen. Ca²⁺ mobilization assays with hM₅ cells were used to obtain CRCs of compounds in the presence of a fixed submaximal (~EC₂₀) concentration of ACh. Data for the two most potent compounds, **4.47** and **4.50**, are bolded. Data represent the mean of at least 3 independent experiments with similar results.



Cmpd #	R =	hM ₅ EC ₅₀ (μM)	% ACh _{Max}
4.6	1,4-benzodioxan-5-sulfonamide	>30	52.8
4.7	benzenesulfonamide	6.2	69.2
4.8	2-methoxybenzenesulfonamide	>30	49.8
4.9	3-methoxybenzenesulfonamide	3.1	76.6
4.10	4-methoxybenzenesulfonamide	3.2	75.3
4.11	3,4-dimethoxybenzenesulfonamide	>30	57.1
4.15	2-chlorobenzenesulfonamide	4.8	53.6
4.16	3-chlorobenzenesulfonamide	4.4	74.2
4.17	4-bromobenzenesulfonamide	3.9	73.5
4.19	3-trifluoromethylbenzenesulfonamide	>30	75.0
4.20	4-trifluoromethylbenzenesulfonamide	>30	65.0
4.24	4-trifluoromethoxybenzenesulfonamide	3.8	74.4
4.25	3-difluoromethoxybenzenesulfonamide	3.1	74.3
4.26	4-difluoromethoxybenzenesulfonamide	5.1	83.9
4.29	3-tolylsulfonamide	3.9	66.2
4.30	4-tolylsulfonamide	5.3	72.6
4.32	4-ethylphenylsulfonamide	5.2	81.5
4.33	4-propylphenylsulfonamide	3.2	75.3
4.39	6-chloropyridine-3-sulfonamide	6.4	48.0
4.41	6-methoxypyridine-3-sulfonamide	>30	53.6
4.43	6-morpholinopyridine-3-sulfonamide	>30	70.0
4.44	quinoline-7-sulfonamide	>10	65.8
4.45	2,1,3-benzothiadiazole-5-sulfonamide	3.0	80.6
4.47	1H-indazole-5-sulfonamide	1.6	85.6
4.48	1-methyl-1H-indazole-5-sulfonamide	5.0	73.8
4.50	1H-indazole-6-sulfonamide	1.7	86.2
4.53	benzofuran-5-sulfonamide	2.4	80.5
4.54	benzo[<i>d</i>][1,3]dioxole-5-sulfonamide	7.4	93.3
4.56	5-methylthiophene-2-sulfonamide	>10	64.5

From these data it was clear that manipulation of the sulfonamide substituent had the potential to greatly increase the potency of the compound over the original HTS lead. The unadorned benzenesulfonamide **4.7** displayed a slight increase in potency over the lead, but further increases in potency were attained by introducing substituents around the ring. Both 3- and 4-methoxybenzenesulfonamide analogs **4.9** and **4.10** greatly increased potency; however, the relative inactivity of the 2-methoxybenzenesulfonamide analog **4.8** again underscored the observation that *ortho*-substituents are not tolerated. Interestingly, the 3,4-dimethoxybenzenesulfonamide analog **4.11** showed greatly reduced potency and efficacy compared to the individual 3- and 4- methoxy substituents as well as the HTS lead.

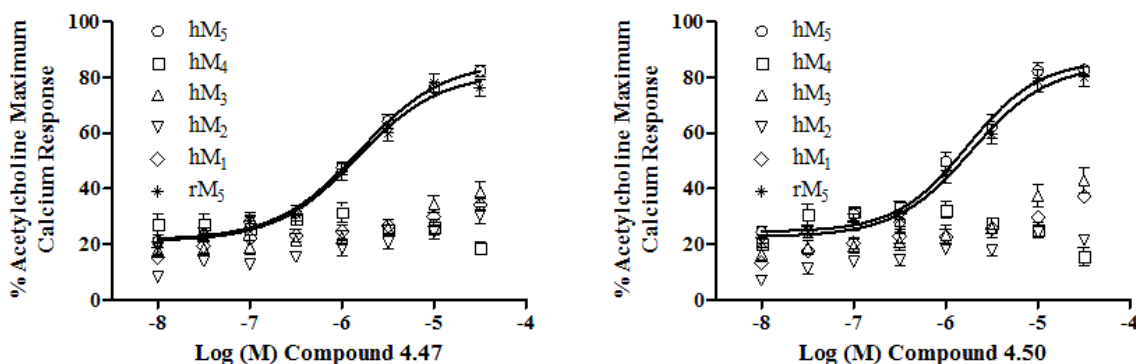


Figure 4.4. Potency and selectivity of analogs **4.47** (VU0475661; left panel) and **4.50** (VU0475778; right panel). Ca^{2+} mobilization assays with hM₁-hM₅ (M₂ and M₄ co-expressing G_{αq15}) and rM₅ cells were used to obtain CRCs of the compounds in the presence of a fixed submaximal (~EC₂₀) concentration of ACh (**4.47** EC₅₀ values: hM₅ EC₅₀ = 1.6 μM, %ACh_{Max} = 86; hM₁-hM₄ EC₅₀ >30 μM; rM₅ EC₅₀ = 1.5 μM, %ACh_{Max} = 82%; **4.50** EC₅₀ values: hM₅ EC₅₀ = 1.7 μM, %ACh_{Max} = 87; hM₁-hM₄ EC₅₀ >30 μM; rM₅ EC₅₀ = 1.9 μM, %ACh_{Max} = 85%). Data represent the mean ± S.E.M. of at least 3 independent experiments with similar results.

Out of all analogs tested, the two indazolyl sulfonamide analogs, compounds **4.47** (VU0475661) and **4.50** (VU0475778), showed the greatest potency and were subjected to further counter screening against the remaining human mAChR subtypes as well as rM₅

(**Figure 4.4**). We were pleased to see that both **4.47** and **4.50** maintained their activity at rM₅ (**4.47**: rM₅ EC₅₀ = 1.5 μM, %ACh_{Max} = 82; **4.50**: rM₅ EC₅₀ = 1.9 μM, % ACh_{Max} = 85) while also maintaining selectivity for M₅ versus other human mAChR subtypes (hM₁-hM₄ EC₅₀ >30 μM). In addition to potency data, fold shift data for **4.47** and **4.50** at 10 μM was gathered at hM₅ and rM₅ (**4.47** hM₅ fold shift = 5.4, rM₅ fold shift = 3.6; **4.50** hM₅ fold shift = 4.8, rM₅ fold shift = 5.2), revealing a ~2-fold improvement over the HTS lead **4.1** (**Figure 4.5**, **Figure 4.6**). In light of the potency increase and efficacy over the HTS lead, we deemed the 5- and 6-indozolyl sulfonamide analogs to be the preferred substituents for the sulfonamide region as we moved forward in the optimization effort.

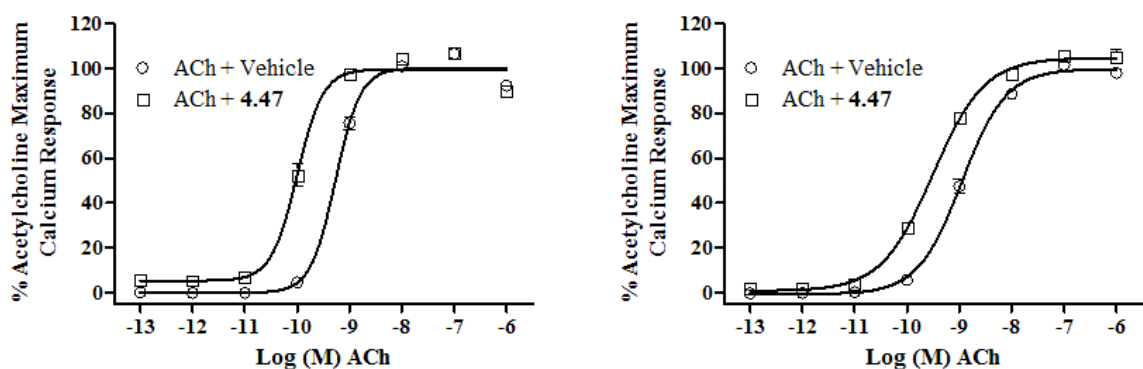


Figure 4.5. ACh CRC fold shifts of compound **4.47** (VU0475661) at hM₅ (left panel) and rM₅ (right panel). Ca²⁺ mobilization assays with hM₅ cells and rM₅ cells were used to obtain ACh CRCs in the presence of vehicle or 10 μM compound **4.47** (EC₅₀ values: hM₅ EC₅₀ of ACh + vehicle = 539 pM, hM₅ EC₅₀ of ACh + **4.47** = 100 pM, hM₅ fold shift = 5.4; rM₅ EC₅₀ of ACh + vehicle = 1.12 nM, rM₅ EC₅₀ of ACh + **4.47** = 313 pM, rM₅ fold shift = 3.6). Data represent the mean ± S.E.M. of at least 3 independent experiments with similar results.

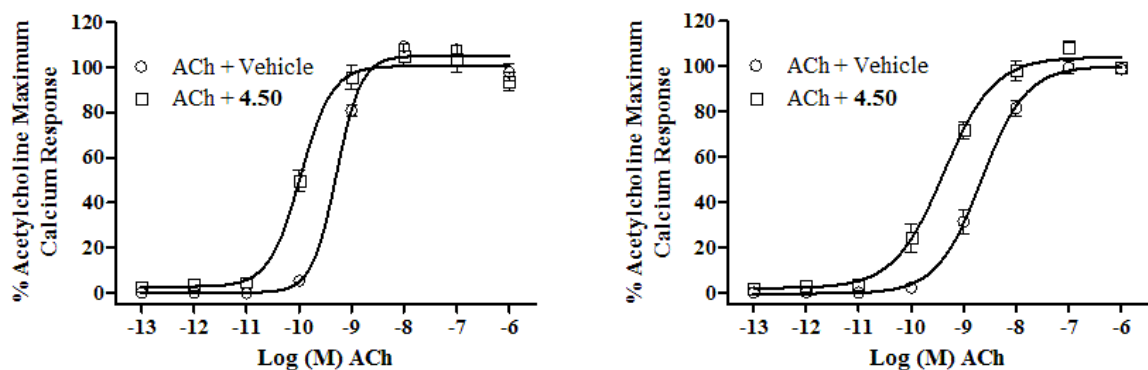
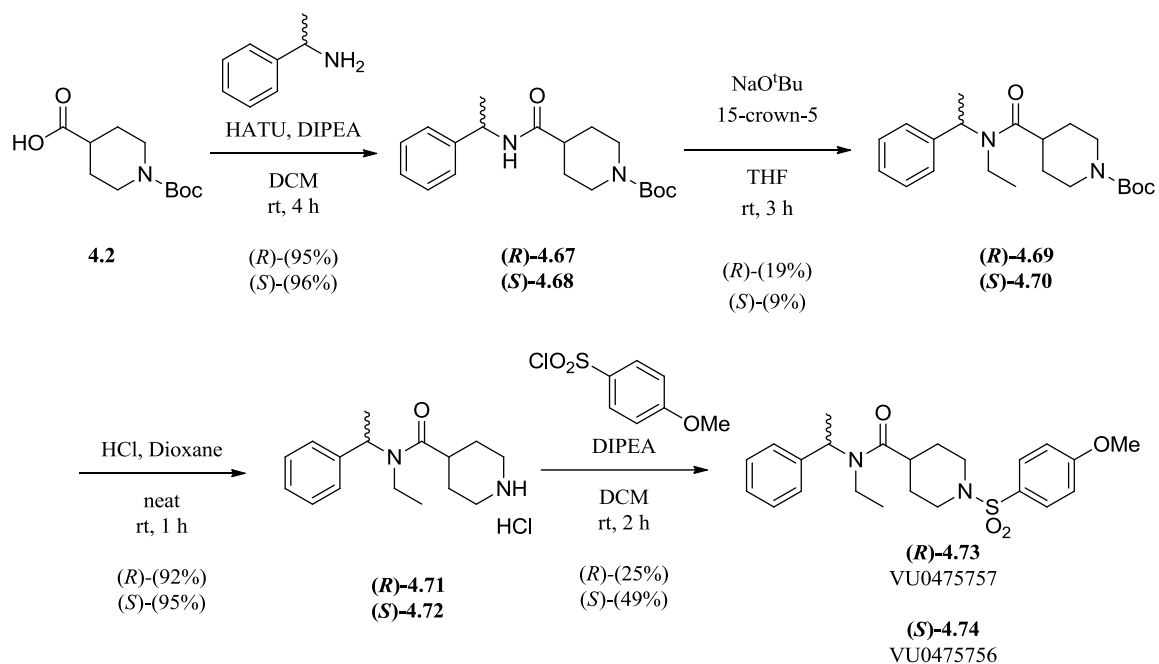


Figure 4.6. ACh CRC fold shifts of compound **4.50** (VU0475778) at hM₅ (left panel) and rM₅ (right panel). Ca²⁺ mobilization assays with hM₅ cells and rM₅ cells were used to obtain ACh CRCs in the presence of vehicle or 10 μM compound **4.50** (EC₅₀ values: hM₅ EC₅₀ of ACh + vehicle = 517 pM, hM₅ EC₅₀ of ACh + **4.50** = 107 pM, hM₅ fold shift = 4.8; rM₅ EC₅₀ of ACh + vehicle = 2.20 nM, rM₅ EC₅₀ of ACh + **4.50** = 421 pM, rM₅ fold shift = 5.2). Data represent the mean ± S.E.M. of at least 3 independent experiments with similar results.

Introduction of benzylic methyl and discovery of enantiospecific activity

Having settled upon a set of optimized sulfonamide moieties for the eastern region of the chemical scaffold we next sought to explore SAR surrounding the western side of the molecule, including the benzyl ring and the amide *N*-alkyl substituent. Noticing an opportunity to introduce chirality, we first experimented with placing a methyl at the benzylic position of the benzyl ring. Due to an inconsistent commercial supply of the preferred indazolyl sulfonyl chlorides, we initially conducted experiments with benzylic SAR in the context of the 4-methoxysulfonamide in the pharmacophore's eastern region. Beginning from the commercial (*S*)- or (*R*)-1-phenylethylamine the analogs (*R*)-**4.73** and (*S*)-**4.74** were synthesized in the previously described manner (**Scheme 4.3**).



Scheme 4.3. Synthesis of benzylic methyl analogs (R) -**4.73** and (S) -**4.74**.

Upon testing the compounds in full CRC Ca^{2+} mobilization assays at hM_5 we observed the compounds to exhibit enantiospecific PAM activity, with (R) -**4.73** (VU0475757) exhibiting sub-micromolar potency (hM_5 EC_{50} = 0.97 μM , % ACh_{Max} = 90) while (S) -**4.74** (VU0475756) displayed no PAM activity (hM_5 EC_{50} > 30 μM ; **Figure 4.7A**).

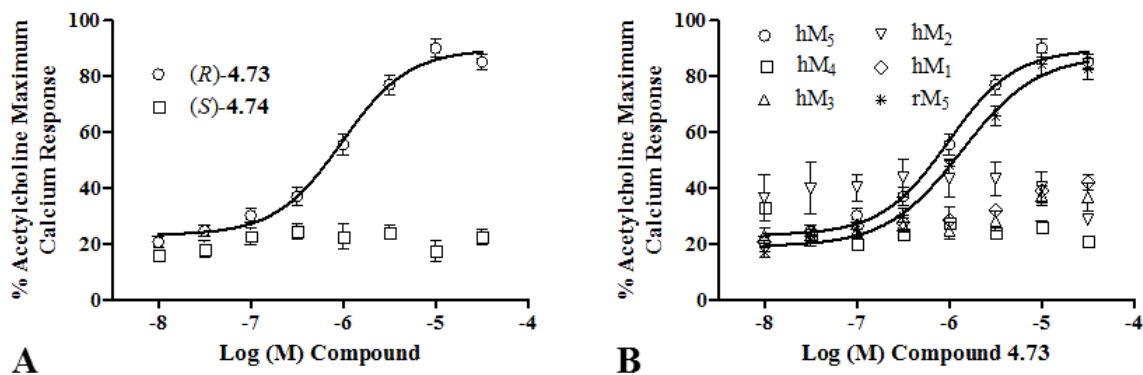


Figure 4.7. **A)** CRCs comparing activities of **4.73** (VU0475757; hM₅ EC₅₀ = 0.97 μM, %ACh_{Max} = 90), and **4.74** (VU0475756; hM₅ EC₅₀ > 30 μM) at hM₅. **B)** Potency and selectivity of analog **4.73**. Ca²⁺ mobilization assays with hM₁-hM₅ (M₂ and M₄ co-expressing G_{αq/15}) and rM₅ cells were used to obtain CRCs of the compounds in the presence of a fixed submaximal (~EC₂₀) concentration of ACh (**4.73** EC₅₀ values: hM₅ EC₅₀ = 0.97 μM, %ACh_{Max} = 90; hM₁-hM₄ EC₅₀ >30 μM; rM₅ EC₅₀ = 1.4 μM, %ACh_{Max} = 88). Data represent the mean ± S.E.M. of at least 3 independent experiments with similar results.

Impressed by yet another leap in the potency of this chemical series we obtained potency and selectivity data for **4.74** at rM₅ as well as at the remaining human mAChRs. The compound exhibited a slight decrease in potency at rM₅ (rM₅ EC₅₀ = 1.4 μM), but it maintained complete selectivity for M₅ versus hM₁-hM₄ (hM₁-hM₄ EC₅₀ >30 μM; **Figure 4.7B**) and, at 10 μM, produced a fold shift of 7.7- and 7.0-fold at hM₅ and rM₅, respectively (**Figure 4.8**). Given these data, **4.73** represented a >10-fold improvement in potency over the HTS lead **4.1** and the first sub-micromolar, M₅-selective, non-isatin M₅ PAM that we had developed.

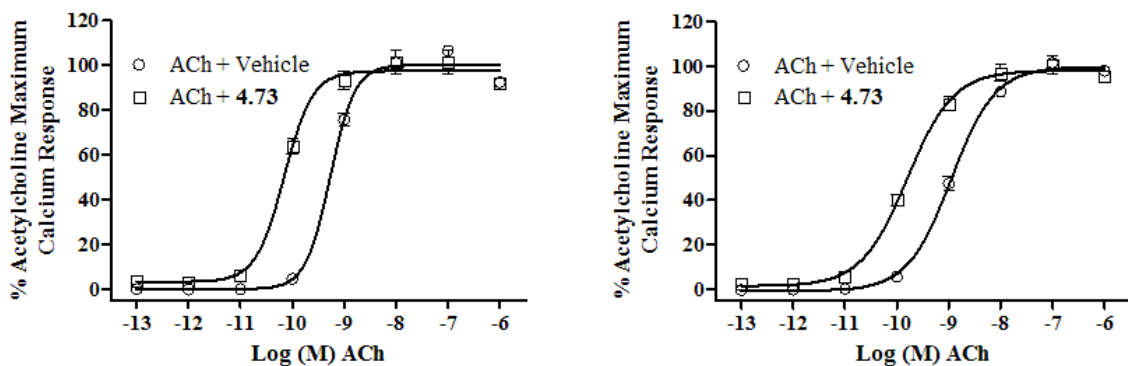
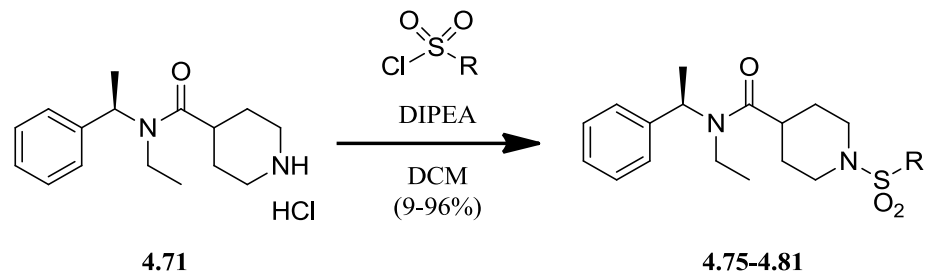


Figure 4.8. ACh CRC fold shifts of compound **4.73** (VU0475757) at hM₅ (left panel) and rM₅ (right panel). Ca²⁺ mobilization assays with hM₅ cells and rM₅ cells were used to obtain ACh CRCs in the presence of vehicle or 10 μ M compound **4.73** (EC₅₀ values: hM₅ EC₅₀ of ACh + vehicle = 539 pM, hM₅ EC₅₀ of ACh + **4.73** = 70.0 pM, hM₅ fold shift = 7.7; rM₅ EC₅₀ of ACh + vehicle = 1.11 nM, rM₅ EC₅₀ of ACh + **4.73** = 159 pM, rM₅ fold shift = 7.0). Data represent the mean \pm S.E.M. of at least 3 independent experiments with similar results.

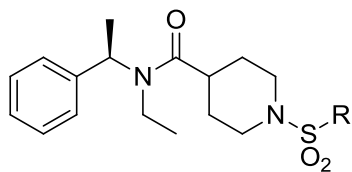
Combination of benzylic methyl and sulfonamide substituent SAR

At this stage we acknowledged the importance of the multidimensional nature of our optimization strategy by combining the two regions of SAR explored thus far. A small library of analogs was constructed that combined the (*R*)-oriented benzylic methyl with the optimal sulfonamide substituents from our previous library. 1*H*-indazol-5-yl, 1*H*-indazol-6-yl, and benzofuran-5-yl were recognized as the optimal sulfonamide substituents to be utilized, while 4 novel sulfonamide substituents were also selected to further explore and expand on the SAR of the sulfonamide region in the context of the benzylic methyl. From intermediate **4.71**, the secondary amine was sulfonylated with the selected sulfonyl chlorides under standard acyl chloride amide coupling conditions (**Scheme 4.4**).



Scheme 4.4. Synthetic scheme for sulfonamide library analogs **4.75-4.81** from intermediate **4.71**. Syntheses performed jointly with M. Kokubo.

Table 4.3. Potencies at hM₅ for 7 sulfonamide analogs, **4.75-4.81**, in the context of the (*R*)-oriented benzylic methyl. Ca²⁺ mobilization assays with hM₅ cells were used to obtain CRCs of compounds in the presence of a fixed submaximal (~EC₂₀) concentration of ACh. VU number denotes the compound identifier assigned by Vanderbilt University. Data represent the mean of at least 3 independent experiments with similar results.



Cmpd #	R =	VU#	hM ₅ EC ₅₀ (μM)	% ACh _{Max}
4.75	1 <i>H</i> -indazol-5-yl	VU0476212	0.74	85.7
4.76	1 <i>H</i> -indazol-6-yl	VU0476213	0.76	87.3
4.77	benzofuran-5-yl	VU0477569	0.93	79.7
4.78	2,3-dihydrobenzofuran-5-yl	VU0477987	1.1	87.8
4.79	2,3-dihydro-1 <i>H</i> -inden-5-yl	VU0477939	0.73	96.8
4.80	3,4,5-trifluorophenyl	VU0477989	2.5	65.1
4.81	4-(1 <i>H</i> -pyrazol-1-yl)phenyl	VU0477932	0.61	97.5

Potency data gathered via CRC Ca²⁺ mobilization assays at hM₅ revealed that the potency seen in **4.73** was maintained in the benzofuran-5-yl analog **4.77**, while substantial gains in potency were seen in 1*H*-indazolyl analogs **4.75** and **4.76** as well as in the novel sulfonamide analogs **4.79** and **4.81** (Table 4.3). Further selectivity data obtained for **4.75** (VU0476212) against rM₅ and the remaining human mAChR subtypes

revealed that **4.75** possessed comparable potency at rM₅ (rM₅ EC₅₀ = 0.64 μM, %ACh_{Max} = 89) and was completely selective versus hM₂ and hM₄ (hM₂, hM₄ EC₅₀ >30 μM). Slight activity was noted at hM₁ and hM₃, albeit with poor efficacy (hM₁ EC₅₀ = 4.8 μM, %ACh_{Max} = 61; hM₃ EC₅₀ = 1.7 μM, %ACh_{Max} = 59; **Figure 4.9**). Along with the increased potency seen at hM₅ and rM₅ with **4.75**, fold shift data revealed that **4.75** displayed an increased fold shift, shifting the ACh EC₅₀ 12- and 17-fold at hM₅ and rM₅, respectively (**Figure 4.10**).

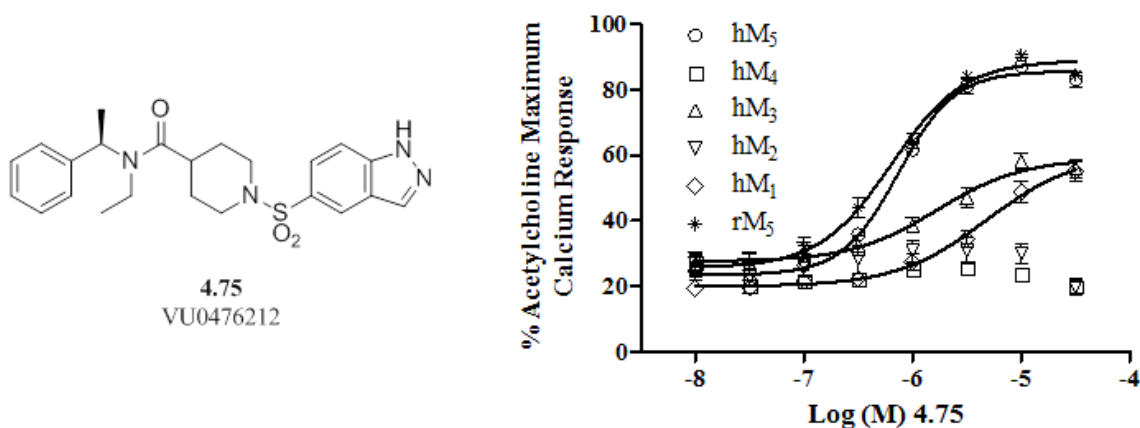


Figure 4.9. Structure, potency, and selectivity of analog **4.75** (VU0476212). Ca²⁺ mobilization assays with hM₁-hM₅ (M₂ and M₄ co-expressing G_{αq15}) and rM₅ cells were used to obtain CRCs of resynthesized compound **4.75** in the presence of a fixed submaximal (~EC₂₀) concentration of ACh (EC₅₀ values: hM₅ EC₅₀ = 0.74 μM, %ACh_{Max} = 86; hM₃ EC₅₀ = 1.7 μM, %ACh_{Max} = 59; hM₁ EC₅₀ = 4.8 μM, %ACh_{Max} = 61; hM₂, hM₄ EC₅₀ >30 μM; rM₅ EC₅₀ = 0.64 μM, %ACh_{Max} = 89). Data represent the mean ± S.E.M. of at least 3 independent experiments with similar results.

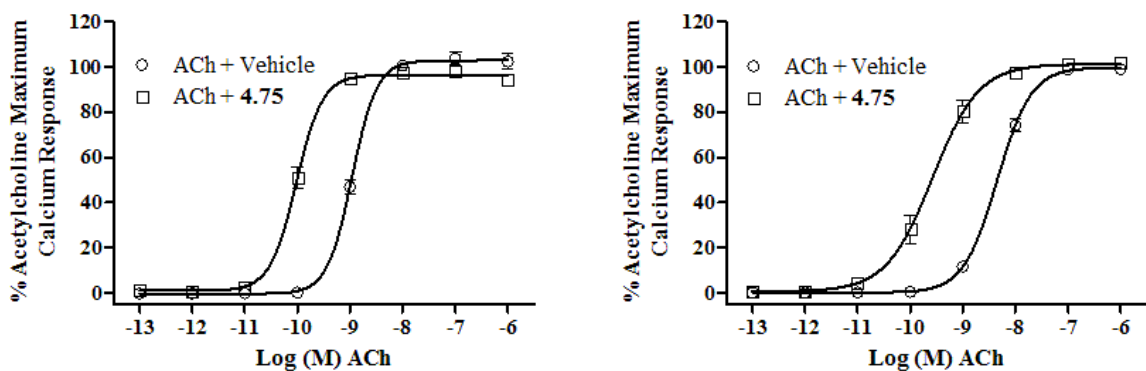


Figure 4.10. ACh CRC fold shifts of compound **4.75** (VU0476212) at hM₅ (left panel) and rM₅ (right panel). Ca²⁺ mobilization assays with hM₅ cells and rM₅ cells were used to obtain ACh CRCs in the presence of vehicle or 10 μM compound **4.75** (EC₅₀ values: hM₅ EC₅₀ of ACh + vehicle = 1.10 nM, hM₅ EC₅₀ of ACh + **4.75** = 95.2 pM, hM₅ fold shift = 11.6; rM₅ EC₅₀ of ACh + vehicle = 4.54 nM, rM₅ EC₅₀ of ACh + **4.75** = 266 pM, rM₅ fold shift = 17.1). Data represent the mean ± S.E.M. of at least 3 independent experiments with similar results.

***In vitro* DMPK characterization of non-isatin M₅ PAM VU0476212**

In vitro DMPK characterization of VU0476212

Considering that **4.75** (VU0476212) represented a ~13-fold improvement in potency over the HTS lead **4.1** and possessed a high degree of M₅-selectivity in both human and rat, we elected to characterize the *in vitro* DMPK profile of **4.75** in order to ascertain if the compound might be a candidate for *in vivo* studies of M₅ in the CNS. The compound was assayed in several *in vitro* DMPK assays, including plasma protein binding, rat and human microsomal stability, and a CYP inhibition panel. The results from these assays are summarized in **Table 4.4**.

Table 4.4. *In vitro* DMPK data for **4.75** (VU0476212) in multiple species. Studies performed by T. Bridges. ---, not determined.

Parameter	Rat	Human
hepatic microsome CL_{int} (mL/min/kg)	5581	2320
predicted CL_{hep} (mL/min/kg)	69.1	20.8
$f_{u,plasma}$	0.023	0.045
CYP inhibition (P450, IC_{50} , μ M)	---	1A2, 2C9: >30; 2D6: 8.1; 3A4: 1.4

Compound **4.75** displayed a moderate CYP inhibition profile, with 3A4 representing the primary liability. In both rat and human **4.75** displayed a low-to-moderate fraction unbound in plasma. In microsomal stability studies **4.75** exhibited high intrinsic clearance, with predicted hepatic clearance values near the hepatic blood flow rate in each species tested.

In addition to the standard DMPK profile studies, a bidirectional Caco-2 transwell assay was also carried out to assess efflux liabilities. When dosed at 5 μ M, **4.75** exhibited a P_{app} of 16.6×10^{-6} cm/sec, indicating moderate-high permeability, and an ER of 0.7, suggesting an absence of P-gp-mediated active efflux liabilities at the BBB.

VU0476212 metabolite identification

From the results of the microsomal stability assay it was clear that we needed to bolster the unstable structural elements of analog **4.75** that were leading to the compound's rapid metabolism and clearance. Thus we sought to determine the relevant biotransformation pathway(s) occurring within the hepatic microsomes via metabolite identification studies (**Figure 4.11**).

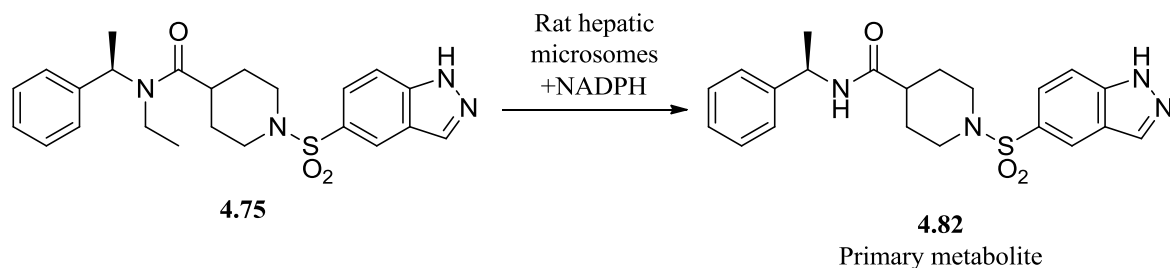
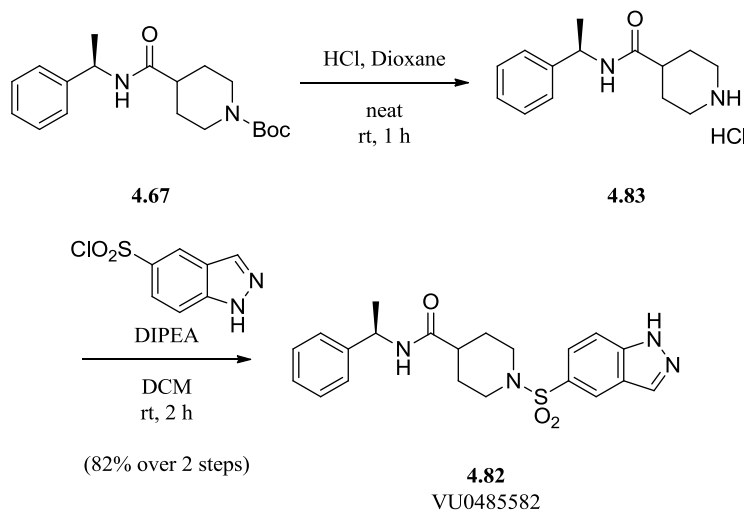


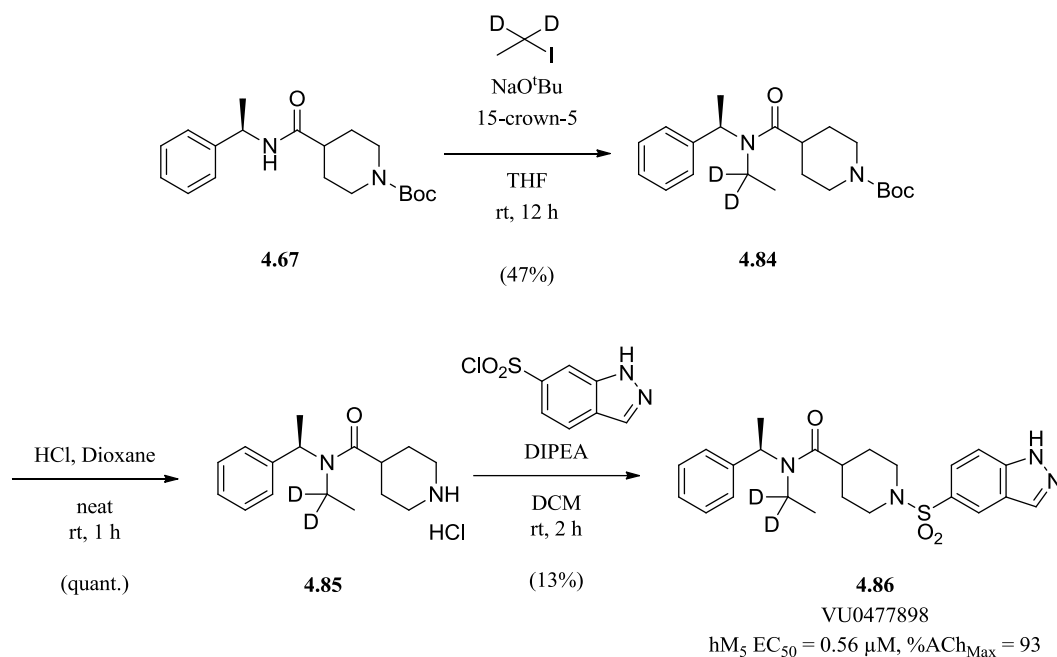
Figure 4.11. Results of metabolite identification following incubation of **4.75** with rat hepatic microsomes and NADPH. The primary metabolite identified, **4.82**, is the product of oxidative (NADPH-dependent) *N*-dealkylation. Studies performed by T. Bridges.

These analyses revealed the oxidative *N*-dealkylation of the amide to be the primary pathway of biotransformation in both plasma and microsomes. To explore the possibility that the primary metabolite may itself be an M₅ PAM we synthesized metabolite **4.82** from intermediate **4.67** (Scheme 4.5). Unfortunately, upon testing **4.82** in a full CRC Ca²⁺ mobilization assay at hM₅, and found the primary metabolite to be inactive (hM₅ EC₅₀ >>30 μM).



Scheme 4.5. Synthesis of **4.82** (VU0485582), the primary metabolite of **4.75** (VU0476212), from intermediate **4.67**. Syntheses performed jointly with M. Kokubo

Since the primary metabolite **4.82** was an inactive species, we attempted to reduce metabolism via deuteration of the methylene position of the amide *N*-ethyl. Through the deuteration of the *N*-alkyl substituent we sought to take advantage of the kinetic isotope effect and thereby perturb the rate of the oxidation by the CYP proteins^{86,87}. The deuterium analog **4.86** was synthesized from intermediate **4.67** with the previously described procedure (**Scheme 4.6**). Upon testing in a CRC Ca²⁺ mobilization assay at hM₅, we were pleased to see that **4.86** maintained sub-micromolar activity at hM₅ (hM₅ EC₅₀ = 0.56 μM, %ACh_{Max} = 93; **Scheme 4.6**). In order to determine if improved metabolic stability accompanied the improved potency, deuterated analog **4.86** was tested in plasma protein binding and microsomal stability assays at rat and human (**Table 4.5**). Although deuteration of the *N*-ethyl methylene position slightly reduced the intrinsic clearance values at rat and human relative to the values seen for **4.75** in **Table 4.4**, the intrinsic clearance values were still exceedingly high and the predicted hepatic clearance values remained near the hepatic blood flow rate.



Scheme 4.6. Synthesis and activity of deuterated analog **4.86** (VU0477898) from intermediate **4.67**. Ca^{2+} mobilization assays in hM_5 cells were used to obtain CRCs of compound **4.86** in the presence of a fixed submaximal ($\sim\text{EC}_{20}$) concentration of ACh. Data represent the mean of at least 3 independent experiments with similar results.

Table 4.5. *In vitro* DMPK data for **4.86** (VU0477898) in multiple species. Studies performed by T. Bridges.

Parameter	Rat	Human
hepatic microsome CL_{int} (mL/min/kg)	3370	1902
predicted CL_{hep} (mL/min/kg)	68.7	20.8
$f_{\text{u,plasma}}$	0.033	0.042

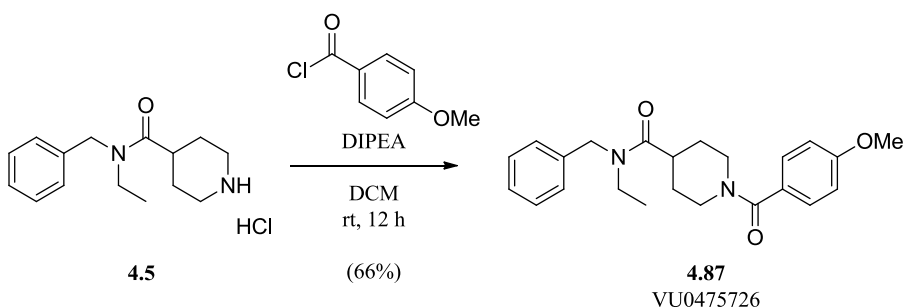
Although we were unsuccessful in our initial attempts to directly address the oxidative dealkylation of **4.75**, the SAR of many regions of the chemical scaffold had yet to have been explored. Thus, we returned to optimizing unexplored chemical space with the confidence that further discoveries found in the course of potency optimization might present a solution to shunt or block the oxidative dealkylation of the amide.

Optimization of VU0476212 to obtain non-isatin M₅ PAM VU0481443

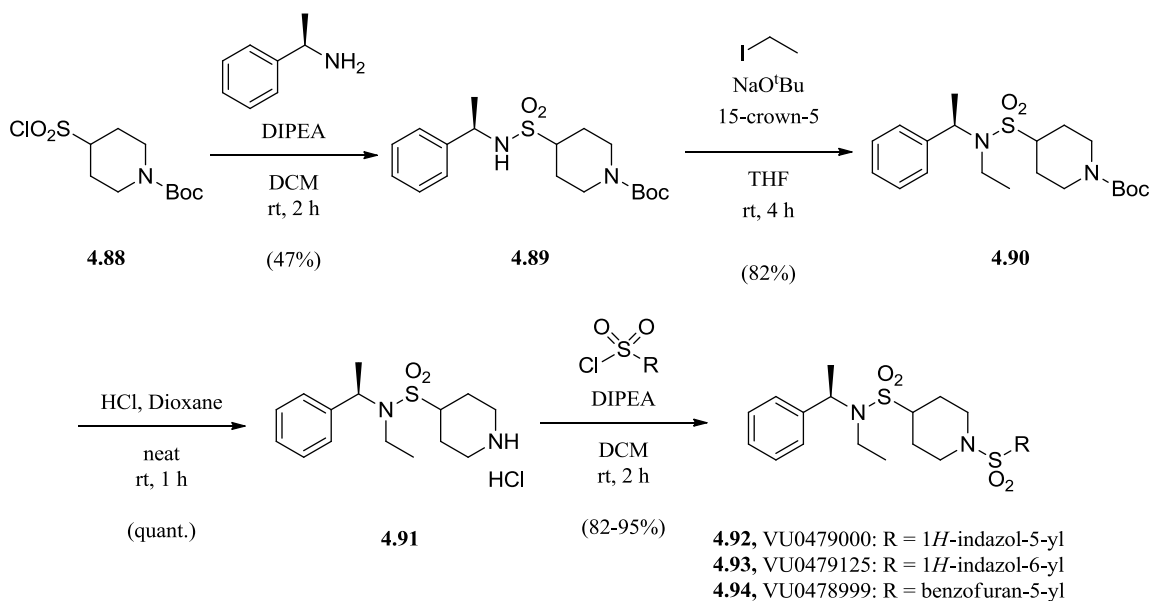
Exploration of amide and sulfonamide SAR

Since it was evident that the DMPK liabilities of compound **4.75** centered on the oxidative dealkylation of the tertiary amide, we next explored the SAR in this area with the goal of altering or masking the amide to the point that it would retard or halt oxidative dealkylation. It should be noted that this particular effort was not concerted, but was carried out over time as a side project to the larger SAR exploration efforts, hence the smattering of different elements of SAR.

Initial studies exploring the SAR around the amide consisted of several standalone compounds and small libraries designed to examine the tractability and necessity of the amide itself. **Scheme 4.7** depicts the synthesis of a bis-amide analog **4.87** from intermediate **4.5**, while **Scheme 4.8** depicts the complete synthesis of bis-sulfonamides **4.92-4.94**. Upon testing these compounds in Ca²⁺ mobilization assays at hM₅, they were shown to be inactive (hM₅ EC₅₀ >>30 μM).

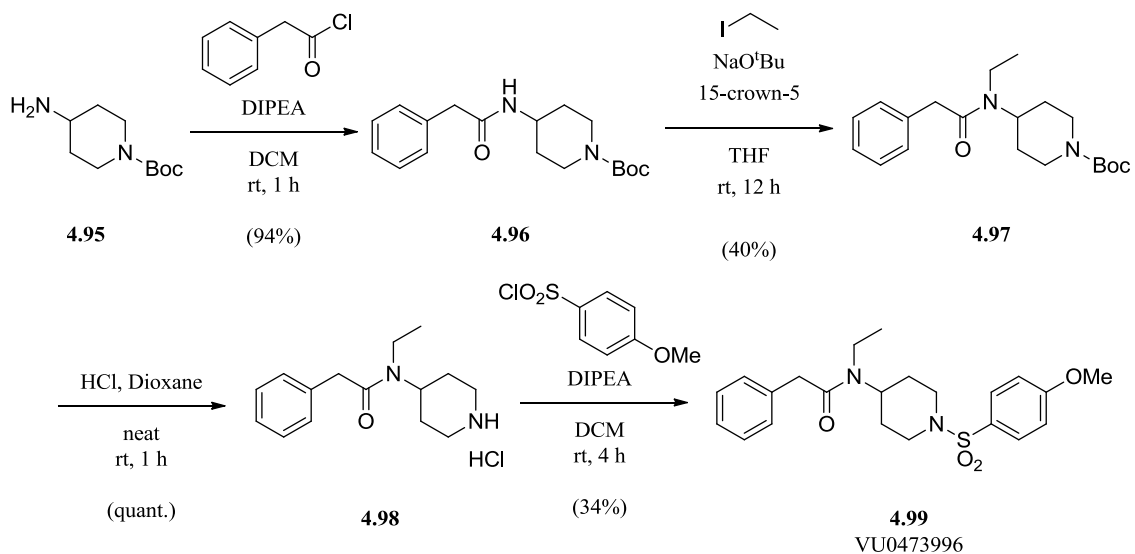


Scheme 4.7. Synthesis of bisamide analog **4.87** (VU0475726) from intermediate **4.5**.



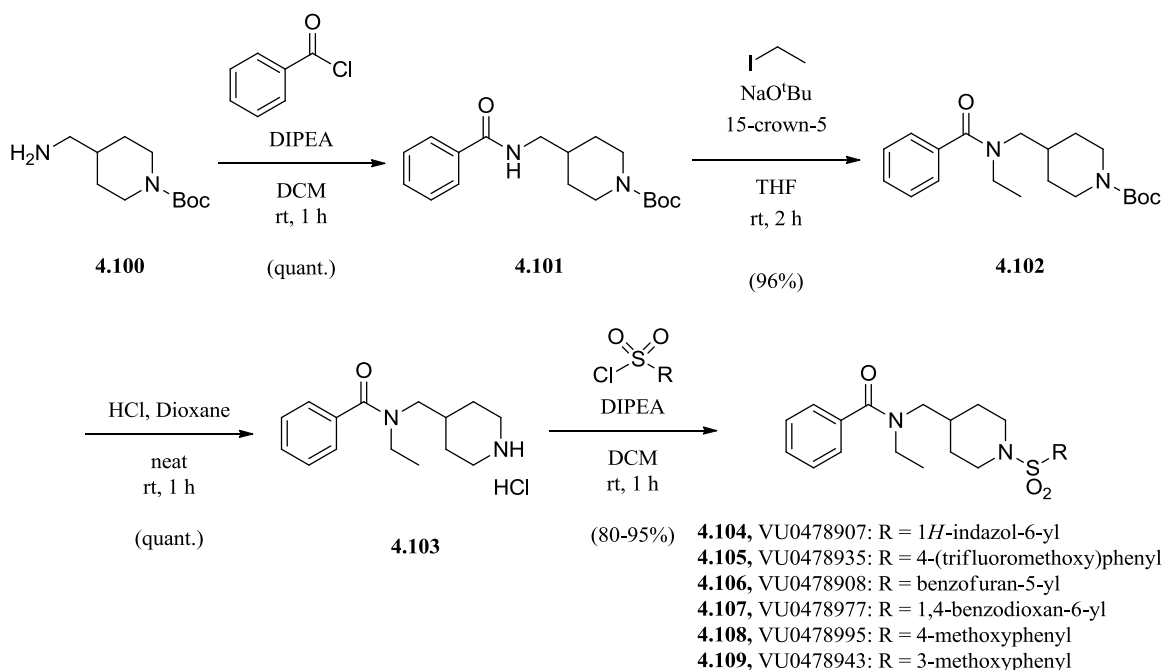
Scheme 4.8. Synthesis of bisulfonamide analogs **4.92-4.94**. Synthesized jointly with M. Kokubo.

Scheme 4.9 depicts the synthesis of the reverse amide, analog **4.99**. This compound was also found to be inactive at hM₅ upon testing in Ca²⁺ mobilization assays (hM₅ EC₅₀ >>30 μM).

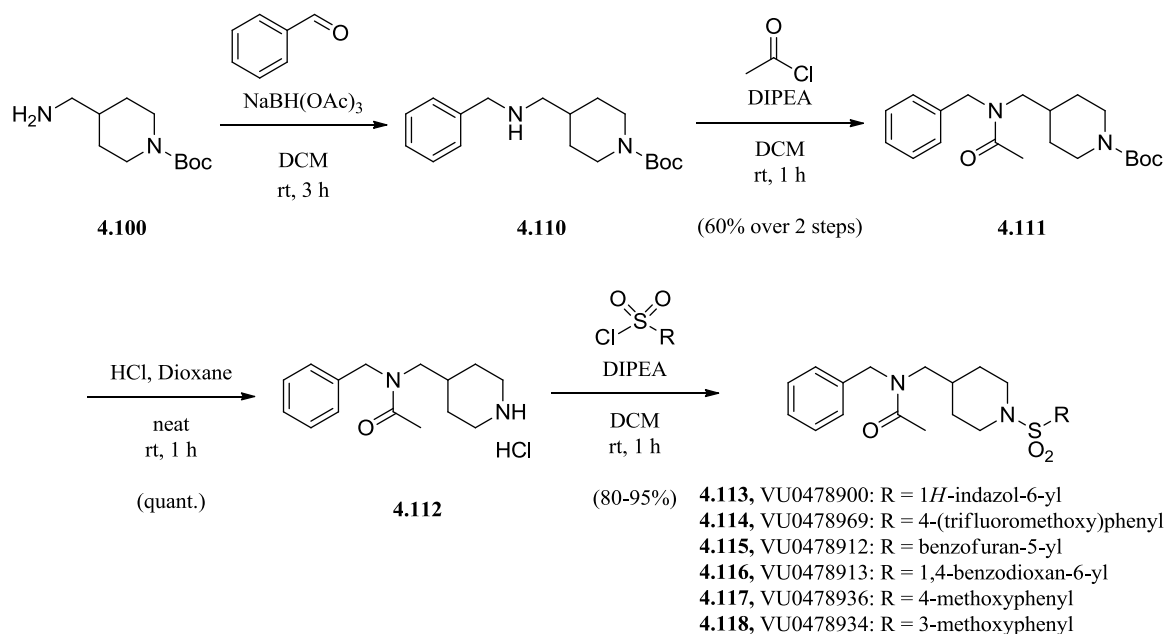


Scheme 4.9. Synthesis of reverse amide analog **4.99** (VU0473996).

Lastly, we synthesized two libraries that examined the migration of the amide carbonyl to form either benzamide analogs (**4.104-4.109**) or acetamide analogs (**4.113-4.118**) in the context of multiple sulfonamide substituents. **Scheme 4.10** and **Scheme 4.11** depict the syntheses of these libraries. As with all other attempts to manipulate the amide carbonyl, these analogs proved to be devoid of activity at hM₅ upon testing in Ca²⁺ mobilization assays. Thus, despite probing multiple variations of amide positioning and composition, persistent inactivity in the resulting analogs suggests that the original amide is a necessary structural element for PAM activity.



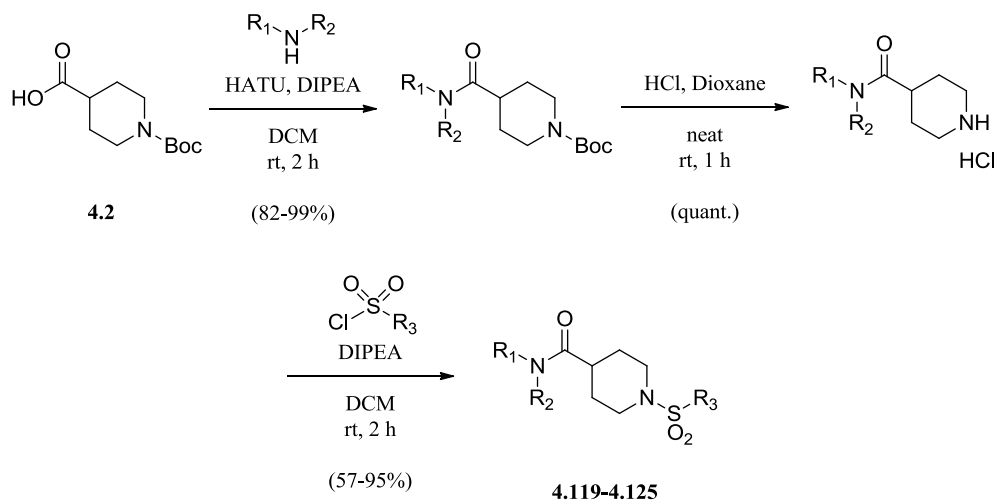
Scheme 4.10. Synthesis of benzamide analogs **4.104-4.109**. Syntheses performed by M. Kokubo.



Scheme 4.11. Synthesis of acetamide analogs **4.113-4.118**. Syntheses performed by M. Kokubo.

Attempts to constrain the N-alkyl moiety

After finding it challenging to modify the amide without losing PAM activity, we investigated other strategies to prevent the oxidative dealkylation of the *N*-ethyl. One intriguing possibility was to constrain the *N*-alkyl by bonding the alkyl chain to either the benzyl ring or the benzylic position. We constructed a small library that examined the effects of tying back the *N*-alkyl to the benzyl ring with varying chain lengths (analog **4.119-4.121**), tying back the *N*-alkyl to the benzyl ring in the context of a benzylic methyl (analog **4.122-4.124**), and tying back the *N*-ethyl to the benzylic methyl (analog **4.125**; **Scheme 4.12**, **Figure 4.12**). Unfortunately, all of the constrained *N*-alkyl library analogs were devoid of PAM activity in Ca^{2+} mobilization assays at hM_5 (**Figure 4.12**).



Scheme 4.12. General synthesis of libraries constraining *N*-alkyl to benzyl moiety, analogs **4.119-4.125**. Synthesized jointly with M. Kokubo.

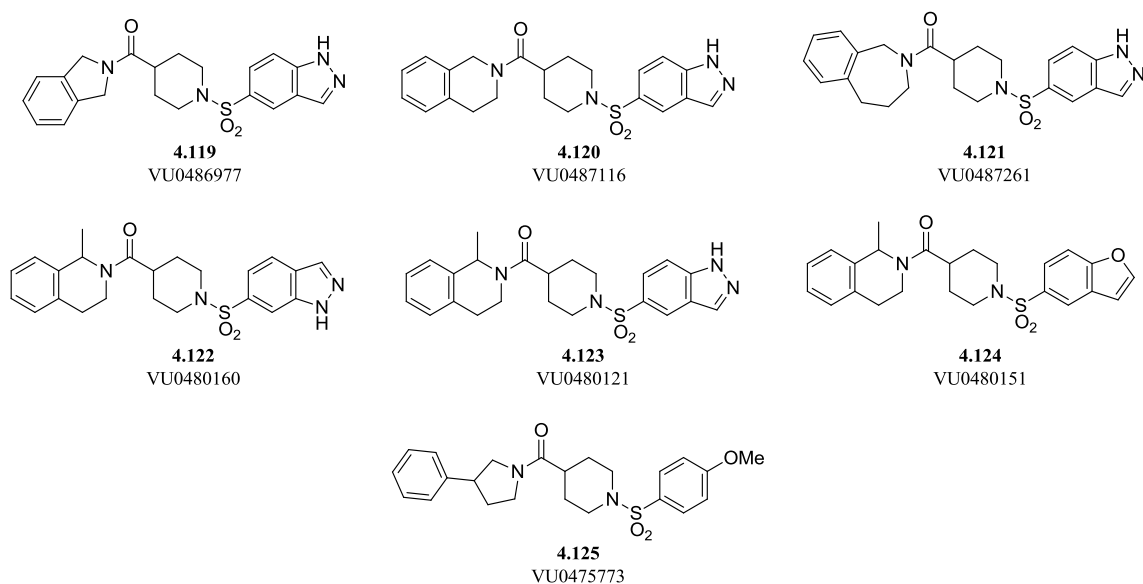


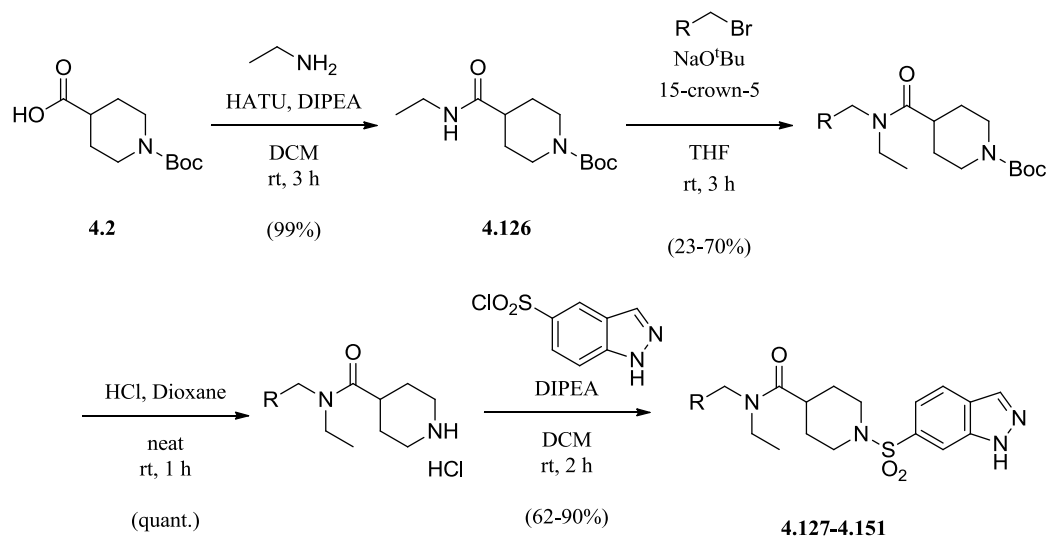
Figure 4.12. Structures of inactive analogs from the constrained *N*-alkyl library, analogs **4.119-4.125**.

Optimization of western benzamide ring substituent SAR

Disappointed by our unsuccessful attempts to directly address the oxidative dealkylation of the *N*-alkyl substituent, we elected to further explore the general SAR of

the chemical scaffold with the expectation that further potency optimization may also result in increased stability to metabolic processes. We next turned our attention to the SAR of the western benzamide region, recalling the marked improvement in potency observed after the introduction of the benzylic methyl during our previous exploration of this region. Up until this point an unadorned benzyl ring was present all of our analogs; therefore, we aimed to construct a library exploring diverse substitutions of the western benzyl ring in order to assess the general SAR of the region.

While planning the library we took great care in deciding which features of existing SAR to include and which to omit. We ultimately decided to use 1*H*-indazol-6-yl to serve as the model sulfonamide substituent to be used throughout the library. We also elected to construct the benzyl library analogs in the absence of the benzylic methyl. This latter decision was due to the estimation that omitting the benzylic methyl allowed us to avoid confusing constructive or destructive SAR interactions between benzyl ring substituents and the benzylic methyl, thus making for a more systematic examination of the benzyl ring SAR.



Scheme 4.13. General synthesis of benzyl bromide library compounds **4.127-4.151**. Synthesized jointly with M. Kokubo.

Beginning from *N*-Boc protected carboxylic acid core **4.2**, a HATU-mediated peptide coupling with ethanamine furnished the secondary amide **4.126**. The amide was deprotonated and alkylated with a library of 25 benzyl bromides and bromomethylpyridines to form the tertiary amides. Removal of the Boc protecting group for each analog intermediate was accomplished under standard anhydrous HCl conditions to provide the HCl salts. Finally, the secondary amines were sulfonylated with 1*H*-indazol-6-sulfonyl chloride to form the final library analogs **4.127-4.151** (Scheme 4.13).

The benzyl ring library analogs were tested in single point (10 μM) Ca^{2+} mobilization assays to assess their general PAM activity. The results of this primary assay are summarized in **Figure 4.13** and **Table 4.6**. The single point library revealed that a number of the benzyl ring modifications were productive. The activity of the benzyl ring substitution followed a general pattern of *ortho* > *meta* > *para*, with halide, methyl, trifluoromethyl, methoxy, and trifluoromethoxy substitutions all exhibiting

strong potentiation of the EC₂₀. Contrastingly, nitrile substitutions and methylpyridyl replacements displayed weak or no PAM activity.

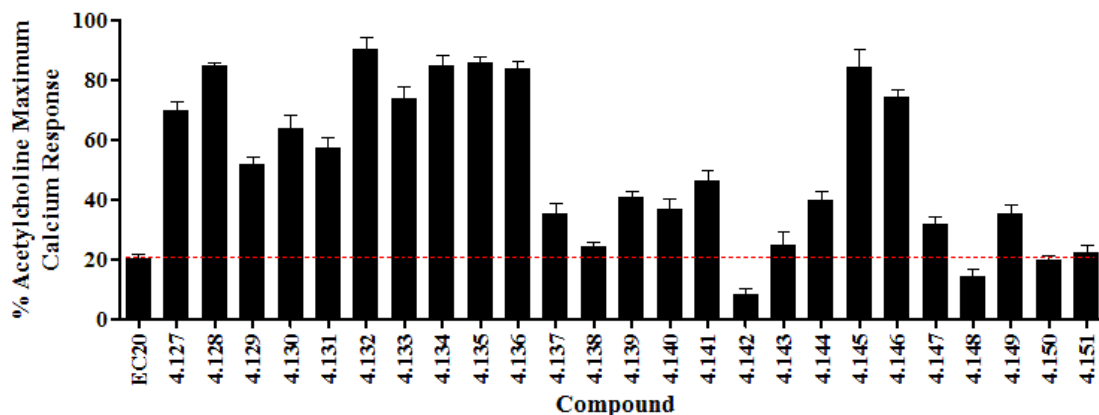
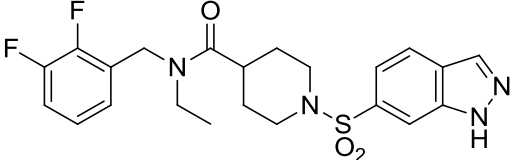
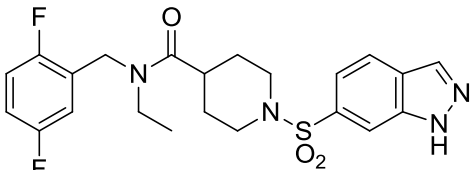
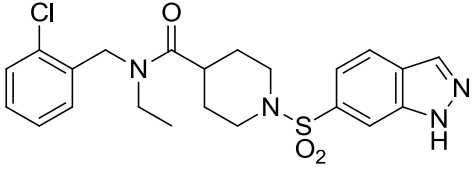
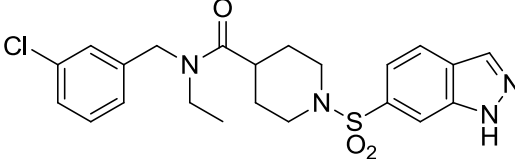
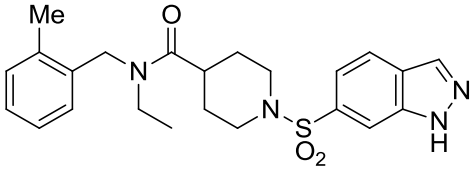
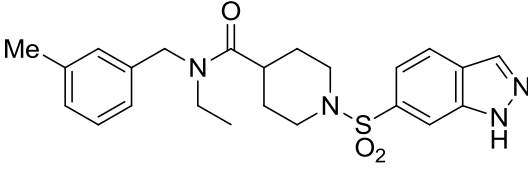
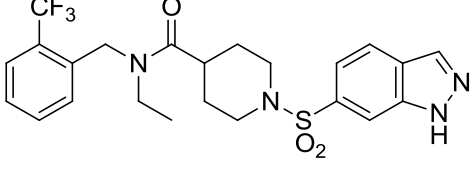
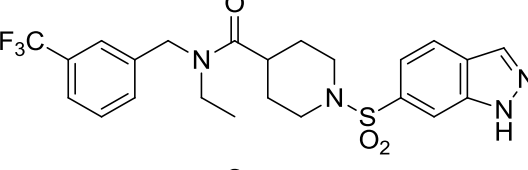
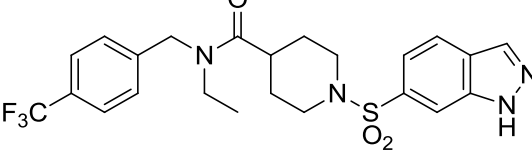
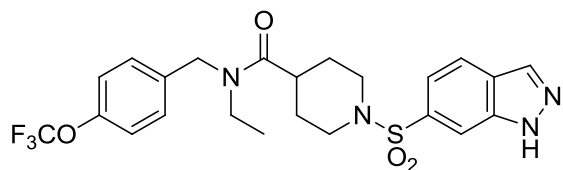
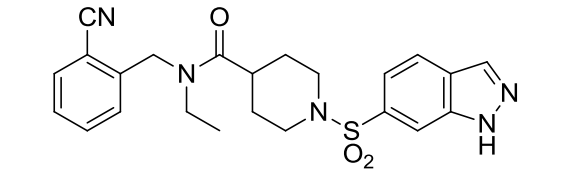
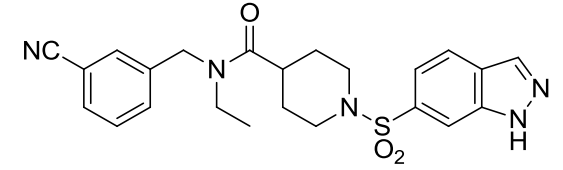
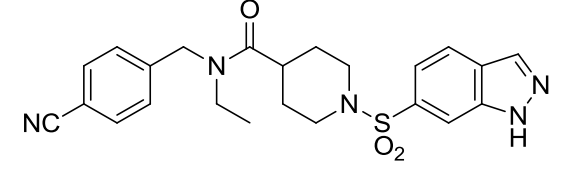
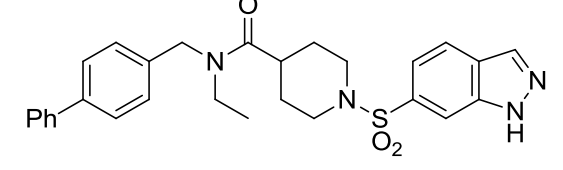
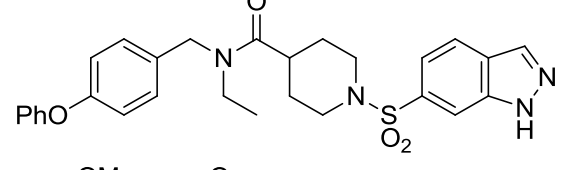
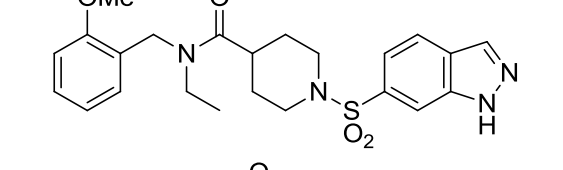
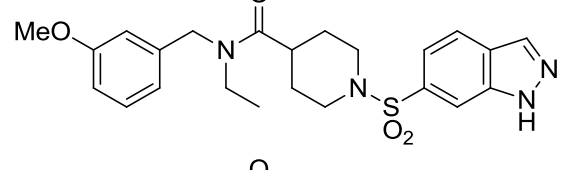
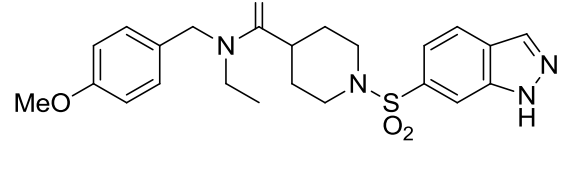


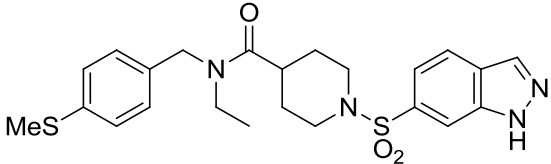
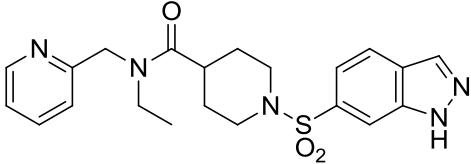
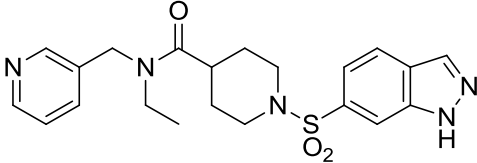
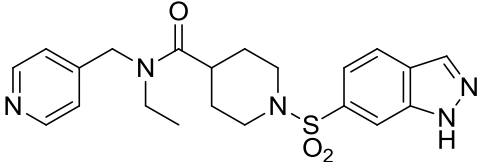
Figure 4.13. Comparison of single point (10 μ M) screen results of the benzyl library, analogs **4.127-4.151**. Ca²⁺ mobilization was used to obtain % ACh_{Max} values for each compound in the presence of a fixed submaximal (\sim EC₂₀) concentration of ACh. Data represent the mean \pm S.E.M. of at least 3 replicate experiments with similar results.

Table 4.6. Structures for benzyl analogs **4.127-4.151** and associated PAM activity data from the single point (10 μ M) screen at hM₅. Ca²⁺ mobilization responses for each compound are reported as a percentage of the maximum ACh response. VU number denotes the compound identifier assigned by Vanderbilt University. Data represent the mean of at least 3 replicate experiments with similar results.

Structure	Cmpd #	VU #	hM ₅ %ACh _{Max}
	4.127	VU0479095	69.9
	4.128	VU0477974	84.8
	4.129	VU0477945	52.1

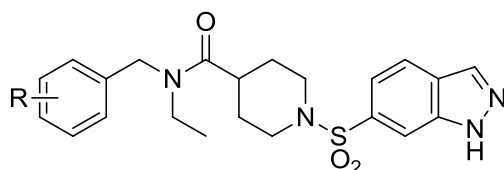
	4.130	VU0487292	63.7
	4.131	VU0477948	57.2
	4.132	VU0481717	90.7
	4.133	VU0479028	73.9
	4.134	VU0481762	85.1
	4.135	VU0481910	85.8
	4.136	VU0479111	84.2
	4.137	VU0482003	35.4
	4.138	VU0479129	24.2

	4.139	VU0477935	40.8
	4.140	VU0481788	36.8
	4.141	VU0480112	46.3
	4.142	VU0479112	8.4
	4.143	VU0480113	24.8
	4.144	VU0477880	39.6
	4.145	VU0487191	84.5
	4.146	VU0479011	74.2
	4.147	VU0480124	32.0

	4.148	VU0479128	14.0
	4.149	VU0480186	35.1
	4.150	VU0480161	19.8
	4.151	VU0481420	22.4

To further corroborate these SAR results we obtained potency data on selected analogs in full CRC Ca²⁺ mobilization assays at hM₅ (**Table 4.7**). As we observed in the single-point screen, the *ortho*-substituted analogs generally provided the greatest improvements in potency, with the *ortho*-CF₃ of compound **4.136** (VU0479111) demonstrating the greatest potency that we had yet observed in a non-isatin M₅ PAM (hM₅ EC₅₀ = 480 nM, %ACh_{Max} = 92).

Table 4.7. Potencies at hM₅ for substituted benzyl ring analogs selected from the single point (10 μM) screen. Ca²⁺ mobilization assays with hM₅ cells were used to obtain CRCs of compounds in the presence of a fixed submaximal (~EC₂₀) concentration of ACh. Data represent the mean of at least 3 independent experiments with similar results.



Cmpd #	R =	hM ₅ EC ₅₀ (μM)	% ACh _{Max}
4.127	2-F	2.1	83.9
4.128	3-F	1.5	88.8
4.129	4-F	>10	54.7
4.132	2-Cl	0.64	93.2
4.133	3-Cl	1.6	77.1
4.134	2-Me	0.87	100.0
4.135	3-Me	0.87	78.0
4.136	2-CF ₃	0.48	92.3
4.137	3-CF ₃	5.6	58.9
4.140	2-CN	6.5	68.0
4.141	3-CN	4.5	53.0
4.145	2-OMe	0.75	92.4
4.146	3-OMe	2.6	84.6

With our earlier lead analog, **4.75**, we had witnessed increased off-target mAChR activity accompanying the compound's sub-micromolar potency at M₅, thus we were interested to further characterize the activity of **4.136** in selectivity assays at the remaining human mAChRs and rM₅, and at fold shift assays at hM₅. The results of these studies are shown in **Figure 4.14** and **Figure 4.15**.

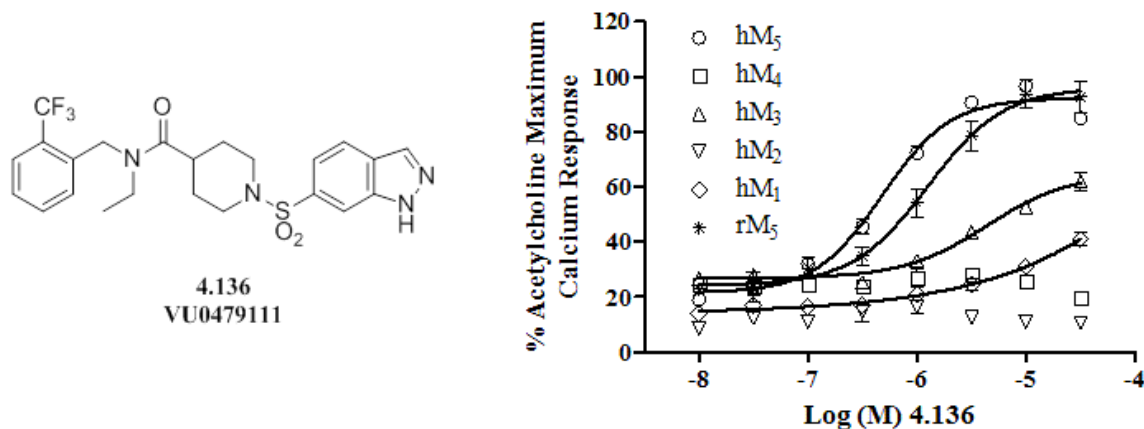


Figure 4.14. Structure, potency, and selectivity of analog **4.136** (VU0479111). Ca^{2+} mobilization assays with hM_1 - hM_5 (M_2 and M_4 co-expressing G_{aqi5}) and rM_5 cells were used to obtain CRCs of compound **4.136** in the presence of a fixed submaximal ($\sim\text{EC}_{20}$) concentration of ACh (EC_{50} values: hM_5 EC_{50} = 0.48 μM , $\% \text{ACh}_{\text{Max}}$ = 92; hM_3 EC_{50} = 4.4 μM , $\% \text{ACh}_{\text{Max}}$ = 65; hM_1 , hM_2 , hM_4 EC_{50} >30 μM ; rM_5 EC_{50} = 1.3 μM , $\% \text{ACh}_{\text{Max}}$ = 96). Data represent the mean \pm S.E.M. of at least 3 independent experiments with similar results.

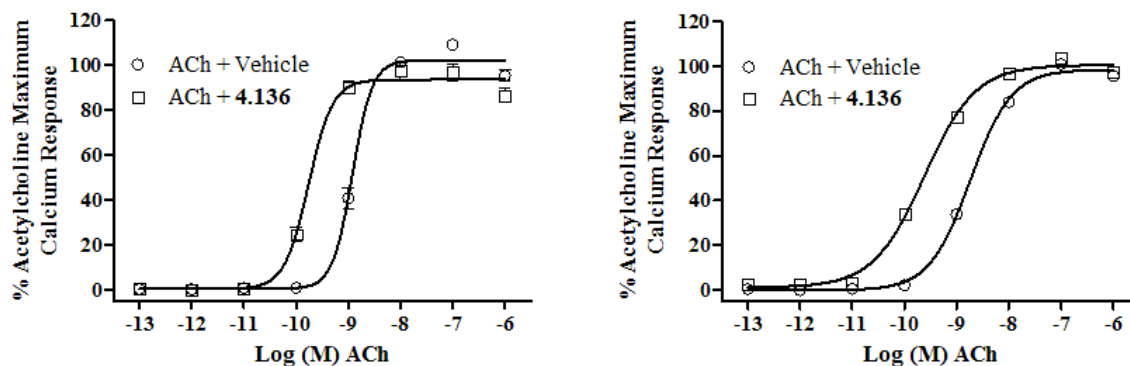


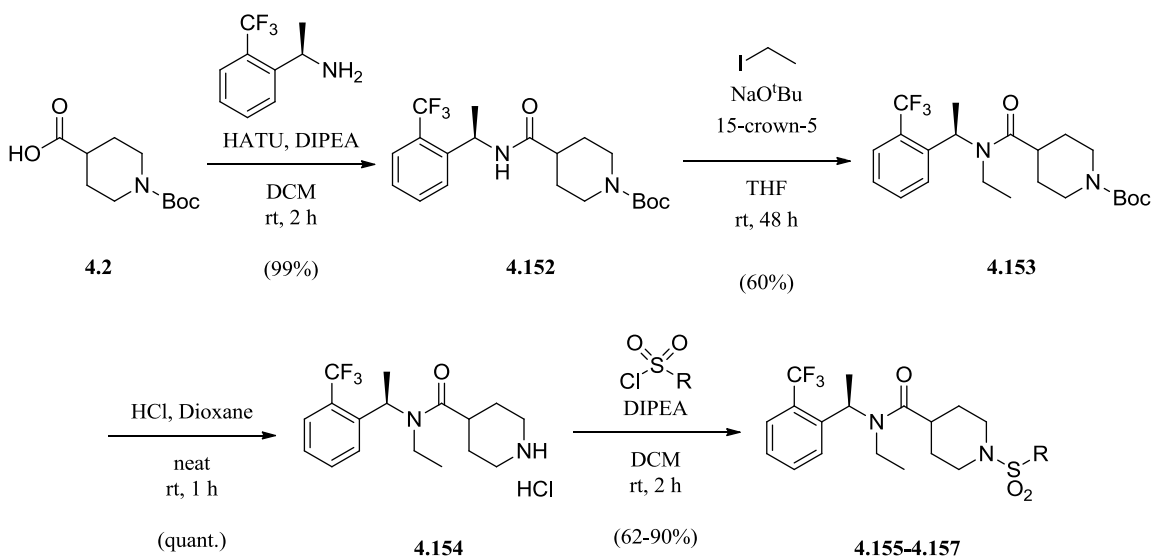
Figure 4.15. ACh CRC fold shifts of compound **4.136** (VU0479111) at hM_5 (left panel) and rM_5 (right panel). Ca^{2+} mobilization assays with hM_5 cells and rM_5 cells were used to obtain ACh CRCs in the presence of vehicle or 10 μM compound **4.136** (EC_{50} values: hM_5 EC_{50} of ACh + vehicle = 1.20 nM, hM_5 EC_{50} of ACh + **4.136** = 174 pM, hM_5 fold shift = 6.9; rM_5 EC_{50} of ACh + vehicle = 1.84 nM, rM_5 EC_{50} of ACh + **4.136** = 241 pM, rM_5 fold shift = 7.6). Data represent the mean \pm S.E.M. of at least 3 independent experiments with similar results.

These data revealed that **4.136** suffers some species difference, being ~ 3 -fold less potent at rM_5 than at hM_5 (rM_5 EC_{50} = 1.3 μM , $\% \text{ACh}_{\text{Max}}$ = 92). The compound is, however highly M_5 -preferring (hM_1 , hM_2 , hM_4 EC_{50} > 30 μM). M_3 remains the primary off-target mAChR activity (hM_3 EC_{50} = 4.4 μM , $\% \text{ACh}_{\text{Max}}$ = 65), yet it displayed ~ 2.5 -

fold less potency than in compound **4.75**. This factor, in combination with the increased potency at M_5 , indicates that the *ortho*-CF₃ benzyl modification of **4.136** considerably increased the selectivity window for the non-isatin M_5 PAMs. Despite the increased potency and selectivity window of **4.136**, fold shift assays revealed the compound is less proficient at shifting an ACh CRC (hM₅ fold shift = 6.9, rM₅ fold shift = 7.6) compared to **4.75** (hM₅ fold shift = 11.6, rM₅ fold shift = 17.1).

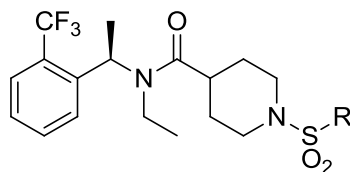
Combination of benzyl region SAR

Pleased with the gain in potency offered by the *ortho*-CF₃ benzyl substituent, we once again combined elements of SAR by synthesizing analogs possessing both the *ortho*-CF₃ as well as the (*R*)-oriented benzylic methyl. In order to maximize the diversity of SAR explored, this combination of SAR was attempted in the context of multiple sulfonamide substituents previously observed to be potent in their own respect.



Scheme 4.14. Synthesis of combined benzyl region SAR compounds **4.155-4.157**. Synthesis performed by M. Kokubo.

Table 4.8. Potencies at hM₅ for combined benzyl region SAR analogs **4.155-4.157**. Ca²⁺ mobilization assays with hM₅ cells were used to obtain CRCs of compounds in the presence of a fixed submaximal (~EC₂₀) concentration of ACh. VU number denotes the compound identifier assigned by Vanderbilt University. Data represent the mean of at least 3 independent experiments with similar results. ---, not determined.



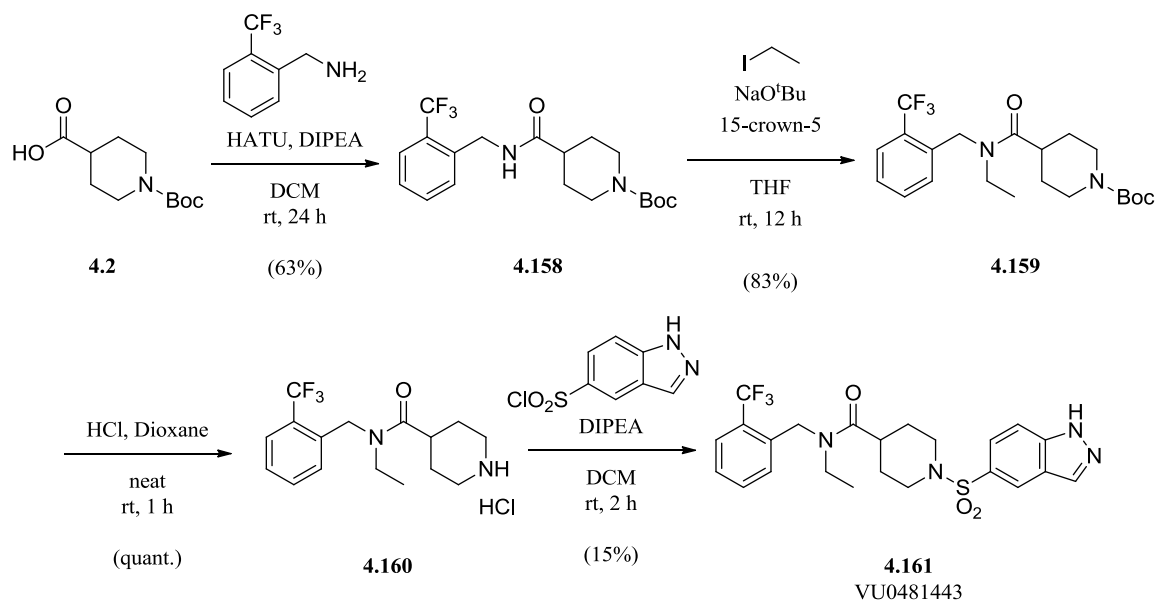
Cmpd #	R =	VU#	hM ₅ EC ₅₀ (μM)	% ACh _{Max}
4.155	1 <i>H</i> -indazol-5-yl	VU0482911	2.4	85.7
4.156	benzofuran-5-yl	VU0482908	>30	---
4.157	4-(1 <i>H</i> -pyrazol-1-yl)phenyl	VU0482909	>30	---

From the *N*-Boc protected carboxylic acid core **4.2**, a HATU-mediated peptide coupling with (*R*)-1-(2-(trifluoromethyl)phenyl)ethanamine furnished the secondary amide **4.152**. The amide was then deprotonated and treated with iodoethane to furnish intermediate **4.153**. Removal of the Boc protecting group was accomplished under standard anhydrous HCl conditions to provide HCl salt **4.154**. Finally, the secondary amine was sulfonylated with 1*H*-indazol-5-, benzofuran-5-, or 4-(1*H*-pyrazol-1-yl)benzene-1-sulfonyl chloride to form analogs **4.155-4.157** (Scheme 4.14). Disappointingly, CRC Ca²⁺ mobilization assays at hM₅ revealed that the SAR of the benzylic methyl group and the *ortho*-CF₃ substituent was not cooperative. Instead, combination of these structural elements resulted in inactive or dramatically weakened compounds (Table 4.8).

Discovery of VU0481443

After finding it unfavorable to combine the SAR of the benzylic methyl group with the *ortho*-CF₃ benzyl ring substituent, we sought alternate means to directly compare these two elements of benzamide SAR. Thus, we synthesized an analog possessing the *ortho*-CF₃ in the context of the 1*H*-indazol-5-sulfonamide substituent, which we previously observed to be slightly more potent than the 1*H*-indazol-6-yl congener in our initial library. This analog would serve as a direct comparator to compound **4.75** (VU0476212), which possessed the benzylic methyl in the context of the 1*H*-indazol-5-sulfonamide substituent.

From the *N*-Boc protected carboxylic acid core **4.2**, a HATU-mediated peptide coupling with 2-(trifluoromethyl)benzylamine furnished the secondary amide **4.158**. The amide was then deprotonated and treated with iodoethane to furnish intermediate **4.159**. Removal of the Boc protecting group was accomplished under standard anhydrous HCl conditions to provide HCl salt **4.160**. Finally, the secondary amine was sulfonylated with 1*H*-indazol-5-sulfonyl chloride to form analog **4.161** (VU0481443) (**Scheme 4.15**).



Scheme 4.15. Synthesis of compound **4.161** (VU0481443). Synthesized jointly with M. Kokubo

Upon testing in a full CRC Ca^{2+} mobilization assay at hM_5 , we were pleased to see that the *1H*-indazol-5-yl analog **4.161** was extremely potent (hM_5 EC_{50} = 190 nM, % ACh_{Max} = 96). Analog **4.161** was thus ~2.5-fold more potent than the *1H*-indazol-6-sulfonamide analog **4.136**, ~4-fold more potent than its benzylic methyl congener **4.75** (VU0476212), and the most potent M_5 PAM that we had observed to date.

***In vitro* pharmacological characterization of non-isatin M_5 PAM VU0481443**

Characterization of VU0481443 mAChR selectivity and fold shift

Impressed by the hM_5 potency of **4.161** (VU0481443), we desired to obtain a more extensive *in vitro* pharmacologic profile. This characterization effort began with a full mAChR subtype-selectivity profile for the compound. Counterscreening was carried

out against human mAChR subtypes as well as for all rat mAChR subtypes (**Figure 4.16**).

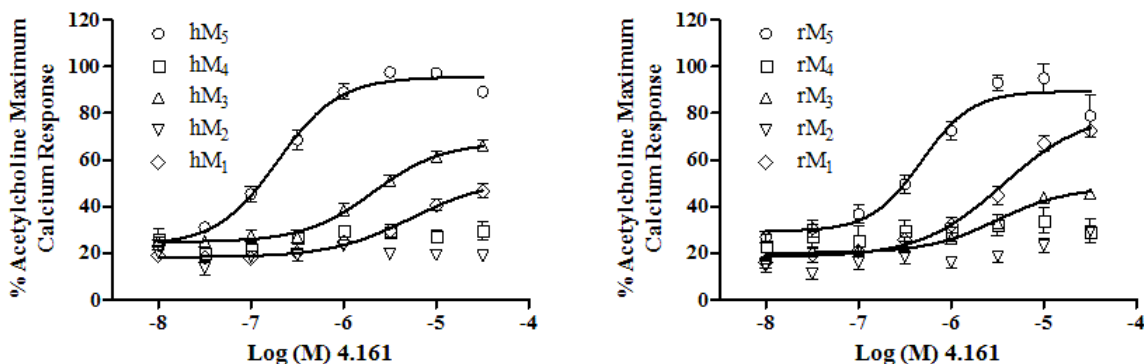


Figure 4.16. Potency and selectivity of compound **4.161** (VU0481443) at all human and rat mAChR subtypes. Ca^{2+} mobilization assays with hM₁-hM₅ cells and with rM₁-rM₅ cells (M₂ and M₄ co-expressing G_{αqis}) were used to obtain CRCs of **4.161** in the presence of a fixed submaximal (~EC₂₀) concentration of ACh (EC₅₀ values: hM₅ EC₅₀ = 0.19 μM, %ACh_{Max} = 96; hM₃ EC₅₀ = 2.1 μM, %ACh_{Max} = 68; hM₁ EC₅₀ = 5.4 μM, %ACh_{Max} = 52; hM₂, hM₄ EC₅₀ >30 μM; rM₅ EC₅₀ = 0.48 μM, %ACh_{Max} = 89; rM₃ EC₅₀ = 3.1 μM, %ACh_{Max} = 48; rM₁ EC₅₀ = 3.6 μM, %ACh_{Max} = 81; rM₂, rM₄ EC₅₀ >30 μM). Data represent the mean ± S.E.M. of at least 3 independent experiments with similar results.

The mAChR selectivity panel revealed that **4.161** possesses a high degree of preference for hM₅ and ~10-fold selectivity for hM₅ over hM₁ and hM₃ (hM₃ EC₅₀ = 2.1 μM, %ACh_{Max} = 68; hM₁ EC₅₀ = 5.4 μM, %ACh_{Max} = 52). Across rat mAChR subtypes, we again observed rM₅ to be ~2.5-fold less potent than the human isoform (rM₅ EC₅₀ = 0.48 μM, %ACh_{Max} = 89). Interestingly, the rat mAChR subtypes displayed different subtype selectivity than the human isoforms, with M₃ activity diminished and M₁ activity becoming the prevalent off target mAChR subtype (rM₃ EC₅₀ = 3.1 μM, %ACh_{Max} = 48; rM₁ EC₅₀ = 3.6 μM, %ACh_{Max} = 81).

Further characterization of the compound's efficacy was probed in fold shift assays. In these assays **4.161** induced a 9.3-fold leftward shift of the ACh CRC in hM₅

and 13.8-fold shift in rM₅ (**Figure 4.17**). Although the fold shifts of **4.161** are greater than most of the previous analogs, the fold shifts of the benzylic methyl congener **4.75** (hM₅: 11.6-fold, rM₅: 17.1 fold) remain the highest values yet observed with this chemical series. Thus, although our exploration of the SAR around the benzyl ring resulted in the greatest potency of this chemical series, the SAR around the benzylic methyl position appears to have a greater ability to shift the CRC of ACh. Nevertheless, the submicromolar potency, M₅-selectivity, and ACh fold shift exhibited by compound **4.161** earned it lead compound status and it was subsequently approved as an MLPCN probe and given the identifier ML380.

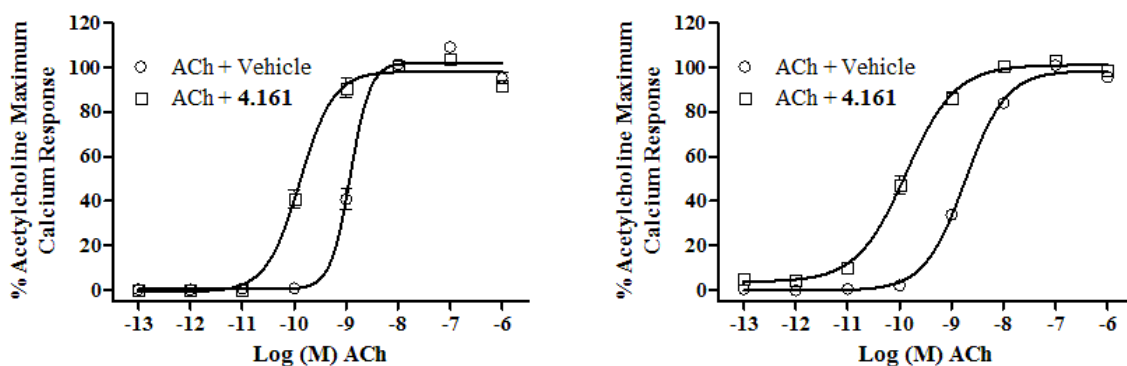


Figure 4.17. ACh CRC fold shifts of compound **4.161** (VU0481443) at hM₅ (left panel) and rM₅ (right panel). Ca²⁺ mobilization assays with hM₅ cells and rM₅ cells were used to obtain ACh CRCs in the presence of vehicle or 10 μM compound **4.161** (EC₅₀ values: hM₅ EC₅₀ of ACh + vehicle = 1.20 nM, hM₅ EC₅₀ of ACh + **4.161** = 129 pM, hM₅ fold shift = 9.3; rM₅ EC₅₀ of ACh + vehicle = 1.84 nM, rM₅ EC₅₀ of ACh + **4.161** = 133 pM, rM₅ fold shift = 13.8). Data represent the mean ± S.E.M. of at least 3 independent experiments with similar results.

Ancillary pharmacology of VU0481443

To more broadly characterize the off-target pharmacology of **4.161**, we assayed the compound in a commercial radioligand competition binding screen of 67 GPCRs, ion channels, and transporters (**Table 4.9**). Pleasingly, **4.161** showed significant inhibition of

binding ($\geq 50\%$ radioligand displacement) at only two of the targets tested: cannabinoid CB₁ (50% displacement) and sigma σ_1 (53% displacement).

Table 4.9. Ancillary/off-target competition binding screen results for **4.161** (VU0481443, ML380). **4.161** was dosed at 10 μM for single point competition binding assays. Targets displaying significant binding ($\geq 50\%$ at 10 μM) are outlined. Data represent the mean of 2 independent experiments with similar results. Studies performed by Eurofins Panlabs, Inc.

Target/Protein	Species	% Inhibition
Adenosine A ₁	Human	-3
Adenosine A _{2A}	Human	3
Adenosine A ₃	Human	14
Adrenergic α_{1A}	Rat	12
Adrenergic α_{1B}	Rat	-10
Adrenergic α_{1D}	Human	5
Adrenergic α_{2A}	Human	37
Adrenergic β_1	Human	3
Adrenergic β_2	Human	-8
Androgen (Testosterone) AR	Rat	11
Bradykinin B ₁	Human	8
Bradykinin B ₂	Human	11
Calcium Channel L-Type, Benzothiazepine	Rat	37
Calcium Channel L-Type, Dihydropyridine	Rat	17
Calcium Channel N-Type	Rat	2
Cannabinoid CB ₁	Human	50
Dopamine D ₁	Human	7
Dopamine D _{2S}	Human	6
Dopamine D ₃	Human	23
Dopamine D _{4.2}	Human	-2
Endothelin ET _A	Human	1
Endothelin ET _B	Human	8
Epidermal Growth Factor (EGF)	Human	9
Estrogen ER α	Human	8
GABA _A , Flunitrazepam, Central	Rat	1
GABA _A , Muscimol, Central	Rat	-2
GABA _{B1A}	Human	-2
Glucocorticoid	Human	1
Glutamate, Kainate	Rat	-6
Glutamate, NMDA, Agonism	Rat	1
Glutamate, NMDA, Glycine	Rat	-2
Glutamate, NMDA, Phencyclidine	Rat	8
Histamine H ₁	Human	26
Histamine H ₂	Human	5
Histamine H ₃	Human	6

Imidazoline I ₂ , Central	Rat	15
Interleukin IL-1	Mouse	-9
Leukotriene, Cysteinyl CysLT ₁	Human	38
Melatonin MT ₁	Human	34
Muscarinic M ₁	Human	1
Muscarinic M ₂	Human	1
Muscarinic M ₃	Human	14
Neuropeptide Y Y ₁	Human	-4
Neuropeptide Y Y ₂	Human	3
Nicotinic Acetylcholine	Human	8
Nicotinic Acetylcholine α 1, Bungarotoxin	Human	1
Opiate δ ₁ (OP1, DOP)	Human	6
Opiate κ (OP2, KOP)	Human	5
Opiate μ (OP3, MOP)	Human	5
Phorbol Ester	Mouse	2
Platelet Activating Factor (PAF)	Human	7
Potassium Channel [K _{ATP}]	Human	5
Potassium Channel hERG	Human	18
Prostanoid EP ₄	Human	33
Purinergic P2X	Rabbit	31
Purinergic P2Y	Rat	4
Rolipram	Rat	4
Serotonin (5-HT _{1A})	Human	0
Serotonin (5-HT _{2B})	Human	32
Serotonin (5-HT ₃)	Human	-4
Sigma σ₁	Human	53
Sodium Channel, Site 2	Rat	49
Tachykinin NK ₁	Human	18
Thyroid Hormone	Rat	5
Transporter, Dopamine (DAT)	Human	39
Transporter, GABA	Rat	-1
Transporter, Norepinephrine (NET)	Human	20
Transporter, Serotonin (SERT)	Human	2

Confirmation of the allosteric mechanism of VU0481443

Although the allosteric mechanism of **4.161** was strongly supported by its behavior in double-add Ca²⁺ mobilization assays (i.e. – **4.161** possesses no inherent activity, yet potentiates an ACh EC₂₀), we desired to confirm the allosteric mechanism via [³H]-NMS competition binding with **4.161** (**Figure 4.18**). As anticipated, when

competing with [³H]-NMS in hM₅ membrane preparations, **4.161** does not compete for the orthosteric site. These competition binding data, when taken into account with the aforementioned evidence of an allosteric mechanism, strongly suggests that **4.161** is indeed an allosteric modulator.

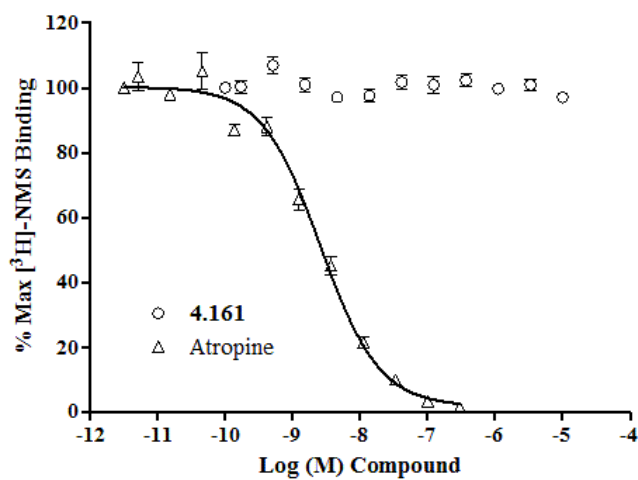


Figure 4.18. [³H]-NMS competition binding assay with **4.161** (VU0481443, ML380) in an hM₅ membrane preparation. [³H]-NMS and a CRC of either atropine (control) or **4.161** were allowed to equilibrate for 3 hours in the hM₅ membrane preparation before filtration and scintillation counting (K_i values: atropine $K_i = 1.5$ nM, **4.161** $K_i \gg 10$ μ M). Data represent the mean \pm S.E.M. of at least 3 independent experiments with similar results.

***In vitro* and *in vivo* DMPK characterization of non-isatin M₅ PAM VU0481443**

Encouraged by the compound's potent and M₅-preferring *in vitro* pharmacological profile, we began investigating the DMPK profile of **4.161** (VU0481443, ML380). **4.161** was entered into multiple studies, including plasma protein binding, rat brain homogenate binding, and rat and human microsomal stability. The results from these assays are summarized in **Table 4.10**. As with compound **4.75**, **4.161** displayed very low metabolic stability, with high intrinsic clearance values and

correspondingly high predicted hepatic clearance values near hepatic blood flow in both rat and human.

Table 4.10. *In vitro* and *in vivo* IV PK/PBL DMPK data for **4.161** (VU0481443, ML380) in multiple species. Studies performed by T. Bridges. ---, not determined.

Parameter	Rat	Human
hepatic microsome CL_{int} (mL/min/kg)	2639	538
predicted CL_{hep} (mL/min/kg)	68.3	20.2
$f_{u,plasma}, f_{u,brain}$	0.014, 0.011	0.015, ---
CL_p (mL/min/kg)	66	---
Elimination, $t_{1/2}$ (min)	22	---
$K_p, K_{p,uu}$ (0.25 h, IV)	0.36, 0.28	---

The instability of **4.161** was reconfirmed in an *in vivo* IV PK/PBL assay where compound was dosed to male Sprague-Dawley rats at 1 mg/kg ($n = 3$). The compound displayed high plasma clearance and a short half-life. A modest K_p of 0.36 was determined at 15 minutes post-administration which translates to a $K_{p,uu}$ of 0.28, indicating that the compound is weakly CNS penetrant, or a substrate for active efflux across the BBB.

To examine this latter hypothesis we tested the compound in an *in vitro*, bidirectional transwell assay employing MDCK-MDR1 cells to assess efflux liabilities at the BBB. When dosed at 5 μ M, **4.161** exhibited an efflux ratio of 16, suggesting that it is a strong substrate for P-gp-mediated active efflux. This high efflux ratio, along with the restricted CNS penetrance demonstrated in the IV PK/PBL study, indicates that **4.161** is impractical as a chemical probe for M_5 within the CNS. Nevertheless, if the stability of

the compound could be improved, its restriction to the periphery may prove to make **4.161** an ideal probe for studying M₅ in the endothelium of the cerebral vasculature.

Given that the tertiary amide of **4.161** was virtually unchanged from that of **4.75**, it appeared probable that the compound was undergoing an identical or similar oxidative dealkylation process. Thus we again turned our synthetic efforts back to exploring novel SAR that could bolster the stability of the chemical scaffold while maintaining its potent M₅ PAM activity.

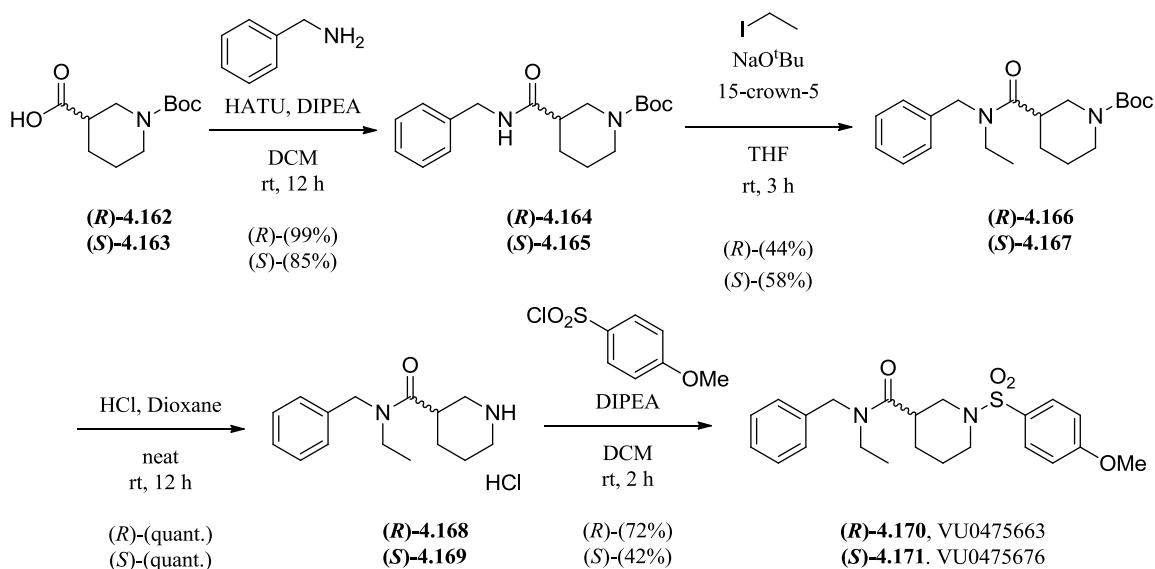
Continued SAR exploration of non-isatin M₅ PAM VU0481443

Exploration of piperidine core modifications

We investigated multiple modifications to the heretofore unexplored piperidine core, hypothesizing that changes to the structure or orientation of the core and its connectivity to the tertiary amide may block the instabilities around this region. As with our earlier exploration of the amide carbonyl composition and orientation, it should be noted that this effort was not concerted, but was compiled from several standalone syntheses performed alongside larger library synthetic efforts, hence the assortment of elements of SAR.

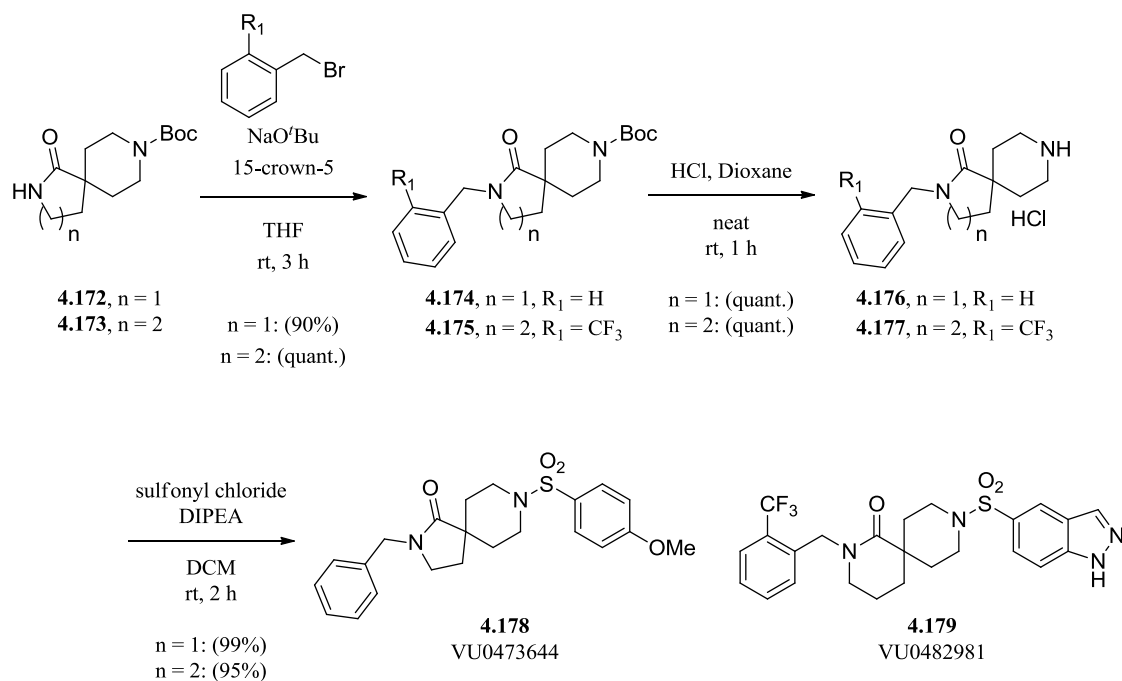
The earliest modification of the core involved simply shifting the connectivity of the amide one carbon over, thus kinking the structure and introducing a chiral center. From the enantiopure starting materials (*S*)- or (*R*)-1-Boc-piperidine-3-carboxylic acid, analogs (*R*)-**4.170** and (*S*)-**4.171** were synthesized in the context of 4-methoxybenzenesulfonamide in the previously detailed fashion (**Scheme 4.16**). Both

analogues were found to be inactive in CRC Ca^{2+} mobilization assays at hM_5 ($\text{hM}_5 \text{EC}_{50} \gg 30 \mu\text{M}$).



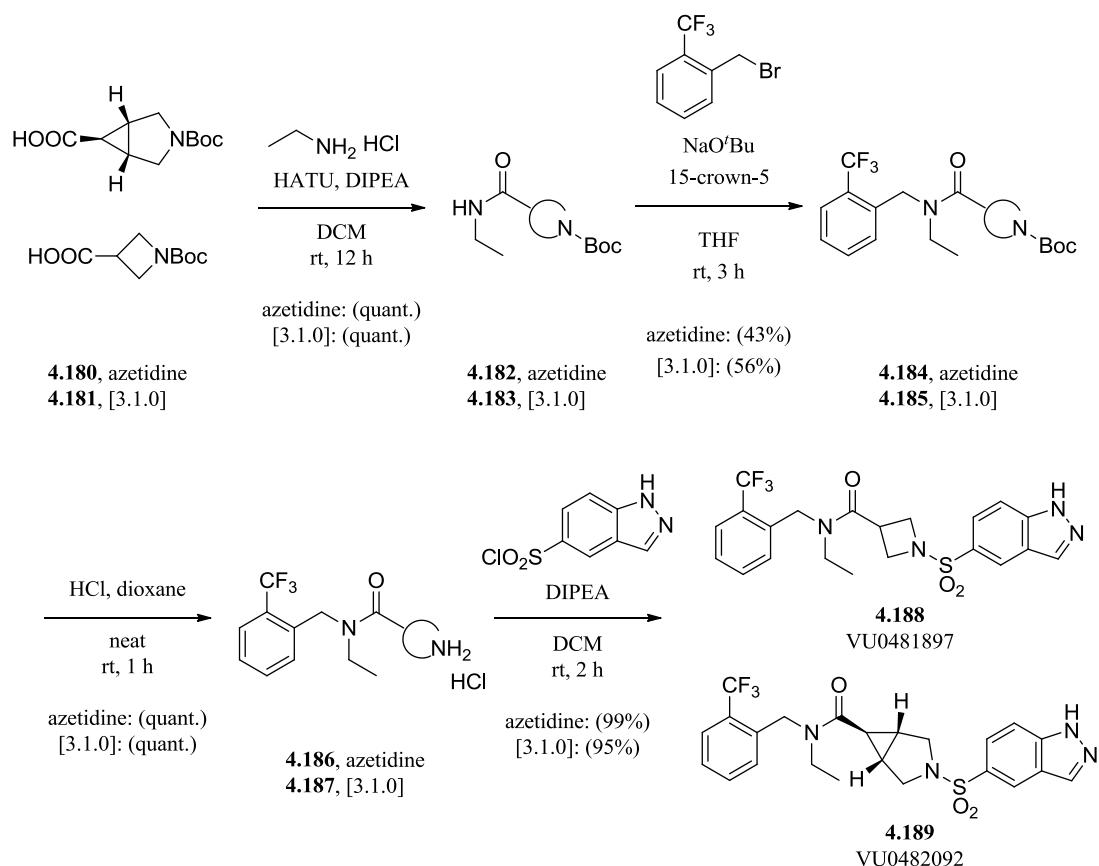
Scheme 4.16. Synthesis of shifted piperidine core analogs **4.170** (VU0475663) and **4.171** (VU0475676).

Echoing our attempts at constraining the *N*-alkyl moiety to the benzyl ring, we synthesized two analogs that constrain the *N*-alkyl to the piperidine core itself in a spirocyclic fashion. In both cases an *N*-Boc-protected spirocyclic amide was alkylated with a benzyl bromide, deprotected, and subsequently sulfonylated in the previously detailed fashion to provide analogs **4.178** and **4.179** (Scheme 4.17). Once again, both analogs proved to be inactive in CRC Ca^{2+} mobilization assays at hM_5 ($\text{hM}_5 \text{EC}_{50} \gg 30 \mu\text{M}$).



Scheme 4.17. Synthesis of spirocyclic core compounds **4.178** (VU0473644) and **4.179** (VU0482981). Synthesized jointly with M. Kokubo.

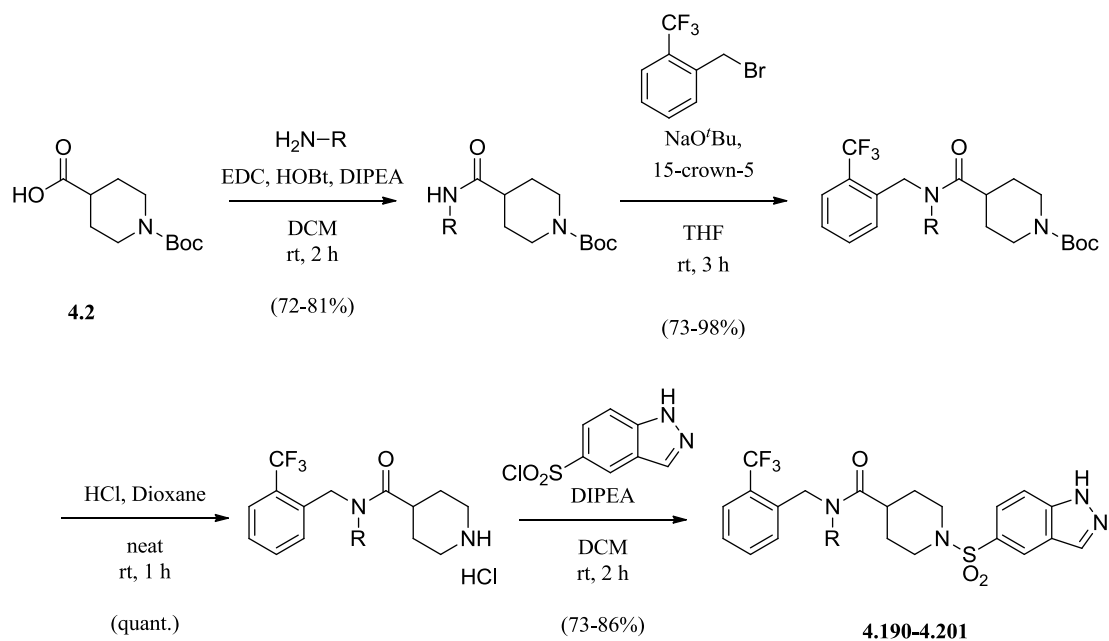
Our final attempt at SAR exploration in this region was the alteration of the core structure itself. In the case of analog **4.188** we substituted an azetidine core, whereas in the case of analog **4.189** we substituted a 3-azabicyclo[3.1.0]hexane core. For both analogs, the synthesis began from the respective *N*-Boc protected acid cores and proceeded in the previously detailed fashion (**Scheme 4.18**). SAR of the core yet again proved to be intractable as both analogs were devoid of activity in CRC Ca²⁺ mobilization assays at hM₅ (hM₅ EC₅₀ >>30 μM).



Scheme 4.18. Synthesis of central core substitutions, analogs **4.188** (VU0481897) and **4.189** (VU0482092). Syntheses performed by M. Kokubo.

Substitution of the amide N-alkyl substituent

As we were thwarted in all attempts to dramatically change the structure or conformation of the sensitive amide region of the chemical scaffold, we opted to take a new approach by substituting the *N*-alkyl substituent. Employing a variety of small alkylamines we were able to construct a library of novel *N*-alkyl analogs in the context of both the *ortho*-CF₃ benzyl substitution and the 1*H*-indazol-5-sulfonamide.



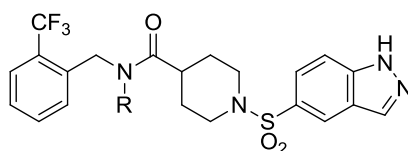
Scheme 4.19. General synthesis of *N*-alkyl library analogs **4.190-4.201**. Syntheses performed by M. Kokubo.

From the *N*-Boc protected carboxylic acid core **4.2**, an EDC-mediated peptide coupling with one of a library of 12 alkyl halides furnished the secondary amide intermediates. The amides were next deprotonated with *tert*-butoxide followed by treatment with 1-(bromomethyl)-2-(trifluoromethyl)benzene to form the tertiary amide intermediates. Removal of the Boc protecting group was accomplished under standard anhydrous HCl conditions to provide the HCl salts. Finally, the secondary amines were sulfonylated with 1*H*-indazol-5-sulfonyl chloride to produce compounds **4.190-4.201** (**Scheme 4.19**).

When the analogs were tested in full CRC Ca²⁺ mobilization assays at hM₅, we were pleased to see that the SAR surrounding the *N*-alkyl substituent was diverse and rich. Multiple *N*-alkyl substitutions resulted in highly potent M₅ PAMs. Aliphatic substitutions were highly productive, with EC₅₀ values as low as 120 nM in the case of

the *N*-neopentyl analog **4.196** (Table 4.11). Many of the *N*-alkyl analogs were submitted to human and rat hepatic microsome stability studies in order to ascertain if these changes in any way affected the scaffold's metabolic instability. Unfortunately, despite the variety of substitutions, all analogs tested were rapidly cleared, with predicted hepatic clearance values at parity with hepatic blood flow in each species. The *N*-cyclopropyl analog **4.197** was cleared at relatively slower rate; however, it was inactive in Ca²⁺ mobilization assays at hM₅ (Table 4.11).

Table 4.11. Potencies at hM₅ for *N*-alkyl library analogs **4.190-4.201** and corresponding microsomal clearance data in rat and human for selected analogs. Ca²⁺ mobilization assays with hM₅ cells were used to obtain CRCs of compounds in the presence of a fixed submaximal (~EC₂₀) concentration of ACh. VU number denotes the compound identifier assigned by Vanderbilt University. Data represent the mean of at least 3 independent experiments with similar results. Microsomal clearance studies performed by T. Bridges. ---, not determined.



Cmpd #	R =	VU#	EC ₅₀ (μM)	%ACh _{Max}	CL _{int} (mL/min/kg)		CL _{hep} (mL/min/kg)	
					human	rat	human	rat
4.190	2-hydroxyethyl	VU0485999	>10	74.0	384	1252	19.9	66.3
4.191	2-fluoroethyl	VU0516506	1.3	94.7	1611	2799	20.7	68.3
4.192	Propyl	VU0516529	0.16	93.7	1596	6013	20.7	69.2
4.193	Allyl	VU0516505	1.8	78.5	1853	7257	20.8	69.3
4.194	Isopropyl	VU0485822	>10	54.8	3475	682	68.6	20.4
4.195	Isobutyl	VU0517948	0.15	100.0	1517	5826	20.7	69.2
4.196	Neopentyl	VU0549968	0.12	104.0	652	1672	20.3	67.2
4.197	Cyclopropyl	VU0516341	>30	---	88	414	17.0	60.0
4.198	Cyclobutyl	VU0517619	1.8	84.2	872	7301	20.5	69.3
4.199	Methylcyclopropyl	VU0603726	0.12	101.5	---	---	---	---
4.200	Methylcyclobutyl	VU0603725	0.13	102.8	---	---	---	---
4.201	Benzyl	VU0650166	0.75	97.9	---	---	---	---

Our previous metabolite identification study that identified oxidative dealkylation as the primary mode of clearance was carried out on the less potency optimized analog **4.75**. In order to investigate if the current series of *N*-alkyl substituted analogs was cleared via the same biotransformation pathways we initiated a second metabolite identification study on the highly potent *N*-neopentyl analog **4.196**.

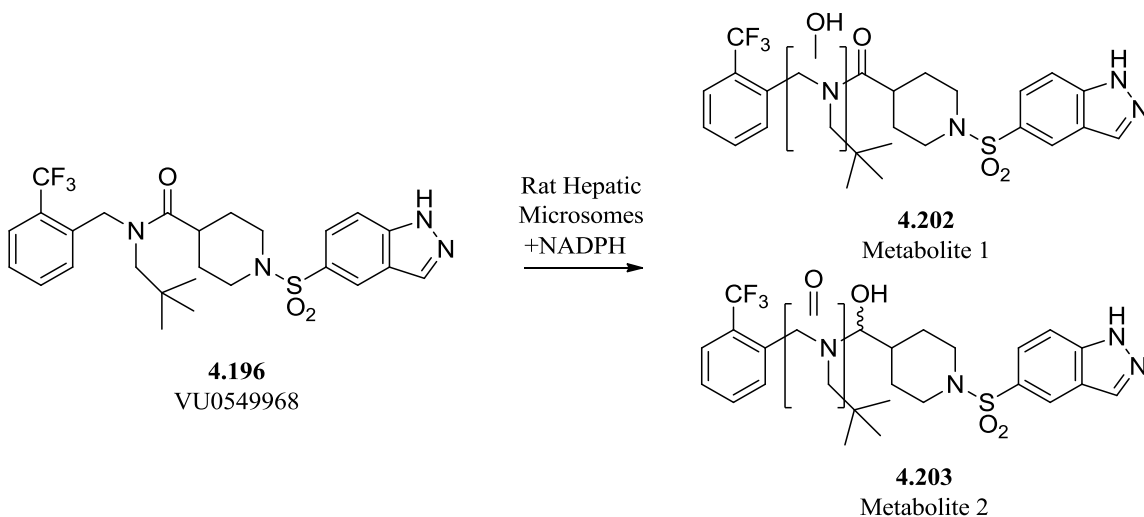


Figure 4.19. Results of metabolite identification following incubation of analog **4.196** (VU0549968) with rat hepatic microsomes and NADPH. Studies performed by A. Rajapakse.

This study revealed a pathway similar to what we had previously observed, but it gave more detailed insight into the clearance pathway (**Figure 4.19**). The primary metabolites detected indicated keto-reduction of the amide (**4.203**) as well as methylene hydroxylation (**4.202**). This latter metabolite could potentially be involved in the dealkylation pathway we previously observed by forming an unstable hemiaminal which subsequently collapses, dealkylating the amide.

Summary and future directions

The first non-isatin M₅ PAM, **4.1** (VU0472882), was discovered in an HTS of the MLPCN screening deck, presenting weak potency at M₅. The HTS lead was subsequently subjected to a multidimensional iterative parallel synthesis optimization effort to explore SAR and improve potency. This effort produced over 170 analogs, culminating in the lead compound, **4.161** (VU0481443, ML380), an M₅-preferring PAM which possessed over 50-fold greater potency at M₅ relative to the HTS lead (**Figure 4.20**).

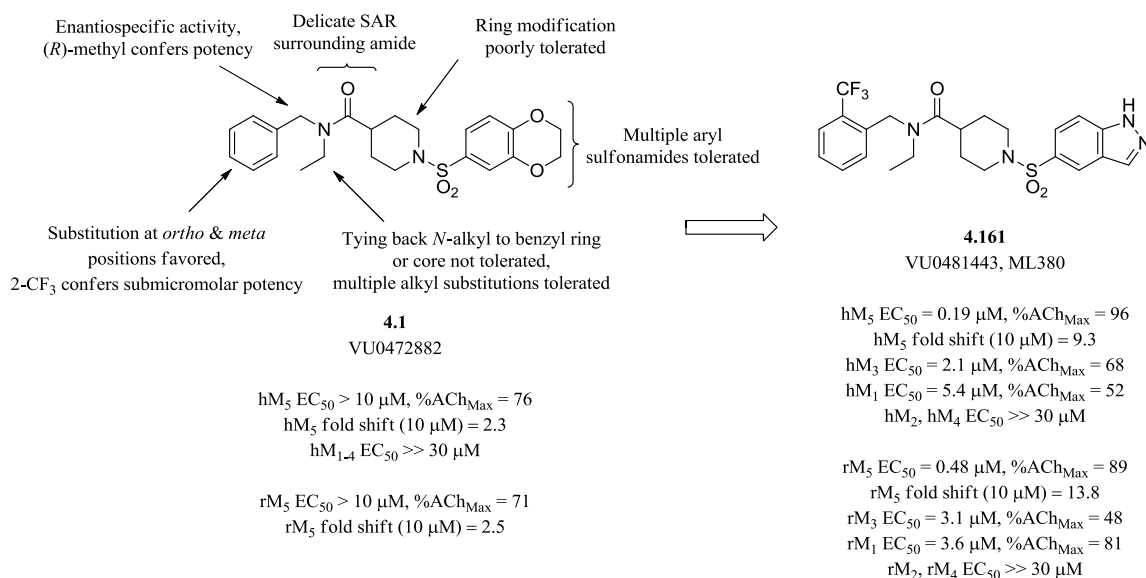


Figure 4.20. Summary and comparison of the structure, potency, and SAR found around the non-isatin M₅ PAM HTS lead **4.1** (VU0472882) that led to the discovery of the novel, sub-micromolar, non-isatin M₅-preferring PAM **4.161** (VU0481443, ML380).

In exploring the SAR of the compound it was found that the sulfonamide region possessed a high degree of flexibility in what substituents were tolerated. Nearly all aryl sulfonamides produced active analogs; however it was found that 6-5 heterocyclic

systems such as 1*H*-indazol-5-, 1*H*-indazol-6-, and benzofuran-5-sulfonamide produced the most potent results (analogs **4.47**, **4.50**, and **4.53**, respectively).

The benzyl region of the molecule was found to have more nuanced SAR. The introduction of a methyl to the benzylic position revealed enantiospecific activity, with the (*R*)-oriented methyl producing sub-micromolar activity in the context of a 1*H*-indazol-5-sulfonamide (analog **4.75**). Sub-micromolar EC₅₀s could also be obtained via the substitution of benzyl ring, with the *ortho* position being highly favored. It was in this region that the introduction of an *ortho*-CF₃ on the benzyl ring in the context of a 1*H*-indazol-5-sulfonamide led to our current lead compound, the highly potent **4.161**. In further characterization, **4.161** was found to be highly M₅-preferring (**Figure 4.20**).

From a DMPK standpoint, **4.161** possessed moderate-to-low plasma protein binding values in rat and human (rat $f_u = 0.014$; human $f_u = 0.015$); however, the intrinsic clearance of the compound was found to be high, with the predicted hepatic clearance values equivalent to hepatic blood flow in rat and human (rat CL_{int} = 2639 mL/min/kg, predicted rat CL_{hep} = 68 mL/min/kg; human CL_{int} = 538, predicted human CL_{hep} = 20 mL/min/kg). Metabolite identification studies indicated that the primary metabolic product was a result of oxidative dealkylation of the *N*-ethyl group. In reaction to these data, all further SAR exploration was aimed at bolstering this metabolic lability. A multitude of analogs were synthesized exploring the migration and substitution of the amide, the cyclization of the *N*-alkyl to either the benzyl ring or core piperidine ring, and the substitution of the piperidine core. Unfortunately, in all cases these our efforts resulted in inactive or weakly potent compounds.

The only further region of tractable SAR that was discovered was the substitution of the *N*-alkyl substituent. A library constructed around this region revealed that bulky aliphatic substituents were highly favored, producing potencies as low as 120 nM. Regrettably, these compounds also suffered from rapid clearance.

At present, compound **4.161** remains our lead non-isatin M₅ PAM. Although **4.161** is not a highly CNS penetrant M₅ PAM, its potency and preference for M₅ make it a potential candidate for pharmacodynamic studies of the relationship between M₅ potentiation and the dilation of rat cerebral vasculature. Currently, **4.161** is entered into such a study that is using functional MRI to monitor changes in cerebral blood volume in response to the presence of an M₅ PAM. The outcome of these experiments hold the potential to answer fundamental questions put forth in studies of the constitutively constricted cerebral vasculature of M₅^{-/-} mice (Chapter I).

Regardless of the outcome of the pharmacodynamic studies, the high rate of hepatic microsome clearance and off-target M₃/M₁ activity of **4.161** leave open the possibility for further optimization of this chemical series. A future optimization effort might begin by reexamining existing analogs that did not undergo full selectivity screens. By counterscreening these analogs against M₃ and M₁, elements of SAR that dial-in or dial-out M₃ and/or M₁ activity may become apparent. Similarly, a counterscreen of all analogs against rM₅ may reveal the elements of SAR that are the basis for the slight species difference in potency between hM₅ and rM₅.

Beyond further scrutiny of existing analogs, many possibilities remain for synthesizing new non-isatin M₅ PAM analogs focusing on the lightly explored regions of the chemical scaffold. For instance, our library of *N*-alkyl substituents revealed that many

substituents produce active compounds, but the majority of these library members were entirely aliphatic. Incorporating *N*-aryl or *N*-heteroaryl groups in this region could reveal new dimensions of SAR while also helping to block oxidative metabolism. Similarly, the series could benefit from searching for new SAR surrounding the barely explored piperidine core. The sulfonamide linkage is another structural element that emerged from this campaign virtually unexplored. Analog **4.87** demonstrated that an amide is an untenable substitution for this linkage, but many other options for alternative linkers remain to be studied.

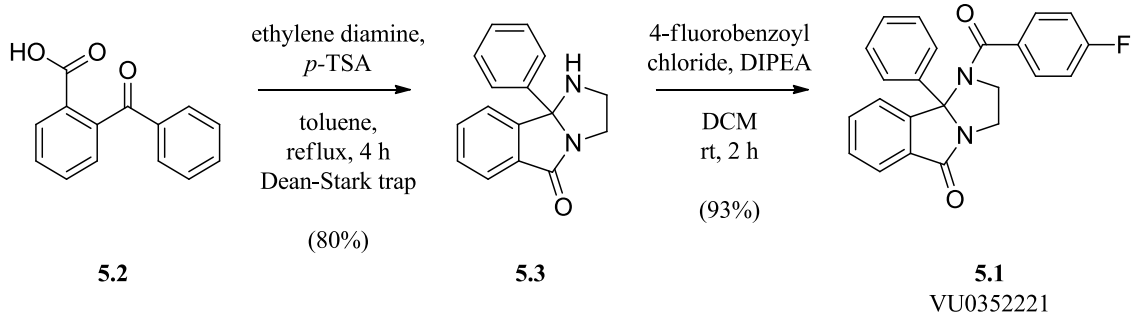
There are many possibilities available to a campaign aiming to further optimize the non-isatin M₅ PAM chemical series. The optimization of the highly potent and M₅-preferring **4.161** has successfully laid the groundwork for such future campaigns, demonstrating that this chemical series possesses highly flexible SAR and the potential to produce highly potent and M₅-selective compounds. The depth of SAR that still remains to be explored within this chemical series promises to generate many more analogs that will be indispensable in the study of M₅.

Chapter V

IDENTIFICATION, OPTIMIZATION, AND CHARACTERIZATION OF THE FIRST HIGHLY SELECTIVE M₅ NEGATIVE ALLOSTERIC MODULATOR

HTS identification of a novel, M₅-selective ligand with antagonist activity

As discussed in the opening of Chapter IV, the 2012 HTS campaign of the MLPCN screening deck identified a number of novel M₅-selective ligands. In addition to the identification of nine confirmed M₅ PAMs (of which VU0472882 and its analogs were discussed in Chapter IV) the screen also identified nine novel M₅ antagonists (discussed here and in Chapter VI). The HTS assay protocol could not determine whether the compounds possessing inhibitory activity were M₅ orthosteric antagonists or NAMs; nevertheless, we proceeded to explore the SAR around these molecules since an M₅-selective ligand of either mode of pharmacology would be highly useful in the study of M₅ in the CNS.



Scheme 5.1. Structure and synthetic pathway for the synthesis of HTS lead **5.1** (VU0352221).

Of the antagonist hits highlighted in the HTS, we focused on compound **5.1** (VU0352221) due to its unique 2,3-dihydro-1*H*-imidazo[2,1-*a*]isoindol-5(9*bH*)-one-based scaffold which, in the HTS screen, was inactive at hM₁ and hM₄ isoforms, but displayed weak inhibition of hM₅ (IC₅₀ >10 μM, data not shown; **Scheme 5.1**). The compound was resynthesized in-house via a two-step synthetic pathway consisting of the condensation of ethylene diamine and 2-benzoylbenzoic acid **5.2** to provide amine **5.3**. Subsequent acylation with 4-fluorobenzoyl chloride provided HTS hit compound **5.1** (**Scheme 5.1**). Full CRCs were obtained in double-add functional Ca²⁺ mobilization assays against all the human mAChR subtypes (M₂ and M₄ co-expressing G_{αq15}) as well as rat M₅. Upon retesting compound **5.1** we were pleased to observe that the resynthesized powder reconfirmed its activity and selectivity with enhanced potency (hM₅ IC₅₀ = 3.5 μM, rM₅ IC₅₀ = 5.7 μM, hM₁-hM₄ IC₅₀ >> 30 μM) (**Figure 5.1**). Reconfirmation of the potency and selectivity of compound **5.1** reinforced our confidence in exploring and optimizing the SAR surrounding the chemical scaffold with the goal of increasing potency while maintaining the high degree of M₅ selectivity exhibited by compound **5.1** (**Figure 5.1**)⁷³.

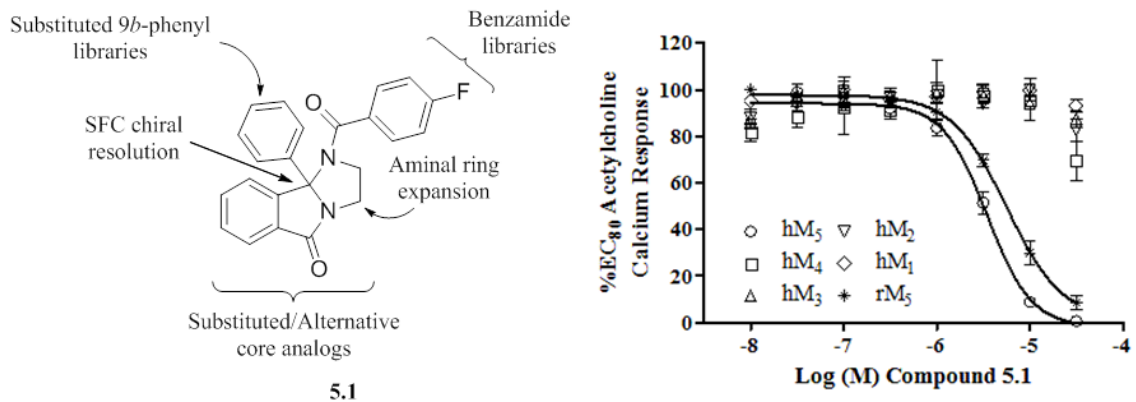
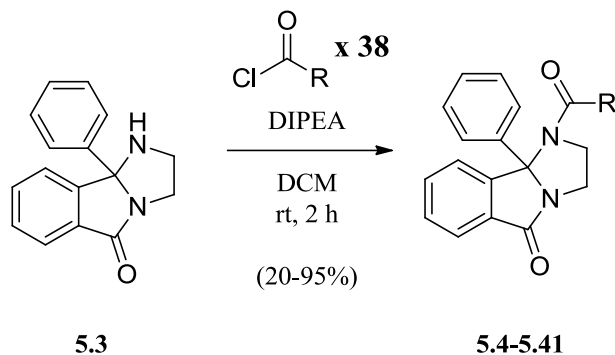


Figure 5.1. Structure, planned SAR exploration, potency, and selectivity of HTS hit compound **5.1** (VU0352221). Ca^{2+} mobilization assays with hM₁-hM₅ (M₂ and M₄ co-expressing G_{αq15}) and rM₅ cells were used to obtain CRCs of resynthesized compound **5.1** in the presence of a fixed submaximal (~EC₈₀) concentration of ACh (IC₅₀ values: hM₅ IC₅₀ = 3.5 μM, hM₁-hM₄ IC₅₀ >>30 μM, rM₅ IC₅₀ = 5.7 μM). Data represent the mean ± S.E.M. of at least 3 independent experiments with similar results.

Optimization of VU0352221 to obtain the first M₅ NAM, VU0483253

Optimization of benzamide region SAR

To begin the optimization of compound **5.1** we turned our attention to the benzamide moiety. We constructed an amide library combining amine **5.3** with a library of 38 acid chlorides (aryl, heteroaryl, and aliphatic) under standard acylation conditions to furnish compounds **5.4-5.41** in yields of 20-95% (**Scheme 5.2**).



Scheme 5.2. Synthesis of benzamide analogs **5.4-5.41** from intermediate **5.3**. Syntheses performed jointly with M. Kokubo.

These library analogs, as well as HTS hit **5.1**, were next screened in single point (10 μM) Ca^{2+} mobilization assays in the presence of an ACh $\sim\text{EC}_{80}$ in CHO cells stably expressing hM₅. The results of this single point screen are shown in **Figure 5.2** and **Table 5.1**.

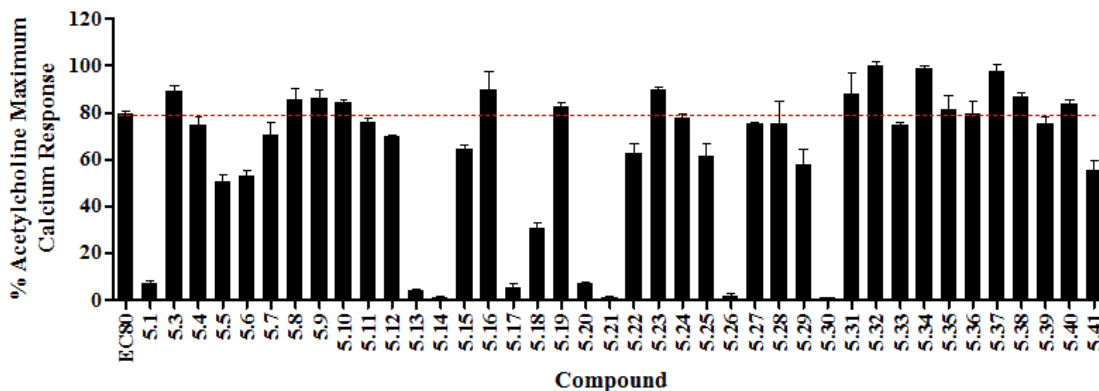
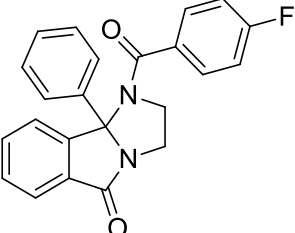
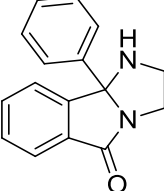
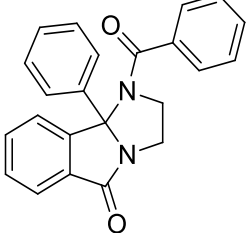
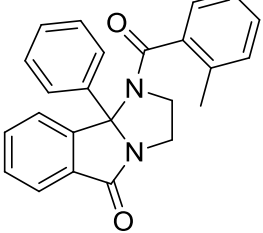
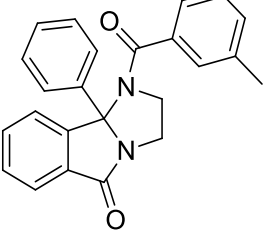
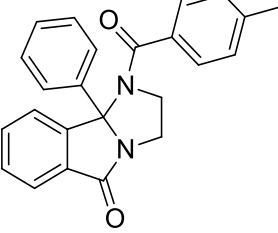
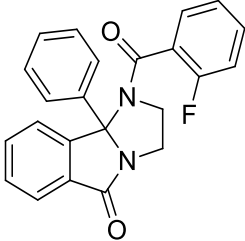
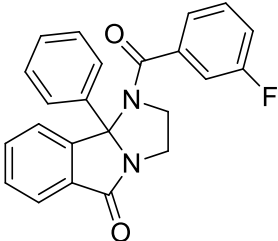
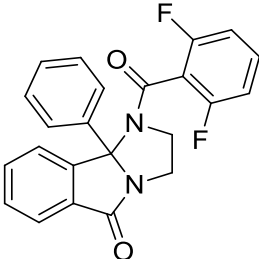
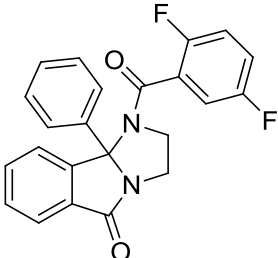
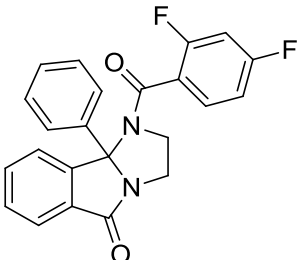
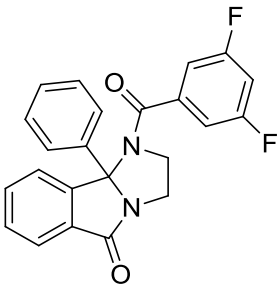
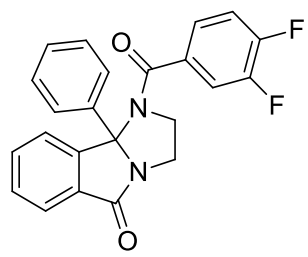
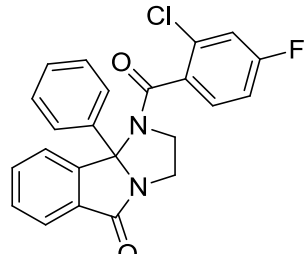
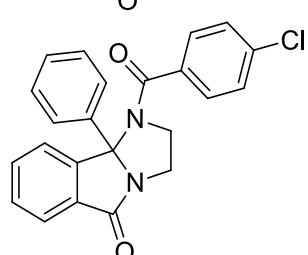
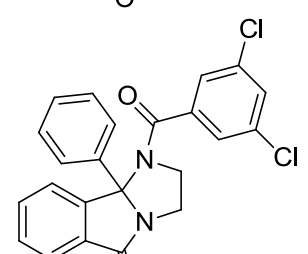
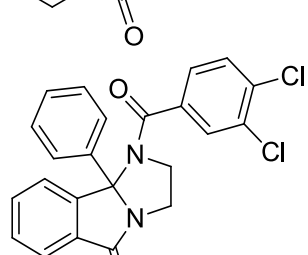
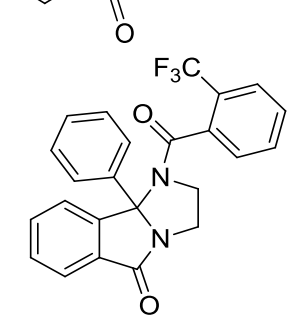


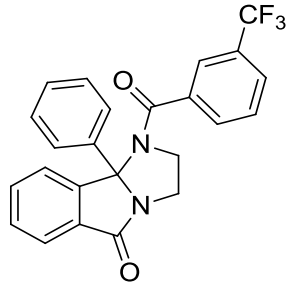
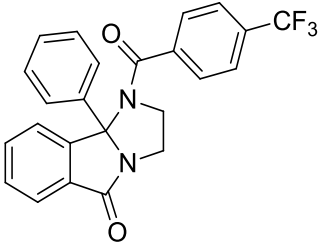
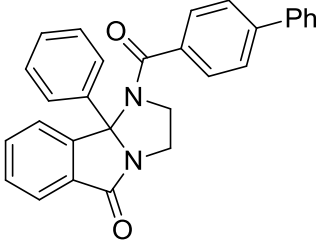
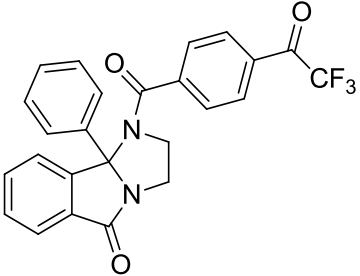
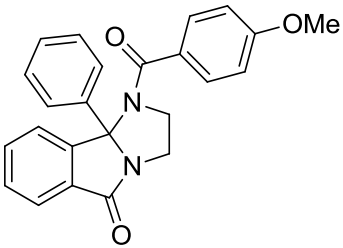
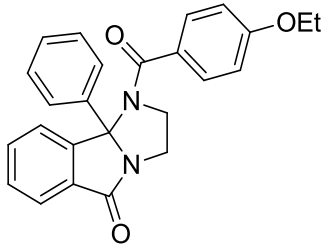
Figure 5.2. Comparison of single point (10 μM) screen results of the benzamide library, analogs **5.3-5.41**. Also included is the single point Ca^{2+} mobilization response of the initial hit, compound **5.1**. Ca^{2+} mobilization was used to obtain $\% \text{ACh}_{\text{Max}}$ values for each compound in the presence of a fixed submaximal ($\sim\text{EC}_{80}$) concentration of ACh. Data represent the mean \pm S.E.M. of at least 3 replicate experiments with similar results.

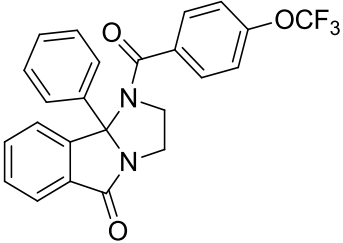
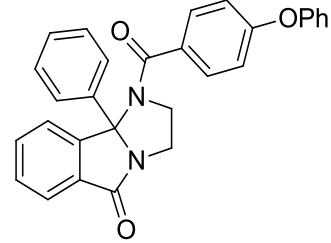
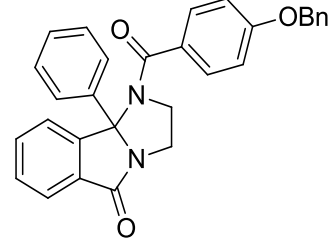
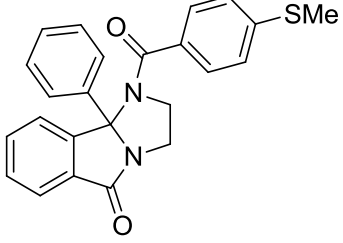
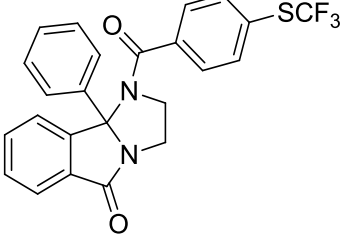
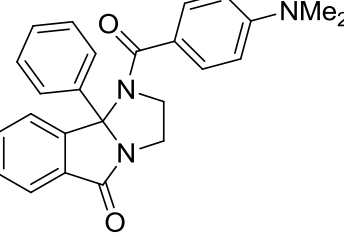
Table 5.1. Structures for benzamide analogs **5.3-5.41** and associated inhibitory activity data from the single point (10 μ M) screen at hM₅. Also included is the structure and single point Ca²⁺ mobilization response of the HTS hit, compound **5.1**. Ca²⁺ mobilization responses for each compound are reported as a percentage of the maximum ACh response. VU number denotes the compound identifier assigned by Vanderbilt University. Data represent the mean of at least 3 replicate experiments with similar results.

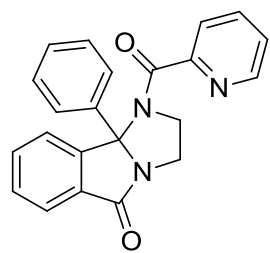
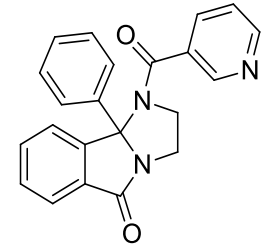
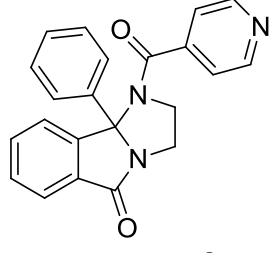
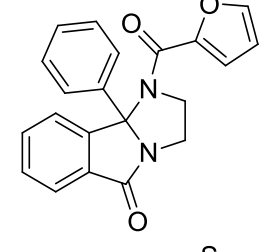
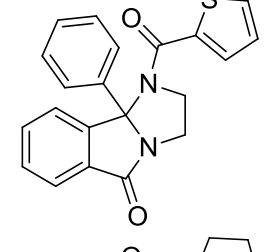
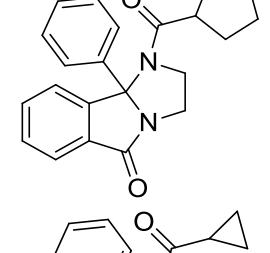
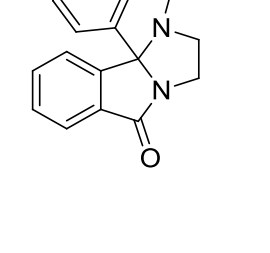
Structure	Cmpd #	VU #	hM ₅ %ACh _{Max}
	5.1	VU0352221	7.0
	5.3	VU0026940	89.3
	5.4	VU0477969	74.8
	5.5	VU0478013	50.5
	5.6	VU0478015	52.7
	5.7	VU0333569	70.2

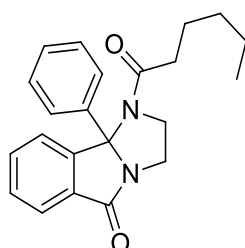
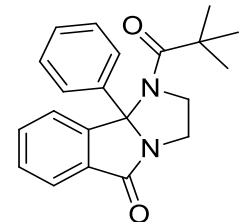
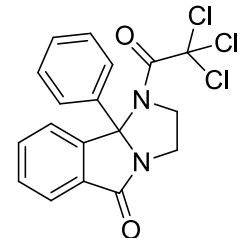
	5.8	VU0477901	85.8
	5.9	VU0477902	86.0
	5.10	VU0478080	84.1
	5.11	VU0478231	76.0
	5.12	VU0478230	69.1
	5.13	VU0478232	4.2

	5.14	VU0478141	0.9
	5.15	VU0478223	64.1
	5.16	VU0477637	89.9
	5.17	VU0477674	5.4
	5.18	VU0478073	30.5
	5.19	VU0478180	82.4

	5.20	VU0478244	6.8
	5.21	VU0478119	1.1
	5.22	VU0478027	62.7
	5.23	VU0478224	64.1
	5.24	VU0477938	77.7
	5.25	VU0477830	61.1

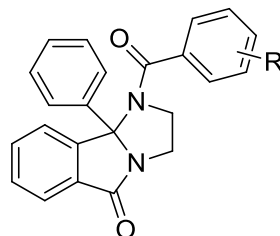
	5.26	VU0478005	1.8
	5.27	VU0477900	75.1
	5.28	VU0477903	75.1
	5.29	VU0478002	58.0
	5.30	VU0478052	1.1
	5.31	VU0477934	88.0

	5.32	VU0477975	100
	5.33	VU0478033	74.8
	5.34	VU0477944	98.6
	5.35	VU0477936	81.3
	5.36	VU0477631	79.5
	5.37	VU0477831	97.8
	5.38	VU0477779	86.4

	5.39	VU0478021	75.3
	5.40	VU0477879	83.6
	5.41	VU0477662	55.1

The majority of the analogs assayed demonstrated little or no ability to inhibit the ACh EC₈₀. Out of the 40 novel analogs tested, only seven antagonized the EC₈₀ to near baseline. Of the active compounds, all were substituted benzamides; all heterocycles and aliphatic analogs were inactive. The seven active compounds were subsequently tested in full CRC in Ca²⁺ mobilization assays at hM₅ to obtain IC₅₀ potencies (**Table 5.2**).

Table 5.2. Potencies at hM₅ for active benzamide analogs selected from the single point (10 μM) screen. Ca²⁺ mobilization assays with hM₅ cells were used to obtain CRCs of compounds in the presence of a fixed submaximal (~EC₈₀) concentration of ACh. Data represent the mean of at least 3 independent experiments with similar results.



Cmpd #	R =	hM ₅ IC ₅₀ (μM)
5.13	3,5-diF	3.8
5.14	3,4-diF	1.0
5.17	3,5-diCl	8.1
5.20	3-CF ₃	3.0
5.21	4-CF ₃	2.0
5.26	4-OCF ₃	4.5
5.30	4-SCF ₃	1.4

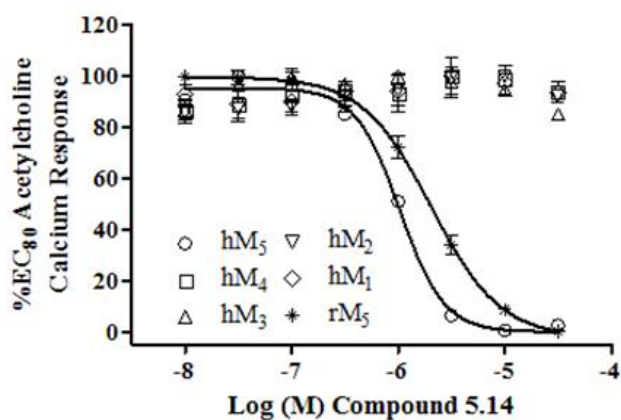
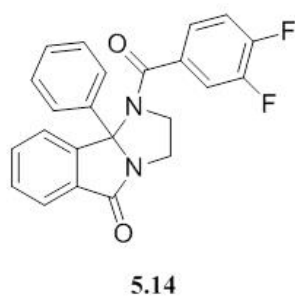
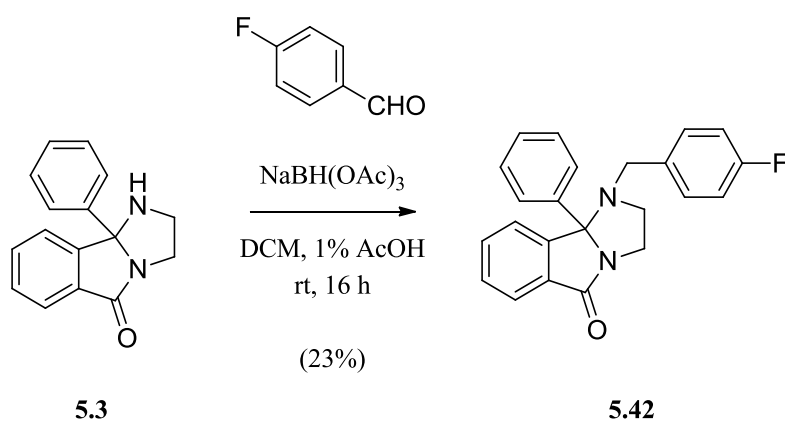


Figure 5.3. Structure, potency, and selectivity of benzamide analog **5.14** (VU0478141). Ca²⁺ mobilization assays with hM₁-hM₅ (M₂ and M₄ co-expressing G_{αq15}) and rM₅ cells were used to obtain CRCs of compound **5.14** in the presence of a fixed submaximal (~EC₈₀) concentration of ACh (IC₅₀ values: hM₅ IC₅₀ = 1.0 μM, hM₁-hM₄ IC₅₀ >> 30 μM, rM₅ IC₅₀ = 2.1 μM). Data represent the mean ± S.E.M. of at least 3 independent experiments with similar results.

We were pleased to see that the majority of these analogs displayed improvement in potency over the HTS hit. Compound **5.14** was the most potent analog, with an hM₅ IC₅₀ = 1.0 μM (**Table 5.2**). Encouraged by this 3-fold jump in potency over the HTS hit, we subjected compound **5.14** to a counterscreen against all human mAChR subtypes as well as rM₅ to insure that M₅-selectivity was maintained with the increased potency (**Figure 5.3**). Compound **5.14** displayed complete selectivity for M₅, with slightly decreased potency at rM₅ (hM₅ IC₅₀ = 1.0 μM, rM₅ IC₅₀ = 2.1 μM, hM₁-hM₄ IC₅₀ >> 30 μM). Based on its ability to maintain selectivity with a 3-fold increase in potency over the HTS lead compound **5.1**, we provisionally declared the 3,4-difluoro substitution pattern to be the optimal benzamide analog.

Concurrent with our efforts to optimize the benzamide ring substituent, we explored the necessity and structural flexibility of the SAR around the amide itself. To begin with, we synthesized the *N*-4-fluorobenzyl analog of compound **5.1** via a reductive amination of 4-fluorobenzaldehyde with compound **5.3** under standard conditions to obtain compound **5.42** (**Scheme 5.3**).



Scheme 5.3. Synthesis of des-carbonyl analog **5.42** (VU0478004). Synthesis performed by M. Kokubo.

In addition to the *N*-4-fluorobenzyl analog **5.42**, a small library of 10 commercially available compounds possessing interesting variations around the amide was acquired to aid in exploring the SAR of this region. This library included analogs that substituted the amide moiety with urea, thiourea, and sulfonamide. The structures and commercial suppliers of these compounds are noted in **Table 5.3**. These compounds were screened along with **5.42** in single point (10 μ M) Ca^{2+} mobilization assays against hM_5 to assess the general inhibitory activity of each analog (**Figure 5.4**, **Table 5.3**).

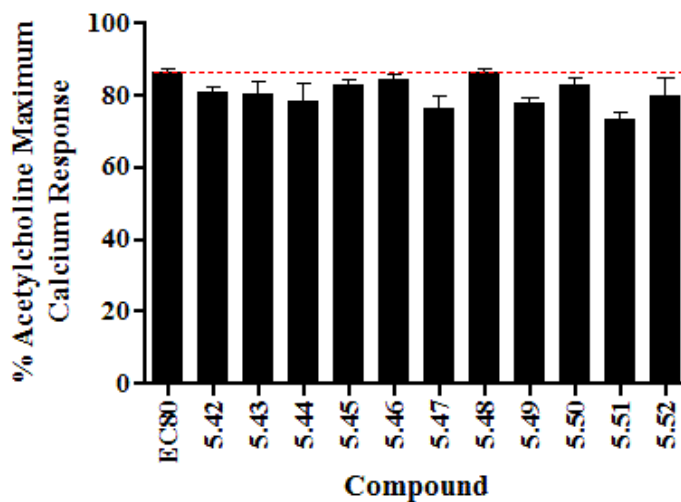
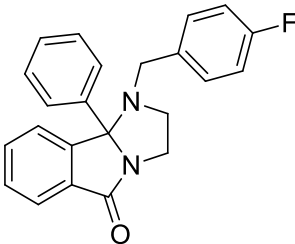
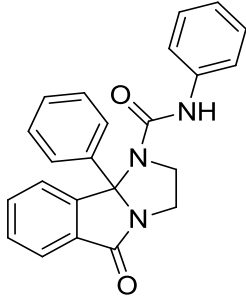
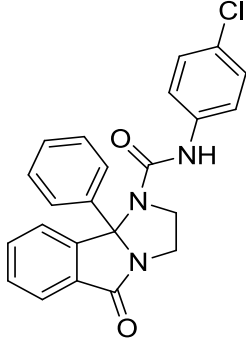
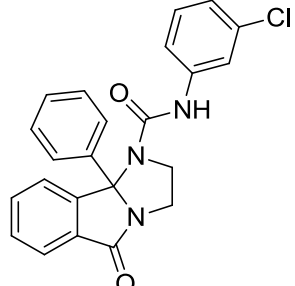
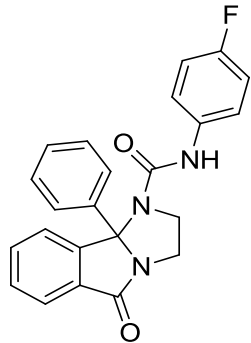
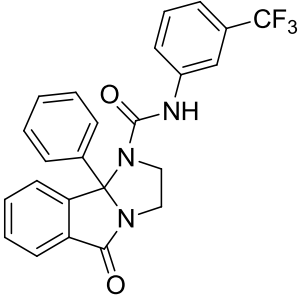
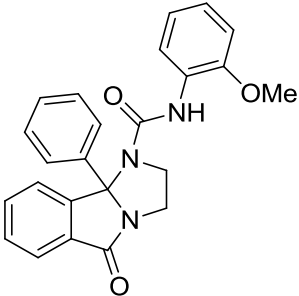
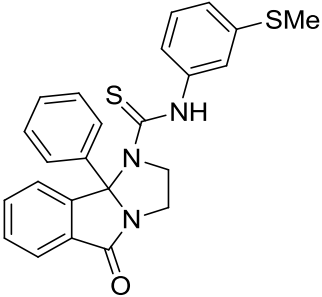
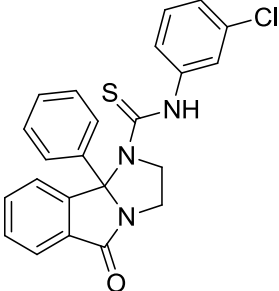
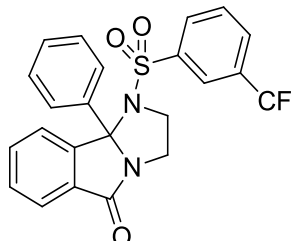


Figure 5.4. Comparison of single point (10 μ M) screen results of the amide library, analogs **5.42-5.52**. Ca^{2+} mobilization was used to obtain $\% \text{ACh}_{\text{Max}}$ values for each compound in the presence of a fixed submaximal ($\sim \text{EC}_{80}$) concentration of ACh. Data represent the mean \pm S.E.M. of at least 3 replicate experiments with similar results.

Table 5.3. Structures for amide analogs **5.42-5.52** and associated inhibitory activity data from the single point (10 μM) screen at hM_5 . Ca^{2+} mobilization responses for each compound are reported as a percentage of the maximum ACh response. VU number denotes the compound identifier assigned by Vanderbilt University. The name of the commercial supplier and the commercial stock number are also provided. Data represent the mean of at least 3 replicate experiments with similar results.

Structure	Cmpd #	VU #	Commercial Supplier	hM_5 %ACh _{Max}
	5.42	VU0478004	n/a	80.8
	5.43	VU0217057	Vitas M. Laboratories, Ltd. (STK777060)	80.4
	5.44	VU0477823	Butt Park, Ltd. (42\07-24)	78.2
	5.45	VU0202910	Vitas M. Laboratories, Ltd. (STK836668)	83.0

	5.46	VU0170704	Vitas M. Laboratories, Ltd. (STK837554)	84.3
	5.47	VU0477746	Butt Park, Ltd. (39\07-92)	76.4
	5.48	VU0099964	Enamine (Z56798121)	86.6
	5.49	VU0477682	Maybridge, Ltd. (DSHS01083)	77.7
	5.50	VU0477813	Maybridge, Ltd. (DSHS01080)	83.0

	5.51	VU0477810	Vitas M. Laboratories, Ltd. (STK724323)	73.4
	5.52	VU0477619	Maybridge, Ltd. (DSHS01055)	80.0

The single point screen against hM₅ revealed that none of the amide analogs displayed any inhibitory activity, suggesting that the amide moiety is necessary for activity in this chemical scaffold. Satisfied with our initial exploration of the benzamide region of the chemical scaffold, we moved on to assess the tractability of SAR in the tricyclic core region.

Exploration of tricyclic core region SAR

As the tricyclic core was the feature of this chemical scaffold that originally attracted our attention, we were interested to test modifications of the core to gauge the flexibility of the SAR in this region. A number of commercially available molecules possessing unique variations on the tricyclic core arrangement of lead compound **5.1** were obtained to serve as a library exploring the SAR of this region. Analogs selected featured disconnections of one or more of the core tricycles, expansions of the aminal ring, and both additions and deletions of rings from the core. In selecting these analogs our goal was to discover if the tricycle is a necessary element for the scaffold's activity, if

only certain constitutive elements are required, or if the core scaffold may be expanded. The structures and commercial suppliers of these core analogs **5.53-5.64** are noted in **Table 5.4**. As with other early libraries, these compounds were assayed in single point (10 μM) Ca^{2+} mobilization assays against hM_5 to assess the general inhibitory activity of each analog (**Figure 5.5**, **Table 5.4**).

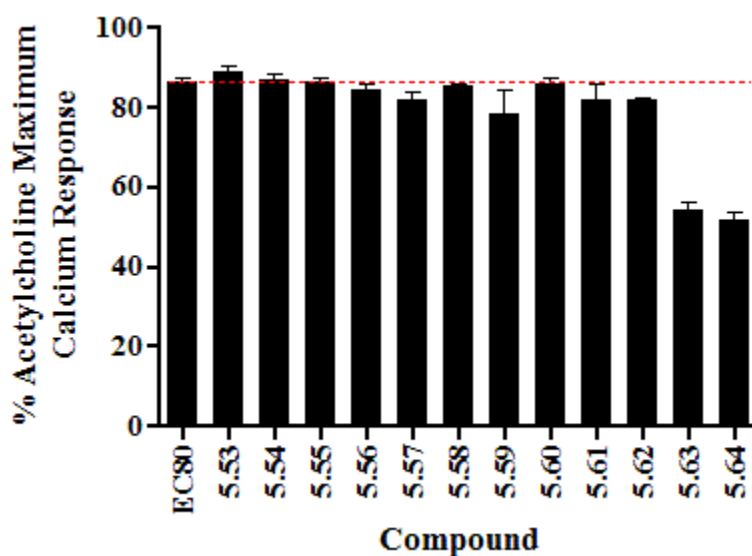
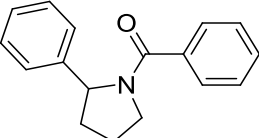
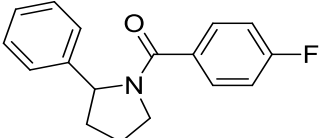
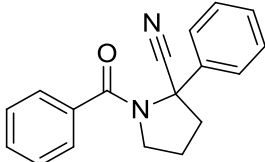
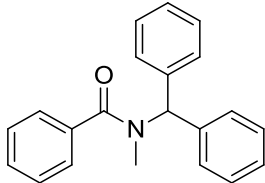
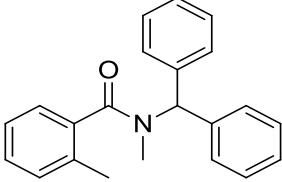
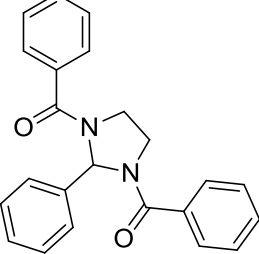
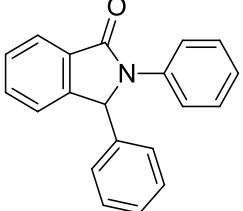
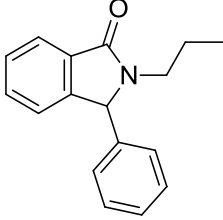
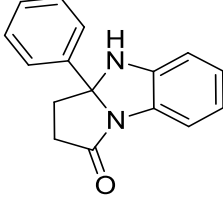
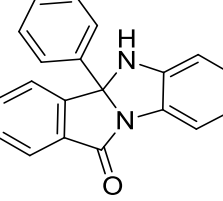
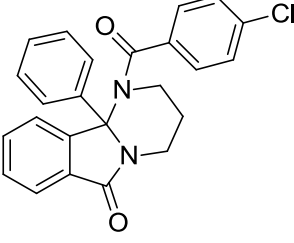
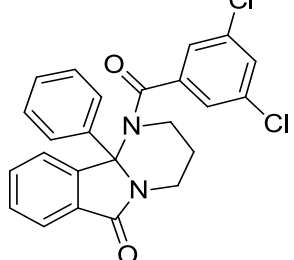


Figure 5.5. Comparison of single point (10 μM) screen results of the core library, analogs **5.53-5.64**. Ca^{2+} mobilization was used to obtain $\% \text{ACh}_{\text{Max}}$ values for each compound in the presence of a fixed submaximal ($\sim \text{EC}_{80}$) concentration of ACh. Data represent the mean \pm S.E.M. of at least 3 replicate experiments with similar results.

Table 5.4. Structures for core analogs **5.53-5.64** and associated inhibitory activity data from the single point (10 μ M) screen at hM₅. Ca²⁺ mobilization responses for each compound are reported as a percentage of the maximum ACh response. VU number denotes the compound identifier assigned by Vanderbilt University. The name of the commercial supplier and the commercial stock number are also provided. Data represent the mean of at least 3 replicate experiments with similar results.

Structure	Cmpd #	VU #	Commercial Supplier	hM ₅ %ACh _{Max}
	5.53	VU0477642	UkrOrgSyn, Ltd. (PB231861070)	88.8
	5.54	VU0477751	UkrOrgSyn, Ltd. (PB281653944)	87.0
	5.55	VU0099964	InterBioScreen, Ltd. (2S-29658)	86.6
	5.56	VU0477660	Enamine (Z29317183)	84.3
	5.57	VU0477650	Enamine (Z29317241)	81.6
	5.58	VU0104716	Vitas M. Laboratories, Ltd. (STK212693)	85.3
	5.59	VU0477745	Labotest (LT00008901)	78.1

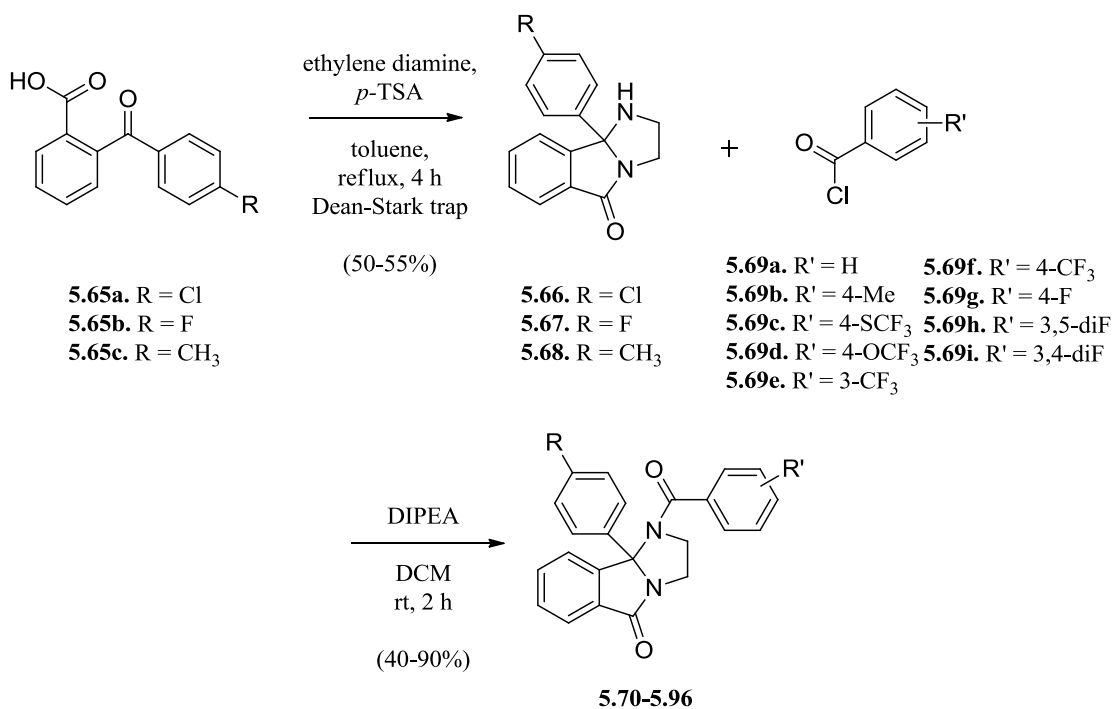
	5.60	VU0477780	Vitas M. Laboratories, Ltd. (STK044900)	86.1
	5.61	VU0477778	Vitas M. Laboratories, Ltd. (STK871398)	81.8
	5.62	VU0477652	Vitas M. Laboratories, Ltd. (STK526400)	81.8
	5.63	VU0477680	Butt Park, Ltd. (39\07-93)	54.0
	5.64	VU0477654	Butt Park, Ltd. (39\07-94)	51.9

The results of the screen of core analogs demonstrated that most modifications of the tricyclic core produced no inhibitory effects at the 10 μ M concentration used in the single point assay. The exceptions to this inactivity were compounds **5.63** and **5.64**, which feature an expanded, 6-membered aminal ring; however, even these compounds showed a relatively weak response. At this point we accepted that dramatic disconnections, expansions, or contractions of the tricyclic core rings were unproductive

pathways for moving forward in our optimization efforts. Thus, we left the core in its original state and moved on to another unexplored region of the molecule, the 9b-phenyl ring.

Optimization of 9b-phenyl ring SAR

Having established the 3,4-difluorobenzamide moiety as the optimal substitution for the benzamide ring system, we next proposed to test substitutions for the 9b-phenyl ring and their impact on activity at M₅. Ideally, when optimizing a chemical lead with multidimensional iterative parallel synthesis, it is simplest for the library step to be the final step of the synthesis, as with the optimization of the benzamide region. In this case, however, the 9b-phenyl library step is the first step in a two-step synthesis, limiting the ease of library preparation (**Scheme 5.4**). Thus, we prepared analogs of the 9b-phenyl ring in a matrix library format (3 x 9) with three functionalized congeners of compound **5.2 (5.68-5.70)** that were acylated with nine benzoyl chlorides possessing the most potent substitution patterns discovered during the optimization of the benzamide region (compounds **5.71-5.79**) to provide analogs **5.80-5.109 (Scheme 5.4)**. This strategy of constructing a matrix library not only provides us with SAR information on a sampling of 9b-phenyl analogs, but also gives us SAR data on how the 9b-phenyl substitution interacts, if at all, with benzamide ring system. The library analogs were assayed in parallel in single point (10 μM) Ca²⁺ mobilization assays against hM₅ to assess the general inhibitory activity of each analog. These results of are shown in **Figure 5.6** and **Table 5.5**.



Scheme 5.4. Synthesis of matrix library exploring substituents in the 9b-phenyl regions, analogs **5.70-5.96**. Three different 9b-phenyl-2,3-dihydro-1*H*-imidazo[2,1-*a*]isoindol-5(9b*H*)-ones (**5.66-5.68**) were acylated under standard conditions with 9 different benzoyl chlorides (**5.69a-5.69i**) to produce a 27 member library (**5.70-5.96**). Syntheses performed by M. Kokubo.

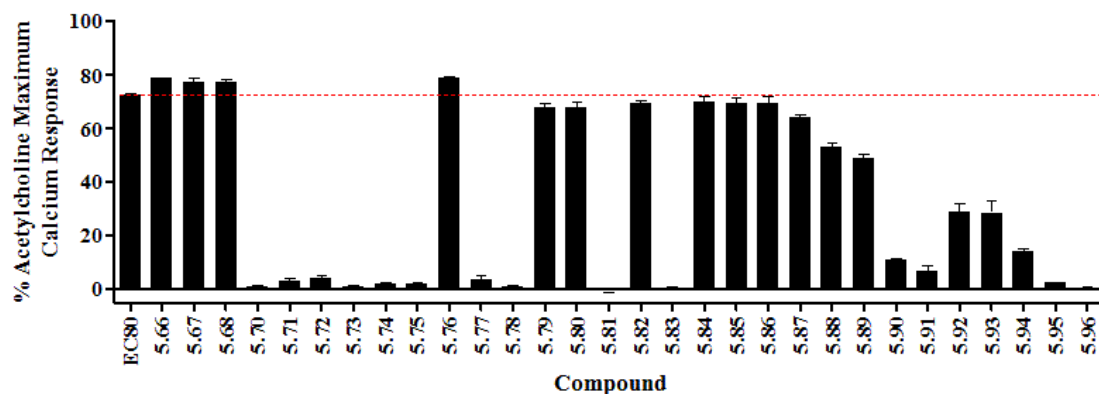
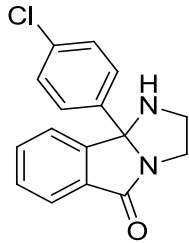
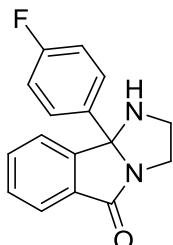
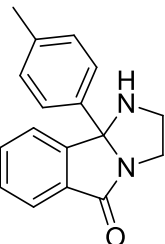
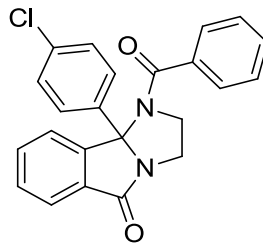
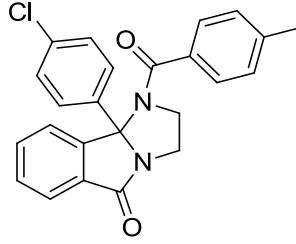
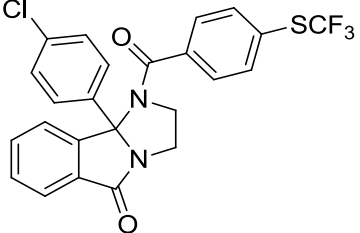
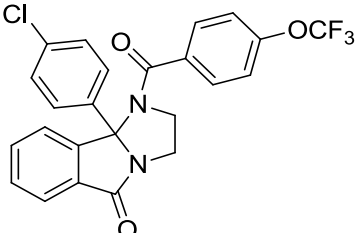
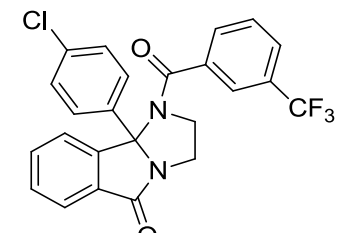
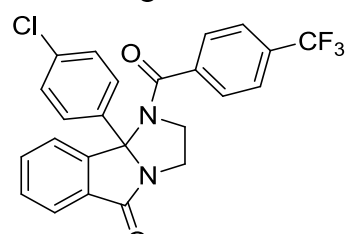
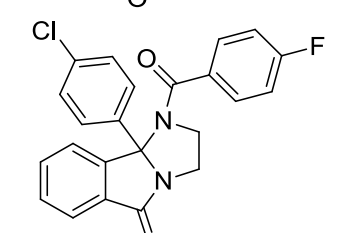
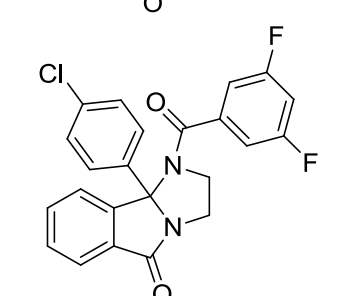
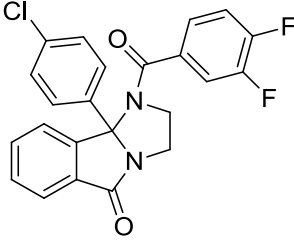
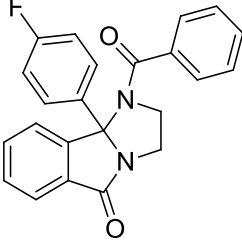
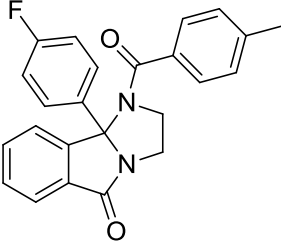
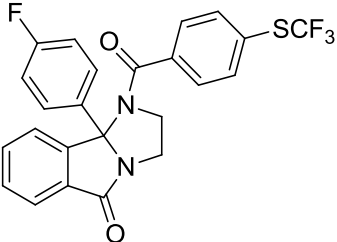
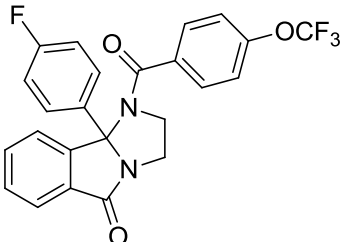
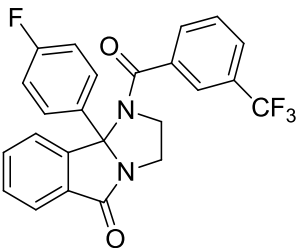


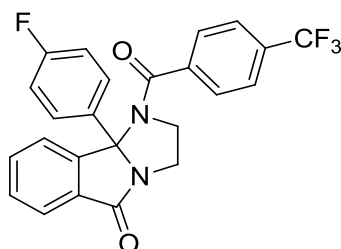
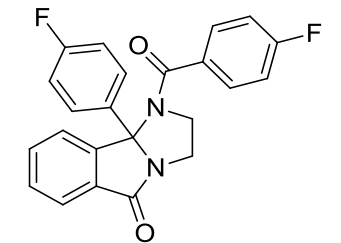
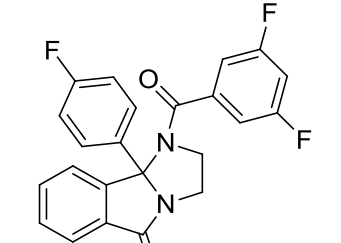
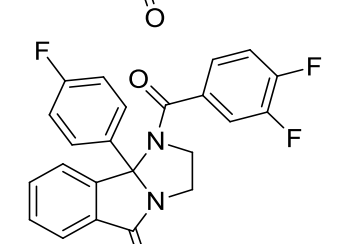
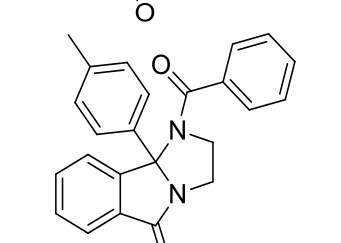
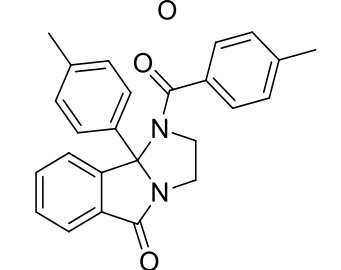
Figure 5.6. Comparison of single point (10 μ M) screen results of the 9b-phenyl matrix library, analogs **5.70-5.96**. Also included in the assay were the unacylated 9b-phenyl-2,3-dihydro-1*H*-imidazo[2,1-*a*]isoindol-5(9b*H*)-ones, **5.66-5.68**. Ca²⁺ mobilization was used to obtain %ACh_{Max} values for each compound in the presence of a fixed submaximal (\sim EC₈₀) concentration of ACh. Data represent the mean \pm S.E.M. of at least 3 replicate experiments with similar results.

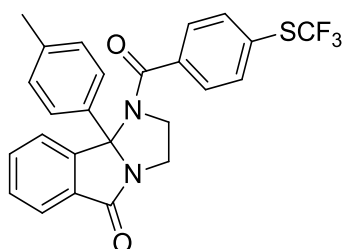
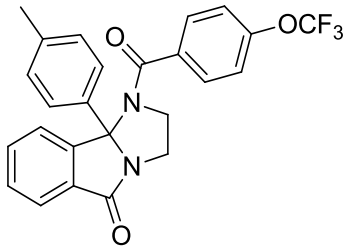
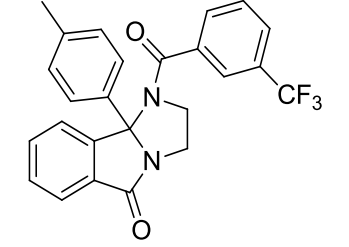
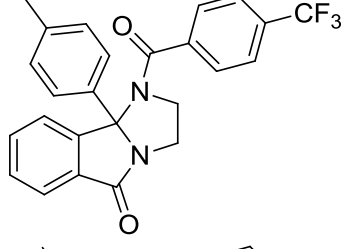
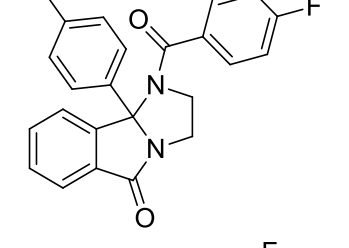
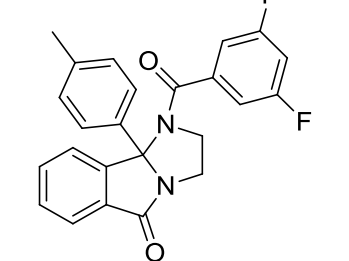
Table 5.5. Structures for 9b-phenyl matrix library analogs **5.70-5.96** and associated inhibitory activity data from the single point (10 μM) screen at hM_5 . Also included are the structures and single point Ca^{2+} mobilization response of the unacylated 9b-phenyl-2,3-dihydro-1*H*-imidazo[2,1-*a*]isoindol-5(9*bH*)-ones, **5.66-5.68**. Ca^{2+} mobilization responses for each compound are reported as a percentage of the maximum ACh response. VU number denotes the compound identifier assigned by Vanderbilt University. Data represent the mean of at least 3 replicate experiments with similar results.

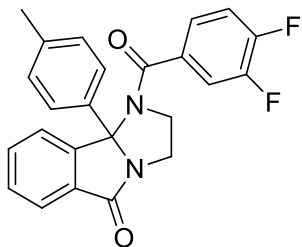
Structure	Cmpd #	VU #	hM_5 %ACh _{Max}
	5.66	VU0066006	78.7
	5.67	VU0331642	77.6
	5.68	VU0478193	77.4
	5.70	VU0156675	1.2
	5.71	VU0156706	3.3

	5.72	VU0478358	4.4
	5.73	VU0478345	1.2
	5.74	VU0478319	1.9
	5.75	VU0478351	2.0
	5.76	VU0326724	78.8
	5.77	VU0478357	3.5

	5.78	VU0478333	0.9
	5.79	VU0478355	67.6
	5.80	VU0478360	67.9
	5.81	VU0478302	-0.7
	5.82	VU0478346	69.4
	5.83	VU0478301	0.2

	5.84	VU0478336	70.3
	5.85	VU0478300	69.7
	5.86	VU0478359	69.3
	5.87	VU0478354	64.5
	5.88	VU0478270	53.3
	5.89	VU0478271	49.1

	5.90	VU0478264	10.9
	5.91	VU0478269	6.6
	5.92	VU0478327	28.8
	5.93	VU0478297	28.6
	5.94	VU0478340	14.1
	5.95	VU0478341	2.4



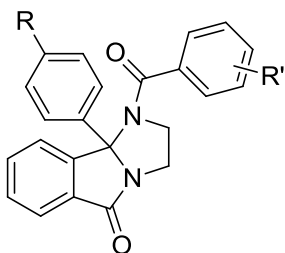
5.96

VU0478268

0.5

The single point assay of the matrix library reveals that the substituent at the 4-position of the 9b-phenyl has a profound effect on analog activity. In general, compounds possessing a 9b-4-fluorophenyl showed the lowest occurrence of activity, although with some highly active exceptions (compounds **5.81** and **5.83**). Compounds with a 9b-4-methylphenyl moiety showed middling results in activity. Compounds with the 9b-4-chlorophenyl moiety were typically active regardless of the substitution on the benzamide moiety; however, a notable exception to this observation is the 9b-4-chlorophenyl analog of the HTS hit compound **5.1**, compound **5.76**. The failure of compound **5.76** to display inhibitory activity at 10 μM hints at a complex relationship between substituents on the 9b-phenyl and those on the benzamide ring.

Table 5.6. Potencies at hM₅ for 9b-phenyl matrix library analogs **5.70-5.96**. Ca²⁺ mobilization assays with hM₅ cells were used to obtain CRCs of compounds in the presence of a fixed submaximal (~EC₈₀) concentration of ACh. Data represent the mean ± S.E.M. of at least 3 independent experiments with similar results. ---, not determined.



Cmpd #	R =	R' =	hM ₅ pIC ₅₀	hM ₅ IC ₅₀ (μM)	ACh _{Min} (%)
5.70	Cl	H	5.80±0.03	1.6	0.2±1.7
5.71	Cl	4-CH ₃	5.58±0.04	2.6	0.1±2.8
5.72	Cl	4-SCF ₃	5.51±0.13	3.1	-9.2±8.7
5.73	Cl	4-OCF ₃	5.63±0.06	2.3	-5.3±4.4
5.74	Cl	3-CF ₃	5.31±0.11	4.9	-7.2±8.0
5.75	Cl	4-CF ₃	5.69±0.04	2.0	0.7±2.3
5.76	Cl	4-F	>4.5	>30	63.8±0.9
5.77	Cl	3,5-diF	6.00±0.04	1.0	2.8±2.0
5.78	Cl	3,4-diF	6.32±0.02	0.48	0.1±1.0
5.79	F	H	---	---	---
5.80	F	4-CH ₃	---	---	---
5.81	F	4-SCF ₃	5.89±0.03	1.3	-0.2±1.7
5.82	F	4-OCF ₃	---	---	---
5.83	F	3-CF ₃	5.68±0.03	2.1	-2.4±1.8
5.84	F	4-CF ₃	---	---	---
5.85	F	4-F	---	---	---
5.86	F	3,5-diF	---	---	---
5.87	F	3,4-diF	---	---	---
5.88	CH ₃	H	---	---	---
5.89	CH ₃	4-CH ₃	---	---	---
5.90	CH ₃	4-SCF ₃	5.39±0.08	4.1	4.1±5.5
5.91	CH ₃	4-OCF ₃	5.46±0.06	3.5	-0.2±4.3
5.92	CH ₃	3-CF ₃	---	---	---
5.93	CH ₃	4-CF ₃	---	---	---
5.94	CH ₃	4-F	---	---	---
5.95	CH ₃	3,5-diF	5.63±0.05	2.3	-1.1±3.3
5.96	CH ₃	3,4-diF	5.58±0.06	2.6	-6.8±4.3

We aimed to explore this relationship in more detail by testing selected matrix analogs in full CRC Ca^{2+} mobilization assays at M_5 (**Table 5.6**). As with the single point data, the CRC data strongly suggests the presence of a complex and cooperative relationship between the benzamide and 9b-phenyl substituents. Excitingly, one analog, compound **5.78**, possessing the 3,4-difluorobenzamide and a 9b-4-chlorophenyl moiety, afforded submicromolar potency ($\text{hM}_5 \text{ IC}_{50} = 0.48 \mu\text{M}$). As this was the first submicromolar antagonist witnessed from this chemical series, compound **5.78** was counterscreened in full CRC Ca^{2+} mobilization assays at the remaining human mAChR subtypes and rM_5 in order to determine if this highly potent compound maintained the M_5 -selectivity previously seen in this chemical series (**Figure 5.7**).

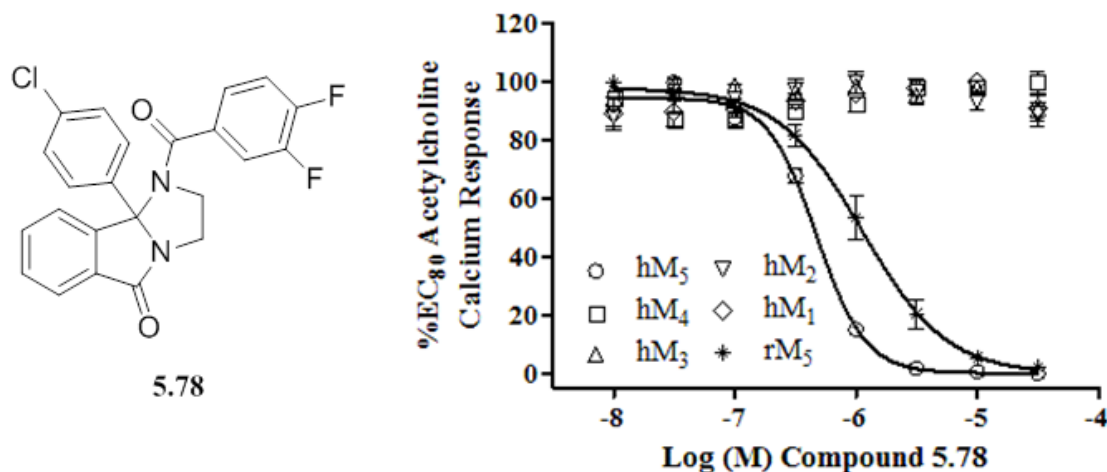


Figure 5.7. Structure, potency, and selectivity of benzamide analog compound **5.78** (VU0478333). Ca^{2+} mobilization assays with hM_1 - hM_5 (M_2 and M_4 co-expressing G_{aqi5}) and rM_5 cells were used to obtain CRCs of compound **5.78** in the presence of a fixed submaximal ($\sim\text{EC}_{80}$) concentration of ACh (IC_{50} values: $\text{hM}_5 \text{ IC}_{50} = 0.47 \mu\text{M}$, hM_1 - $\text{hM}_4 \text{ IC}_{50} \gg 30 \mu\text{M}$, $\text{rM}_5 \text{ IC}_{50} = 1.1 \mu\text{M}$). Data represent the mean \pm S.E.M. of at least 3 independent experiments with similar results.

The results of the counterscreen demonstrated that compound **5.78** maintained complete M_5 -selectivity, although we again observed attenuated potency at the rat

isoform (hM₁-hM₄ IC₅₀ >> 30 μM, hM₅ IC₅₀ = 0.48 μM, rM₅ IC₅₀ = 1.1 μM). With such encouraging results in potency and selectivity with the racemic **5.78** we were anxious to resolve the enantiomers in order to investigate the potential for enantioselective inhibition of M₅.

Using a supercritical fluid chromatography purification system we developed conditions to separate the pure enantiomers of **5.78** to furnish **5.97** (VU0483253) and **5.98** (VU0483252) in >99% ee. Optical rotations were recorded, and the two enantiomers were compared in a full CRC Ca²⁺ mobilization assay in hM₅ cells. The (–)-enantiomer **5.97** was found to be the active enantiomer (hM₅ IC₅₀ = 0.30 μM), while the (+)-enantiomer **5.98** was devoid of activity at M₅ (hM₅ IC₅₀ >>30 μM; **Figure 5.8A**). Single crystal X-ray crystallography ultimately revealed that the active (–)-enantiomer **5.97** possessed (*S*)-stereochemistry (**Figure 5.8B, C**).

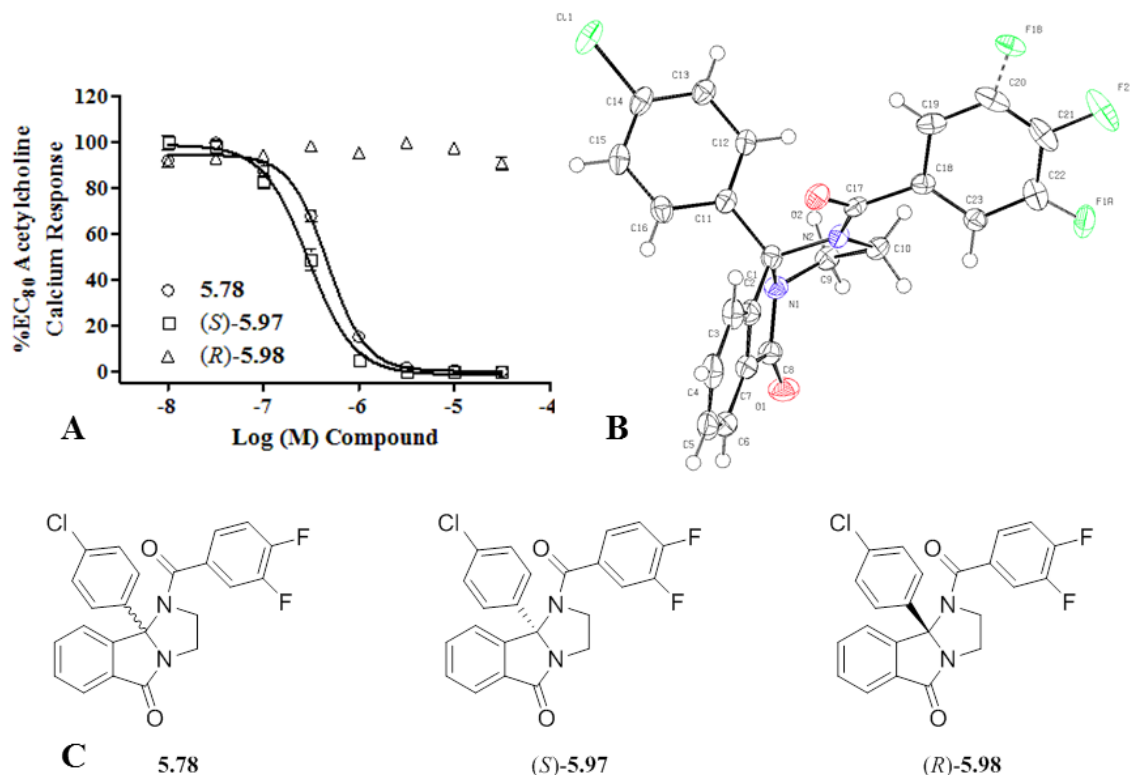


Figure 5.8. **A**) CRCs comparing activities of **5.78** (VU0478333), **5.97** (VU0483253), and **5.98** (VU0483252). Ca^{2+} mobilization assays with hM_5 cells were used to obtain CRCs of compounds **5.76** (hM_5 $\text{IC}_{50} = 0.47 \mu\text{M}$), **5.97** (hM_5 $\text{IC}_{50} = 0.30 \mu\text{M}$), and **5.98** (hM_5 $\text{IC}_{50} \gg 30 \mu\text{M}$) in the presence of a fixed submaximal ($\sim\text{EC}_{80}$) concentration of ACh. Data represent the mean \pm S.E.M. of at least 3 independent experiments with similar results. **B**) Crystal structure of the isolated active (–)-enantiomer of **5.97**, revealing its (S)-stereochemistry. Note that the fluorine in the *meta*-position of the benzamide (F1A/B) appears doubled because, when crystallized, this fluorine exhibits 50% occupancy in both the upper and lower position. Single crystal X-ray crystallography performed by J. Harp. **C**) Structures of **5.78**, **5.97**, and **5.98**.

In vitro pharmacological characterization of M_5 NAM VU0483253

Characterization of mAChR subtype selectivity of VU0483253

In light of the enantiospecific, submicromolar activity of compound **5.97** (VU0483253), we next obtained a full mAChR subtype-selectivity profile of **5.97**. Counterscreening was carried out against the remaining human mAChR subtypes to insure that M_5 -selectivity had been maintained by the pure enantiomer; furthermore, since

we ultimately desired an *in vivo* tool compound with which to study M₅, we also evaluated **5.97** against all rat mAChR subtypes to similarly insure that the compound possessed no species-specific activity outside of M₅ (**Figure 5.9**).

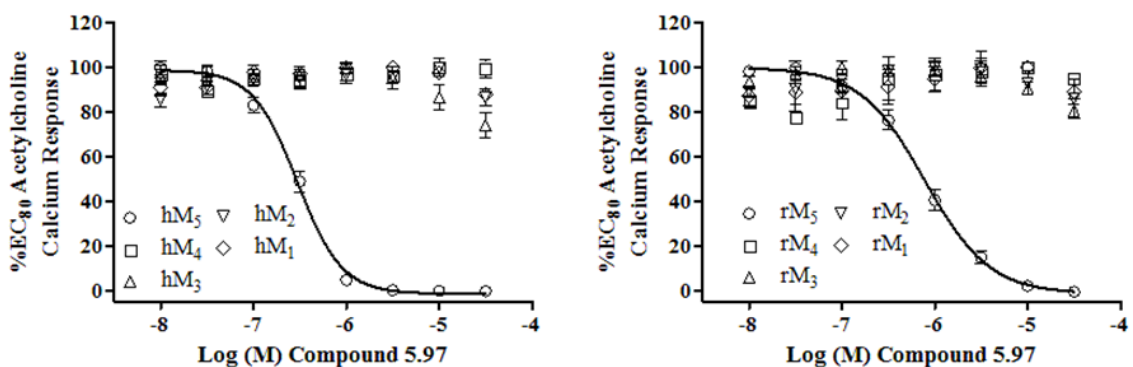


Figure 5.9. Potency and selectivity of compound **5.97** (VU0483253) at all human and rat mAChR subtypes. Ca²⁺ mobilization assays with hM₁-hM₅ cells and with rM₁-rM₅ (M₂ and M₄ co-expressing G_{α_{q15}}) cells were used to obtain CRCs of **5.97** in the presence of a fixed submaximal (~EC₈₀) concentration of ACh (IC₅₀ values: hM₅ IC₅₀ = 0.30 μM, hM₁-hM₄ IC₅₀ >> 30 μM, rM₅ IC₅₀ = 0.79 μM, rM₁-rM₄ IC₅₀ >> 30 μM). Data represent the mean ± S.E.M. of at least 3 independent experiments with similar results.

Gratifyingly, we observed no off-target mAChR activity in rat or human isoforms. Although we observed a slight species difference in potency between human and rat M₅ (hM₅ IC₅₀ = 0.30 μM, rM₅ IC₅₀ = 0.79 μM), **5.97** was inactive at hM₁-hM₄ and rM₁-rM₄, thus making it the first M₅-selective small molecule inhibitor with submicromolar potency.

Investigation of allosteric mechanism of VU0483253

At this point in our optimization and characterization of this chemical series it was still unknown whether **5.97** and its related analogs were orthosteric antagonists or NAMs. Because both a NAM and an orthosteric antagonist are functionally capable of

inhibiting an ACh EC₈₀ response, the Ca²⁺ mobilization assays that have driven the project to this point are unable distinguish between the two. In order to probe the mechanism of action by which compound **5.97** exerts its inhibitory effect, we performed radioligand competition binding experiments in hM₅ membrane preparations with the orthosteric mAChR antagonist [³H]-NMS (**Figure 5.10A**). We observed that compound **5.97** exhibited no competition with [³H]-NMS, suggesting an allosteric mode of receptor inhibition. However, this outcome represented a lack of an observable response; therefore, additional experiments were needed to conclusively declare compound **5.97** a NAM.

To further substantiate the allosteric mechanism, we performed [³H]-NMS dissociation kinetics experiments in hM₅ membrane preparations (**Figure 5.10B**). In these experiments, [³H]-NMS was allowed to bind to the hM₅ membrane preparation before a fixed concentration (10 μM) of the orthosteric antagonist atropine and **5.97** were added at multiple time points to observe any perturbation of the dissociation rate of [³H]-NMS when compared to the dissociation rate of [³H]-NMS in the presence atropine (and vehicle) alone. These experiments revealed that, in the presence of **5.97**, the dissociation rate of [³H]-NMS is retarded (Atropine + vehicle $t_{1/2}$ = 49.9 min, Atropine + **5.97** $t_{1/2}$ = 68.8 min). Together, these binding experiments demonstrated that **5.97** exerts an allosteric effect on the orthosteric site, which led us to conclude that **5.97** is the first M₅-selective NAM. Based on the unprecedented submicromolar potency, M₅-selectivity, and NAM mode of action displayed by compound **5.97**, it was declared an MLPCN probe and given the identifier ML375.

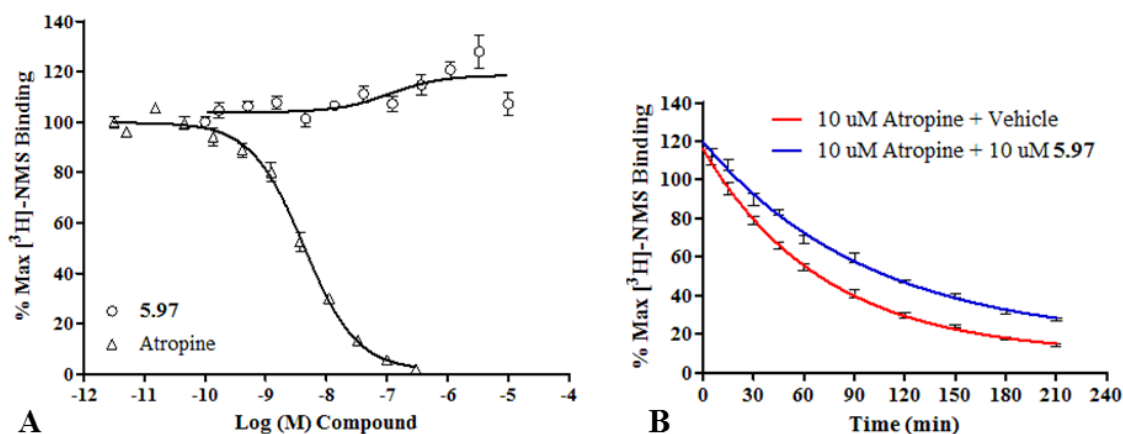


Figure 5.10. A) [^3H]-NMS competition binding assay with **5.97** (VU0483253, ML375) in an hM₅ membrane preparation. [^3H]-NMS and a CRC of either Atropine (control) or **5.97** were allowed to equilibrate for 3 hours in the hM₅ membrane preparation before filtration and scintillation counting (K_i values: Atropine $K_i = 2.5$ nM, **5.97** $K_i \gg 10$ μM). B) [^3H]-NMS dissociation kinetics assay with **5.97** in an hM₅ membrane preparation. [^3H]-NMS was allowed to label the hM₅ membrane preparation for 3 hours before the application of a fixed concentration (10 μM) of either Atropine + vehicle (control) or Atropine + **5.97** at various time points ($t_{1/2}$ values: Atropine + vehicle $t_{1/2} = 49.9$ min, Atropine + **5.97** $t_{1/2} = 68.8$ min). Data represent the mean \pm S.E.M. of at least 3 independent experiments with similar results.

Ancillary pharmacology of the VU0483253

Having optimized several major regions of SAR around the **5.97** chemical scaffold, we paused our chemical optimization and pharmacological characterization efforts to determine what, if any, wider ancillary pharmacology **5.97** may possess. In order to do this we employed a commercial radioligand competition binding screen of 68 GPCRs, ion channels, and transporters (**Table 5.7**).

Table 5.7. Ancillary/off-target competition binding screen results for compound **5.97** (VU0483253, ML375). Compound **5.97** was dosed at 10 μM for single point competition binding assays. Targets displaying significant binding ($\geq 50\%$ at 10 μM) are outlined. Data represent the mean of 2 independent experiments with similar results. Studies performed by Eurofins Panlabs, Inc.

Target/Protein	Species	% Inhibition
Adenosine A ₁	Human	10
Adenosine A _{2A}	Human	20
Adenosine A ₃	Human	42
Adrenergic α_{1A}	Rat	16

Adrenergic α_{1B}	Rat	10
Adrenergic α_{1D}	Human	7
Adrenergic α_{2A}	Human	7
Adrenergic β_1	Human	-12
Adrenergic β_2	Human	13
Androgen (Testosterone) AR	Rat	42
Bradykinin B ₁	Human	21
Bradykinin B ₂	Human	3
Calcium Channel L-Type, Benzothiazepine	Rat	33
Calcium Channel L-Type, Dihydropyridine	Rat	18
Calcium Channel N-Type	Rat	-2
Cannabinoid CB₁	Human	66
Dopamine D ₁	Human	27
Dopamine D _{2S}	Human	1
Dopamine D ₃	Human	28
Dopamine D _{4,2}	Human	1
Endothelin ET _A	Human	10
Endothelin ET _B	Human	15
Epidermal Growth Factor (EGF)	Human	4
Estrogen ER α	Human	-20
GABA _A , Flunitrazepam, Central	Rat	-3
GABA _A , Muscimol, Central	Rat	2
GABA _{B1A}	Human	13
Glucocorticoid	Human	27
Glutamate, Kainate	Rat	31
Glutamate, NMDA, Agonism	Rat	27
Glutamate, NMDA, Glycine	Rat	15
Glutamate, NMDA, Phencyclidine	Rat	6
Histamine H ₁	Human	23
Histamine H ₂	Human	-7
Histamine H ₃	Human	12
Imidazoline I ₂ , Central	Rat	13
Interleukin IL-1	Mouse	3
Leukotriene, Cysteinyl CysLT ₁	Human	4
Melatonin MT ₁	Human	32
Muscarinic M ₁	Human	9
Muscarinic M ₂	Human	14
Muscarinic M ₃	Human	11
Neuropeptide Y Y ₁	Human	14
Neuropeptide Y Y ₂	Human	14
Nicotinic Acetylcholine	Human	-21
Nicotinic Acetylcholine α_1 , Bungarotoxin	Human	12
Opiate δ_1 (OP1, DOP)	Human	9
Opiate κ (OP2, KOP)	Human	7
Opiate μ (OP3, MOP)	Human	3
Phorbol Ester	Mouse	3

Platelet Activating Factor (PAF)	Human	19
Potassium Channel [K _{ATP}]	Human	9
Potassium Channel hERG	Human	39
Prostanoid EP ₄	Human	1
Purinergic P2X	Rabbit	-6
Purinergic P2Y	Rat	7
Rolipram	Rat	20
Serotonin (5-HT _{1A})	Human	8
Serotonin (5-HT _{2B})	Human	13
Serotonin (5-HT ₃)	Human	-4
Sigma σ_1	Human	42
Sodium Channel, Site 2	Rat	49
Tachykinin NK ₁	Human	7
Thyroid Hormone	Rat	3
Transporter, Dopamine (DAT)	Human	28
Transporter, GABA	Rat	45
Transporter, Norepinephrine (NET)	Human	21
Transporter, Serotonin (SERT)	Human	0

Pleasingly, among all 68 targets tested, compound **5.97** displayed significant binding (>50% at 10 μ M) at only one target, the cannabinoid CB₁ receptor (66% inhibition). Compound **5.97** was subsequently tested in a functional assay at CB₁, but no functional activity was found at this target (data not shown, experiment performed by Eurofins Panlabs, Inc.).

***In vitro* & *in vivo* DMPK characterization of M₅ NAM VU0483253**

Now that we possessed a highly selective M₅ NAM with submicromolar potency, we sought to determine the *in vitro* DMPK profile of compound **5.97** (VU0483253, ML375) in order to evaluate its potential to serve as a future *in vivo* tool compound with which so study M₅ in the CNS. The compound was assayed in several *in vitro* DMPK assays, including plasma protein binding, rat and human microsomal stability, and a CYP

inhibition panel. These studies revealed **5.97** to have a very robust DMPK profile with strong microsomal stability and low predicted hepatic clearance in human, rat, and cynomolgus monkey (**Table 5.8**).

Table 5.8. *In vitro* and *in vivo* DMPK data for **5.97** (VU0483253) in multiple species. Human and rat studies performed by T. Bridges. Non-human primate cynomolgus monkey studies performed by Frontage Laboratories, Inc.

Parameter	Rat	Cynomolgus monkey	Human
hepatic microsome CL_{int} (mL/min/kg)	24	20	2.6
predicted CL_{hep} (mL/min/kg)	18	14	2.3
$f_{u,plasma} \cdot f_{u,brain}$	0.029, 0.003	0.001, ---	0.013, ---
CYP inhibition (P450, IC_{50})	---	---	3A4, 2D6, 1A2: >15; 2C9: 7.4
CL_p (mL/min/kg)	2.5	3.0	---
Elimination, $t_{1/2}$ (hr)	80	10	---
V_{ss} (L/kg, IV)	16	1.9	---
%F (PO)	80	---	---
K_p , $K_{p,uu}$ (1 h, PO)	1.8, 0.2	---	---

Given its promising *in vitro* profile, we moved on to testing the *in vivo* DMPK properties of **5.97** in rat. In a rat IV/PO PK study the parameters of plasma clearance (CL_p), elimination half-life ($t_{1/2}$), volume of distribution at steady state (V_{ss}), bioavailability through oral dosing (%F), and the brain:plasma partition coefficient (K_p) were determined (**Table 5.8**). We were pleased to observe low plasma clearance rates that correlated well with the low hepatic clearance predicted by the *in vitro* microsomal intrinsic clearance data. Furthermore, with an oral bioavailability of 80%, the compound appears to be readily available systemically when dosed orally. Most excitingly, a K_p of

1.8 indicates the compound is CNS penetrant; however, when combined with the $f_{u,plasma}$ and $f_{u,brain}$, a K_p of 1.8 translates to an unbound brain:plasma partition coefficient ($K_{p,uu}$) of 0.20, indicating that the compound is either highly bound to protein and lipids in the brain or possibly subject to active efflux. Unfortunately, bidirectional efflux experiments with Caco-2 and MDCK-P-gp cells were confounded by the poor solubility of **5.97** in the assay buffer, so the potential involvement of active transporter activity at the BBB is presently unknown.

Altogether, these DMPK data demonstrate that compound **5.97** possesses a robust metabolic profile and is CNS penetrant. Unfortunately, the free fraction of compound within the brain was extremely low and hence, the amount of compound free at the site of action would be extremely low as well, for a free fraction-driven effect. In light of this data, the optimization effort now turned towards focusing on means by which to increase either the free fraction or overall potency of the chemical series.

Continued SAR exploration and physicochemical optimization of M₅ NAM

VU0483253

Having gained knowledge of the DMPK properties of compound **5.97** (VU0483253, ML375) we returned to further optimization efforts. As previously mentioned, **5.97** possesses an excellent potency and selectivity profile, the primary hindrance to employing compound **5.97** as an *in vivo* probe is its low $K_{p,uu}$. Given the compound's excellent K_p value, it is clear that the compound is CNS penetrant; however, once within the brain the compound is likely highly protein and lipid bound. The low free

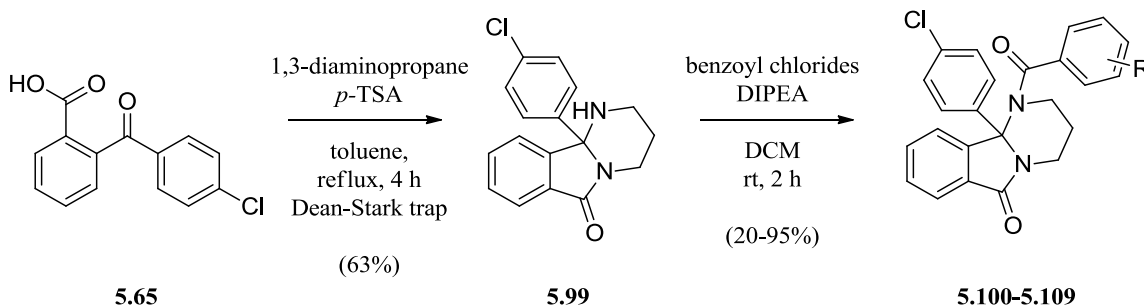
fraction within the brain may be due to the compounds highly bound nature alone, or it may be further exacerbated by the active transport of unbound compound out of the CNS (a factor which we have thus far been unable to test, *vide supra*). In either scenario, the notably high lipophilicity of compound **5.97** (CLogP = 5.0, as calculated by ChemBioDraw Ultra, version 12.0.2.1076) is very likely contributing to the high level of protein and lipid binding in the brain. As a result, the goals of our continued optimization efforts were twofold: (1) Decrease the scaffold's lipophilicity in order to increase the CNS free fraction of compound and/or (2) explore untapped SAR in order to increase the potency to a level that the observed low concentration of free compound will be sufficient to exert an effect.

Historically, the manner in which medicinal chemists have decreased lipophilicity is by introducing hydrogen bond donors and acceptors and by increasing the molecule's total polar surface area through the introduction of heteroatoms^{88,89}. Since compound **5.97** currently contains few of either of these features, we envisioned many opportunities to improve the molecule's physicochemical properties. In addition to these efforts, we also planned to continue generally exploring the chemical scaffold's SAR in the event that such efforts may yield even more potent analogs.

Continued exploration of tricyclic core region SAR

In searching for areas of the chemical scaffold to experiment with our revised optimization strategy, we returned to the tricyclic core. Although we had previously found little tractable SAR around this region (*vide supra*), we felt that the structural composition of the previous library, consisting of relatively radical variations on the

tricyclic core, warranted a more nuanced approach that examined more targeted changes to the core that may improve the physical properties of the chemical scaffold. Thus we sought to make analogs of compounds **5.63** and **5.64**, which contained an expanded, 6-membered aminal ring and showed weak activity in the previous screen of the core library (**Figure 5.5**, **Table 5.4**). The added conformational freedom allowed by a 6-membered aminal ring lessens the planarity of the chemical scaffold and marginally improves the ClogP of the scaffold when compared to the 5-membered version (ClogP = 4.8). We hypothesized that, by combining this new core with the potent 9b-4-chlorophenyl moiety, we might improve the potency of the 6-membered aminal scaffold while also improving the physicochemical properties of the overall scaffold



Scheme 5.5. Synthesis of 6-membered aminal core library analogs **5.100-5.109**. Syntheses performed by M. Kokubo.

6-membered aminal analogs were easily accessed by modifying the general synthesis of the NAM scaffold with the substitution of 1,3-diaminopropane for ethylene diamine. The resulting 6-membered aminal analog **5.99** was subsequently acylated with 10 benzoyl chlorides selected for their strong activity in earlier libraries (**Scheme 5.5**). The library analogs as well as the unacylated **5.99** were assayed in parallel in single point

(10 μM) Ca^{2+} mobilization assays against hM_5 to assess the activity of each analog (Figure 5.11, Table 5.9).

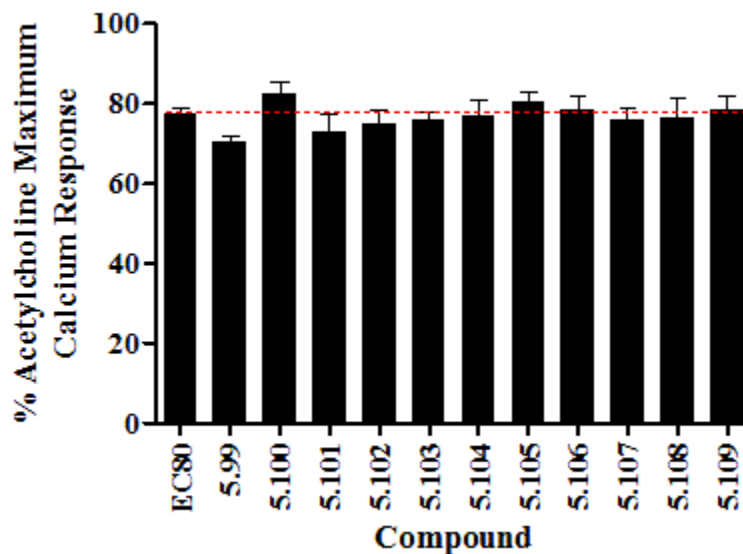
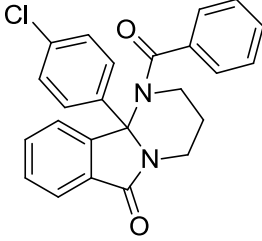
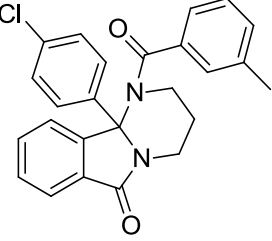
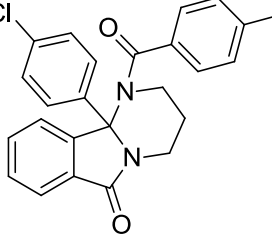
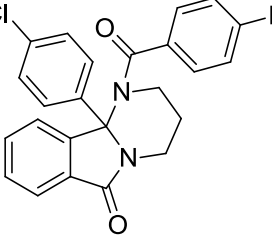
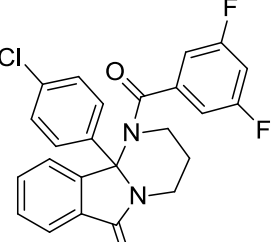
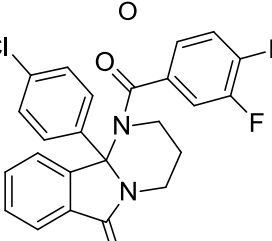
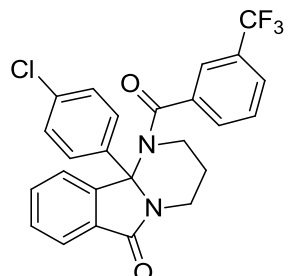
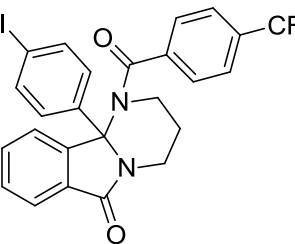
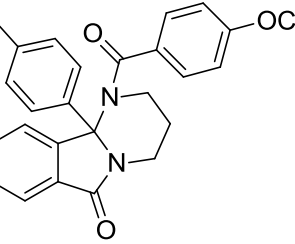
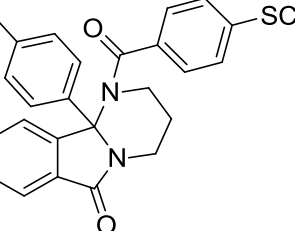


Figure 5.11. Comparison of single point (10 μM) screen results of the 6-membered aminal core library, analogs **5.99-5.109**. Ca^{2+} mobilization was used to obtain $\%ACh_{\text{Max}}$ values for each compound in the presence of a fixed submaximal ($\sim\text{EC}_{80}$) concentration of ACh. Data represent the mean \pm S.E.M. of at least 3 replicate experiments with similar results.

Table 5.9. Structures for 6-membered aminal core analogs **5.99-5.109** and associated inhibitory activity data from the single point (10 μM) screen at hM_5 . Ca^{2+} mobilization responses for each compound are reported as a percentage of the maximum ACh response. VU number denotes the compound identifier assigned by Vanderbilt University. Data represent the mean of at least 3 replicate experiments with similar results.

Structure	Cmpd #	VU #	hM_5 $\%ACh_{\text{Max}}$
	5.99	VU0485459	70.4

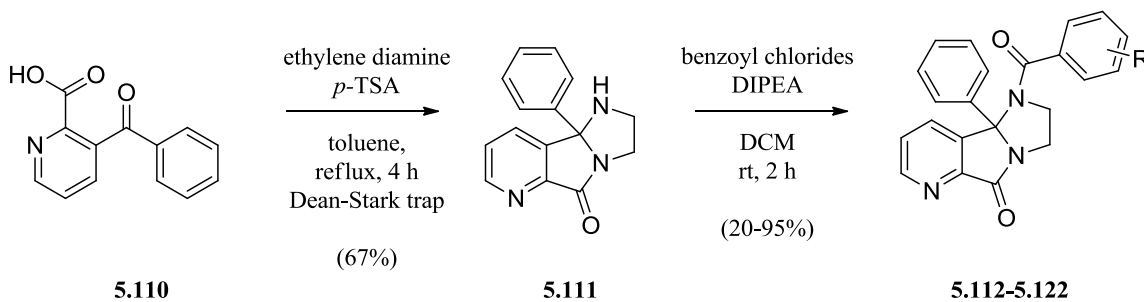
	5.100	VU0478978	82.5
	5.101	VU0478903	72.9
	5.102	VU0478886	74.8
	5.103	VU0478910	76.0
	5.104	VU0478911	76.8
	5.105	VU0478914	80.4

	5.106	VU0478894	78.6
	5.107	VU0478906	75.7
	5.108	VU0478996	76.4
	5.109	VU0478862	78.5

Unfortunately, all 6-membered aminal ring analogs were devoid of activity in the Ca^{2+} mobilization assays at hM_5 . That a seemingly minor ring expansion should cause such a dramatic loss in potency further underscores the paucity of SAR surrounding the NAM chemical scaffold.

Discouraged from further manipulation of the size and orientation of the core, we next attempted the strategy of increasing the molecule's total polar surface area via the introduction of heteroatoms to the core benzo ring. Specifically, we aimed to replace the core benzo ring with a pyridyl version. From 3-(4-chlorobenzoyl)picolinic acid,

condensation with ethylene diamine furnished amine intermediate **5.111**. The amine was subsequently acylated with 11 benzoyl chlorides to furnish library analogs **5.112-5.122** (Scheme 5.6). The library analogs as well as the unacylated **5.111** were assayed in parallel in single point (10 μM) Ca^{2+} mobilization assays against hM_5 to assess the activity of each analog (Figure 5.12, Table 5.10).



Scheme 5.6. Synthesis of pyridyl core library analogs **5.112-5.122**. Syntheses performed by M. Kokubo.

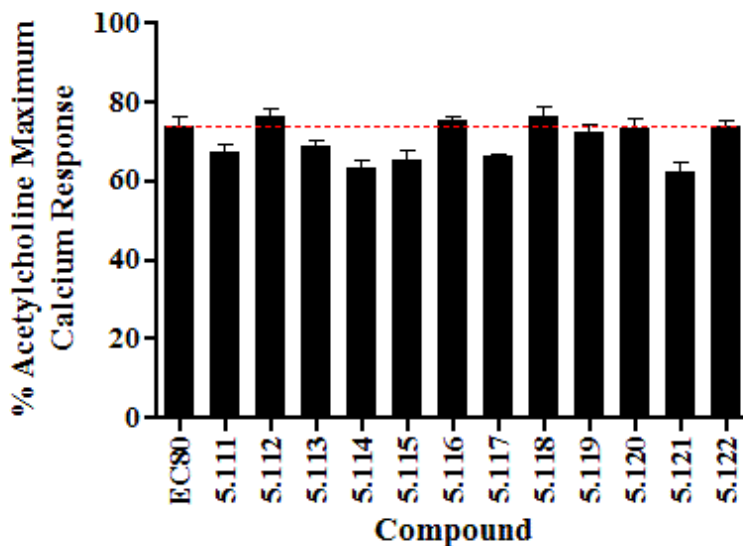
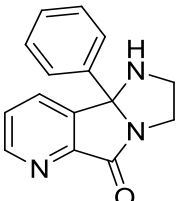
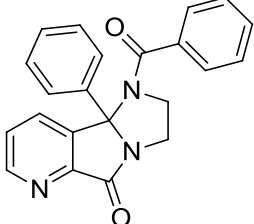
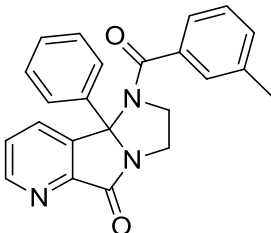
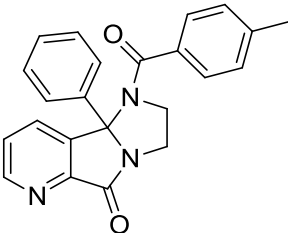
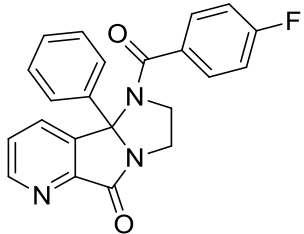
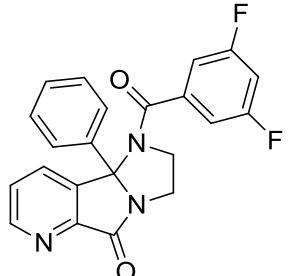
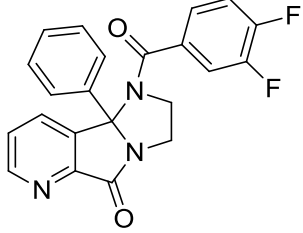
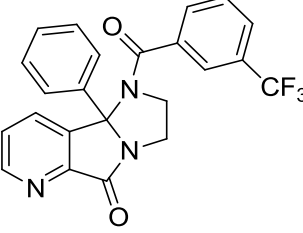
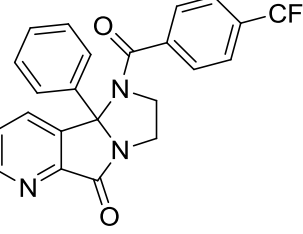
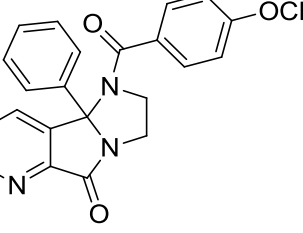
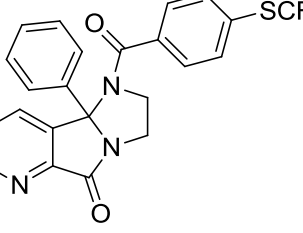
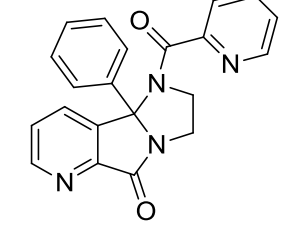


Figure 5.12. Comparison of single point (10 μM) screen results of the pyridyl core library, analogs **5.112-5.122**. Ca^{2+} mobilization was used to obtain $\% \text{ACh}_{\text{Max}}$ values for each compound in the presence of a fixed submaximal ($\sim \text{EC}_{80}$) concentration of ACh. Data represent the mean \pm S.E.M. of at least 3 replicate experiments with similar results.

Table 5.10. Structures for pyridyl core analogs **5.112-5.122** and associated inhibitory activity data from the single point (10 μ M) screen at hM₅. Ca²⁺ mobilization responses for each compound are reported as a percentage of the maximum ACh response. VU number denotes the compound identifier assigned by Vanderbilt University. Data represent the mean of at least 3 replicate experiments with similar results.

Structure	Cmpd #	VU #	hM ₅ %ACh _{Max}
	5.111	VU0481528	67.2
	5.112	VU0481905	76.7
	5.113	VU0481890	68.9
	5.114	VU0481888	63.1
	5.115	VU0482002	65.2
	5.116	VU0481787	75.2

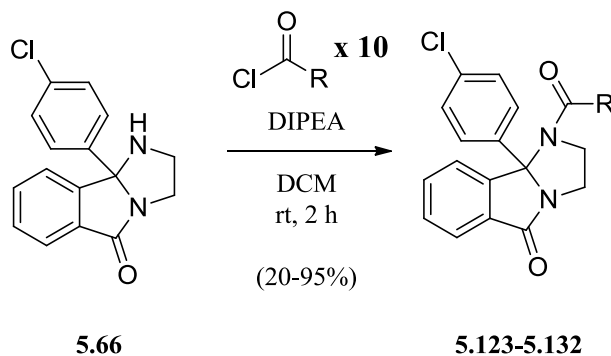
	5.117	VU0481760	66.4
	5.118	VU0481886	76.6
	5.119	VU0481887	72.2
	5.120	VU00481969	73.1
	5.121	VU0481970	62.1
	5.122	VU0481909	73.8

As with the aminal library, all core pyridyl library analogs failed to display activity in the Ca^{2+} mobilization assays at hM_5 . Thwarted by the delicate SAR of the core

tricycle, we again were forced to leave the core in its original state as we shifted our renewed optimization efforts to a different region of the chemical scaffold.

Continued optimization of benzamide region SAR

Disheartened by the lack of productive SAR in the core region, we returned to the relatively diverse SAR of the benzamide region in order to try our strategy of introducing heteroatoms and proton donors/acceptors to improve the physicochemical profile of the chemical scaffold. Beginning from amine intermediate **5.66**, we synthesized a small library of benzamide analogs by acylating the amine with 10 acyl chlorides possessing heteroatoms and proton donors/acceptors (**Scheme 5.7**). The new benzamide library analogs were subsequently assayed in single point (10 μM) Ca^{2+} mobilization assays against hM_5 to assess the activity of each analog (**Figure 5.13**, **Table 5.11**).



Scheme 5.7. Synthesis of benzamide library analogs **5.123-5.132**. Syntheses performed by M. Kokubo.

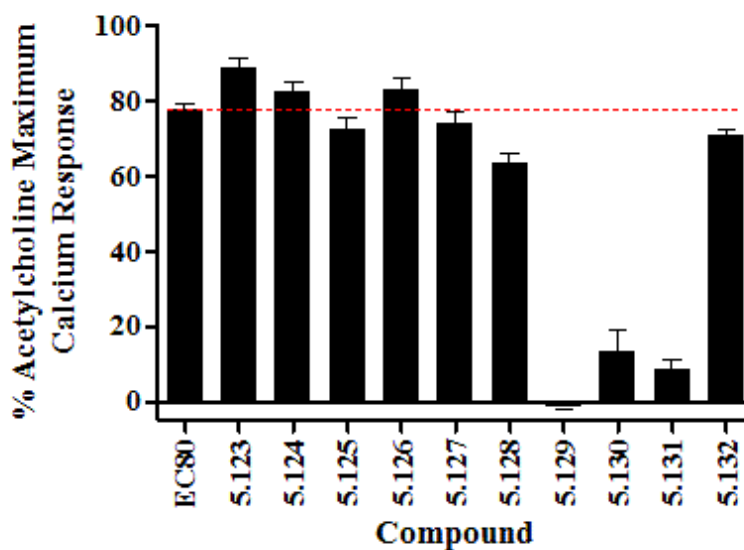
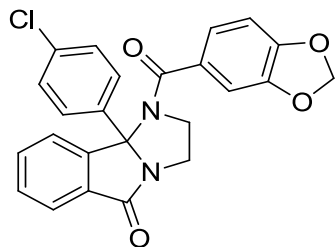


Figure 5.13. Comparison of single point (10 μM) screen results of the benzamide library, analogs **5.123-5.132**. Ca^{2+} mobilization was used to obtain $\%ACh_{\text{Max}}$ values for each compound in the presence of a fixed submaximal ($\sim\text{EC}_{80}$) concentration of ACh. Data represent the mean \pm S.E.M. of at least 3 replicate experiments with similar results.

Table 5.11. Structures for benzamide analogs **5.123-5.132** and associated inhibitory activity data from the single point (10 μM) screen at hM_5 . Ca^{2+} mobilization responses for each compound are reported as a percentage of the maximum ACh response. VU number denotes the compound identifier assigned by Vanderbilt University. Data represent the mean of at least 3 replicate experiments with similar results.

Structure	Cmpd #	VU #	hM_5 $\%ACh_{\text{Max}}$
	5.123	VU0480132	88.9
	5.124	VU0480152	82.6

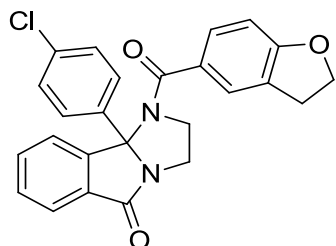
	5.125	VU0480187	72.4
	5.126	VU0480125	82.9
	5.127	VU0486204	74.0
	5.128	VU0486268	63.4
	5.129	VU0486240	-1.4
	5.130	VU0486205	13.3



5.131

VU0486177

8.7



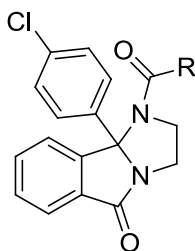
5.132

VU0486162

71.1

We were interested to see a range of SAR displayed in the results of the single point screen. All three regioisomers of the pyridyl analogs proved to be inactive. The three active analogs, **5.129**, **5.130**, and **5.131**, all share the feature an oxygen stemming from the 4-position of the benzamide. Nevertheless, this trait obviously is not a guarantee of activity as other analogs such as **5.127**, **5.128**, and **5.132** share this structural element, but are inactive. The three active compounds were subsequently tested in full CRC Ca^{2+} mobilization assays at hM_5 (**Table 5.12**).

Table 5.12. Potencies at hM₅ for selected benzamide analogs **5.129-5.131**. Ca²⁺ mobilization assays with hM₅ cells were used to obtain CRCs of compounds in the presence of a fixed submaximal (~EC₈₀) concentration of ACh. Data represent the mean of at least 3 independent experiments with similar results.

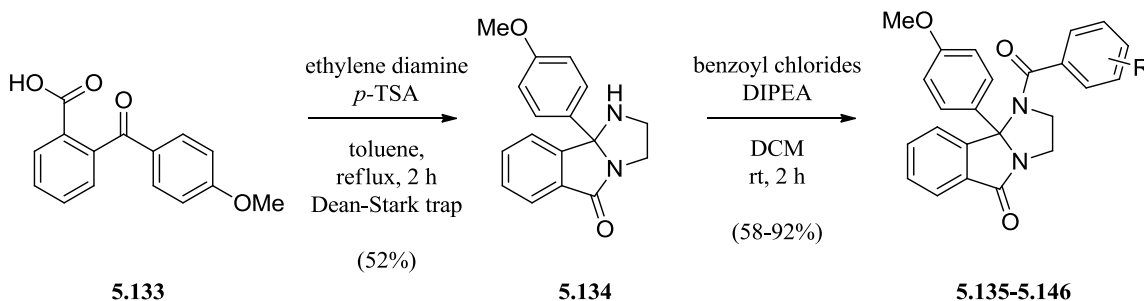


Cmpd #	R =	hM ₅ EC ₅₀ (μM)
5.129	4-isopropoxyphenyl	0.79
5.130	4-difluoromethoxyphenyl	4.9
5.131	benzo[<i>d</i>][1,3]dioxol-5-yl	2.1

Although none of the active benzamide analogs proved as potent as the lead M₅ NAM **5.97** or its racemic precursor, **5.76**, the 4-isopropoxyphenyl analog **5.129** demonstrated submicromolar potency while also possessing the added physicochemical benefit of a proton acceptor. Despite this, its CLogP was increased relative to **5.97** (CLogP = 5.7). Nevertheless, this small benzamide library demonstrates that it is possible to incorporate substituents containing proton donors/acceptors into the relatively diverse SAR of the benzamide region. Moving forward in the optimization of this series, such groups will be necessary to tweak and refine the physicochemical properties of the chemical series in order to obtain an M₅ NAM analog with a DMPK profile suitable for the *in vivo* study of M₅.

Continued exploration of 9b-phenyl region SAR

Having revisited the core and the benzamide with our mandate to decrease lipophilicity and explore SAR we continued on to the 9b-phenyl region to test its response to the incorporation of a proton-accepting substituent. In this case we tested the effect of a 4-methoxy on the potency and DMPK profile of the chemical series. Beginning from 2-(4-methoxybenzoyl)benzoic acid, condensation with ethylene diamine furnished amine **5.134**. Subsequent acylation with a library of 12 acid chlorides provided analogs **5.135-5.146** (Scheme 5.8). The 9b-4-methoxyphenyl library analogs were subsequently tested in in single point (10 μM) Ca^{2+} mobilization assays against hM_5 to assess the activity of each analog (Figure 5.14, Table 5.13).



Scheme 5.8. Synthesis of 9b-phenyl library analogs **5.135-5.146**. Syntheses performed by M. Kokubo.

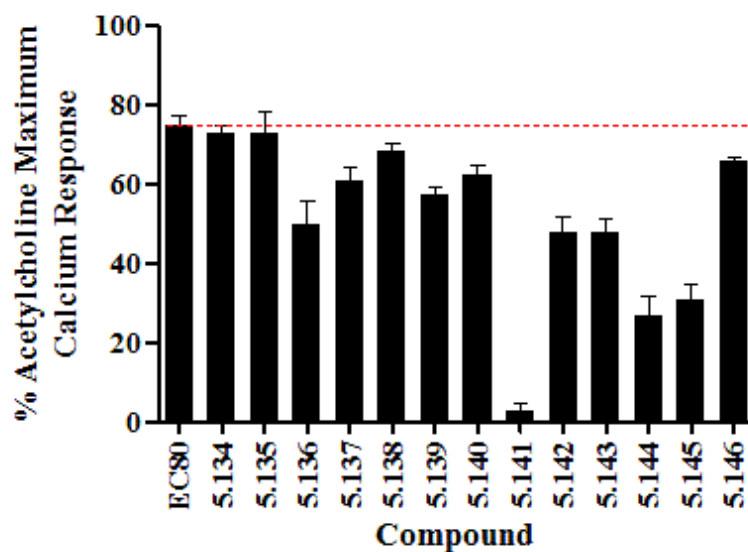
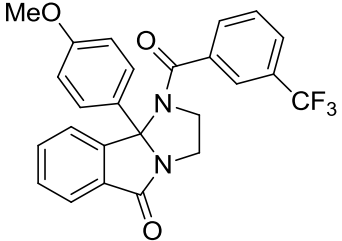
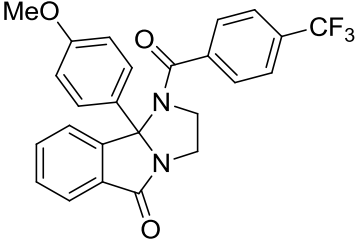
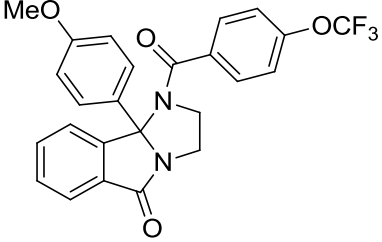
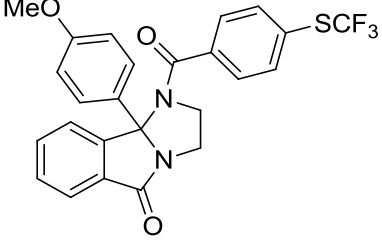
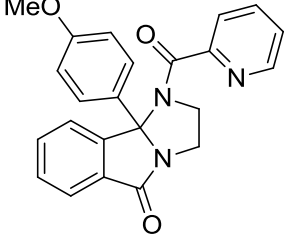


Figure 5.14. Comparison of single point (10 μM) screen results of the 9b-4-methoxyphenyl library, analogs **5.134-5.146**. Ca^{2+} mobilization was used to obtain %ACh_{Max} values for each compound in the presence of a fixed submaximal ($\sim\text{EC}_{80}$) concentration of ACh. Data represent the mean \pm S.E.M. of at least 3 replicate experiments with similar results.

Table 5.13. Structures for 9b-4-methoxyphenyl analogs **5.134-5.146** and associated inhibitory activity data from the single point (10 μM) screen at hM₅. Ca^{2+} mobilization responses for each compound are reported as a percentage of the maximum ACh response. VU number denotes the compound identifier assigned by Vanderbilt University. Data represent the mean of at least 3 replicate experiments with similar results..

Structure	Cmpd #	VU #	hM ₅ %ACh _{Max}
	5.134	VU0487631	72.7
	5.135	VU0515835	73.0

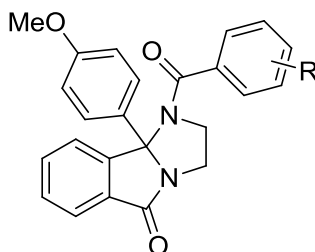
	5.136	VU0515833	49.9
	5.137	VU0515834	61.1
	5.138	VU0515979	68.4
	5.139	VU0515980	57.4
	5.140	VU0515981	62.4
	5.141	VU0487632	2.9

	5.142	VU0515827	47.9
	5.143	VU0515982	48.0
	5.144	VU0515828	26.7
	5.145	VU0515829	30.7
	5.146	VU0515830	66.1

In general, the 9b-4-methoxyphenyl library produced weak or inactive compounds, with the one exception of the 3,4-difluorobenzamide analog **5.141** (VU0487632). The fact that many of the observed benzamide substituents were formerly active in the presence of different 9b-phenyl substituents and were now inactive in the presence of the 9b-4-methoxyphenyl once again underscored the complex interaction

between the 9b-phenyl moiety and the benzamide moiety. To ascertain IC₅₀ potencies, analog **5.141** as well as the relatively active analogs **5.144** and **5.145** were tested in full CRC Ca²⁺ assays (**Table 5.14**)

Table 5.14. Potencies at hM₅ for selected 9b-4-methoxyphenyl analogs **5.141**, **5.144**, and **5.145**. Ca²⁺ mobilization assays with hM₅ cells were used to obtain CRCs of compounds in the presence of a fixed submaximal (~EC₈₀) concentration of ACh. Data represent the mean of at least 3 independent experiments with similar results.



Cmpd #	R =	hM ₅ EC ₅₀ (μM)
5.141	3,4-diF	1.3
5.144	4-OCF ₃	6.7
5.145	4-SCF ₃	8.1

Although analogs **5.144** and **5.145** were relatively weak, we were pleased to see a higher degree of potency from analog **5.141**. Despite the fact that this analog was nowhere near as potent as the lead M₅ NAM **5.97** or its racemic precursor **5.76**, its CLogP was markedly decreased (CLogP = 4.2) and we rationalized that a slightly weaker compound with a higher free fraction may still have the potential to be useful in an *in vivo* study. Thus we submitted **5.141** to a plasma protein binding studies to assess its free fractions in human and rat. Gratifyingly, **5.141** displayed a >2-fold increase in free fraction compared to **5.97** (**5.97** human $f_{u,plasma} = 0.013$, rat $f_{u,plasma} = 0.029$; **5.141** human $f_{u,plasma} = 0.037$, rat $f_{u,plasma} = 0.064$), demonstrating that the incorporation of even a single

proton acceptor can improve the physicochemical properties of the chemical series. Despite this, the low-micromolar potency of **5.141** leaves much to be desired. Although its exhibition of an improved plasma free fraction is a positive advance, more optimization will be necessary to increase the potency and/or physicochemical properties to a level that will be suitable for *in vivo* studies of M₅ in the CNS

Summary and Future Directions

The HTS of the MLPCN screening deck that interrogated the chemical landscape surrounding M₅ selective ligands revealed a weakly active M₅-selective inhibitor, **5.1** (VU0352221). The SAR of each region of the lead compound was subsequently analyzed and optimized with a multidimensional iterative parallel synthesis strategy. This effort produced over 130 analogs, including the highly potent and M₅-selective lead compound **5.97** (VU0483253, ML375). Moreover, analysis of the mechanism of action of **5.97** revealed that the compound acts as a NAM, making it the first M₅-selective NAM ever reported (**Figure 5.15**).

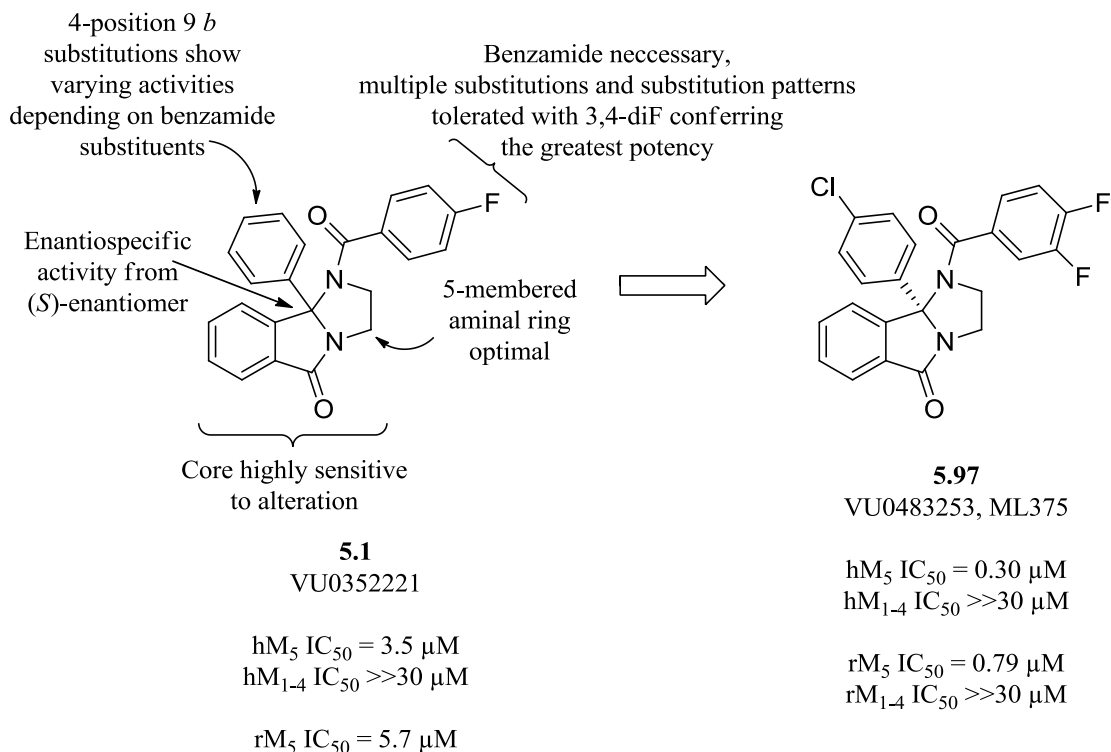


Figure 5.15. Summary and comparison of the structure, potency, and SAR surrounding the M_5 antagonist HTS lead **5.1** (VU0352221) that led to the discovery of the first sub-micromolar, M_5 -selective NAM **5.97** (VU0483253, ML375).

Optimization efforts up to this point have given us a general understanding of the SAR surrounding the novel M_5 NAM chemical series. Although the unique tricyclic core was what originally drew our attention to this chemical series, SAR around this region was found to be extremely delicate, and any disturbance to the original tricyclic arrangement resulted in inactive compounds. Contrastingly, the benzamide region exhibited far more flexible SAR. In this region we found that the amide connectivity is required for activity, but the benzyl ring itself tolerates a multitude of substituents and substitution patterns. Out of the 40+ benzamide analogs we analyzed, 3,4-difluorobenzamide was the most optimal benzamide found. It was also discovered that the benzamide substituents are not independent from the 9*b*-phenyl in their influence on

activity. Depending on the substituents of the 9b-phenyl region, formerly active benzamide substituents may be rendered inactive, or *vice versa*. A stark example of this interesting relationship was found between the original HTS hit **5.1** ($\text{hM}_5 \text{ IC}_{50} = 3.5 \mu\text{M}$) and its 9b-4-chlorophenyl analog **5.76** ($\text{hM}_5 \text{ IC}_{50} \gg 10 \mu\text{M}$). Despite this example, the 9b-4-chlorophenyl moiety was generally found to increase potency in the presence of most benzamide substituents. It was the combination of this 9b-4-chlorophenyl and the 3,4-difluorobenzamide which produced the highly potent analog **5.76**. By resolving the enantiomers of **5.76** we discovered that the chemical scaffold exhibits enantiospecific inhibition, with the (*S*)-enantiomer, our lead M_5 NAM **5.97** (VU0483253, ML375), being the active arrangement (**Figure 5.15**).

In vitro DMPK studies revealed that **5.97** possesses a robust metabolic and pharmacokinetic profile with strong microsomal stability and low predicted hepatic clearance in human, rat, and cynomolgus monkey (rat $\text{CL}_{\text{int}} = 24 \text{ mL/min/kg}$, predicted rat $\text{CL}_{\text{hep}} = 18 \text{ mL/min/kg}$; human $\text{CL}_{\text{int}} = 2.6 \text{ mL/min/kg}$, predicted human $\text{CL}_{\text{hep}} = 2.3 \text{ mL/min/kg}$; cyno $\text{CL}_{\text{int}} = 20 \text{ mL/min/kg}$, predicted cyno $\text{CL}_{\text{hep}} = 14 \text{ mL/min/kg}$). Based on this profile **5.97** was entered into *in vivo* rat pharmacokinetic studies. These studies corroborated that the compound was highly stable. Furthermore, **5.97** exhibited high oral bioavailability and CNS penetrance (%F = 80, $K_p = 1.8$). Unfortunately these studies, along with plasma protein/rat brain homogenate binding studies, also revealed that **5.97** is highly protein and lipid bound in the brain ($f_{u,\text{brain}} = 0.003$), likely precluding its ability to reach an effective concentration in the CNS.

In response to this DMPK profile, our optimization efforts shifted towards revisiting regions of the chemical scaffold with the goal of improving the

physicochemical properties of the chemical series. Although the majority of these newer analogs have been inactive or far less potent than **5.97**, several analogs, including the 4-isopropoxybenzamide analog **5.129** and the 9b-4-methoxy analog **5.141** are promising leads for future campaigns seeking to improve the *in vivo* potential for this scaffold.

Indeed, there are many options for further exploration and optimization of the SAR and physicochemical properties of the M₅ NAM chemical series. The 9b-phenyl remains an underexplored region. Thus far only 4-substituted phenyl rings have been tested. Any number of substituents, substitution patterns, and/or heterocycles in the 9b-position could lead to entirely new dimensions of SAR. Similarly, further study of the synergy between the 9b-phenyl ring and the benzamide is warranted. At this point the phenomenon of fluctuations in potency resulting from the interaction of these regions is poorly understood. A large matrix library comparing these two regions may be able to provide a deeper understanding of this interaction. Conveniently, such an effort could be accomplished alongside the aforementioned expanded study of SAR in the 9b-phenyl region. Finally, this chemical series could benefit from a counterscreen of all analogs against rM₅ with the goal of discovering the elements of SAR that are the basis for the species difference in potency between hM₅ and rM₅.

Although the M₅ NAM **5.97** may not be optimal for systemic dosing in *in vivo* studies due to its highly protein-bound nature, its M₅-selectivity, potency, and unique NAM pharmacology make it an invaluable probe for a number of studies into M₅ receptor structure and function. For instance, insight into the role of M₅ in regulating dopamine release in neurons of the VTA or SNc could be accomplished using the M₅ NAM in electrophysiological studies of *ex vivo* brain slices. Alternatively, **5.97** could be utilized

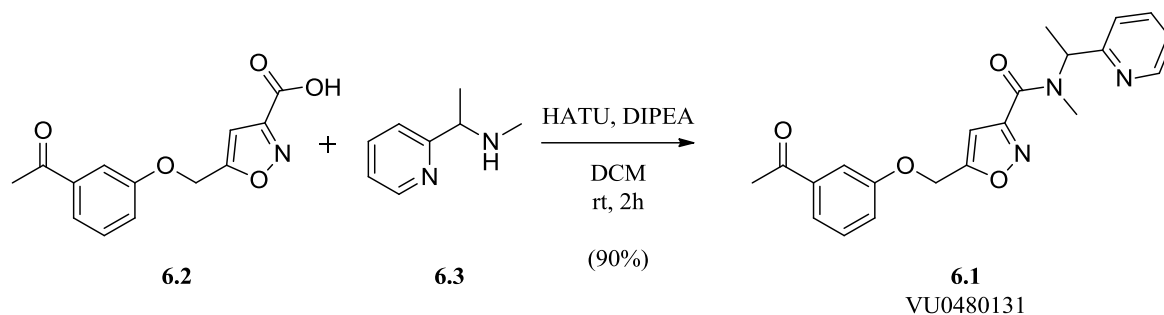
in X-ray crystallography studies of M_5 to gain greater insight into the structural biology of negative allosteric modulation of M_5 . Such a study may also provide insight into the binding orientation of **5.97** and its interaction with amino acid residues, possibly explaining the basis of the aforementioned relationship between the 9b-phenyl and benzamide regions. Finally, direct perfusion via an intracerebral cannula could represent a viable method by which to administer a high concentration of **5.97** to the site of action in a pharmacodynamic study. However **5.97** is used in the future, this first series of M_5 NAMs represents a landmark achievement and has greatly expanded the tools available to pharmacologists for the study of the neurobiology of M_5 .

Chapter VI

DISCOVERY, OPTIMIZATION, AND CHARACTERIZATION OF A HIGHLY SELECTIVE M₅ ORTHOSTERIC ANTAGONIST

HTS Identification of a novel, M₅-selective ligand with antagonist activity

As discussed in the opening of Chapter IV, the 2012 HTS campaign of the MLPCN screening deck identified a number of novel M₅-selective ligands. In addition to the identification of nine confirmed M₅ PAMs (discussed in Chapter IV) the screen also identified nine novel M₅ antagonists (discussed here and in Chapter V). At the time of the project's initiation it was not clear whether the compounds possessing inhibitory activity were M₅ orthosteric antagonists or NAMs; nevertheless, we proceeded to explore the SAR around these molecules as an M₅-selective ligand of either mode of pharmacology would be highly useful in the study of M₅ in the CNS. Where Chapter V discussed a ligand that was ultimately characterized as the first highly M₅-selective NAM, this chapter will examine another HTS hit with inhibitory activity which was ultimately revealed to be an M₅-selective orthosteric antagonist.



Scheme 6.1. Structure and synthetic pathway for the synthesis of compound **6.1** (VU0480131). Synthesis performed by M. Kokubo.

During examination of the HTS results the weak, yet M_5 -selective, isoxazole-based amide **6.1** drew our attention. The HTS reported **6.1** as having an $IC_{50} = 9.3 \mu\text{M}$ at hM_5 and selectivity against hM_1 and hM_4 ($hM_1 IC_{50} >30 \mu\text{M}$, $hM_4 IC_{50} >30 \mu\text{M}$). Compound **6.1** (VU0480131) was synthesized in-house via the amide coupling of the commercially available acid **6.2** and the secondary amine **6.3** under HATU-mediated conditions (**Scheme 6.1**). Upon retesting the freshly prepared compound in full CRC Ca^{2+} mobilization assays against all mAChR subtypes, we were pleased to see that **6.1** displayed increased potency at human and rat M_5 ($hM_5 IC_{50} = 1.1 \mu\text{M}$, $rM_5 IC_{50} = 3.5 \mu\text{M}$) and high selectivity versus hM_1 - hM_4 (hM_1 - $hM_4 IC_{50} >30 \mu\text{M}$) (**Figure 6.1**). Given the innate high potency and M_5 -selectivity of **6.1**, we were confident that, by exploring and optimizing the SAR around the multiple dimensions of the chemical scaffold, we could further increase the compound's potency and maintain its selectivity for M_5 (**Figure 6.1**)⁹⁰.

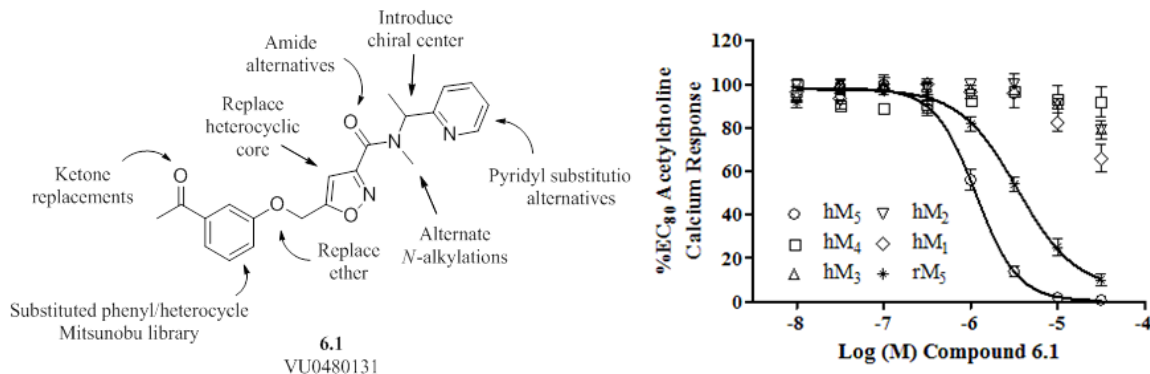


Figure 6.1. Structure, planned SAR exploration, potency, and selectivity of HTS hit compound **6.1** (VU0480131). Ca^{2+} mobilization assays with hM₁-hM₅ and rM₅ cells were used to obtain CRCs of resynthesized compound **6.1** in the presence of a fixed submaximal (~EC₈₀) concentration of ACh (EC₅₀ values: hM₅ IC₅₀ = 1.1 μM ; hM₁-hM₄ EC₅₀ >30 μM ; rM₅ EC₅₀ > 3.5 μM). Data represent the mean \pm S.E.M. of at least 3 independent experiments with similar results.

Before initiating our campaign of multidimensional iterative parallel synthesis, we first desired to analyze the mechanism of action of **6.1**. Thus, we performed competition binding experiments against the *pan*-mAChR antagonist radioligand [³H]-NMS. Interestingly, these experiments demonstrated that **6.1** displaces [³H]-NMS in a concentration-dependent manner (**6.1** K_i = 1.3 μM ; **Figure 6.2**). Such behavior suggests that **6.1** competes with [³H]-NMS for the orthosteric site. As discussed in Chapter 1, the residues of the orthosteric site are highly conserved across mAChR subtypes. So the revelation that **6.1** possesses an orthosteric mechanism of action while also being M₅-selective was particularly unexpected and stressed the need for an extensive exploration of the compound's SAR.

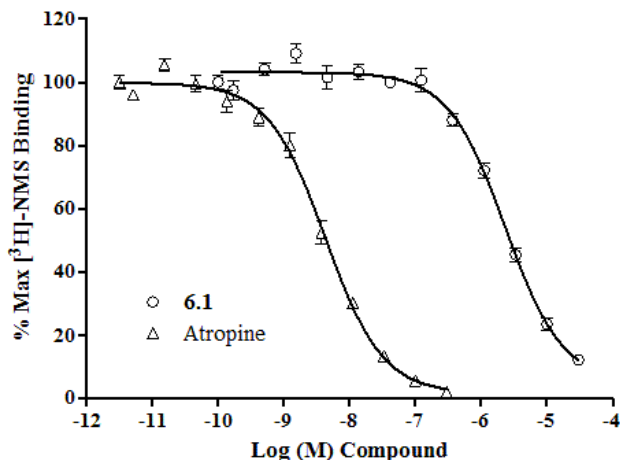


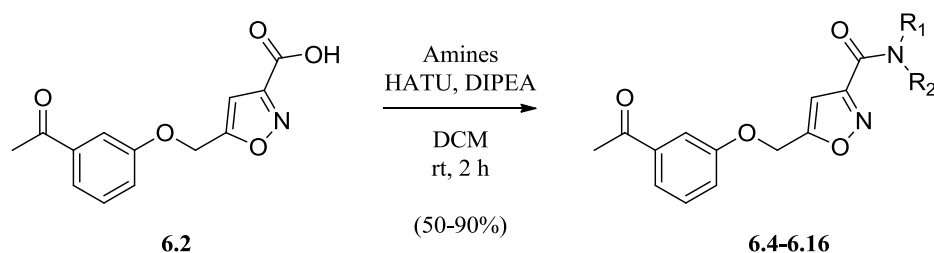
Figure 6.2. [³H]-NMS competition binding assay with **6.1** (VU0480131) in an hM₅ membrane preparation. [³H]-NMS and a CRC of either atropine (control) or **6.1** were allowed to equilibrate for 3 hours in the hM₅ membrane preparation before filtration and scintillation counting (K_i values: atropine $K_i = 2.5$ nM, **6.1** $K_i = 1.3$ μ M). Data represent the mean \pm S.E.M. of at least 3 independent experiments with similar results.

Optimization of VU0480131 to obtain M₅ orthosteric antagonist VU0488130

Exploration of eastern amide region SAR

As we already possessed the acid starting material **6.2**, we initially focused our synthetic efforts on constructing an amide library to explore the easternmost amide region of compound **6.1**. Specifically we desired to explore the effects of the deletion or expansion of the amide *N*-methyl, including joining the *N*-alkyl to the pyridine ring system to create a bicyclic system. We also used the amide library as an opportunity to explore the deletion or regioisomers of the pyridyl ring and the deletion or substitution of the chiral methyl. To construct the library, a library of commercial primary and secondary amines were coupled with acid **6.2** under HATU-mediated conditions to furnish analogs **6.4-6.16** (Scheme 6.2, Table 6.1). Upon testing the library in our single point (10 μ M) Ca²⁺ mobilization assay at hM₅ it became readily apparent that SAR was

very delicate in this region as the majority of amide region analogs proved to be inactive (**Figure 6.3**, **Table 6.1**). The exception to this inactivity was found in the *N*-ethyl homolog **6.16**; however, the compound was later found to be only weakly potent in a full CRC Ca²⁺ mobilization assays at human and rat M₅ (hM₅ IC₅₀ = 5.6 μM, rM₅ IC₅₀ >10 μM).



Scheme 6.2. Synthesis of amide region library analogs **6.4-6.16**. Syntheses performed by M. Kokubo.

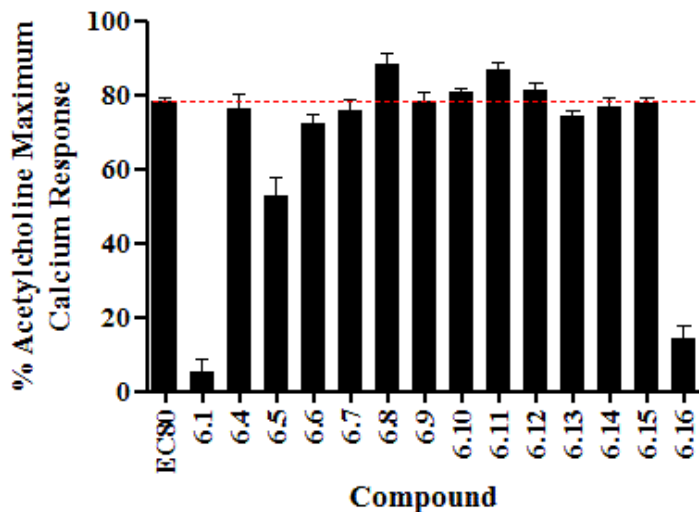
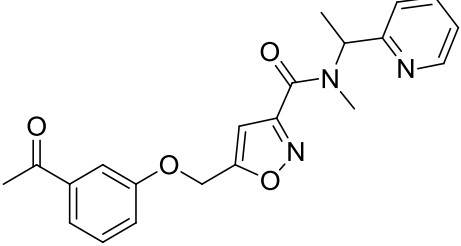
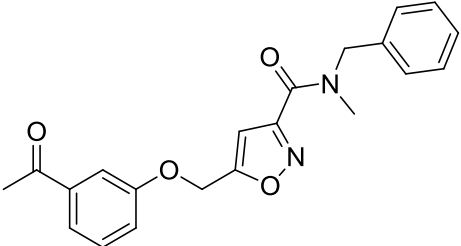
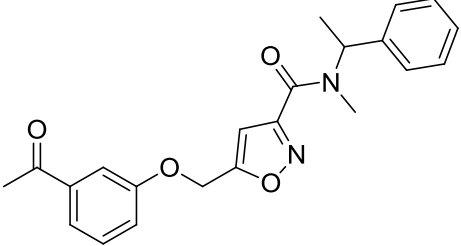
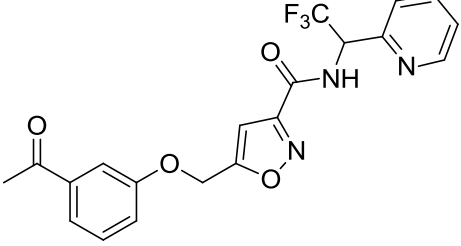
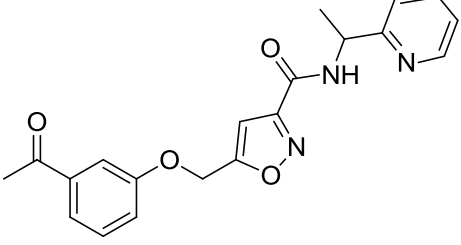
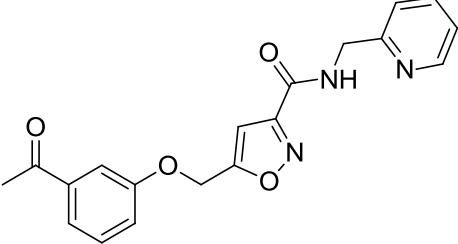
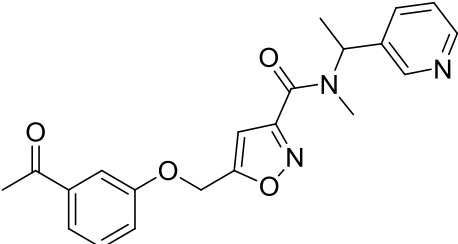
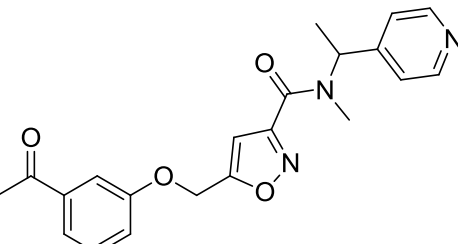
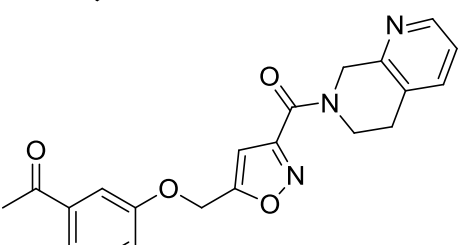
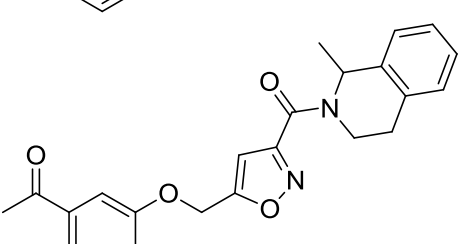
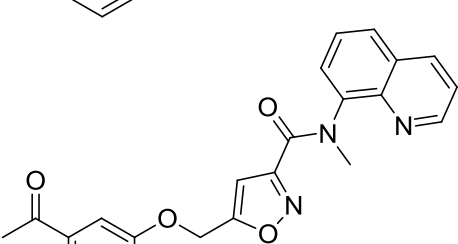
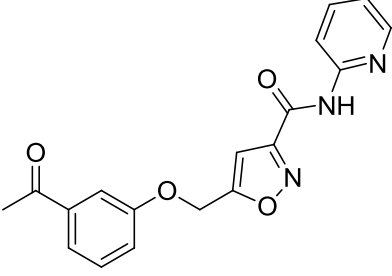
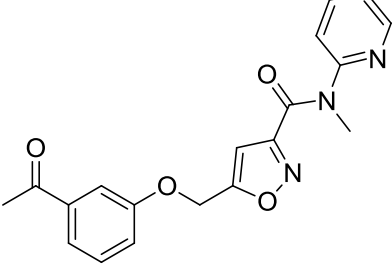
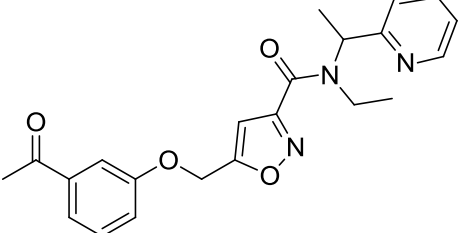


Figure 6.3. Comparison of single point (10 μM) screen results of the amide region library, analogs **6.4-6.16**. Also included is the single point Ca²⁺ mobilization response of the initial hit, compound **6.1**. Ca²⁺ mobilization was used to obtain %ACh_{Max} values for each compound in the presence of a fixed submaximal (~EC₈₀) concentration of ACh. Data represent the mean ± S.E.M. of at least 3 replicate experiments with similar results.

Table 6.1. Structures for amide analogs **6.4-6.16** and associated inhibitory activity data from the single point (10 μ M) screen at hM₅. Also included are the structure and single point Ca²⁺ mobilization response of the HTS hit, compound **6.1**. Ca²⁺ mobilization responses for each compound are reported as a percentage of the maximum ACh response. VU number denotes the compound identifier assigned by Vanderbilt University. Data represent the mean of at least 3 replicate experiments with similar results.

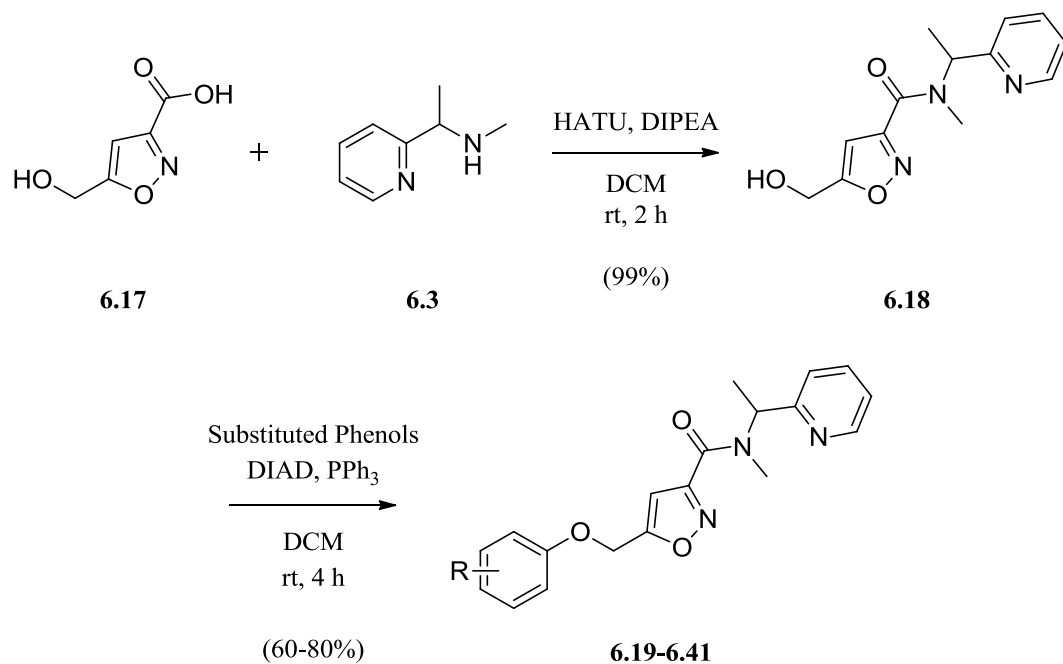
Structure	Cmpd #	VU #	hM ₅ %ACh _{Max}
	6.1	VU0480131	5.3
	6.4	VU0480164	76.6
	6.5	VU0481440	52.9
	6.6	VU0481381	72.6
	6.7	VU0481906	76.0

	6.8	VU0481408	88.7
	6.9	VU0481344	78.2
	6.10	VU0481377	80.9
	6.11	VU0481422	86.8
	6.12	VU0481348	81.5
	6.13	VU0485707	74.2

	6.14	VU0481349	77.1
	6.15	VU0481529	77.8
	6.16	VU0481461	14.2

Exploration of the western aryl ether SAR

With the amide region of **6.1** seemingly resistant to modification, we next turned our attention to optimizing the aryl ether moiety at the opposite end of the chemical scaffold. We aimed to explore the SAR of this region utilizing the Mitsunobu reaction and a library of phenols. Beginning from acid **6.17**, a HATU-mediated amide coupling with secondary amine **6.3** furnished intermediate **6.18**. The subsequent Mitsunobu reactions furnished analogs **6.19-6.41** (Scheme 6.4, Table 6.2). Despite surveying nitro, halogen, alkoxy, and alkyl moieties around the pendant phenyl ring, as well as reduced variations of the 3-acetyl group, no analogs in this library displayed any notable activity at hM₅ in single point (10 μM) Ca²⁺ mobilization assays at hM₅ (Figure 6.4, Table 6.2).



Scheme 6.3. Synthesis of aryl ether library analogs **6.19-6.41**. Syntheses performed by M. Kokubo.

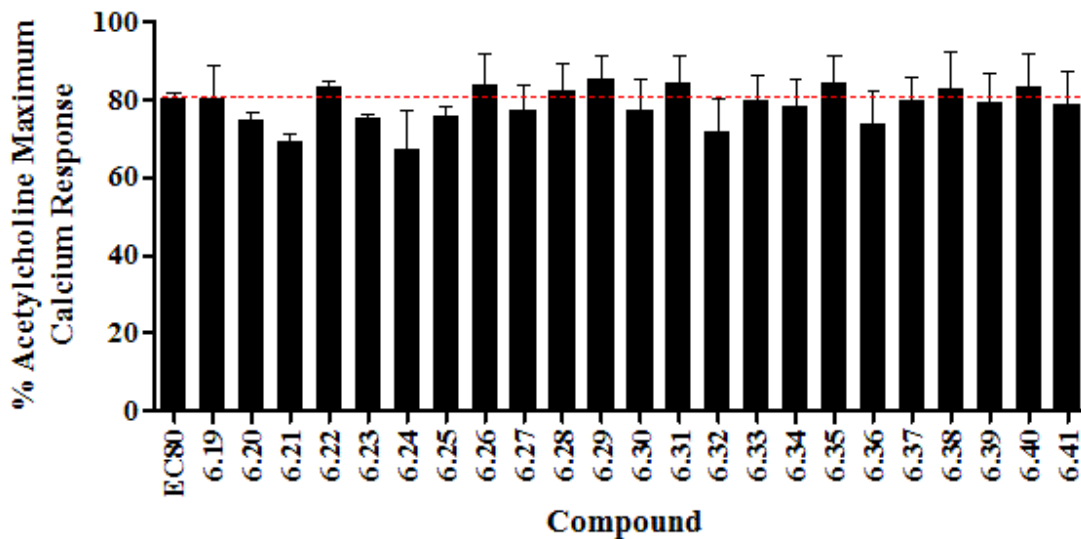
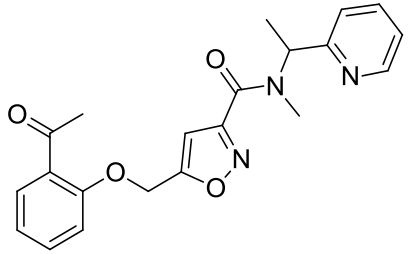
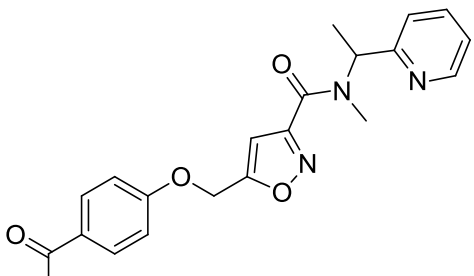
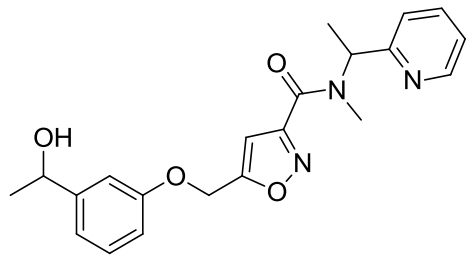
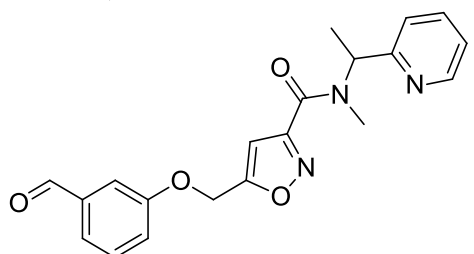
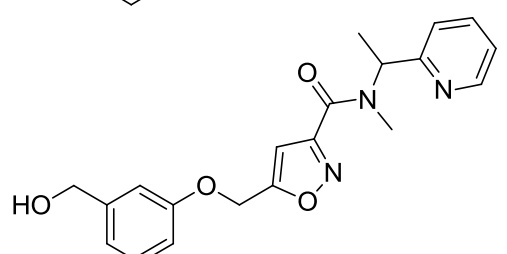
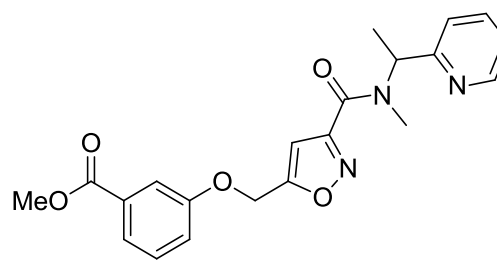
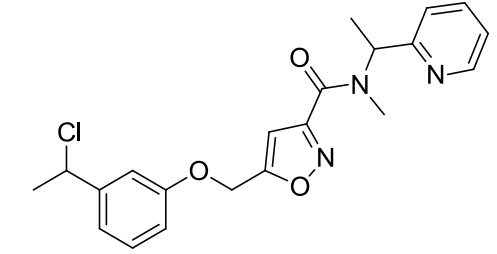
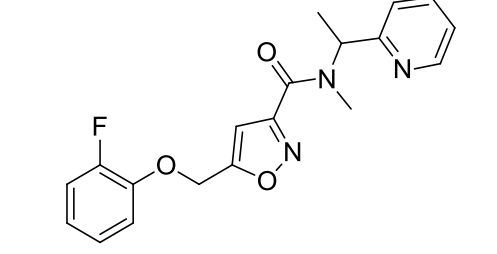
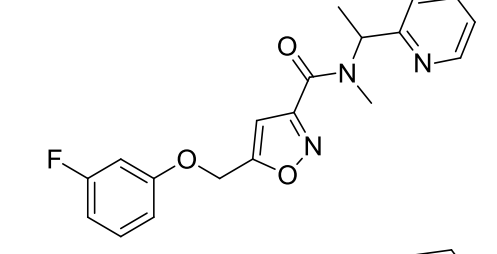
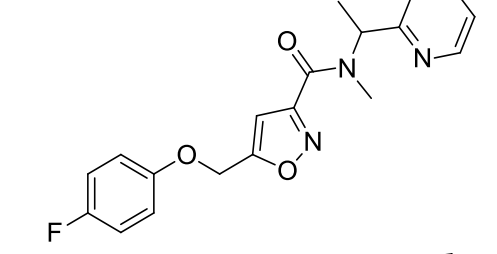
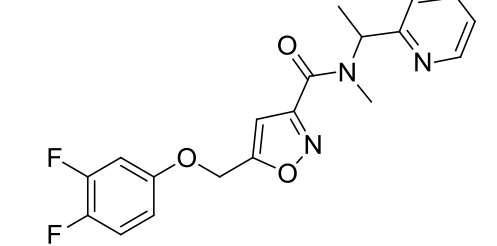
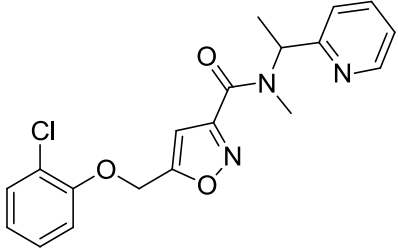
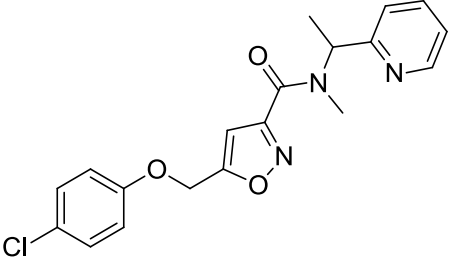
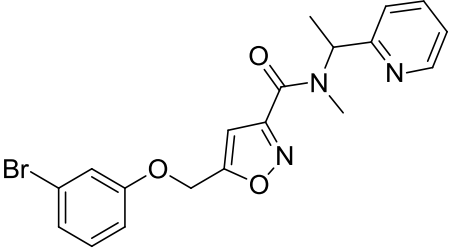
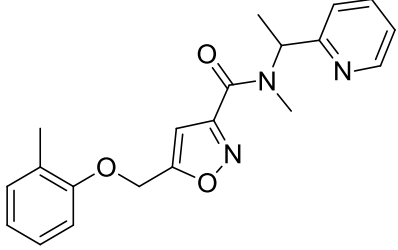
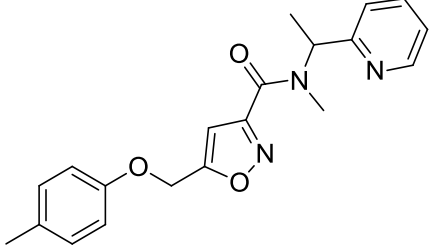
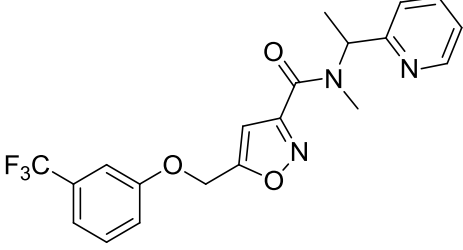


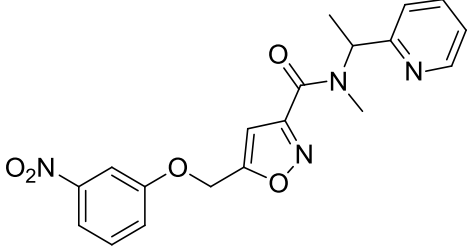
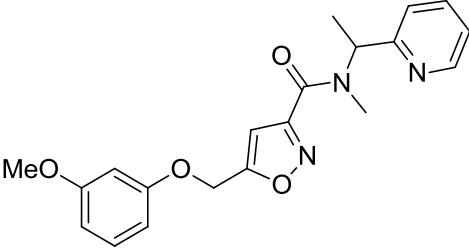
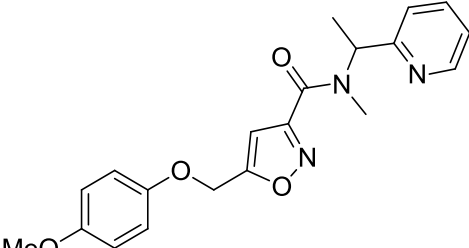
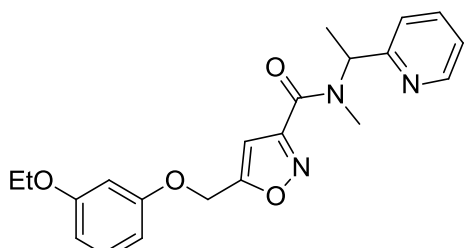
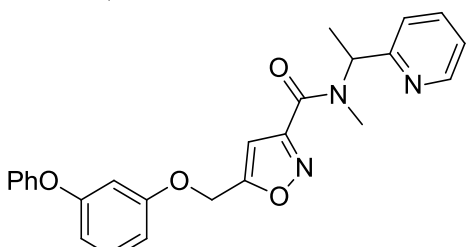
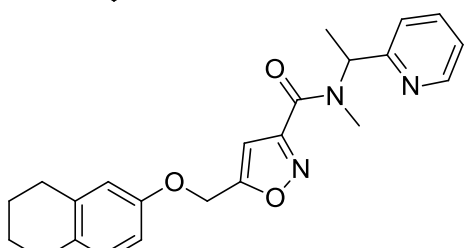
Figure 6.4. Comparison of single point (10 μM) screen results of the aryl ether library, compounds **6.19-6.41**. Ca^{2+} mobilization was used to obtain %ACh_{Max} values for each compound in the presence of a fixed submaximal ($\sim\text{EC}_{80}$) concentration of ACh. Data represent the mean \pm S.E.M. of at least 3 replicate experiments with similar results.

Table 6.2. Structures for aryl ether analogs **6.19-6.41** and associated inhibitory activity data from the single point (10 μ M) screen at hM₅. Ca²⁺ mobilization responses for each compound are reported as a percentage of the maximum ACh response. VU number denotes the compound identifier assigned by Vanderbilt University. Data represent the mean of at least 3 replicate experiments with similar results.

Structure	Cmpd #	VU #	hM ₅ %ACh _{Max}
	6.19	VU0483374	80.4
	6.20	VU0484029	75.0
	6.21	VU0483913	69.3
	6.22	VU0485567	83.1
	6.23	VU0485666	75.5

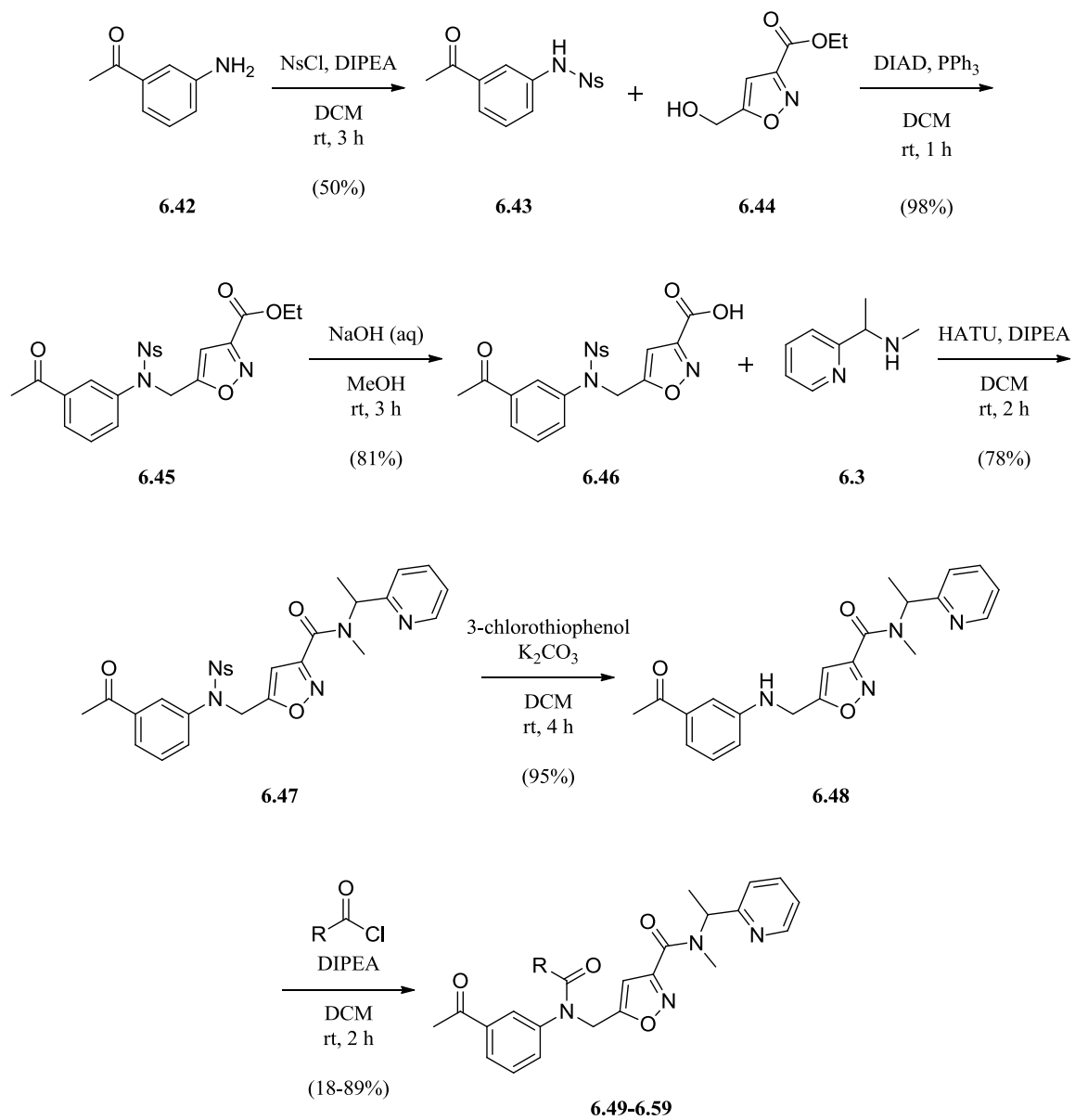
	6.24	VU0483387	67.3
	6.25	VU0485568	76.1
	6.26	VU0483513	83.7
	6.27	VU0483517	77.1
	6.28	VU0483510	82.2
	6.29	VU0483482	85.3

	6.30	VU0483421	77.2
	6.31	VU0483432	84.2
	6.32	VU0483509	71.7
	6.33	VU0483467	79.9
	6.34	VU0483385	78.5
	6.35	VU0483375	84.1

	6.36	VU0483481	73.7
	6.37	VU0483438	79.8
	6.38	VU0483386	82.8
	6.39	VU0483429	79.2
	6.40	VU0483376	83.1
	6.41	VU0483430	79.0

Concurrent with the aryl ether library, we constructed a similar library in which the ether linker was replaced with a secondary amine, or tertiary amide congeners. Beginning from the aniline **6.42**, nosyl protection of the amine and a subsequent Mitsunobu reaction with alcohol **6.44** furnished ester **6.45**. The ester was saponified to acid **6.46** and a HATU-mediated amide coupling with secondary amine **6.3** furnished the nosyl-protected amine linker analog **6.47**. Deprotection of the amine with 3-chlorothiophenol provided the amine linker analog **6.48**. Finally, acylation with a library of 11 acyl chlorides furnished analogs **6.49-6.59** (Scheme 6.4).

Disappointingly, all tertiary amide congeners as well as the nosyl protected intermediate **6.47** led to complete loss of hM₅ inhibitory activity in single point (10 μM) Ca²⁺ mobilization assays at hM₅ (Figure 6.5, Table 6.3). The secondary amine linker analog **6.48** displayed promising activity in the single point assay (%ACh_{Min} at 10 μM = 21.4); however, further investigation in a full CRC Ca²⁺ mobilization assays at human and rat M₅ revealed it to be only weakly active (hM₅ IC₅₀ >10 μM, rM₅ IC₅₀ >10 μM).



Scheme 6.4. Synthesis of amine and amide linker library analogs **6.47-6.59**. Syntheses performed by M. Kokubo

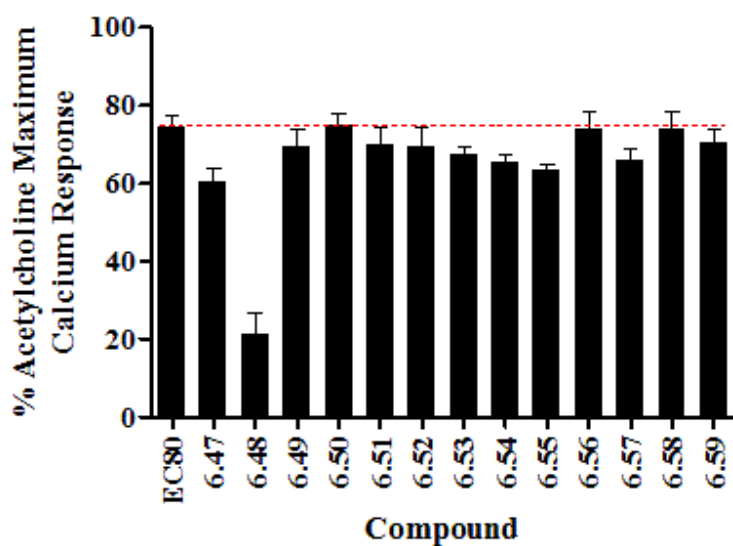
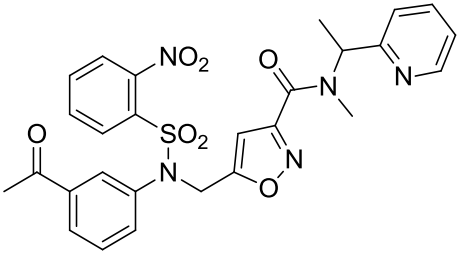
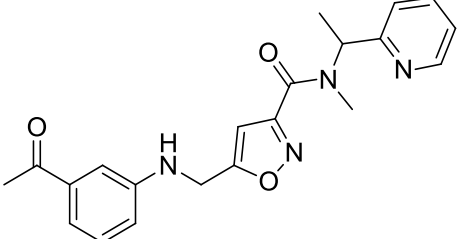
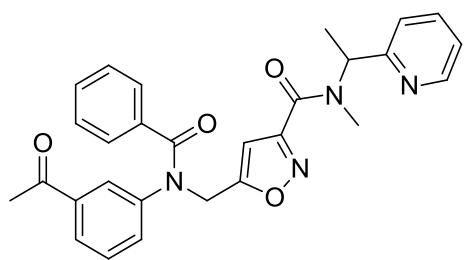
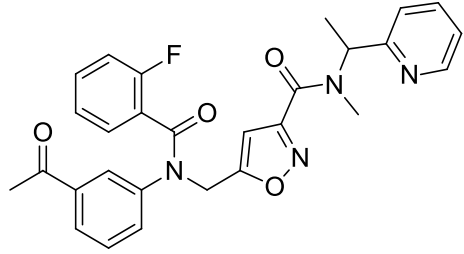
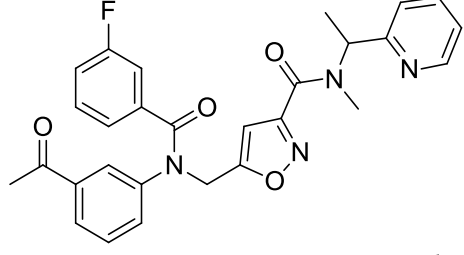
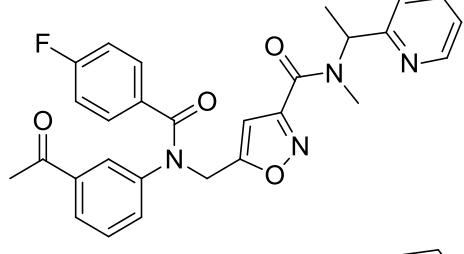
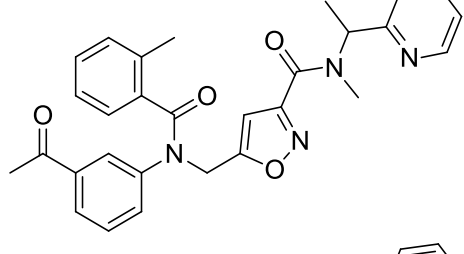
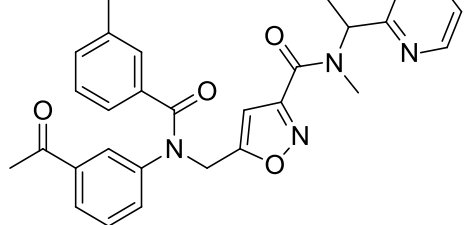
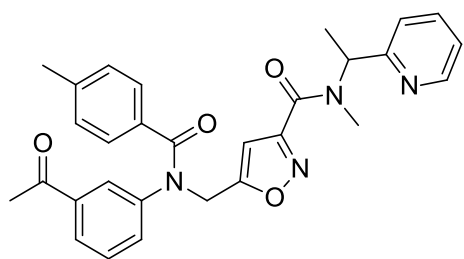
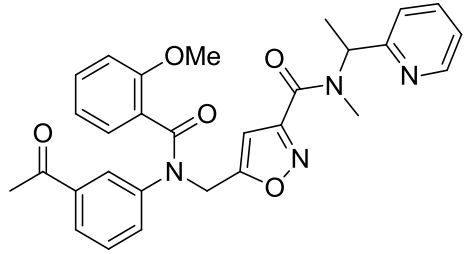
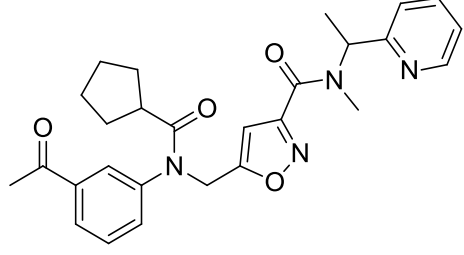
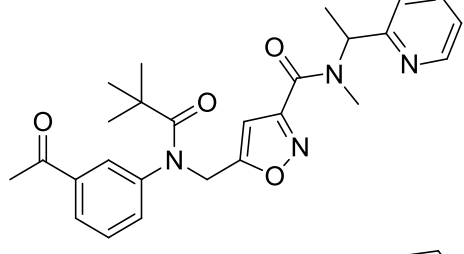
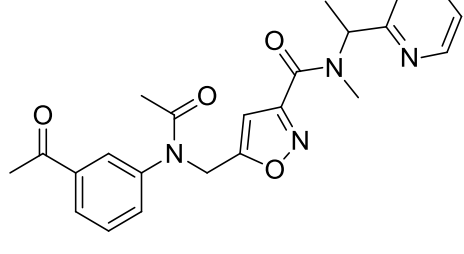


Figure 6.5. Comparison of single point (10 μM) screen results of the amine and amide linker library, analogs **6.47-6.59**. Ca^{2+} mobilization was used to obtain $\%ACh_{\text{Max}}$ values for each compound in the presence of a fixed submaximal ($\sim\text{EC}_{80}$) concentration of ACh. Data represent the mean \pm S.E.M. of at least 3 replicate experiments with similar results.

Table 6.3. Structures for amine and amide linker analogs **6.47-6.59** and associated inhibitory activity data from the single point (10 μM) screen at hM_5 . Ca^{2+} mobilization responses for each compound are reported as a percentage of the maximum ACh response. VU number denotes the compound identifier assigned by Vanderbilt University. Data represent the mean of at least 3 replicate experiments with similar results.

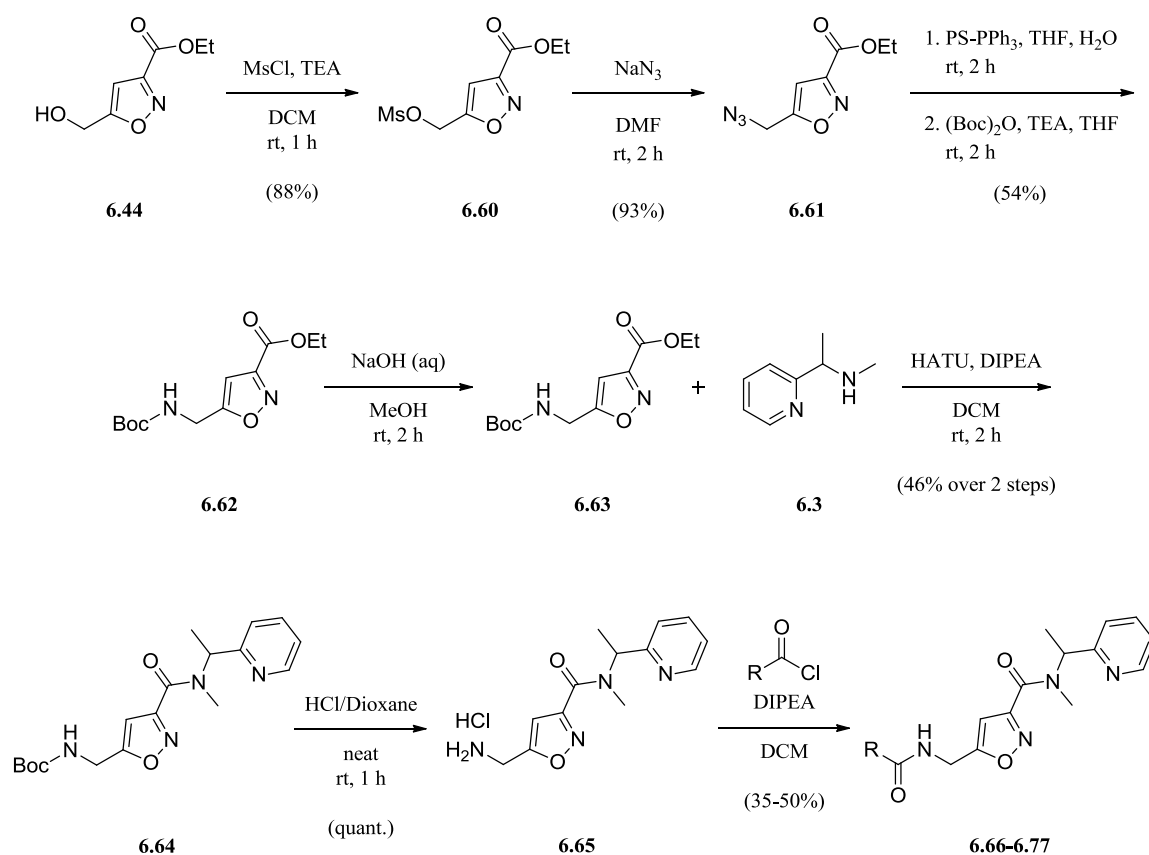
Structure	Cmpd #	VU #	hM_5 $\%ACh_{\text{Max}}$
	6.47	VU0486654	60.6
	6.48	VU0486512	21.4

	6.49	VU0486435	69.6
	6.50	VU0486433	74.8
	6.51	VU0486598	70.0
	6.52	VU0486653	69.3
	6.53	VU0486539	67.3
	6.54	VU0486514	65.5

	6.55	VU0486572	63.5
	6.56	VU0486599	73.8
	6.57	VU0486624	66.0
	6.58	VU0486597	73.9
	6.59	VU0486434	70.4

The final library exploring the SAR in the western aryl ether region tested the replacement of the ether linker with a secondary amide moiety. Alcohol **6.44** was protected with mesyl chloride to provide the mesylate **6.60**. Treatment with NaN_3 furnished azide **6.61** which was reduced to the amine under modified Staudinger

conditions. The amine was subsequently protected with Boc anhydride to furnish ester **6.62**. The ester was saponified and the resulting acid **6.63** was coupled to secondary amine **6.3** under HATU-mediated conditions to provide **6.64**. Removal of the Boc protecting group was accomplished under anhydrous HCl conditions to provide HCl salt **6.65**. Finally, **6.65** was acylated with a library of 12 acyl chlorides to furnish analogs **6.66-6.77** (Scheme 6.5, Table 6.4). Once again, when tested in single point (10 μM) Ca^{2+} mobilization assays at hM_5 , the library revealed itself to be completely devoid of inhibitory activity (Figure 6.6, Table 6.4).



Scheme 6.5. Synthesis of secondary amide linker library analogs **6.66-6.77**. Syntheses performed by M. Kokubo

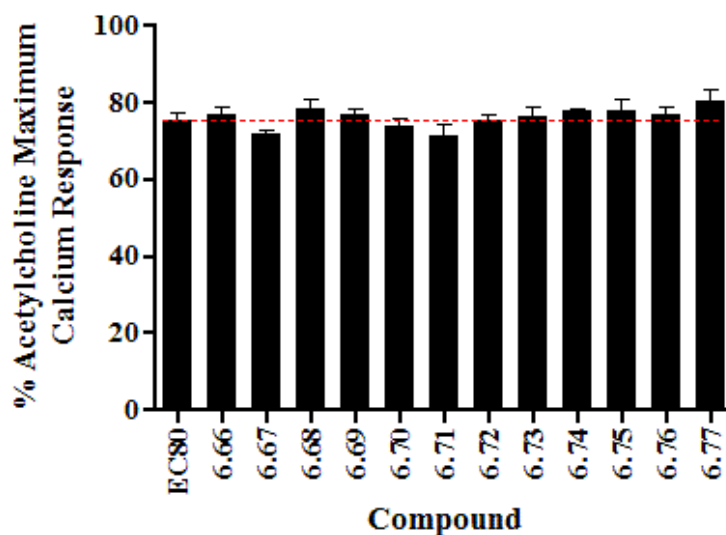
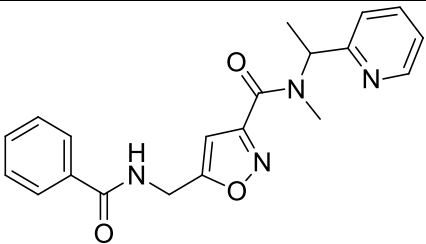
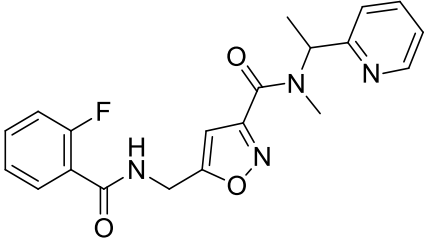
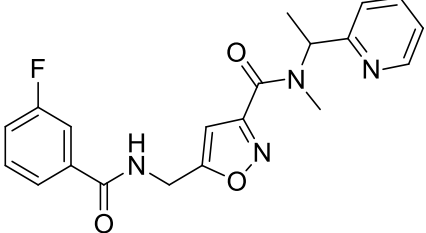
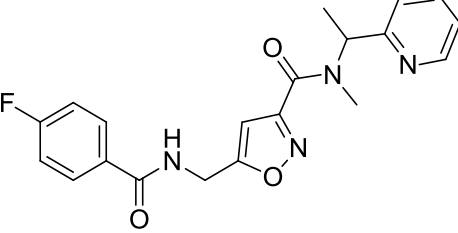
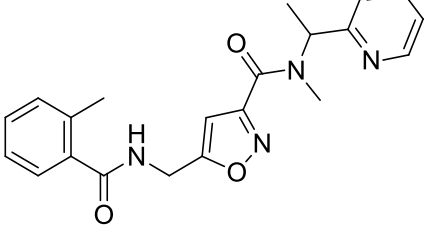
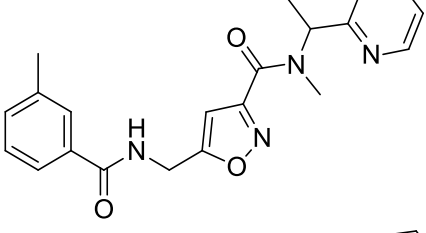
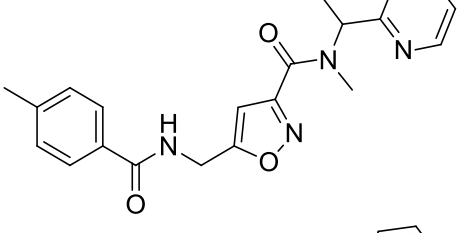
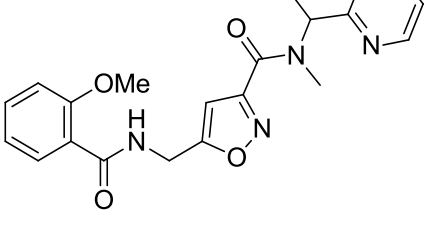
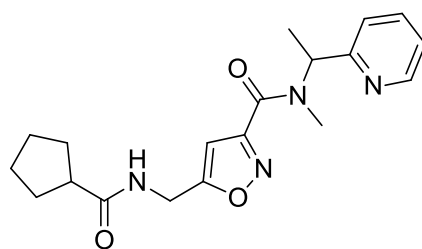
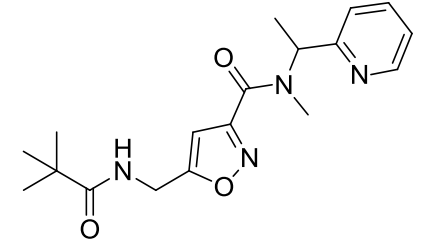
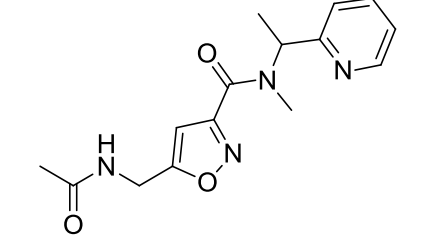
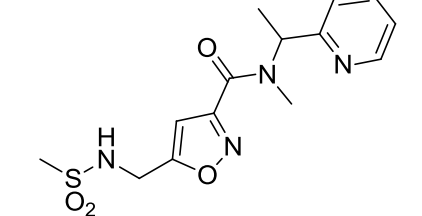


Figure 6.6. Comparison of single point (10 μM) screen results of the secondary amide linker library, analogs **6.66-6.77**. Ca^{2+} mobilization was used to obtain $\%ACh_{\text{Max}}$ values for each compound in the presence of a fixed submaximal ($\sim\text{EC}_{80}$) concentration of ACh. Data represent the mean \pm S.E.M. of at least 3 replicate experiments with similar results.

Table 6.4. Structures for secondary amide linker analogs **6.66-6.77** and associated inhibitory activity data from the single point (10 μM) screen at hM_5 . Ca^{2+} mobilization responses for each compound are reported as a percentage of the maximum ACh response. VU number denotes the compound identifier assigned by Vanderbilt University. Data represent the mean of at least 3 replicate experiments with similar results.

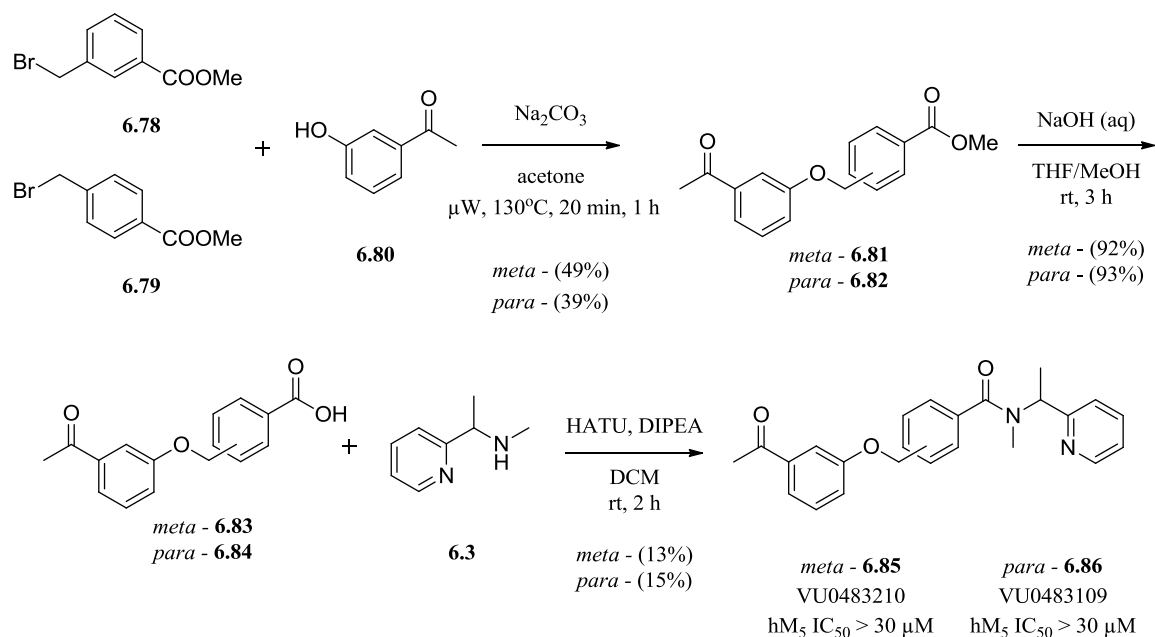
Structure	Cmpd #	VU #	hM_5 $\%ACh_{\text{Max}}$
	6.66	VU0486671	76.7
	6.67	VU0486884	71.8

	6.68	VU0486747	78.2
	6.69	VU0486811	77.0
	6.70	VU0486948	73.8
	6.71	VU0486735	71.5
	6.72	VU0486808	75.1
	6.73	VU0486810	76.4

	6.74	VU0486681	77.7
	6.75	VU0486857	77.8
	6.76	VU0486736	76.8
	6.77	VU0486675	80.4

Exploration of isoxazole core region SAR

Faced with intractable SAR in both the amide and aryl ether regions of the chemical scaffold, we turned our focus to the remaining unexplored region, the isoxazole core. Discouraged by failure of our larger libraries to reveal tractable SAR, we chose to synthesize only a couple of test analogs for the core region. **Scheme 6.6** details the synthesis of benzyl ring replacements for the isoxazole core, with regioisomers in the *meta*- (**6.85**) and *para*- (**6.86**) positions. Upon testing in full CRC Ca²⁺ mobilization assays at hM₅, both analogs proved to be inactive (hM₅ IC₅₀ >30 μM).



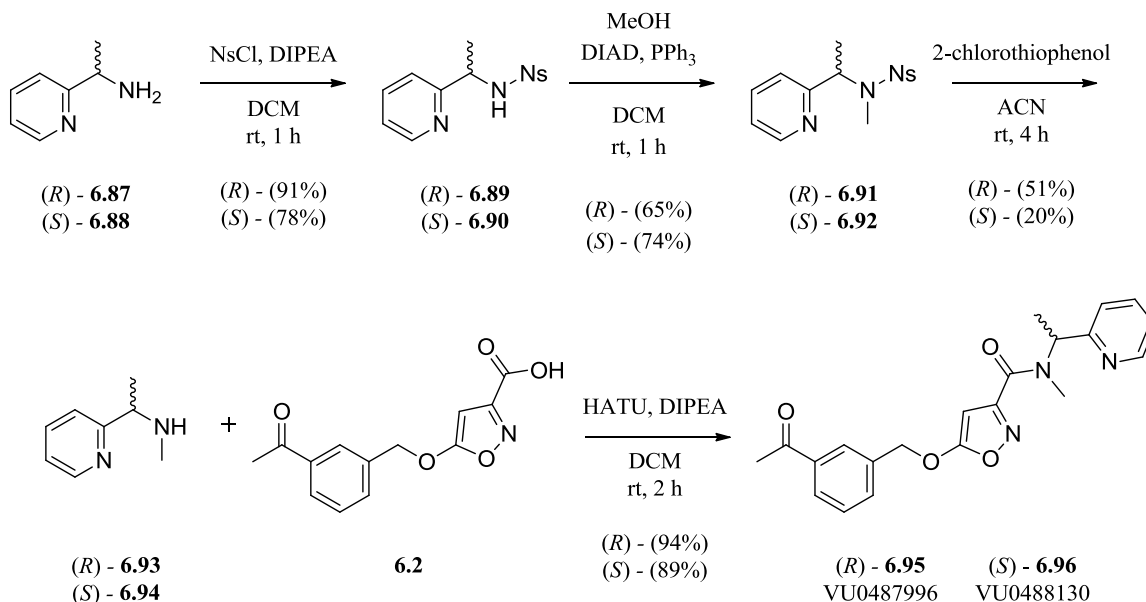
Scheme 6.6. Synthesis of core substitution analogs **6.85** (VU0483210) and **6.86** (VU0483109). Ca^{2+} mobilization assays in hM_5 cells were used to obtain CRCs of compounds **6.85** and **6.86** in the presence of a fixed submaximal ($\sim\text{EC}_{80}$) concentration of ACh. Data represent the mean of at least 3 independent experiments with similar results. Syntheses performed by M. Kokubo.

Synthesis of VU0480131 enantiomers

Having studied a diverse range of analogs designed to test structural modifications throughout the orthosteric antagonist chemical scaffold, we found no tractable SAR. All analogs tested in single point or CRC Ca^{2+} mobilization assays demonstrated little or no inhibitory activity at M_5 , and none showed activity remotely equal to HTS lead **6.1**. Thus, we elected to proceed by synthesizing the pure enantiomers of **6.1** in search of the active enantiomer.

Beginning from the commercial (*S*)- or (*R*)-1-(pyridine-2-yl)ethanamine (*R*)-**6.87** and (*S*)-**6.88**, treatment with N_3Cl provided protected amines (*R*)-**6.89** and (*S*)-**6.90**. The *N*-methyl moiety was installed via a Mitsunobu reaction with methanol to furnish the

tertiary sulfonamides (*R*)-**6.91** and (*S*)-**6.92**. Next, nosyl deprotection with 3-chlorothiophenol resulted in the chiral secondary amines (*R*)-**6.93** and (*S*)-**6.94**. Finally, the amines were coupled to acid **6.2** under HATU conditions to afford the single enantiomers of **6.1**, (*R*)-**6.95** (VU0487996) and (*S*)-**6.96** (VU0488130; **Scheme 6.7**).



Scheme 6.7. Synthesis of single enantiomers of HTS lead **6.1**, analogs (*R*) - **6.95** (VU0487996) and (*S*) - **6.96** (VU0488130). Syntheses performed by M. Kokubo

When screened in full CRC Ca²⁺ mobilization assays at hM₅, enantiospecific inhibition was observed, with (*S*)-**6.96** (VU0488130) exhibiting sub-micromolar potency (hM₅ IC₅₀ = 450 nM) while (*R*)-**6.95** (VU0487996) displayed no activity (hM₅ IC₅₀ >10 μM; **Figure 6.7**).

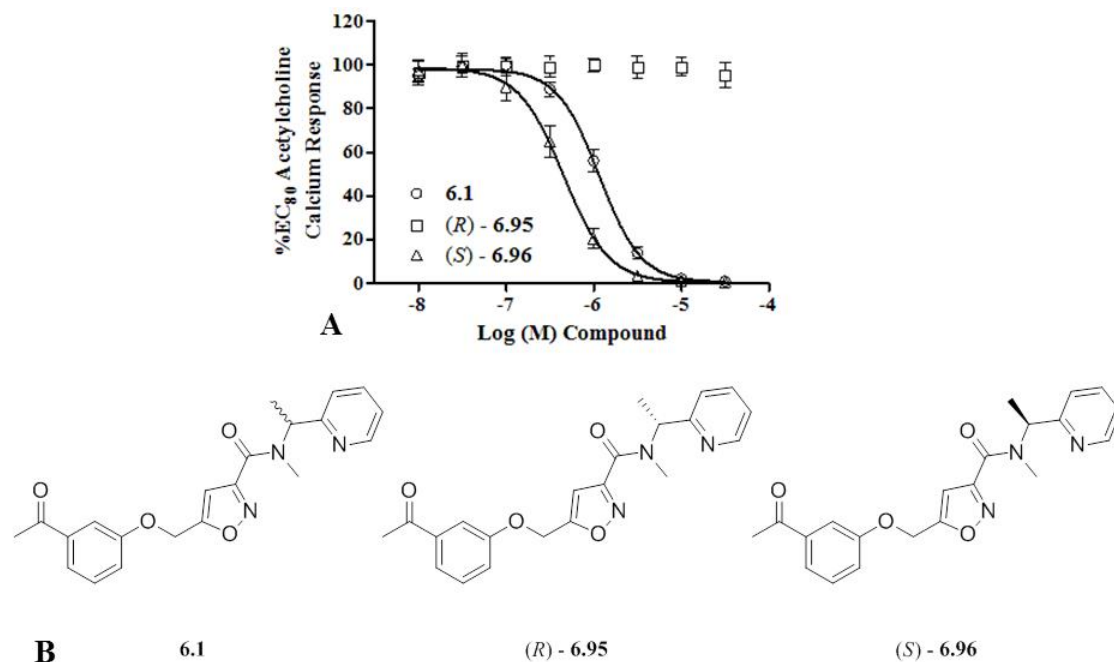


Figure 6.7. A) CRCs comparing activities of HTS lead **6.1** (VU0480131), **6.95** (VU0487996), and **6.96** (VU0488130). Ca^{2+} mobilization assays with hM_5 cells were used to obtain CRCs of compounds **6.1** (hM_5 IC_{50} = 1.1 μM), **6.95** (hM_5 IC_{50} > 30 μM), and **6.96** (hM_5 IC_{50} = 0.45 μM) in the presence of a fixed submaximal ($\sim\text{EC}_{80}$) concentration of ACh. Data represent the mean \pm S.E.M. of at least 3 independent experiments with similar results. B) Structures of **6.1**, **6.95**, and **6.96**.

***In vitro* pharmacological characterization of M_5 orthosteric antagonist VU0488130**

Characterization of mAChR subtype selectivity of VU0488130

Having finally arrived at a compound with greater potency than the original HTS hit **6.1**, we were interested to see if **6.96** (VU0488130) maintained selectivity for human M_5 . Furthermore, because an M_5 -selective orthosteric antagonist would be a unique chemical tool in the study of M_5 in *in vivo* studies, we also surveyed the compound's selectivity in rat mAChR isoforms. Thus a full rat and human mAChR subtype selectivity panel was run in CRC Ca^{2+} mobilization assays (**Figure 6.8**). The selectivity panel showed that **6.96** possesses exceptional selectivity for M_5 in both human and rat mAChR

isoforms; however, a ~4-fold reduction in potency was noted at rat M₅ (hM₅ IC₅₀ = 0.45 μM, hM₁-hM₄ IC₅₀ >30 μM; rM₅ IC₅₀ = 1.7 μM, rM₁-rM₄ IC₅₀ >30 μM). Based on the potency and M₅-selectivity of **6.96**, it was approved as an MLPCN probe and given the identifier ML381.

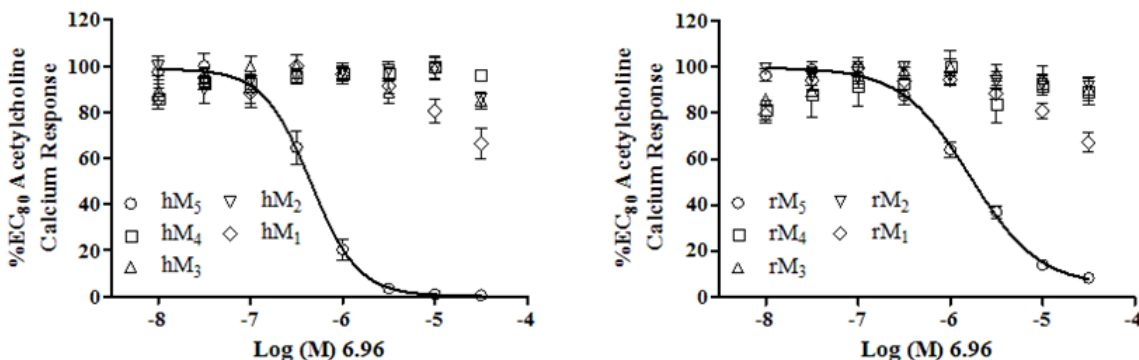


Figure 6.8. Potency and selectivity of compound **6.96** (VU0488130, ML381) at all human and rat mAChR subtypes. Ca²⁺ mobilization assays with hM₁-hM₅ cells and with rM₁-rM₅ (M₂ and M₄ co-expressing G_{α_{q15}}) cells were used to obtain CRCs of **6.96** in the presence of a fixed submaximal (~EC₈₀) concentration of ACh (IC₅₀ values: hM₅ IC₅₀ = 0.45 μM, hM₁-hM₄ IC₅₀ >30 μM, rM₅ IC₅₀ = 1.7 μM, rM₁-rM₄ IC₅₀ >30 μM). Data represent the mean ± S.E.M. of at least 3 independent experiments with similar results.

Confirmation of the orthosteric mechanism of VU0488130

As with the original HTS lead **6.1**, we desired to confirm the mechanism of action of **6.96** via competition binding with the radioligand [³H]-NMS in hM₅ membrane preparations. As with the parent **6.1**, **6.96** appeared to act with an orthosteric mode of action, displacing [³H]-NMS in a concentration-dependent manner (K_i = 0.34 μM; **Figure 6.9**).

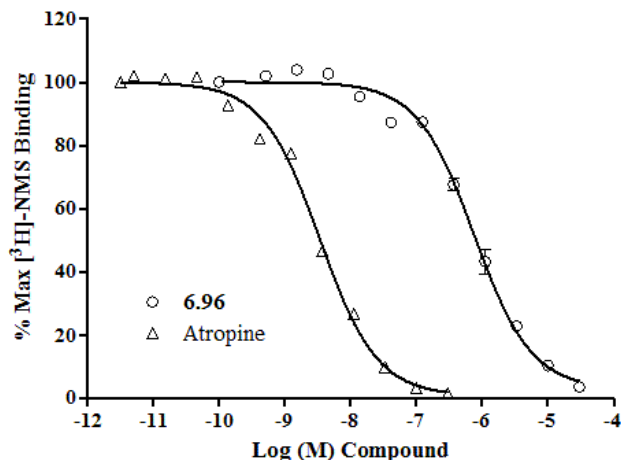


Figure 6.9. [³H]-NMS competition binding assay with **6.96** (VU0488130, ML381) in an hM₅ membrane preparation. [³H]-NMS and a CRC of either atropine (control) or **6.96** were allowed to equilibrate for 3 hours in the hM₅ membrane preparation before filtration and scintillation counting (K_i values: atropine K_i = 1.5 nM, **6.96** K_i = 0.34 μM). Data represent the mean ± S.E.M. of at least 3 independent experiments with similar results.

Ancillary pharmacology of VU0488130

To gain a general impression of off-target binding outside of the mAChRs, **6.96** was entered into a commercial radioligand competition binding screen of 67 GPCRs, ion channels, and transporters (**Table 6.5**). Significant binding was seen only at the 5-HT_{2B} receptor (50% inhibition). Thus, in addition to selectivity versus the mAChR subtypes, **6.96** also displays relatively clean ancillary pharmacology with respect to binding against a diverse array of discrete molecular targets.

Table 6.5. Ancillary/off-target competition binding screen results for **6.96** (VU0488130, ML381). **6.96** was dosed at 10 μM for single point competition binding assays. Targets displaying significant binding (≥50% at 10 μM) are highlighted. Data represent the mean of 2 independent experiments with similar results. Studies performed by Eurofins Panlabs, Inc.

Target/Protein	Species	% Inhibition
Adenosine A ₁	Human	-4
Adenosine A _{2A}	Human	-2
Adenosine A ₃	Human	12

Adrenergic α_{1A}	Rat	-10
Adrenergic α_{1B}	Rat	-18
Adrenergic α_{1D}	Human	12
Adrenergic α_{2A}	Human	5
Adrenergic β_1	Human	-3
Adrenergic β_2	Human	-16
Androgen (Testosterone) AR	Rat	2
Bradykinin B ₁	Human	-1
Bradykinin B ₂	Human	-1
Calcium Channel L-Type, Benzothiazepine	Rat	11
Calcium Channel L-Type, Dihydropyridine	Rat	-9
Calcium Channel N-Type	Rat	-4
Cannabinoid CB ₁	Human	21
Dopamine D ₁	Human	13
Dopamine D _{2S}	Human	2
Dopamine D ₃	Human	6
Dopamine D _{4,2}	Human	3
Endothelin ET _A	Human	14
Endothelin ET _B	Human	-1
Epidermal Growth Factor (EGF)	Human	3
Estrogen ER α	Human	-9
GABA _A , Flunitrazepam, Central	Rat	30
GABA _A , Muscimol, Central	Rat	2
GABA _{B1A}	Human	13
Glucocorticoid	Human	-6
Glutamate, Kainate	Rat	11
Glutamate, NMDA, Agonism	Rat	-9
Glutamate, NMDA, Glycine	Rat	-2
Glutamate, NMDA, Phencyclidine	Rat	4
Histamine H ₁	Human	-5
Histamine H ₂	Human	6
Histamine H ₃	Human	2
Imidazoline I ₂ , Central	Rat	4
Interleukin IL-1	Mouse	8
Leukotriene, Cysteinyl CysLT ₁	Human	2
Melatonin MT ₁	Human	3
Muscarinic M ₁	Human	0
Muscarinic M ₂	Human	12
Muscarinic M ₃	Human	13
Neuropeptide Y Y ₁	Human	-2
Neuropeptide Y Y ₂	Human	-2
Nicotinic Acetylcholine	Human	11
Nicotinic Acetylcholine α_1 , Bungarotoxin	Human	1
Opiate δ_1 (OP1, DOP)	Human	1
Opiate κ (OP2, KOP)	Human	8
Opiate μ (OP3, MOP)	Human	1

Phorbol Ester	Mouse	-20
Platelet Activating Factor (PAF)	Human	43
Potassium Channel [K _{ATP}]	Human	4
Potassium Channel hERG	Human	6
Prostanoid EP ₄	Human	28
Purinergic P2X	Rabbit	16
Purinergic P2Y	Rat	18
Rolipram	Rat	-3
Serotonin (5-HT _{1A})	Human	13
Serotonin (5-HT _{2B})	Human	50
Serotonin (5-HT ₃)	Human	-6
Sigma σ_1	Human	6
Sodium Channel, Site 2	Rat	6
Tachykinin NK ₁	Human	4
Thyroid Hormone	Rat	-1
Transporter, Dopamine (DAT)	Human	2
Transporter, GABA	Rat	-2
Transporter, Norepinephrine (NET)	Human	-2
Transporter, Serotonin (SERT)	Human	6

In vitro and *in vivo* DMPK characterization of

M₅ orthosteric antagonist VU0488130

In vitro DMPK characterization of VU0488130

Enthused by the excellent potency and selectivity profile of the M₅ orthosteric antagonist **6.96** (VU0488130, ML381), we were eager to characterize the compound's DMPK profile in order to assess its fitness for future *in vivo* studies of M₅ in the CNS. We entered **6.96** into an in-house *in vitro* DMPK panel which included plasma protein binding, rat brain homogenate binding, rat and human microsomal stability, and CYP inhibition. The results of these studies are summarized in **Table 6.6**.

Table 6.6. *In vitro* DMPK data for **6.96** (VU0488130) in multiple species. Studies performed by T. Bridges.

Parameter	Rat	Human
hepatic microsome CL_{int} (mL/min/kg)	772	92.7
predicted CL_{hep} (mL/min/kg)	64.2	17.1
$f_{u,plasma}, f_{u,brain}$	0.584, 0.136	0.111, ---
CYP inhibition (P450, IC_{50} , μ M)	---	3A4, 2D6, 1A2: >30; 2C9: 6.3

Compound **6.96** displayed a relatively clean CYP inhibition profile, with 2C9 representing the primary liability. In microsomal stability studies **6.96** exhibited high intrinsic clearance, with predicted hepatic clearance values near the hepatic blood flow rate in each species tested. Curiously, the results of the protein binding studies showed that **6.96** exhibits high $f_{u,brain}$ in rat and exceptionally high $f_{u,plasma}$ values in rat and human. These unusually high $f_{u,plasma}$ values forced us to question if the compound might be unstable in the plasma of the species tested. To test the plasma stability of the compound we monitored the percent of parent remaining after the compound was incubated at 37 °C in rat and human plasma for a total of four hours. This experiment revealed **6.96** is markedly unstable in rat plasma and a moderately unstable in human plasma, ultimately precluding our ability to acquire an accurate value of $f_{u,plasma}$.

In addition to our standard *in vitro* DMPK profile studies, we also submitted **6.96** to an *in vitro*, bidirectional transwell assay employing MDCK-MDR1 cells in order to assess efflux liabilities of **6.96** at the BBB. When dosed at 5 μ M, **6.96** exhibited an ER of 1.6, suggesting an absence of P-gp-mediated active efflux liabilities at the BBB.

M₅ antagonist VU0488140 metabolite identification

Given the pronounced instability of **6.96** in both microsomes and plasma, we sought to determine the relevant biotransformation pathway(s) at work in hopes that further medicinal chemistry optimization efforts may improve the stability of the compound. Metabolite identification experiments were carried out using rat and human hepatic microsomes and plasma (**Figure 6.10**). These analyses revealed hydrolytic cleavage of the amide to (**6.97**) be a primary pathway of biotransformation in both plasma and microsomes. Additionally, an array of NADPH-dependent mono-oxidation pathways were also identified in rat and human microsomes, including *O*-dearylation (**6.98**), phenyl hydroxylation (**6.99**), keto-reduction (**6.100**), and *N*-dealkylations at the amide (**6.101, 6.102; Figure 6.10**).

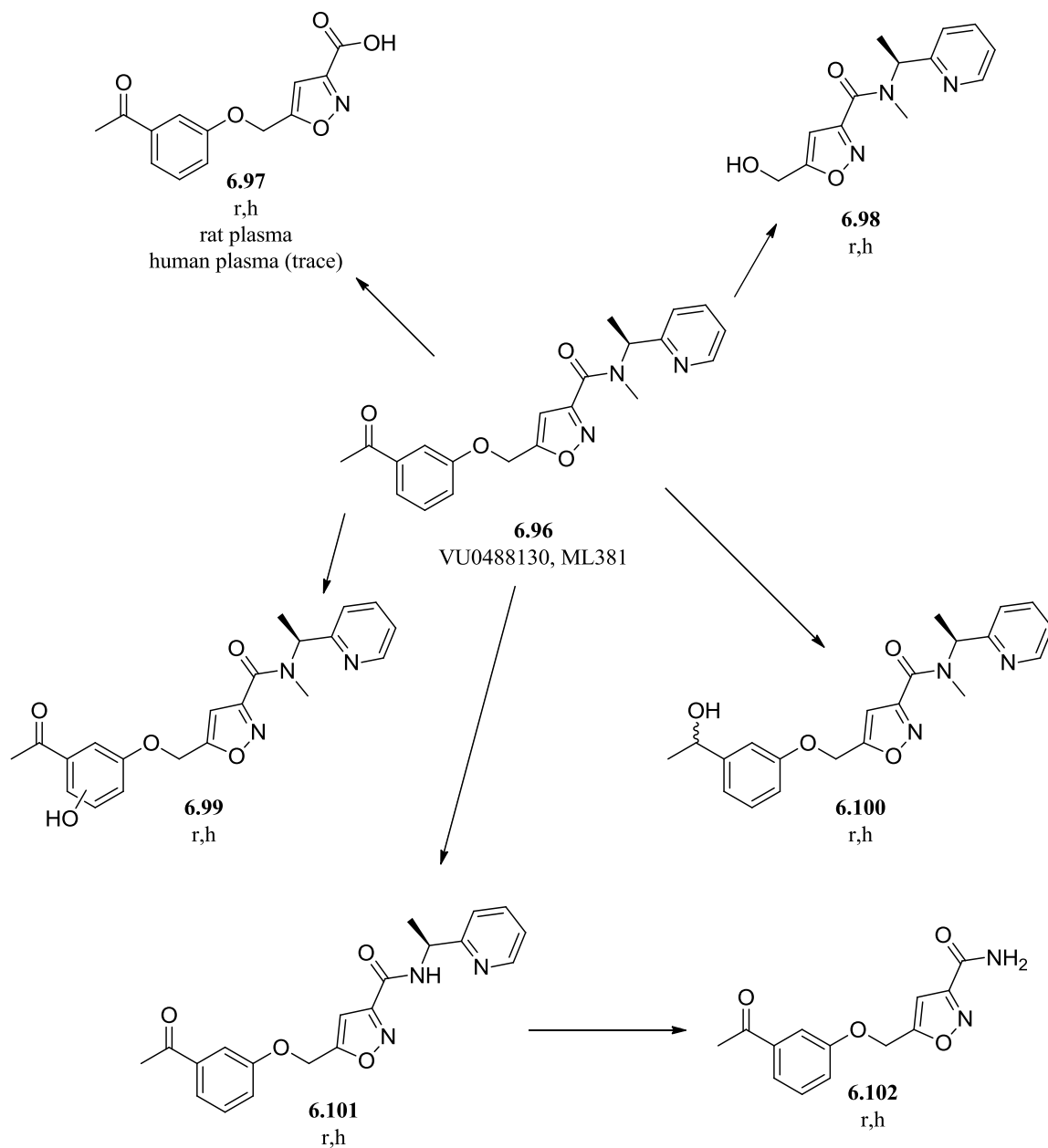


Figure 6.10. Metabolite identification results for **6.96** (VU0488130, ML381) in rat and human. Multiple metabolites were identified (M1-M6), stemming from six major routes of metabolism. Metabolite identification studies performed by T. Bridges.

In vivo DMPK characterization of VU0488130

Although **6.96** had demonstrated itself to be extremely unstable to both plasma and microsomes, we desired to gauge how well the compound might distribute to the CNS in an *in vivo* administration. Thus **6.96** was dosed in a single IV injection (0.2

mg/kg) to male Sprague-Dawley rats ($n = 2$). Whole brains and plasma were collected at a single time point 15 minutes later and compound distribution was quantitated. The study revealed a $K_p = 0.58$, suggesting moderate distribution to the CNS. Calculation of $K_{p,uu}$ was precluded by our aforementioned inability to obtain accurate $f_{u,plasma}$ values.

Summary and Future Directions

This project began with the goals of exploring the SAR and improving the potency of the M_5 -selective orthosteric antagonist HTS lead **6.1** (VU0480131). In the course of exploring the chemical space of this series we synthesized over 60 novel analogs that focused on structural variation of the amide, pyridyl, isoxazole, and aryl ether regions of the molecule. Unfortunately we found SAR to be extremely delicate, with even the most subtle modifications leading to complete loss of inhibitory activity at M_5 . HTS lead **6.1** was ultimately found to possess enantiospecific inhibition, with all activity being found in the (*S*)-enantiomer, compound **6.96** (VU0488130, ML381). **6.96** was subsequently shown to be the most potent and selective M_5 orthosteric antagonist reported to date (**Figure 6.11**). Moreover, **6.96** possesses an overall favorable DMPK profile with moderate CNS penetrance; however, the compound's extreme instability in hepatic microsomes and plasma limit its *in vivo* utility.

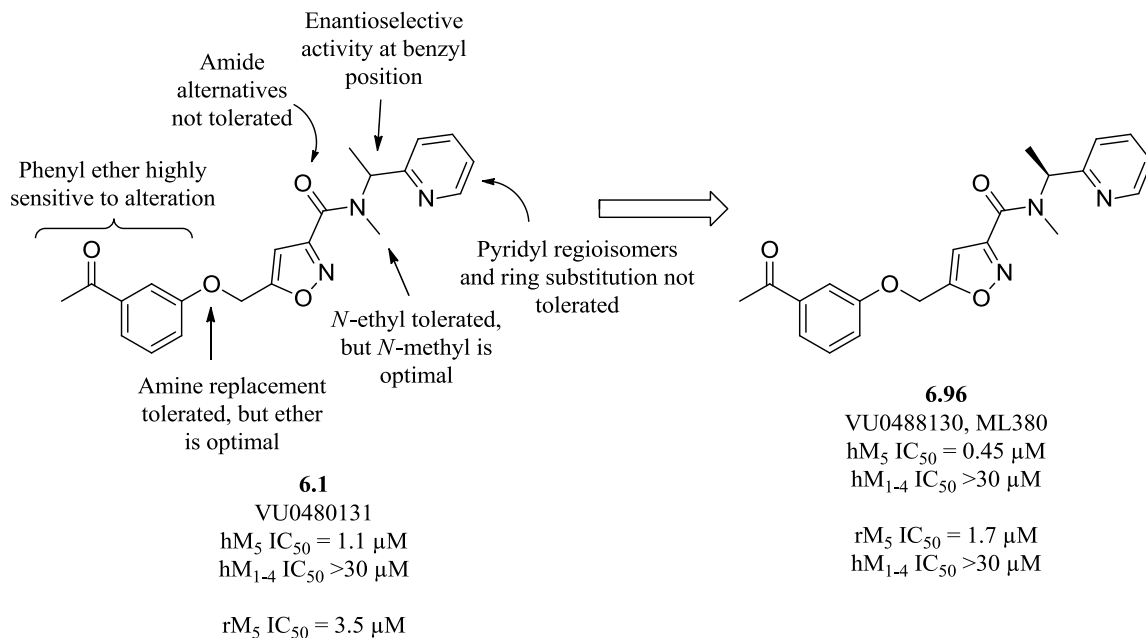


Figure 6.11. Summary and comparison of the structure, potency, and SAR surrounding the M₅ antagonist HTS lead **6.1** (VU0480131) that led to the discovery of the first sub-micromolar, M₅-selective orthosteric antagonist **6.96** (VU0488130, ML381).

Through metabolite identification studies we traced the instability of **6.96** to multiple metabolically labile spots on the chemical scaffold. Due to the combination of compound **6.96**'s delicate SAR and the wide-ranging nature of its metabolic instability, further chemical optimization with the goal of bolstering metabolically labile regions while maintaining potency is an extremely challenging task. Out of all of the chemical regions of this scaffold, the core isoxazole remains the least explored and may present the best opportunity for beneficial modifications.

Although unsuited for *in vivo* systemic dosing, **6.96** is an extremely interesting chemical probe for the study of M₅. That **6.96** possesses an orthosteric mechanism of action while still maintaining M₅-selectivity makes it an interesting tool for structural biology studies with M₅ probing the source of its selectivity. That is, structural biology

studies could reveal if the selectivity of **6.96** for M₅ is purely orthosteric or if **6.96** interacts with both the allosteric and orthosteric sites in a bitopic fashion. From a pharmacological standpoint, inhibitors of M₅ are desirable tool compounds for the study of M₅ on the dopaminergic neurons of the midbrain (Chapter I) and orthosteric antagonist **6.96** could be extremely valuable in *in vitro* pharmacology and electrophysiology experiments aiming to study the effect of M₅ inhibition in the CNS.

REFERENCES

- (1) Smythies, J. Section I. The Cholinergic System. *Int. Rev. Neurobiol.* **2005**, *64*, 1–122.
- (2) Amenta, F.; Tayebati, S. K. Pathways of Acetylcholine Synthesis, Transport and Release as Targets for Treatment of Adult-Onset Cognitive Dysfunction. *Curr. Med. Chem.* **2008**, *15*, 488–498.
- (3) Woolf, N. J.; Butcher, L. L. Cholinergic Systems Mediate Action from Movement to Higher Consciousness. *Behav. Brain Res.* **2011**, *221*, 488–498.
- (4) Schmiedeberg, O.; Koppe, R. *Das Muscarin, Das Giftige Alkaloid Des Fliegenpilzes*; Vogel: Leipzig, 1869.
- (5) Van der Zee, E. A.; Luiten, P. G. Muscarinic Acetylcholine Receptors in the Hippocampus, Neocortex and Amygdala: A Review of Immunocytochemical Localization in Relation to Learning and Memory. *Prog. Neurobiol.* **1999**, *58*, 409–471.
- (6) Schmiedeberg, O.; Harnack, E. Über Die Synthese Des Muscarins Und Über Muscarinartig Wirkende Ammoniumbasen. *Arch. für Exp. Pathol. und Pharmakologie* **1877**, *6*, 101–112.
- (7) Toadstool <http://www.publicdomainpictures.net/view-image.php?image=12241&picture=toadstool> (accessed Jun 13, 2014).
- (8) Dale, H. The Action of Certain Esters and Ethers of Choline, and Their Relation to Muscarine. *J. Pharmacol. Exp. Ther.* **1914**, *6*, 147–190.
- (9) Ewins, A. J. Acetylcholine, a New Active Principle of Ergot. *Biochem. J.* **1914**, *8*, 44–49.
- (10) Loewi, O. Über Humorale Übertragbarkeit Der Herznervenwirkung. *Pflüger's Arch. für die gesamte Physiol. des Menschen und der Tiere* **1924**, *204*, 629–640.
- (11) Hammer, R.; Berrie, C. P.; Birdsall, N. J.; Burgen, A. S.; Hulme, E. C. Pirenzepine Distinguishes between Different Subclasses of Muscarinic Receptors. *Nature* **1980**, *283*, 90–92.
- (12) Brown, D. A.; Forward, A.; Marsh, S. Antagonist Discrimination between Ganglionic and Ileal Muscarinic Receptors. *Br. J. Pharmacol.* **1980**, *71*, 362–364.
- (13) Hammer, R.; Giachetti, A. Muscarinic Receptor Subtypes: M1 and M2 Biochemical and Functional Characterization. *Life Sci.* **1982**, *31*, 2991–2998.

- (14) Birdsall, N. J. M.; Hulme, E. C. Muscarinic Receptor Subclasses. *Trends Pharmacol. Sci.* **1983**, *4*, 459–463.
- (15) Kubo, T.; Fukuda, K.; Mikami, A.; Maeda, A.; Takahashi, H.; Mishina, M.; Haga, T.; Haga, K.; Ichiyama, A.; Kangawa, K. Cloning, Sequencing and Expression of Complementary DNA Encoding the Muscarinic Acetylcholine Receptor. *Nature* **1986**, *323*, 411–416.
- (16) Kubo, T.; Maeda, a; Sugimoto, K.; Akiba, I.; Mikami, a; Takahashi, H.; Haga, T.; Haga, K.; Ichiyama, a; Kangawa, K. Primary Structure of Porcine Cardiac Muscarinic Acetylcholine Receptor Deduced from the cDNA Sequence. *FEBS Lett.* **1986**, *209*, 367–372.
- (17) Bonner, T. I.; Buckley, N. J.; Young, A. C.; Brann, M. R. Identification of a Family of Muscarinic Acetylcholine Receptor Genes. *Science* **1987**, *237*, 527–532.
- (18) Peralta, E. G.; Ashkenazi, A.; Winslow, J. W.; Smith, D. H.; Ramachandran, J.; Capon, D. J. Distinct Primary Structures, Ligand-Binding Properties and Tissue-Specific Expression of Four Human Muscarinic Acetylcholine Receptors. *EMBO J.* **1987**, *6*, 3923–3929.
- (19) Bonner, T. I.; Young, A. C.; Brann, M. R.; Buckley, N. J. Cloning and Expression of the Human and Rat m5 Muscarinic Acetylcholine Receptor Genes. *Neuron* **1988**, *1*, 403–410.
- (20) Liao, C. F.; Themmen, A. P.; Joho, R.; Barberis, C.; Birnbaumer, M.; Birnbaumer, L. Molecular Cloning and Expression of a Fifth Muscarinic Acetylcholine Receptor. *J. Biol. Chem.* **1989**, *264*, 7328–7337.
- (21) Caulfield, M. P.; Birdsall, N. J. International Union of Pharmacology. XVII. Classification of Muscarinic Acetylcholine Receptors. *Pharmacol. Rev.* **1998**, *50*, 279–290.
- (22) Caulfield, M. P. Muscarinic Receptors--Characterization, Coupling and Function. *Pharmacol. Ther.* **1993**, *58*, 319–379.
- (23) Wess, J. Molecular Biology of Muscarinic Acetylcholine Receptors. *Crit. Rev. Neurobiol.* **1996**, *10*, 69–99.
- (24) Yasuda, R. P.; Ciesla, W.; Flores, L. R.; Wall, S. J.; Li, M.; Satkus, S. A.; Weisstein, J. S.; Spagnola, B. V.; Wolfe, B. B. Development of Antisera Selective for m4 and m5 Muscarinic Cholinergic Receptors: Distribution of m4 and m5 Receptors in Rat Brain. *Mol. Pharmacol.* **1993**, *43*, 149–157.

- (25) Vilaró, M. T.; Palacios, J. M.; Mengod, G. Localization of m5 Muscarinic Receptor mRNA in Rat Brain Examined by in Situ Hybridization Histochemistry. *Neurosci. Lett.* **1990**, *114*, 154–159.
- (26) Weiner, D. M.; Levey, A. I.; Brann, M. R. Expression of Muscarinic Acetylcholine and Dopamine Receptor mRNAs in Rat Basal Ganglia. *Proc. Natl. Acad. Sci. U. S. A.* **1990**, *87*, 7050–7054.
- (27) Foster, D. J.; Gentry, P. R.; Lizardi-Ortiz, J. E.; Bridges, T. M.; Wood, M. R.; Niswender, C. M.; Sulzer, D.; Lindsley, C. W.; Xiang, Z.; Conn, P. J. M5 Receptor Activation Produces Opposing Physiological Outcomes in Dopamine Neurons Depending on the Receptor's Location. *J. Neurosci.* **2014**, *34*, 3253–3262.
- (28) Elhousseiny, A.; Cohen, Z.; Olivier, A.; Stanimirović, D. B.; Hamel, E. Functional Acetylcholine Muscarinic Receptor Subtypes in Human Brain Microcirculation: Identification and Cellular Localization. *J. Cereb. Blood Flow Metab.* **1999**, *19*, 794–802.
- (29) Tayebati, S. K.; Di Tullio, M. A.; Tomassoni, D.; Amenta, F. Localization of the m5 Muscarinic Cholinergic Receptor in Rat Circle of Willis and Pial Arteries. *Neuroscience* **2003**, *122*, 205–211.
- (30) Yamada, M.; Lamping, K. G.; Duttaroy, A.; Zhang, W.; Cui, Y.; Bymaster, F. P.; McKinzie, D. L.; Felder, C. C.; Deng, C. X.; Faraci, F. M.; et al. Cholinergic Dilation of Cerebral Blood Vessels Is Abolished in M(5) Muscarinic Acetylcholine Receptor Knockout Mice. *Proc. Natl. Acad. Sci. U. S. A.* **2001**, *98*, 14096–14101.
- (31) Faraci, F. M.; Sigmund, C. D. Vascular Biology in Genetically Altered Mice : Smaller Vessels, Bigger Insight. *Circ. Res.* **1999**, *85*, 1214–1225.
- (32) Araya, R.; Noguchi, T.; Yuhki, M.; Kitamura, N.; Higuchi, M.; Saido, T. C.; Seki, K.; Itohara, S.; Kawano, M.; Tanemura, K.; et al. Loss of M5 Muscarinic Acetylcholine Receptors Leads to Cerebrovascular and Neuronal Abnormalities and Cognitive Deficits in Mice. *Neurobiol. Dis.* **2006**, *24*, 334–344.
- (33) Forster, G. L.; Blaha, C. D. Laterodorsal Tegmental Stimulation Elicits Dopamine Efflux in the Rat Nucleus Accumbens by Activation of Acetylcholine and Glutamate Receptors in the Ventral Tegmental Area. *Eur. J. Neurosci.* **2000**, *12*, 3596–3604.
- (34) Forster, G. L.; Yeomans, J. S.; Takeuchi, J.; Blaha, C. D. M5 Muscarinic Receptors Are Required for Prolonged Accumbal Dopamine Release after Electrical Stimulation of the Pons in Mice. *J. Neurosci.* **2002**, *22*, RC190.

- (35) Forster, G. L.; Blaha, C. D. Pedunculo-pontine Tegmental Stimulation Evokes Striatal Dopamine Efflux by Activation of Acetylcholine and Glutamate Receptors in the Midbrain and Pons of the Rat. *Eur. J. Neurosci.* **2003**, *17*, 751–762.
- (36) Steidl, S.; Miller, A. D.; Blaha, C. D.; Yeomans, J. S. M5 Muscarinic Receptors Mediate Striatal Dopamine Activation by Ventral Tegmental Morphine and Pedunculo-pontine Stimulation in Mice. *PLoS One* **2011**, *6*, e27538.
- (37) Wise, R. A. Neurobiology of Addiction. *Curr. Opin. Neurobiol.* **1996**, *6*, 243–251.
- (38) Koob, G. F.; Sanna, P. P.; Bloom, F. E. Neuroscience of Addiction. *Neuron* **1998**, *21*, 467–476.
- (39) Basile, A. S.; Fedorova, I.; Zapata, A.; Liu, X.; Shippenberg, T.; Duttaroy, A.; Yamada, M.; Wess, J. Deletion of the M5 Muscarinic Acetylcholine Receptor Attenuates Morphine Reinforcement and Withdrawal but Not Morphine Analgesia. *Proc. Natl. Acad. Sci. U. S. A.* **2002**, *99*, 11452–11457.
- (40) Fink-Jensen, A.; Fedorova, I.; Wörtwein, G.; Woldbye, D. P. D.; Rasmussen, T.; Thomsen, M.; Bolwig, T. G.; Knitowski, K. M.; McKinzie, D. L.; Yamada, M.; et al. Role for M5 Muscarinic Acetylcholine Receptors in Cocaine Addiction. *J. Neurosci. Res.* **2003**, *74*, 91–96.
- (41) Thomsen, M.; Woldbye, D. P. D.; Wörtwein, G.; Fink-Jensen, A.; Wess, J.; Caine, S. B. Reduced Cocaine Self-Administration in Muscarinic M5 Acetylcholine Receptor-Deficient Mice. *J. Neurosci.* **2005**, *25*, 8141–8149.
- (42) Zhang, W.; Yamada, M.; Gomeza, J.; Basile, A. S.; Wess, J. Multiple Muscarinic Acetylcholine Receptor Subtypes Modulate Striatal Dopamine Release, as Studied with M1-M5 Muscarinic Receptor Knock-out Mice. *J. Neurosci.* **2002**, *22*, 6347–6352.
- (43) Wang, S. Z.; Zhu, S. Z.; El-Fakahany, E. E. Efficient Coupling of m5 Muscarinic Acetylcholine Receptors to Activation of Nitric Oxide Synthase. *J. Pharmacol. Exp. Ther.* **1994**, *268*, 552–557.
- (44) Elhusseiny, A.; Hamel, E. Muscarinic--but Not Nicotinic--Acetylcholine Receptors Mediate a Nitric Oxide-Dependent Dilation in Brain Cortical Arterioles: A Possible Role for the M5 Receptor Subtype. *J. Cereb. Blood Flow Metab.* **2000**, *20*, 298–305.
- (45) Anney, R. J. L.; Lotfi-Miri, M.; Olsson, C. A.; Reid, S. C.; Hemphill, S. a; Patton, G. C. Variation in the Gene Coding for the M5 Muscarinic Receptor (CHRM5) Influences Cigarette Dose but Is Not Associated with Dependence to Drugs of Addiction: Evidence from a Prospective Population Based Cohort Study of Young Adults. *BMC Genet.* **2007**, *8*, 1–9.

- (46) Yang, G. Muscarinic Receptors: A Novel Therapeutic Target for Drug Addiction. *Trends Pharmacol. Sci.* **2002**, *23*, 551.
- (47) Holzman, R. S. The Legacy of Atropos, the Fate Who Cut the Thread of Life. *Anesthesiology* **1998**, *89*, 241–249.
- (48) Bodick, N. C.; Offen, W. W.; Shannon, H. E.; Satterwhite, J.; Lucas, R.; van Lier, R.; Paul, S. M. The Selective Muscarinic Agonist Xanomeline Improves Both the Cognitive Deficits and Behavioral Symptoms of Alzheimer Disease. *Alzheimer Dis. Assoc. Disord.* **1997**, *11 Suppl 4*, S16–22.
- (49) Okamoto, H.; Prestwich, S. A.; Asai, S.; Unno, T.; Bolton, T. B.; Komori, S. Muscarinic Agonist Potencies at Three Different Effector Systems Linked to the M(2) or M(3) Receptor in Longitudinal Smooth Muscle of Guinea-Pig Small Intestine. *Br. J. Pharmacol.* **2002**, *135*, 1765–1775.
- (50) Bymaster, F. P.; McKinzie, D. L.; Felder, C. C.; Wess, J. Use of M1-M5 Muscarinic Receptor Knockout Mice as Novel Tools to Delineate the Physiological Roles of the Muscarinic Cholinergic System. *Neurochem. Res.* **2003**, *28*, 437–442.
- (51) Conn, P. J.; Christopoulos, A.; Lindsley, C. W. Allosteric Modulators of GPCRs: A Novel Approach for the Treatment of CNS Disorders. *Nat. Rev. Drug Discov.* **2009**, *8*, 41–54.
- (52) Melancon, B. J.; Hopkins, C. R.; Wood, M. R.; Emmitte, K. A.; Niswender, C. M.; Christopoulos, A.; Conn, P. J.; Lindsley, C. W. Allosteric Modulation of Seven Transmembrane Spanning Receptors: Theory, Practice, and Opportunities for Central Nervous System Drug Discovery. *J. Med. Chem.* **2012**, *55*, 1445–1464.
- (53) Wenthur, C. J.; Gentry, P. R.; Mathews, T. P.; Lindsley, C. W. Drugs for Allosteric Sites on Receptors. *Annu. Rev. Pharmacol. Toxicol.* **2014**, *54*, 165–184.
- (54) Kenakin, T.; Miller, L. J. Seven Transmembrane Receptors as Shapeshifting Proteins: The Impact of Allosteric Modulation and Functional Selectivity on New Drug Discovery. *Pharmacol. Rev.* **2010**, *62*, 265–304.
- (55) Christopoulos, A. Allosteric Binding Sites on Cell-Surface Receptors: Novel Targets for Drug Discovery. *Nat. Rev. Drug Discov.* **2002**, *1*, 198–210.
- (56) Gregory, K. J.; Sexton, P. M.; Christopoulos, A. Allosteric Modulation of Muscarinic Acetylcholine Receptors. *Curr. Neuropharmacol.* **2007**, *5*, 157–167.
- (57) Luttrell, L. M.; Kenakin, T. P. Refining Efficacy: Allosterism and Bias in G Protein-Coupled Receptor Signaling. *Methods Mol. Biol.* **2011**, *756*, 3–35.

- (58) Schwartz, T. W.; Holst, B. Allosteric Enhancers, Allosteric Agonists and Ago-Allosteric Modulators: Where Do They Bind and How Do They Act? *Trends Pharmacol. Sci.* **2007**, *28*, 366–373.
- (59) Mohr, K.; Tränkle, C.; Kostenis, E.; Barocelli, E.; De Amici, M.; Holzgrabe, U. Rational Design of Dualsteric GPCR Ligands: Quests and Promise. *Br. J. Pharmacol.* **2010**, *159*, 997–1008.
- (60) Valant, C.; Gregory, K. J.; Hall, N. E.; Scammells, P. J.; Lew, M. J.; Sexton, P. M.; Christopoulos, A. A Novel Mechanism of G Protein-Coupled Receptor Functional Selectivity. Muscarinic Partial Agonist McN-A-343 as a Bitopic Orthosteric/allosteric Ligand. *J. Biol. Chem.* **2008**, *283*, 29312–29321.
- (61) Valant, C.; Robert Lane, J.; Sexton, P. M.; Christopoulos, A. The Best of Both Worlds? Bitopic Orthosteric/allosteric Ligands of G Protein-Coupled Receptors. *Annu. Rev. Pharmacol. Toxicol.* **2012**, *52*, 153–178.
- (62) Klein, M. T.; Vinson, P. N.; Niswender, C. M. *Approaches for Probing Allosteric Interactions at 7 Transmembrane Spanning Receptors.*; 1st ed.; Elsevier Inc., 2013; Vol. 115, pp. 1–59.
- (63) Bridges, T. M.; Lindsley, C. W. G-Protein-Coupled Receptors: From Classical Modes of Modulation to Allosteric Mechanisms. *ACS Chem. Biol.* **2008**, *3*, 530–541.
- (64) Jakubík, J.; Bacáková, L.; El-Fakahany, E. E.; Tucek, S. Subtype Selectivity of the Positive Allosteric Action of Alcuronium at Cloned M1-M5 Muscarinic Acetylcholine Receptors. *J. Pharmacol. Exp. Ther.* **1995**, *274*, 1077–1083.
- (65) Stahl, E.; Ellis, J. Novel Allosteric Effects of Amiodarone at the Muscarinic M5 Receptor. *J. Pharmacol. Exp. Ther.* **2010**, *334*, 214–222.
- (66) Lazareno, S.; Gharagozloo, P.; Kuonen, D.; Popham, A.; Birdsall, N. J. Subtype-Selective Positive Cooperative Interactions between Brucine Analogues and Acetylcholine at Muscarinic Receptors: Radioligand Binding Studies. *Mol. Pharmacol.* **1998**, *53*, 573–589.
- (67) Christopoulos, A.; Sorman, J. L.; Mitchelson, F.; El-Fakahany, E. E. Characterization of the Subtype Selectivity of the Allosteric Modulator Heptane-1,7-Bis-(dimethyl-3'-Phthalimidopropyl) Ammonium Bromide (C7/3-Phth) at Cloned Muscarinic Acetylcholine Receptors. *Biochem. Pharmacol.* **1999**, *57*, 171–179.
- (68) Ellis, J.; Huyler, J.; Brann, M. R. Allosteric Regulation of Cloned m1-m5 Muscarinic Receptor Subtypes. *Biochem. Pharmacol.* **1991**, *42*, 1927–1932.

- (69) Marlo, J. E.; Niswender, C. M.; Days, E. L.; Bridges, T. M.; Xiang, Y.; Rodriguez, A. L.; Shirey, J. K.; Brady, A. E.; Nalywajko, T.; Luo, Q.; et al. Discovery and Characterization of Novel Allosteric Potentiators of M1 Muscarinic Receptors Reveals Multiple Modes of Activity. *Mol. Pharmacol.* **2009**, *75*, 577–588.
- (70) Bridges, T. M.; Marlo, J. E.; Niswender, C. M.; Jones, C. K.; Jadhav, S. B.; Gentry, P. R.; Plumley, H. C.; Weaver, C. D.; Conn, P. J.; Lindsley, C. W. Discovery of the First Highly M5-Preferring Muscarinic Acetylcholine Receptor Ligand, an M5 Positive Allosteric Modulator Derived from a Series of 5-Trifluoromethoxy N-Benzyl Isatins. *J. Med. Chem.* **2009**, *52*, 3445–3448.
- (71) Bridges, T. M.; Kennedy, J. P.; Cho, H. P.; Breininger, M. L.; Gentry, P. R.; Hopkins, C. R.; Conn, P. J.; Lindsley, C. W. Chemical Lead Optimization of a Pan G(q) mAChR M(1), M(3), M(5) Positive Allosteric Modulator (PAM) Lead. Part I: Development of the First Highly Selective M(5) PAM. *Bioorg. Med. Chem. Lett.* **2010**, *20*, 558–562.
- (72) Brady, A. E.; Jones, C. K.; Bridges, T. M.; Kennedy, J. P.; Thompson, A. D.; Heiman, J. U.; Breininger, M. L.; Gentry, P. R.; Yin, H.; Jadhav, S. B.; et al. Centrally Active Allosteric Potentiators of the M4 Muscarinic Acetylcholine Receptor Reverse Amphetamine-Induced Hyperlocomotor Activity in Rats. *J. Pharmacol. Exp. Ther.* **2008**, *327*, 941–953.
- (73) Gentry, P. R.; Kokubo, M.; Bridges, T. M.; Kett, N. R.; Harp, J. M.; Cho, H. P.; Smith, E.; Chase, P.; Hodder, P. S.; Niswender, C. M.; et al. Discovery of the First M5-Selective and CNS Penetrant Negative Allosteric Modulator (NAM) of a Muscarinic Acetylcholine Receptor: (S)-9b-(4-Chlorophenyl)-1-(3,4-Difluorobenzoyl)-2,3-Dihydro-1H-imidazo[2,1-A]isoindol-5(9bH)-One (ML375). *J. Med. Chem.* **2013**, *56*, 9351–9355.
- (74) Bridges, T. M.; Kennedy, J. P.; Hopkins, C. R.; Conn, P. J.; Lindsley, C. W. Heterobiaryl and Heterobiaryl Ether Derived M5 Positive Allosteric Modulators. *Bioorg. Med. Chem. Lett.* **2010**, *20*, 5617–5622.
- (75) Gentry, P. R.; Bridges, T. M.; Lamasal, A.; Vinson, P. N.; Smith, E.; Chase, P.; Hodder, P. S.; Engers, J. L.; Niswender, C. M.; Scott Daniels, J.; et al. Discovery of ML326: The First Sub-Micromolar, Selective M5 PAM. *Bioorg. Med. Chem. Lett.* **2013**, *23*, 2996–3000.
- (76) Bridges, T. M.; Phillip Kennedy, J.; Noetzel, M. J.; Breininger, M. L.; Gentry, P. R.; Conn, P. J.; Lindsley, C. W. Chemical Lead Optimization of a Pan Gq mAChR M1, M3, M5 Positive Allosteric Modulator (PAM) Lead. Part II: Development of a Potent and Highly Selective M1 PAM. *Bioorg. Med. Chem. Lett.* **2010**, *20*, 1972–1975.

- (77) Melancon, B. J.; Poslusney, M. S.; Gentry, P. R.; Tarr, J. C.; Sheffler, D. J.; Mattmann, M. E.; Bridges, T. M.; Utley, T. J.; Daniels, J. S.; Niswender, C. M.; et al. Isatin Replacements Applied to the Highly Selective, Muscarinic M1 PAM ML137: Continued Optimization of an MLPCN Probe Molecule. *Bioorg. Med. Chem. Lett.* **2013**, *23*, 412–416.
- (78) Poslusney, M. S.; Melancon, B. J.; Gentry, P. R.; Sheffler, D. J.; Bridges, T. M.; Utley, T. J.; Daniels, J. S.; Niswender, C. M.; Conn, P. J.; Lindsley, C. W.; et al. Spirocyclic Replacements for the Isatin in the Highly Selective, Muscarinic M1 PAM ML137: The Continued Optimization of an MLPCN Probe Molecule. *Bioorg. Med. Chem. Lett.* **2013**, *23*, 1860–1864.
- (79) Powers, J. C.; Asgian, J. L.; Ekici, O. D.; James, K. E. Irreversible Inhibitors of Serine, Cysteine, and Threonine Proteases. *Chem. Rev.* **2002**, *102*, 4639–4750.
- (80) Bridges, T. M. Discovery, Optimization, and Characterization of Novel Subtype-Selective Muscarinic Acetylcholine Receptor M4 and M5 Positive Allosteric Modulators, Vanderbilt University, 2010.
- (81) Meshram, H. M.; Ramesh, P.; Sanjeeva Kumar, A.; Swetha, A. An Efficient and Environmentally Friendly DABCO Catalyzed Henry Reaction of Isatins. *Tetrahedron Lett.* **2011**, *52*, 5862–5864.
- (82) Zhang, J.; Chen, J.; Ding, J.; Liu, M.; Wu, H. Copper-Catalyzed Arylation of Indolin-2,3-Ones with Arylboronic Acids. *Tetrahedron* **2011**, *67*, 9347–9351.
- (83) Niu, R.; Xiao, J.; Liang, T.; Li, X. Facile Synthesis of Azaarene-Substituted 3-Hydroxy-2-Oxindoles via Brønsted Acid Catalyzed sp³ C-H Functionalization. *Org. Lett.* **2012**, *14*, 676–679.
- (84) Meanwell, N. A. Synopsis of Some Recent Tactical Application of Bioisosteres in Drug Design. *J. Med. Chem.* **2011**, *54*, 2529–2591.
- (85) Gentry, P. R.; Kokubo, M.; Bridges, T. M.; Noetzel, M. J.; Cho, H. P.; Lamsal, A.; Smith, E.; Chase, P.; Hodder, P. S.; Niswender, C. M.; et al. Development of a Highly Potent, Novel Series of M5 Positive Allosteric Modulators (PAMs) Demonstrating CNS Exposure and Encouraging Subtype Selectivity for the Probe Compound ML380. [*Manuscript in preparation*].
- (86) Miwa, G. T.; Walsh, J. S.; Lu, A. Y. Kinetic Isotope Effects on Cytochrome P-450-Catalyzed Oxidation Reactions. The Oxidative O-Dealkylation of 7-Ethoxycoumarin. *J. Biol. Chem.* **1984**, *259*, 3000–3004.

- (87) Miwa, G. T.; Harada, N.; Lu, a Y. Kinetic Isotope Effects on Cytochrome P-450-Catalyzed Oxidation Reactions: Full Expression of the Intrinsic Isotope Effect during the O-Deethylation of 7-Ethoxycoumarin by Liver Microsomes from 3-Methylcholanthrene-Induced Hamsters. *Arch. Biochem. Biophys.* **1985**, *239*, 155–162.
- (88) Strazielle, N.; Ghersi-Egea, J. F. Physiology of Blood-Brain Interfaces in Relation to Brain Disposition of Small Compounds and Macromolecules. *Mol. Pharm.* **2013**, *10*, 1473–1491.
- (89) Di, L.; Rong, H.; Feng, B. Demystifying Brain Penetration in Central Nervous System Drug Discovery. Miniperspective. *J. Med. Chem.* **2013**, *56*, 2–12.
- (90) Gentry, P. R.; Kokubo, M.; Bridges, T. M.; Cho, H. P.; Smith, E.; Chase, P.; Hodder, P. S.; Utley, T. J.; Rajapakse, A.; Byers, F.; et al. Discovery, Synthesis and Characterization of a Highly Muscarinic Acetylcholine Receptor (mAChR)-Selective M5 -Orthosteric Antagonist, VU0488130 (ML381): A Novel Molecular Probe. *ChemMedChem* **2014**, *33548*, 1–7.